Channelling traditional techniques to microfluidic approaches for the analysis of stimuli-responsive lipid-based dispersions

Linda Hong
Bachelor of Pharmaceutical Sciences (Honours)
Monash University

A thesis submitted for the degree of

Doctor of Philosophy

at

Monash University

FEBRUARY 2019

Drug Delivery, Disposition and Dynamics
Monash Institute of Pharmaceutical Science
381 Royal Parade
Parkville, Victoria

To mama and baba

for everything

Copyright Notice

Contents

Abstract

Stimuli-responsive liquid crystalline nanoparticles present a novel mode of drug delivery where the location and duration of drug release can be manipulated upon exposure of the formulation to specific and controllable conditions. The mechanism operates where nanoparticles are induced to alter the configuration of their complex internal network of water and lipid channels, which can enhance or hinder release. Therefore, it is crucial to understand the kinetics of structural changes to optimise and control the availability of drug from the stimuli-responsive formulation so that patients receive a safe and effective dose of medicine. However, the nature of current experimental configurations to characterise the structural transformations of lipid-based formulations cannot achieve the stimulation (combining the stimulus with the formulation) and data acquisition (determining the internal structure) simultaneously. This results in a time delay between the processes which can lead to a mismatch of the kinetics of the detected changes from the inherent properties of the system.

Microfluidics integrated with synchrotron-based scattering techniques and microscopy-based techniques has been proposed in this work to combine the processing and analytics into one combined configuration to facilitate a finer control over the homogeneity of the application of stimuli and the consequent phase transitions. Various microfluidic devices were evaluated for their suitability to monitor phase transitions ranging from a commercial device to an "off-the-shelf" built device to a custom-designed and fabricated device. The formulations studied in the commercial and "off-the-shelf" devices exhibited inefficient mixing behaviours which led to inconsistent phase transformations. Ultimately, the custom-fabricated device featuring a flow focusing junction was able to yield a controlled phase transition via diffusion-limited transfer of the stimulus to the stimuli-responsive formulation. The device enabled resolution of the phase transitions from the moment of contact with the stimulus to up to 25 mins of equilibration time. Additionally, droplet-based microfluidics were also explored for digestion-responsive systems, showing that phase transitions occurred as a gradient across the particle and demonstrating that mixed phases can coexist in the one particle in non-equilibrium conditions.

The outcomes of this thesis further the understanding of the kinetics of the transformations of the lipid-based liquid crystalline formulations. It offers an alternative experimental configuration that can control the application of stimulus and access the earliest of kinetic structures during a transformation which could ultimately accelerate formulation optimisation for clinical use. Additionally, the

trials and tribulations during the development of a suitable microfluidic device offer insight into factors such as mixing, material compatibility and channel design that require inquiry to ensure consistent and accurate monitoring of kinetic data. It is not as simple as repurposing a commercial microfluidic device.

Declaration of Authorship

This thesis contains no material which has been accepted for the award of any other degree or diploma at any university or equivalent institution and that, to the best of my knowledge and belief, this thesis contains no material previously published or written by another person, except where due reference is made in the text of the thesis.

This thesis includes studies and figures from one submitted publications. The core theme of the thesis is the understanding of the structural transformations of stimuli-responsive liquid crystalline systems using microfluidic technologies. The ideas, development and authorship of all the papers in the thesis were the principal responsibility of myself, the candidate, working within the theme of Drug Delivery, Disposition and Dynamics at the Monash Institute of Pharmaceutical Sciences, under the supervision of Professor Ben J. Boyd.

The inclusion of co-authors reflects the fact that the work came from active collaboration between researchers and acknowledges input into team-based research.

In the case of *chapter 3* my contribution to the work involved the following:

Thesis Chapter	Publication Title	Status *(published, in press, accepted or returned for revision, submitted)*	Nature and % of student contribution	Co-author name(s) Nature and % of Co-author's contribution*	Co-author(s), Monash student Y/N*
3	Comparison of bulk and microfluidic methods for the in situ deter-mination of structural progression during the digestion of lipid-based drug formulations	Submitted	80%. Concept, collecting data and writing first draft	1) Muhsincan Sesen/ Adrian Neild: helped design the microfluidic (S-MF) chip 4% 2) Adrian Hawley: Advice on SAXS analysis 3% 3) Patrick Spicer: input into manuscript 5% 4) Ben Boyd: input into manuscript 8%	Yes/No No No No

I have not renumbered sections of submitted papers in order to generate a consistent presentation within the thesis.

Student signature: Linda   Date: 26/2/19

The undersigned hereby certify that the above declaration correctly reflects the nature and extent of the student's and co-authors' contributions to this work. In instances where I am not the responsible author I have consulted with the responsible author to agree on the respective contributions of the authors.

Main supervisor signature: Ben Boyd   Date: 26/2/19

Publications

Du, J. D.; Hong, L.; Tan, A.; Boyd, B. J. Naphthalocyanine as a New Photothermal Actuator for Lipid-Based Drug Delivery Systems. *The Journal of Physical Chemistry B* **2018**, 122, 1766—1770.

Tan, A.; Hong, L.; Du, J. D.; Boyd, B. J. Self-Assembled Nanostructured Lipid Systems: Is There a Link between Structure and Cytotoxicity? *Advanced Science* **2019**, 21, 1801223

Acknowledgements

Firstly, I would like to thank my supervisor and academic father, Professor Ben Boyd. You have been a very patient and understanding mentor who provided much wisdom and experience in science and life. You have been integral to my academic and professional development, giving the encouragement and advice necessary to get me out of my comfort zone and grow. For that, I am forever grateful. I certainly wasn't here for a haircut, and you made sure of that! Thanks also to my co-supervisor, associate professor Patrick Spicer. Another great mentor who has provided a lot of good advice and helped me out so much! Dr. Charlie Dong, you were great support as co-supervisor too!

A huge thanks to my parents! They came to Australia with "not a cent in [their] pocket" (N. Hong, 1988) but they showed me that "the harder you work, the lucky [sic] you get." I am eternally in their debt and I will continue to work hard until they are proud!

My little Hairy Maclary deserves all the love. I don't think I would have finished my PhD without my dog by my side! My cousins, you've all been amazing! Thanks for all the wild times :3 Shout out to the L4DIES aka the earthquake crew, Joanne Ly, Victoria Tang and Christine Wun, for their support and keeping my sanity in check. LOVE YOUS!

I want to also give thanks to the Boyd group (and friends in 230) who shared laughter and frustrations with me over hotpots and lab work. Nicolas Alcaraz, Nicole Bisset, Igor Chekhtman, Andrew Clulow, Joanne Du, Khay Fong, Shayna Jia, Liang Jin, Jamal Khan[1], Tang Li[2], Matthias Lindquist, Jason Liu, Kellie May, Oliver Montagnat, Mubtasim Murshed, Stephanie Phan, Anna Pham, Gisela Ramirez, Malinda Salim, Stefan Salentinig, Xiaohan Sun, Sarah Streck, Angel Tan, Kristian SoyJoy Tangso, Kapil Vithani, Graham Webster, Cindy Xiao and Bo Yun. Also, to Catherine Mak and the CBNS cousins on level 4!

Thanks also to the Australian Government who funded my studies and research with the Research Training Program Scholarship, to the beam line scientists, Adrian Hawley, Nigel Kirby and Stephen Mudie at the Australian Synchrotron, and to Brett Johnson from Melbourne University for the Raman results that were never meant to be.

---

[1] RE: Feta Fetish; as promised, this senpai is also in the footnotes
[2] As is my lab partner in crime >:3c

List of abbreviations

1D	1-dimensional
2D	2-dimensional
4-BPBA	4-bromophenylboronic acid
A.U.	arbitrary units
AOT	sodium dioctyl sulfosuccinate
BA	butyric acid
CA	caprylic acid
COC	cyclic olefin copolymer
CPLM	crossed polarised light microscopy
CPP	critical packing parameter
cryoFESEM	cryogenic field emission scanning electron microscopy
cryoTEM	cryogenic transmission electron microscopy
DDAB	didodecyldimethylammonium bromide
DLS	dynamic light scattering
DP	digestion products
DT-MF	droplet trapping microfluidic
FRR	flow rate ratio
GLY	glycerol
H_2	inverse hexagonal phase
HCl	hydrochloric acid
hr(s)	hours
L_2	inverse micellar phase
L_α	lamellar phase
LCNP	Liquid crystalline nanoparticle
LOM	lipid-only mixture
LP	lattice parameter
MC	monocaprylin
MF	microfluidics
min(s)	minutes
msec(s)	millisecconds
NA chip	NanoAssemblr^{TM} chip
NaOH	sodium hydroxide
NMR	nuclear magnetic resonance
OTS-MF	"off-the-shelf" microfluidic
PHYT15TC	dispersion containing phytantriol with 15%w/w tricaprylin
PHYT20TB	dispersion containing phytantriol with 20%w/w tributyrin
PDMS	polydimethylsiloxane
PHYT	phytantriol
PMMA	polymethyl methacrylate
SA25TB	dispersion containing selachyl alcohol with 25% w/w tributyrin (chapter 2) lipid only mixture containing selachyl alcohol with 25% w/w tributyrin (chapter 3)
SA	selachyl alcohol
SANS	small angle neutron scattering
SAXS	small angle x-ray scattering
sec(s)	seconds
S-MF	serpentine microfluidic
TB	tributyrin
TBU	tributyrin units
TC	tricaprylin

TFR	total flow rate
V_2	bicontinuous cubic phase

Chapter 1: Introduction

1.1 Introduction

Nanoparticles have been extensively studied for drug delivery applications in recent years because of their potential to improve targeting to sites of disease, increase retention, and control the release of the drug, resulting in improved therapeutic outcome.[1] Common nanosystems include liposomes, solid nanoparticles, polymeric micelles, and nanotubes. The systems have the capacity to encapsulate material such as drug particles and biomolecules for applications such as drug delivery, gene therapy and biosensing.[2]

Surface functionalisation or incorporation of particular additives can render the nanoparticles sensitive to certain stimulus to enable controlled and 'on-demand' release. The response to the stimulus induces a change in structure – this may be particle disassembly (an irreversible process) or a transition between structures which returns to the original state when the stimulus is removed (reversible), and this has been illustrated in **Figure 1-1**. As the structure of the particle controls the retention and release of drug, different structures will provide different rates of drug release.[3–5] Ideally, this then enables a system to deliver a dose when the formulation is exposed to the correct stimulus conditions. For a reversible system, upon removal of the stimulus, the drug release should also cease, thus accomplishing controlled and 'on-demand' pulsatile drug release. A delivery system such as this has the potential to deliver drugs more efficiently to the target tissue with control over the timing of drug release and therefore reduce the total amount of drug required, reduce side effects, and reduce the frequency of administration to increase patient compliance.
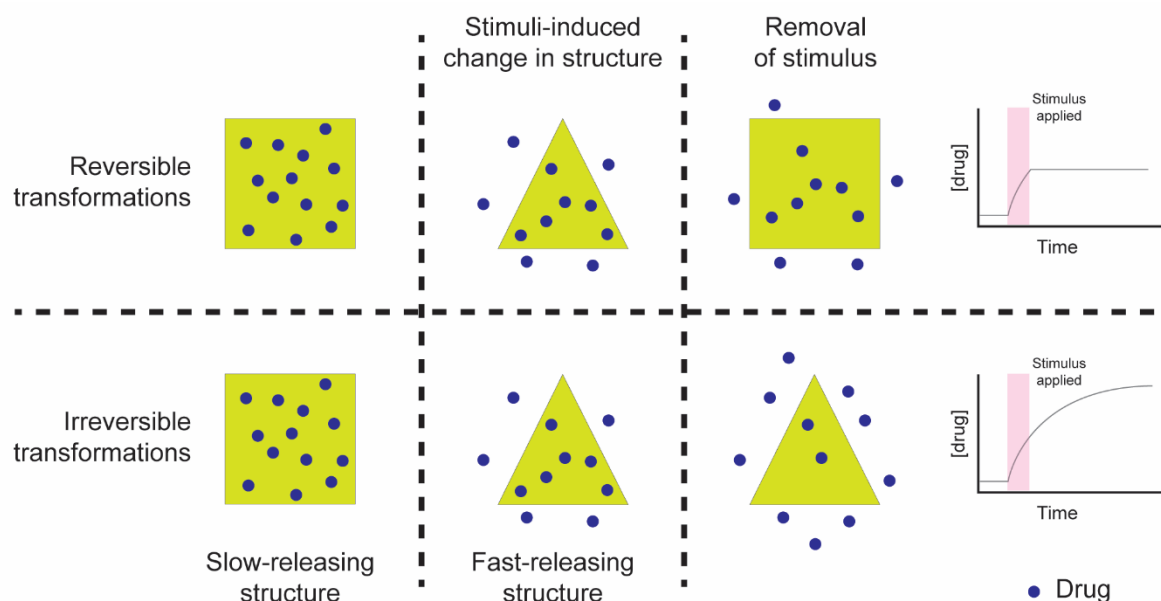
Figure 1-1. Schematic of irreversible and reversible stimuli-responsive systems of drug release. When stimulus is applied to both systems, a structural change can occur which results in the release of drug. Upon removal of the stimulus, the reversible system can revert back to the original structure and inhibit further drug release, while the irreversible system would continue to release drug.

One class of nanoparticulate drug delivery system that could achieve this is lipid-based liquid crystalline nanoparticles (LCNP). These systems can be rendered responsive to different conditions such as pH,[6,7] enzymes,[8,9] temperature,[3,10] and light,[11,12] all of which can be compatible with human administration. The applications and advantages are promising, however there are no such stimuli-responsive products that currently exist on the market.[13] There is still little understanding of these systems to aid in their advance into commercialisation which can be attributed to our inability to consistently and accurately characterise their mechanism of transformation and release. Developing a methodology to reliably analyse these systems is fundamental to their optimisation and eventual clinical use.

The following chapter provides an overview of the nanoparticulate systems and summarises the current forms of stimuli-responsive transformations. The standard techniques used to characterise these phase transitions are discussed whilst also addressing the current limitations. Microfluidics was then explored as a tool to overcome these problems, detailing factors such as the various types of devices, current applications, and potential functions.

1.2 Lipid-based liquid crystal nanoparticles (LCNPs)

Amphiphilic lipid molecules can self-assemble in water into 'bulk phases' that exhibit complex networks of lipophilic and hydrophilic domains in defined geometric arrangements. These ordered networks, also known as mesophases, are shown in **Figure 1-2** and can include: inverse cubic phases (V_2) consisting of the diamond (*Pn3m*), gyroid (*Ia3d*) and primitive (*Im3m*) space groups; inverse micellar cubic (I_2) including the *Fd3m* space group; inverse hexagonal (H_2); and lamellar (L_α) phases.[14] The V_2 phases are bicontinuous and possess two discrete but interlacing lattices of water and lipid channels, and generally exhibit rapid release of hydrophilic components.[4,14] The H_2 phase is essentially micellar rods arranged in a hexagonal formation, where the ends of the rods are capped to inhibit drug release.[4,14] L_α phases consist of stacked bilayers.[14] The bulk phases of these liquid crystalline mesophases may also be dispersed into nanoparticles and retain a similar internal structure as the corresponding bulk phase.[15] Dispersed particles of L_α phase, known as liposomes, may possess one or more bilayers depending on preparation methods and lipid composition.[16]

The types of LCNPs formed depend on the critical packing parameter (CPP) of the amphiphile, which is defined by the equation:

Equation 1-1. Equation to calculate the critical packing parameter,[17] where *v* is the volume of the non-polar tail group; *a* is the effective area of the hydrophilic head group at the interface; and *l* is the chain length of the hydrophobic portion in the liquid state.

$$CPP = {v}/{al}$$
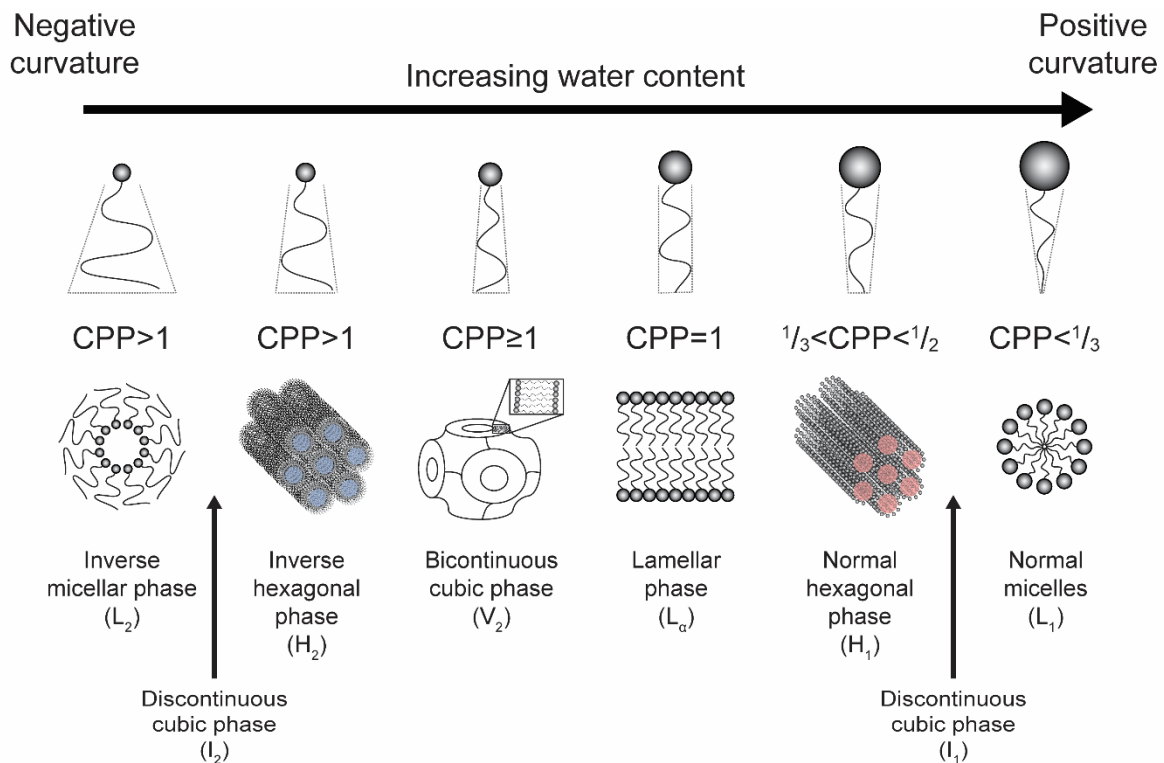
Figure 1-2. Schematic of the various structures that can arise from amphiphiles of different critical packing parameter (CPP). A larger CPP displays a more negative curvature, and vice versa, a smaller CPP exhibits a more positive curvature. Figure adapted from Sagalowicz *et al.*[18] and Israelachvili.[19]

For a specific lipid at a specific extent of hydration, it can self-assemble into one nanostructure, or a specific combination of coexisting nanostructures. Additionally, variations in temperature and pressure can transition the system into another nanostructure for that same lipid composition. One example of this is shown in **Figure 1-3** where the phase behaviour of 1-monoelaidin transitioned from the lamellar crystalline phase to cubic phases with increasing temperature. It was also noted that the slope of the phase transitions decreased with increasing pressure at a fixed composition.[20]
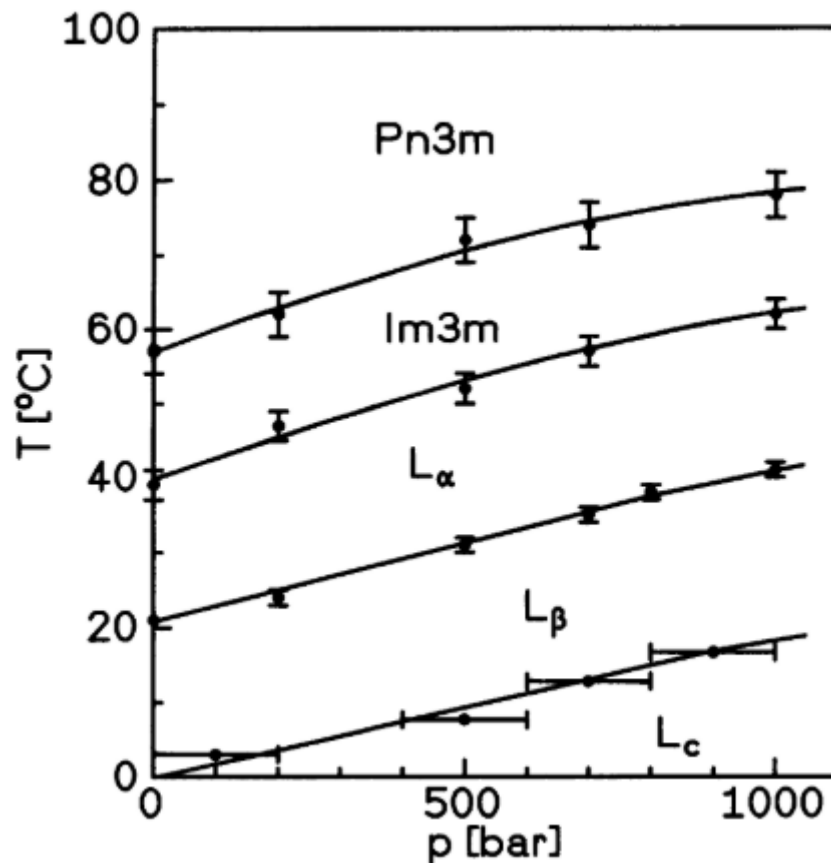
Figure 1-3. Phase diagram of the lyotropic lipid, 1-monoelaidin, in excess water with changing temperature and pressure. The system transitions from lamellar phase (L_c) to the L_β gel phase, the L_a liquid-crystalline phase, the cubic Im3m phase and finally the cubic *Pn3m* phase with increasing temperature. Increasing the pressure increased the temperature required for a phase transition. Figure adapted with permission from Czeslik *et al.*[20]

1.2.1 Formation of liquid crystalline dispersions

The bulk form of these systems is often a viscous gel that is difficult to manipulate or administer as drug products. However, the mesophases described above, when prepared using hydrophobic lipids, can often be stable to dilution in excess water, allowing the dispersion of the bulk phases into particles which retain the internal structure of the parent phase. Cubosomes, hexosomes and liposomes are the terms used to describe the dispersed particles of bulk cubic, hexagonal and lamellar phases, respectively. Hence, to exploit on the unique properties of these liquid crystalline systems, they are often dispersed in excess water to form nanoparticle-based dispersions.

These nanoparticles are often prepared by applying energy in the form of homogenisation or ultrasonication to the bulk lipid in excess aqueous solution.[21] This method is the most common, however the heat generated during the process may be inappropriate for heat-sensitive materials. Alternatively, dissolving the poorly water soluble lipids in low boiling point solvents and then removing said

solvent, or dissolution in a hydrotropic solvent and subsequent dilution in an aqueous solution have also been shown to generate the nanostructures.[22,23] These methods require less energy, however the formation of particles is not comparably uniform, leading to poor size distribution. Homogeneous nucleation was thought to be the process which produced the liquid crystal particles during dilution.[22] An additional step is required to remove the volatile solvents via evaporation for further use.

1.2.2 Structure-forming lipids

A wide range of lipids, including phospholipids, monoglycerides and alcohols, have been shown individually and in combination to form mesophases in excess water.[24] Although they are lipids, the molecules also possess a region of hydrophilicity to satisfy the CPP for self-assembly to occur upon hydration. Of recent interest for potential application in drug delivery are the three lipids shown in **Figure 1-4**.

Phytantriol (3,7,11,15-tetramethylhexadecane-1,2,3-triol) is a lipid commonly used for the formation of LCNPs and has also previously been used in skin-care products[25] with minor allergies to the skin at higher concentrations.[26] It has been formulated with drugs and tested on animal models and on human cells.[27–30] At various temperatures and water content, the lipid can form L_2, L_α, V_2 (of the *Pn3m* and *Ia3d* geometries) and H_2 phases when hydrated in excess water.[31,32]

Glyceryl monooleate (GMO), or monoolein, also forms L_α and V_2 phases when immersed in water.[33] An ester bond is present in the chemical structure of GMO making it liable to hydrolysis and thus, less stable in the presence of hydrolytic enzymes as would be encountered in oral administration.[34] It also consists of two regioisomers, sn-1 and sn-2, which racemise on contact with aqueous solution. The unsaturated bond is also susceptible to oxidation.

Selachyl alcohol is analogous to the structure of GMO, excluding the ester group, but instead self-assembles into the H_2 phase.[35] The lipid lacks a hydrolysable functional group so is resistant to hydrolases in the body, maintaining the integrity of the structure longer than lipids such as GMO.
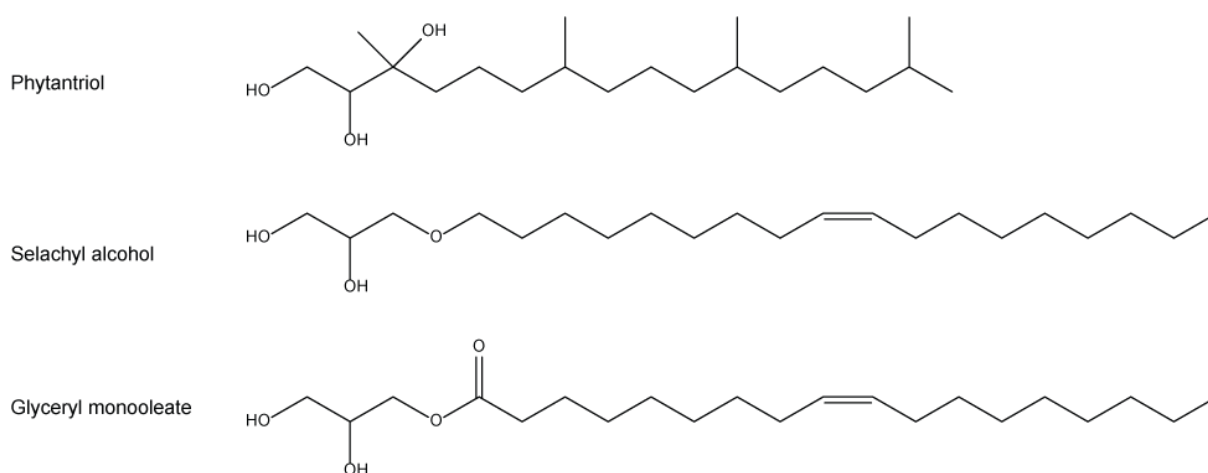
Figure 1-4. Chemical structure of lyotropic amphiphilic lipid molecules, phytantriol, selachyl alcohol and glyceryl monooleate (sn-1 version of GMO is shown in this case).

1.3 Characterisation of liquid crystalline structures

The most common techniques used to analyse the internal structure of these nanoparticles include imaging and scattering techniques. Imaging techniques such as cryogenic transmission electron microscopy (cryoTEM) or crossed polarised light microscopy (CPLM) can qualitatively identify the internal structure of bulk systems. Scattering techniques, including small angle X-ray scattering (SAXS) and small angle neutron scattering (SANS), produce quantitative data that is transformed to reveal the geometry of the unit cell comprising the material and consequently the mesophase. There are other less common structural characterisation techniques including pulsed magnetic field gradient spin echo nuclear magnetic resonance (NMR)[36] and cryo-field emission scanning electron microscopy (cryoFESEM)[37] which will not be covered in this chapter.

1.3.1 Microscopic-based analytical techniques

CryoTEM is the main microscopy-based technique used to confirm the size, morphology and mesophase of the LCNPs.[22,23,38–42] Fast Fourier transform analysis may also be conducted on the image to quantitatively confirm the mesophase.[38] Standard transmission electron microscopy cannot be used as the samples need to be dried and free of solvent, ultimately interfering with the packing of the lipid molecules of the LCNPs. Therefore, cryoTEM, which requires vitrification of the liquid film containing the particles, is advantageous as it can maintain the structural integrity of the mesophase for analysis.

Structural data may also be inferred from optical properties of the bulk non-dispersed mesophase, and this can be resolved using CPLM.[42] Samples are viewed between two crossed polarisers on a regular microscope and depending on the structure of the sample, the sample can appear bright

(if it rotates the plane of polarised light) or dark if it is an isotropic structure. H_2 and L_α phases are anisotropic and exhibit birefringence under polarised light (**Figure 1-5**).[42] V_2 phases are isotropic and lack birefringence but can be identified under CPLM at the lipid-water interface by the distortion due to the high viscosity of the cubic phase.[42] In a typical coloured micrograph such as that shown in **Figure 1-5**, the hue and saturation of the birefringence can represent the orientation and ellipticity, respectively.[43]
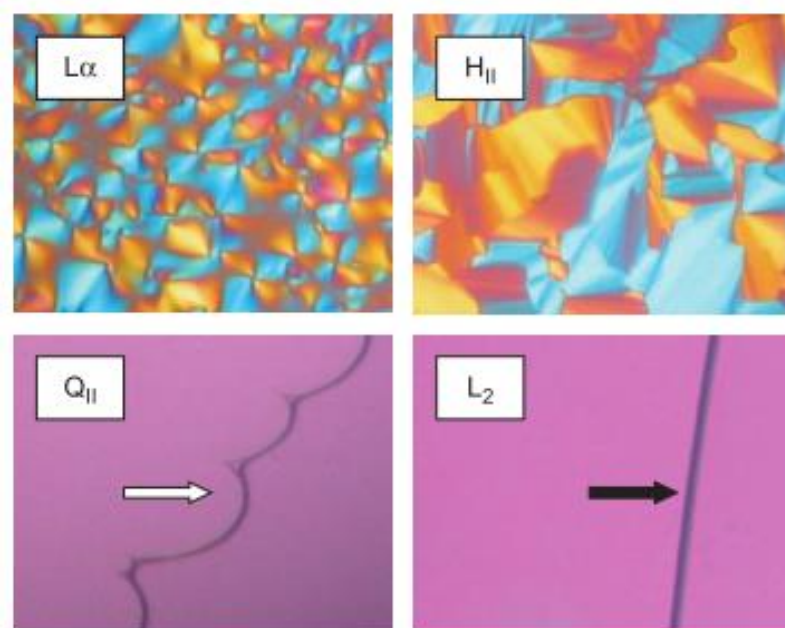
Figure 1-5. Images of liquid crystalline systems observed with CPLM. The L_α and H_2 phases on the top panels demonstrate different birefringent patterns while the images of the V_2 and L_2 phases in the bottom panels show no birefringence due to their isotropy. However, the latter two phases can be distinguished by the behaviour of the lipid-water interface. Image used with permission from Boyd *et al.*[44]

1.3.2 Scattering-based analytical techniques

Small angle X-ray scattering (SAXS) is perhaps the most widely accepted technique used to identify liquid crystalline mesophases. A collimated X-ray beam at a fixed energy (and wavelength, λ) is focused on the sample. The crystalline property of these mesophases features planes of atoms with similar electron density in the repeat units which scatter the photons leading to constructive and destructive interference at the detector. The result is a collection of bright and dark pixels, at various positions on a 2D image depending on the scattering angle (2θ) and azimuth angle (Φ), averaged over the acquisition time.[45] The regions of bright intensity form the diffraction peaks when the 2D image is converted to a 1D scattering profile as a function of intensity versus scattering vector, q (**Figure 1-6**). The relationship between the ordered structure and the 2D scattering pattern can be

defined by Bragg's law (**Equation 1-2**), and determination of q for the 1D scattering profile can be calculated with **Equation 1-3**.

Equation 1-2. Bragg's law where λ is the wavelength, d is the interplanar distance and θ is the angle at which the radiation is diffracted.[45]

$$n\lambda = 2\mathrm{d}\,sin(\theta)$$

Equation 1-3. The equation defining the scattering vector, q, which is used to convert the 1D scattering image to the 2D scattering profile.[45]

$$q = \frac{4\pi}{\lambda} \cdot sin(\theta)$$

The scattering profiles are unique to each different mesophase and can enable identification of the type of structure.[14] The profiles feature diffraction peaks (or Bragg peaks) which originate from diffraction from planes of like atoms or similar electron density within the crystalline structures. The spacing ratios between the peak maxima can be indexed by assigning each diffraction peak to a set of planes within the crystal lattice according to their Miller indices (hkl) and correlated with documented reflection laws specific to each phase as shown in **Figure 1-6**.[14,46] In addition to identifying structure, the profiles can also determine the interplanar distance, d, lattice parameter, a, and the size of the water channels.[5,14,47,48] The d which defines the distance between two aligned lattice planes, can be determined from the q value of the diffraction peak using **Equation 1-4**. Further to this, the lattice parameter, a, which describes the dimensions of the repeating unit cells of the crystal lattice can be determined by **Equation 1-5** for V_2 phases and **Equation 1-6** for H_2 phases. For the inverse micellar phase (L_2), the d-spacing is also known as the characteristic distance, which refers to the distance between each micelle.
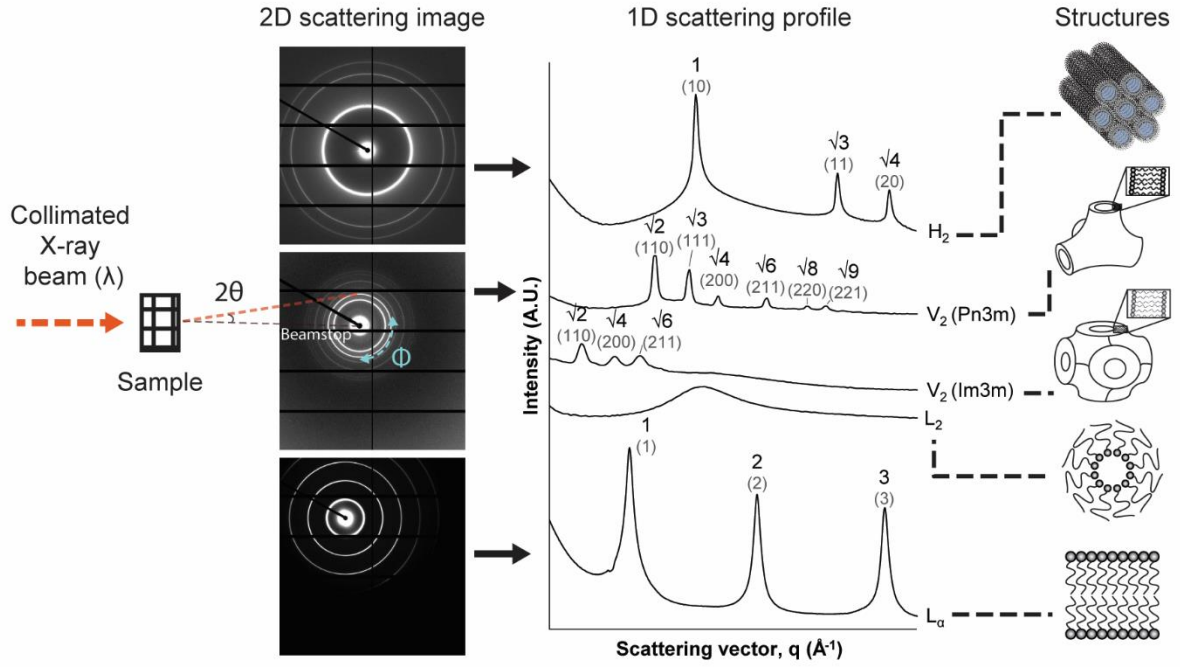
Figure 1-6. A simplified schematic of the analysis of liquid crystalline structures using SAXS. From left: the collimated X-ray beam passed through sample. The sample diffracts the beam at a scattering angle (2Θ) to yield 2D scattering images which are then converted to the 1D profiles (middle) as an intensity vs. q plot. The azimuthal angle has been marked as Φ. The profiles are unique to various liquid crystal phases as denoted by the spacing ratios between the peak positions; the associated Miller indices (hkl) of each peak have also been included.[14,44] The top profile with peaks at 1, √3 and √4 is characteristic of H_2 phase. The next two profiles include the cubic phases of the *Pn3m* and *Im3m* space groups. The fourth profile from the top is the inverse micellar phase, L_2, which is a disordered phase and not a liquid crystalline structure but will be observed often throughout this thesis. The profile at the bottom is indicative of L_α phase. The scattering profiles are correlated to the structures on the right.

Equation 1-4. The equation to determine the *d*-spacing when using the scattering vector, q.[45]

$$d = {2\pi}/{q}$$

Equation 1-5. Lattice parameter equation for cubic phases. Terms, h, k and l, denote the Miller indices for the different mesophases.[49]

$$a = d\sqrt{h^2 + k^2 + l^2}$$

Equation 1-6. Lattice parameter equation for hexagonal phases.[49]

$$a = d\sqrt{\frac{4}{3}(h^2 + k^2 + hk)}$$

There are two types of SAXS instruments, traditional X-ray tube (often called bench-top) and synchrotron sources. X-rays from synchrotron sources are generated from the acceleration of electrons via magnets moving at speeds close to the speed of light whereas lab scale instruments use X-rays

generated from the collision of electrons with a metal filament.[45,50] Therefore, bench-top instruments are relatively lower flux than synchrotron sources, and require upwards of hours to acquire data from static equilibrated samples and are not typically useful for time-resolved measurements. Synchrotron-based SAXS has considerably greater flux (up to 10^{12} times as much)[51] and is capable of resolving structural data within milliseconds making it ideal to study the kinetics of fast structural changes in LCNP systems. The drawback of the synchrotron source is that the higher flux of the X-rays can damage samples, hence the instrument parameters such as flux, exposure time and energy need to be adjusted to circumvent this.[50]

1.4 Transformations

The nanostructure formed by the LCNPs at equilibrium is dictated by the effective CPP of the lipid molecules. Nanostructures that are not in thermodynamic equilibrium (known as non-equilibrium structures) can also exist after the system has been stressed and where it takes time for the structure to relax back to the equilibrium structure.[15,52] In accordance with **Equation 1-1**, modulation of the relative sizes of the hydrophobic and hydrophilic regions of the molecule can alter the CPP thereby causing a structural change and thus achieving transformation of the mesophase. Various stimuli such as light, pH, ionic strength and heat can influence the apparent ratio of the sizes of the polar and non-polar ends which alters the CPP to trigger a phase transition. Examples of some phase transitions and the hypothesised mode of action have been compiled in **Table 1-1**.

Table 1-1. Examples of phase transitions and the common mechanism of transformation.

From	To	Stimulus	Mode of action	Reference
H_2	V_2	Cooling	Reduces chain splay and apparent size of tail group	3
L_2	V_2	Addition of enzyme	Hydrolysis of additive, removing disruptive behaviour of the additive for self-assembly of lipids	9
V_2	H_2	UV irradiation	Photoisomerisation of additive (spiropyran) and change in geometric packing of the lipids around the additive	11
L_α	V_2	Increase in salt concentration	Charge neutralisation of head groups and decrease in apparent size of head group	39
I_2	H_2	Increase in pH	Ionisation of additive (oleic acid) and increase in apparent size of head group	53
L_α	H_2	Increase in salt concentration	Charge neutralisation of head groups and decrease in apparent size of head group	54

The general mechanism of these phase transitions involves the lyotropic lipid transforming under the influence of external stimuli intrinsically or responding to an 'actuator' added to the system to

render it responsive to a particular stimulus. A list of stimuli-responsive LCNP systems with the associated additive and stimulus has been tabulated in **Table 1-2**. Certain stimuli such as direct heat do not require any additives as the packing of some lyotropic lipids is inherently temperature responsive.[15,31,33,35] Temperature can alter the packing behaviour and hydration of the lipids, and the consequent CPP.[55] Inclusion of responsive additives can impact on intrinsic phase behaviour of the system – this can be used to an advantage where the inherent phase formed by the core lipid system occurs under the influence of the stimulus. For example, addition of ionic surfactants can draw a phytantriol-water system towards the L_α structure, and shield the charge by addition of salt can switch it back to V_2 phase.[56] Additionally, the additives are not just limited to other lipids and surfactants, pH-labile drugs can also be incorporated which can change the phase behaviour of the delivery vehicle depending on ionisation state of the drug.[57] In a practical setting, triggering a phase transition can be achieved by diluting the dispersion to reduce the concentration of the additive in the locality of the lipid nanoparticles.

Table 1-2. Various transformations of lyotropic LCNPs in the current literature.

Transformation type	Lyotropic lipid	Additive	Stimuli	Reference
Temperature	Phytantriol GMO Myverol	-	Heat	15
Temperature	Monoelaidin	-	Heat	58
Temperature	1-palmitoyl-2-oleoyl-sn-phosphatidylethanolamine	-	Heat	59
Temperature	GMO	Iron oxide nanoparticles	Low-frequency alternating magnetic field	60
Photothermal	Phytantriol	Graphene	Near infrared radiation	12
Photothermal	Phytantriol	Gold nanorods	Near infrared radiation	61
Photothermal	1,2-dipalmitoyl-sn-glycero-3-phosphocholine 1,2-distearoylsn-glycero-3-phosphocholine 1-stearoyl-2-hydroxy-snglycero-3-phosphocholine 1,2-distearoyl-sn-glycero3-phosphoethanolamine-N-[methoxy(polyethylene glycol)-2000]	Gold nanorods Gold nanostars	Near infrared radiation	62
Pressure	Dimodan Phytantriol	-	Pressure	63
Pressure	1-monoelaidin 1-monoolein	-	Pressure	20
Ionic strength	Phytantriol	Sodium bis(2-ethylhexyl)sulfosuccinate Didodecyldimethylammonium bromide	Ionic strength	56
Ionic strength	Phytantriol	Didodecyldimethylammonium bromide	Phosphate buffered saline	39

Table 1-2. (cont.) Various transformations of lyotropic LCNPs in the current literature.

Transformation type	Lyotropic lipid	Additive	Stimuli	Reference
Ionic strength	GMO	Dioleoyl-phosphatidylglycerol	Calcium ion solution	54
Digestion	Monoolein, Oleic acid, Diolein, Sodium oleate	(lyotropic lipids are digestible)	Thermomyces lanuginosa lipase	64
Digestion	Phytantriol, Selachyl alcohol	Tributyrin, Tricaprylin, Trilaurin	Pancreatic lipase	9,65
Digestion	Soy phosphatidylcholine	Glycerol dioleate	Triacylglycerol lipases	66
Digestion	Phytantriol, Decyl betainate chloride	Polysorbate 80	Lipase B from Candida antarctica, Lipase from Rhizomucor miehei	67
pH	Phytantriol	Oleic acid	Acid/base	6
pH	Monoolein	Oleic acid	Acid/base	53
pH	Monolinolein	Pyridin-4-ylmethyl linoleate	Acid/base	7
Light	Phytantriol	Donor–acceptor Stenhouse adducts (photochromic molecules)	Green light (532 nm)	68
Light	Phytantriol, GMO	Spiropyran derivative	UV light (375 nm)	11,69
Light	Phytantriol	Naphthalocyanine (photochromic)	Near infrared radiation (808 nm)	70
Light	Azo-surfactant	-	UV light (365 nm), Visible light (540 nm)	71

Phase transitions have been exploited for 'on-demand' controlled drug delivery to modulate the nanostructure and consequently the rate of release.[3,61,72] The different mesophases can exhibit different drug release profiles, as shown for a series of mesophases by Phan *et al.*, where the H_2 phase and L_2 phase presented considerably slower release than the V_2 phase.[4] However, the corresponding dispersed systems show burst release which has been suggested to be a result of the higher surface area to volume ratio compared to the bulk phase.[73] Additionally, the internal structure of the nanoparticle has regions of hydrophobicity and hydrophilicity which can internalise molecules of any polarity. Despite the ideal release properties of the bulk phases, the dispersed systems are preferred as delivery systems as they are easier to handle due to the lower viscosity. Consequently, efforts have been sought to translate this type of controlled release behaviour into the dispersed nanoparticle system.

1.4.1 Current limitations in monitoring the kinetics of phase transitions

It is important to fully understand the complexities of LCNPs including accurate characterisation of their transformations and the factors that influence this. This can enable improvement of the formulations and optimise the manner in which they are transformed or produced. Furthermore, knowing which phases to expect and for how long they persist can allow better predictions on the release properties of the drug delivery system.

Stimuli can be applied to the stimuli-responsive formulations in a number of ways, including chemical, enzymatic and using remote stimuli such as heat, light and magnetic field. The experimental configurations to analyse the dynamic transformations of LCNPs is therefore dependent on the type of stimuli. A review of various experimental configurations with SAXS to characterise the formation of the non-equilibrium structures has been previously covered,[74] however the following section will focus more on those for the analysis of stimuli-responsive systems and the limitations.

The phase transitions of samples in response to changes in temperature are usually monitored by loading samples into glass capillaries which are then inserted into a temperature controlled capillary holder in line with the beam.[12,61,75] Samples are equilibrated for an appropriate amount of time before data is acquired. Temperature jump and temperature drop experiments are also possible where sample is heated by an infrared laser.[76,77] Another example of temperature drop configuration to study the non-equilibrium behaviour of LCNPs is illustrated in **Figure 1-7** where a temperature-sensitive sample was pushed through a stainless steel needle immersed across two water baths set

to two different temperatures depending on the experiment.[15] Structural data were acquired at the second temperature over time as the equilibration of structure between the first and second temperatures was found to be almost instantaneous. In these studies, the kinetic structures of liquid crystalline samples being heated and cooled were resolved, noting that the lyotropic behaviour of the lipids in nanoparticle and bulk systems are not always the same, and that the supercooling effect was observed with both systems; where a greater effect was observed for the dispersed formulations.
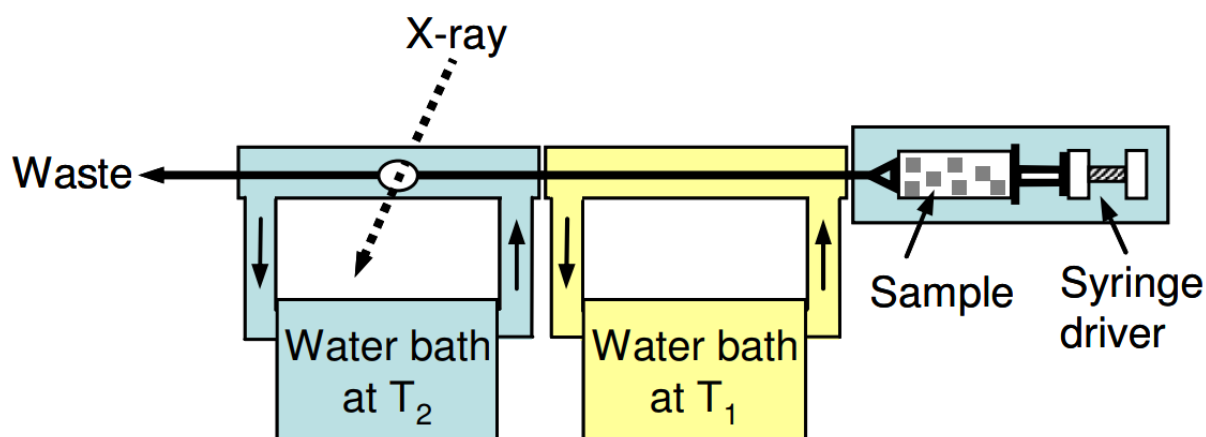
Figure 1-7. Experimental configuration to study the kinetic structures formed when samples were subject to changes in temperature by modulation of the water bath temperatures. Image used with permission from Dong *et al.*[15]

Approaches for incorporating solution-based stimulus (such as pH, salts or enzyme for example) into a formulation require some form of mixing prior to analysis. In the simplest of methods, a digestion-sensitive liquid crystalline sample (30 mg) was mixed with a hydrolytic enzyme (20 µL) using a spatula and then enclosed in a sample holder with X-ray transparent windows; the structural kinetics were monitored over time using SAXS showing the loss of structure over the course of the digestion.[64] A stopped flow configuration can be also integrated with SAXS (shown in **Figure 1-8**) which employs a mixing chamber to combine a solution containing vesicles with a solution of calcium ions from separate syringes within 10 msecs.[54] The mixture (100 µL) was then discharged into a capillary in line with SAXS where the non-equilibrium structures could be resolved over time. Other configurations would require a vessel that can hold volumes in the order of millilitres where the solution containing the stimuli can be incorporated and mixed before being analysed. A self nano-emulsifying formulation (dispersed in 300 mL of digestion media) was combined with lipase (100 mL), and samples at specific times were manually removed and a lipase inhibitor was added to stop the digestion process.[78] The samples were then transferred to the appropriate sample holder (for

example 96-well plates, quartz capillaries) for analysis where digestion had induced the transition from a structureless system to one containing L_α and H_2 phases.[78] The process is not ideal for real-time studies due to the delay presented by the extra processing of the digested mixture.
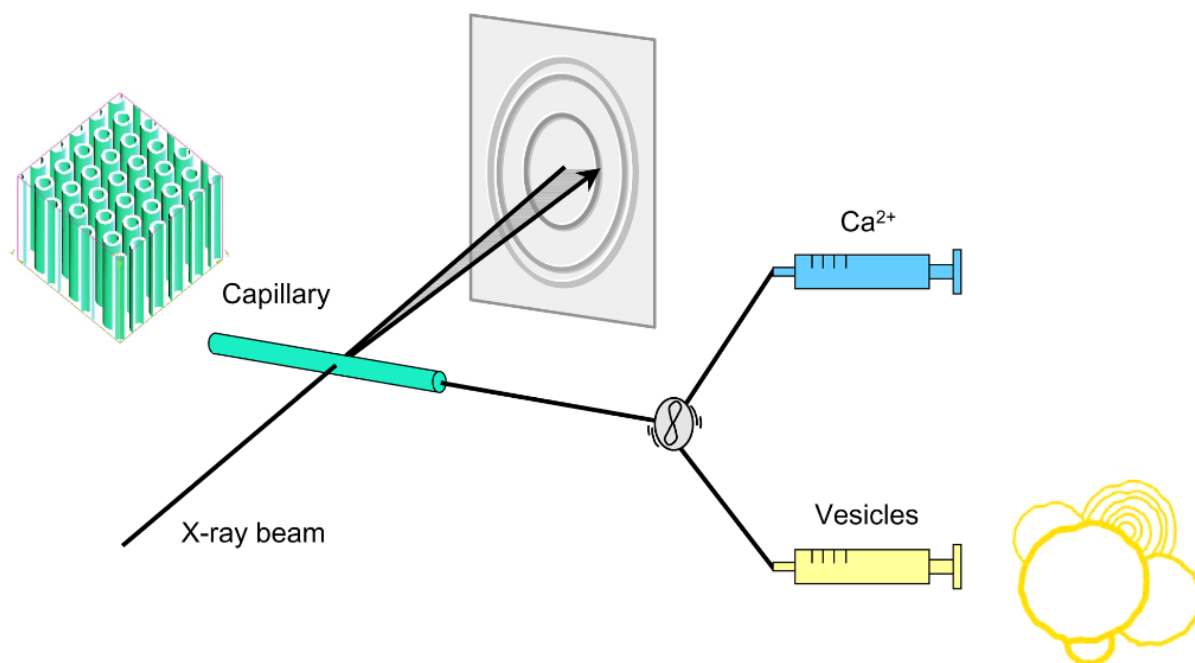
Figure 1-8. A stopped-flow apparatus integrated with SAXS. The salt-sensitive sample and the solution containing the calcium ions were combined in a mixing chamber before being released into a capillary for SAXS analysis. Image used with permission from Yaghmur *et al.*[54]

Alternatively, the sample in the vessel can be circulated via a closed-loop system fitted with a quartz capillary for SAXS measurements given that the vessel itself cannot be directly placed in line with the X-ray beam due to its size or composition. **Figure 1-9** illustrates the pH-stat apparatus for an enzymatic digestion,[9,34,65] but simpler mixing configurations have also been reported for other systems.[6,79] Briefly, sample is mixed with the stimulus in one vessel before it is transferred via a pump and tubing to a capillary (in line with the X-ray) and then back into the bulk. In this configuration, the formulation is under constant flow whilst the X-ray acquires data from a single position. The X-ray beam requires an exposure time within which data is collected, needing as little as milliseconds for acquisition. However, for flow through models and dispersed systems, approximately 5 secs (or more depending on which synchrotron source) is an appropriate time to yield adequate resolution of the sample. As the sample is constantly transforming, the resolution of the kinetics in the flow through model is therefore limited by the acquisition time and the configuration would not be suitable for rapidly transforming systems.
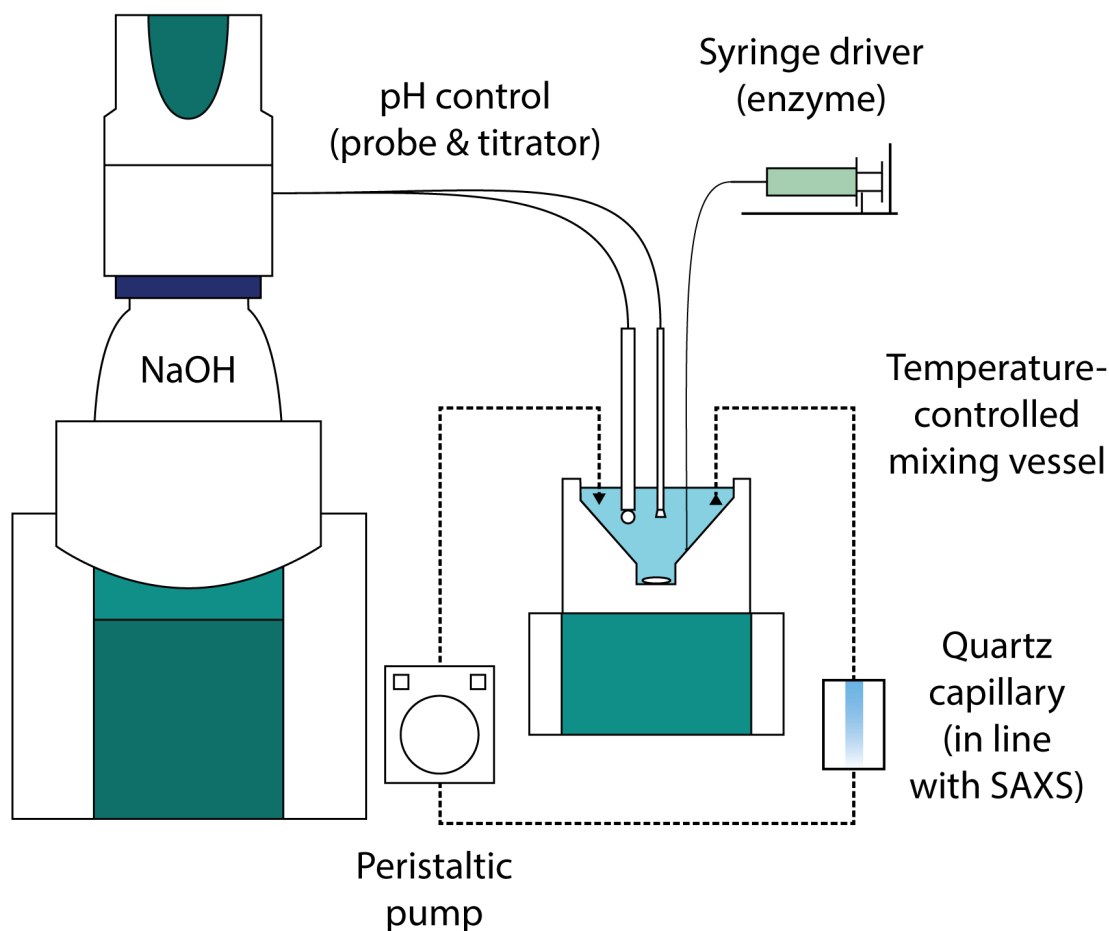
Figure 1-9. Schematic of the pH-stat apparatus for analysing the digestion of formulations using SAXS.[34] Formulation is housed in the temperature-controlled mixing vessel. Stimulus such as an enzyme solution is remotely added to the vessel as the magnetic flea mixes the solutions. At the same time, pH is monitored and maintained constant with the titrator. The mixture is continuously delivered to a capillary in line with the X-ray beam with a peristaltic pump.

For the application of non-physical stimuli such as lasers and electromagnetic fields, there are volume limitations to consider given that this type of stimuli is not easily applied simultaneously to the whole formulation. Unlike solution-based stimulus, the application of this stimuli usually covers a small area so introducing uncertainty around the application to all areas of the sample. For example, in typical laser activated transformation experiments performed in a capillary, the size of the collimated laser spot is important because of the size of the collimated X-ray beam in one example, and typically for many synchrotron sources is approximately 200 μm x 100 μm.[75] Although the region of sample in the path of the X-ray beam would be irradiated, convection may mix the non-irradiated sample in the bulk volume with irradiated sample to potentially reduce the apparent effect of the laser and alter the kinetics. Absorbance of the laser beam by the sample is a second consideration

which could lead to non-uniform exposure. For the study of magnetic-sensitive systems, a low frequency alternating magnetic field is generated by the magnetic coil pictured in **Figure 1-10**.[60] Similar to the light-activated studies, the size of the sample is limited to the gap in the magnet, and it was remarked that the application of the magnetic field was not isotropic within the sample space.[60] Mixing was also absent in the experimental design.
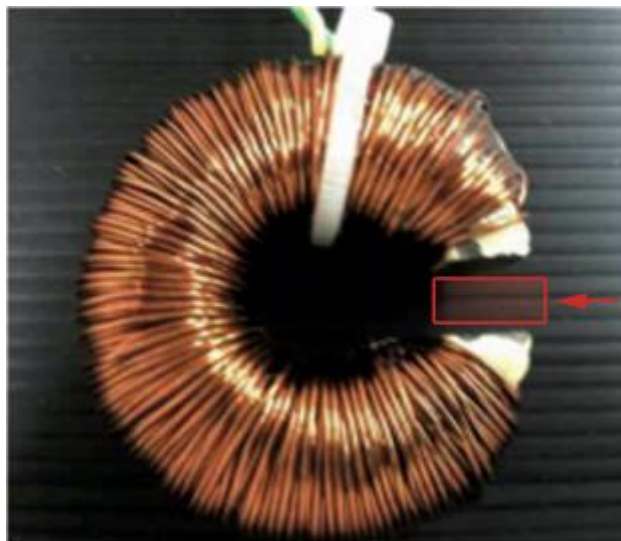
Figure 1-10. Image of a toroidal magnet used for the study of magnetic-sensitive systems. The area highlighted in red denotes where the sample was positioned during application of the magnetic field. Image used with permission from Banchelli *et al.*[80]

In each of these experimental configurations, there are limitations to the kinetic analysis when coupled to analytical techniques such as SAXS. Most configurations do not facilitate the instantaneous mixing and uniform exposure of the stimulus to all the sample, which can lead to heterogeneous transformations. As data is collected over an area of sample, this results in an average of the heterogeneously transitioning particles which can alter the perceived kinetics of the transformation. Some configurations require large volumes of sample in order for stimulus to be applied, potentially precluding study of biological systems or custom synthesised materials, whereas other configurations are limited to smaller volumes and cannot facilitate a mixing component to evenly distribute the stimulus. Additionally, the pH-stat apparatus for example, requires equipment to induce the transformation which may have a large footprint making it difficult to interface with analytical instrumentation, such as spectrometers, microscopes, or beamlines at the synchrotron. The experimental configurations may require extensive setup and preparation, making them low throughput and potentially not of practical utility for industrial analytical methods. Most importantly, many of the configurations are not performed in real-time as the sample is transferred to another location from where

it is initially mixed with the stimulus, and the delay can potentially overlook transient intermediate structures. If there is no transfer and the system is not under any flow, there is a possibility of over-exposing the sample to X-rays which could influence the transformation of the system.

1.5   Statement of the Problem

The translation of lipid-based LCNPs from lab to drug delivery product has proved a challenge for the past few decades. Although there have been numerous studies where researchers have demonstrated the application of LCNPs as various drug delivery systems,[27,81–86] few have actually succeeded into the market. Currently, only liposomal systems have been approved for clinical use, including Doxil® and Exparel®,[87,88] but the potential for non-lamellar LCNP systems has yet to achieve the same feat. These systems have demonstrated biocompatibility and capabilities of encapsulating drugs with different polarities.[41,82,85,89–93] Despite this, inefficient production methods and kinetic instability of the non-lamellar liquid crystal dispersions have contributed to the lack of commercial success in pharmaceutics. There are also limitations to the current methods of accurately investigating the complexities of these systems and this has further confounded advances.

Research on LCNPs in recent years has mostly been performed using traditional experimental configurations as described in the previous section. The methods allow the measurement of the kinetic structures, but the results can be inconsistent and potentially misleading. This can be attributed to a non-uniform application and distribution of the stimulus as a result of the expanse of sample volume and sample surface area in contact with the stimuli at any one time. Therefore, a new approach using microfluidics is proposed to overcome these issues. By miniaturising the process into the confines of microfluidic channels, it may be possible to achieve finer control over the application of stimulus and mixing behaviour. The microfluidic devices would be integrated with the traditional analytical techniques such as SAXS and microscopy-based techniques to offer a different perspective on investigating the structural changes over time. Additionally, different formats, materials and channel designs of microfluidics would be explored for their suitability in this type of kinetic analysis.

1.6   Microfluidics

Microfluidics is a rapidly developing field of technology that deals with the highly controlled manipulation of fluids through micron-scale channels, affording many advantages over conventional methods.[94] The narrow channels allow finer control and efficient use of materials for improved yield, and also requires only microlitre volumes of sample and reagents.[95] Experiments can be modulated

by the flow rates of the fluids to affect results such as kinetics of a reaction or particle size. The design can also enable time-resolved analysis where the position along the channel relative to the starting point of the reaction correlates to a proportional time point with the reaction.[96] Furthermore, smaller volumes can facilitate more rapid mixing of samples, faster kinetics, and faster analyses.[95]

Different channel designs can enable various types of manipulations. The size and arrangement of the channels can allow for different flow behaviours and manipulate the content to yield various results. This can include, but is not limited to, mixing,[96–98] sorting[99,100] or droplet formation.[101–107] The addition of other components into the device can enable more functionality such as inter-digital transducers which can actuate surface acoustic waves to halt the movement of droplets.[101] The customisability of microfluidics is endless so long as materials and facilities are available.

Although microfluidic devices can be custom-designed and fabricated to achieve almost any desired outcome, there are also commercially available devices which aim to standardize microfluidic analytics.[108] These commercially available chips cater to more common functions such as biological studies,[109] generation of nanoparticles[110,111] or mixing of components.[112] The devices are readily accessible with some companies also offering starter kits inclusive of syringe drivers.[113]

Microfluidics has also been integrated with analytical techniques. The device can be used to prepare samples whilst simultaneously acting as the sample holder in which the samples can be analysed. In literature so far, microfluidics has been integrated with SAXS,[103,106,114–119] cryoTEM,[120] NMR[121] and Raman spectroscopy[122,123] amongst many other techniques to enhance the resolution of analysis. This is advantageous because:

- There is potential to analyse the systems as they are manipulated *in situ*;
- Preparation and analysis can be achieved in the one device, enabling uniformity of application of the remote stimulus; and
- In particular for analytical techniques where samples are exposed to damaging levels of energy, the continuous flow of microfluidics and its time-resolved nature can reduce the likelihood of radiation damage.[106,114]

1.6.1 Composition of microfluidic devices

Microfluidic devices can be manufactured from a range of different materials. Aside from economics, selection of the material also depends on chemical compatibility to the materials of interest and its

compatibility with the analytical technique. When coupling the microfluidic device with analytical techniques that require energy sources such as X-rays or photons to pass through the channel and thereby the device walls, the material of the device needs to be selected appropriately. Ideally, there would be minimal attenuation of the energy source and the size of the device conforms to dimension limits of the apparatus without hindrance. It is generally easier to redesign the device than the analytical instrument. Additionally, it should be durable to withstand the flow pressures resulting from viscosities and flow rates of the fluids.

Common materials used in the construction of microfluidic devices include polymers such as polydimethylsiloxane (PDMS), polymethyl methacrylate (PMMA), cyclic olefin copolymer (COC) and thiolene-based polymers, as well as glass or quartz. The polymers are compatible with a limited number of solvents, but they are relatively cheaper to produce via soft-lithographic techniques than glass or silicon-based microfluidic devices.[124,125] Furthermore, all are optically transparent, however their transparency to energy sources of the integrated analytical technique such as X-rays and photons is dependent on the thickness of the material. Khvostichenko *et al.* demonstrated that PDMS and COC-based microfluidic devices can be used to observe the cubic liquid crystalline phases using SAXS as the analytical technique. The device was limited to a maximum combined thickness of 250 μm including 70 and 150 μm for PDMS and COC, respectively.[115]

The polarity of the samples can also influence the choice of polymer used to form the microfluidic devices. If the substance of interest, whether a liquid or solid, is the same polarity as the walls of the channel, then adhesion may occur which can foul the chip and impede the flow through the microchannel.[126] For hydrophobic substances such as lipids or proteins, it is best to avoid the hydrophobic COC as it is prone to blockage.[127] Although also hydrophobic, PDMS can be treated using plasma oxidation to render the walls of the microchannels reversibly hydrophilic for up to 6 hrs.[128] The Weitz research group developed a method that coats the PDMS channel walls with sol-gel, allowing it to be functionalised and in turn enable customisable domains of hydrophobicity and hydrophilicity.[129] Oxygen plasma treatment can also be performed on PMMA, along with a polyvinyl alcohol coating.[130]

1.6.2 Functions of microfluidics

The configuration of channels within the microfluidic devices can control the mixing of samples and facilitate the different manipulations. This can consist of particle formation, sorting of nanoparticles,

and droplet formation. The arrangement of the channels coordinates the flow of sample and how the contents of each channel interact with one another.

1.6.2.1 Microfluidic mixers

Microfluidic channels generally exhibit laminar flow. This behaviour is determined by the Reynold's number, which is a balance between the viscous and inertial forces of the solutions of interest (**Equation 1-7**).[131,132] At Reynold's numbers lower than 2000, the viscous forces dominate and laminar flow results where the direction of flow is along the length of the channel without deviation in the perpendicular plane. Turbulent flow, noted at Reynold's numbers between 2000 and 4000, is generally not observed in microfluidics but the Reynold's number can be increased towards turbulence by decreasing the solution viscosity or adding mixing elements to the microfluidic design.[97]

Equation 1-7. The relationship between the forces that define Reynold's number.

$$Reynolds\ number\ (Re) = {inertial\ forces}/{viscous\ forces}$$

Mixing elements in microfluidic devices aim to enhance the diffusivity of the fluids by increasing the surface area of contact between the solutions.[133] It is important to do so to ensure complete mixing before elution from the chip, and to minimise the channel length required for reaching homogeneity, thus making the channel design more efficient. There exists two types of mixers, active and passive, and their selection in the design can be based on factors such as time required for complete mixing and feasibility. Active mixing involves energy input into the device to induce mixing which includes acoustic waves, pressure and temperature. Passive mixing does not require external energy input and mixing occurs via diffusion or disruption of the laminar flow by the channel design such as with staggered herringbone structures (**Figure 1-11**). A thorough review of the different types of mixers has been explored elsewhere by Nguyen *et al.*[134] The mixing efficiency can also be affected by the viscosities of the fluids and so it must be noted that one particular microfluidic device which is compatible for the analysis of one system may not translate as well to another.
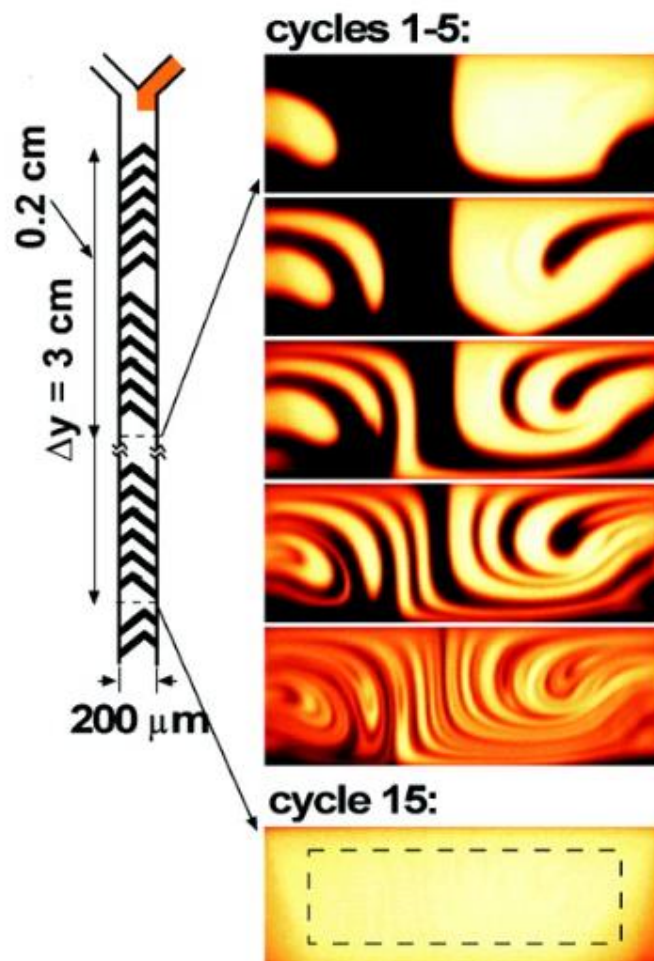
Figure 1-11. Schematic of the mixing behaviour of two fluids in a microfluidic device featuring staggered herringbone structures. The two solutions generate more and more layers as they flow through the sequential herringbone structures until one homogeneous solution persists. Figure adapted with permission from Stroock et al.[98]

1.6.2.2 Co-axial flow

Co-axial flow can occur where streams of sample flow in parallel within one microchannel (**Figure 1-12**). The channels containing the individual streams of sample converge in any customised arrangement to achieve this. The parallel flows share an interface between each stream where material can be transferred across and reactions can occur. The transfer, or diffusion, of material between the flows can also be characterised and controlled.

The diffusion of material between streams in a co-axially flowing microfluidic device can be used to determine the position of complete mixing along the channel. The point of complete mixing can be defined by the position along the length of the microchannel where the material in one stream has reached the maximum distance of another stream. In the case where one stream is in between two other streams of the same material, then the point of complete diffusion occurs where the material

reaches the centre of the middle stream. Ghazal *et al.* and With *et al.* have calculated the position of complete mixing in their systems.[119,135] The diffusion coefficient of the molecule of interest, flow rates and dimensions of the microchannel were taken into account in the calculations.
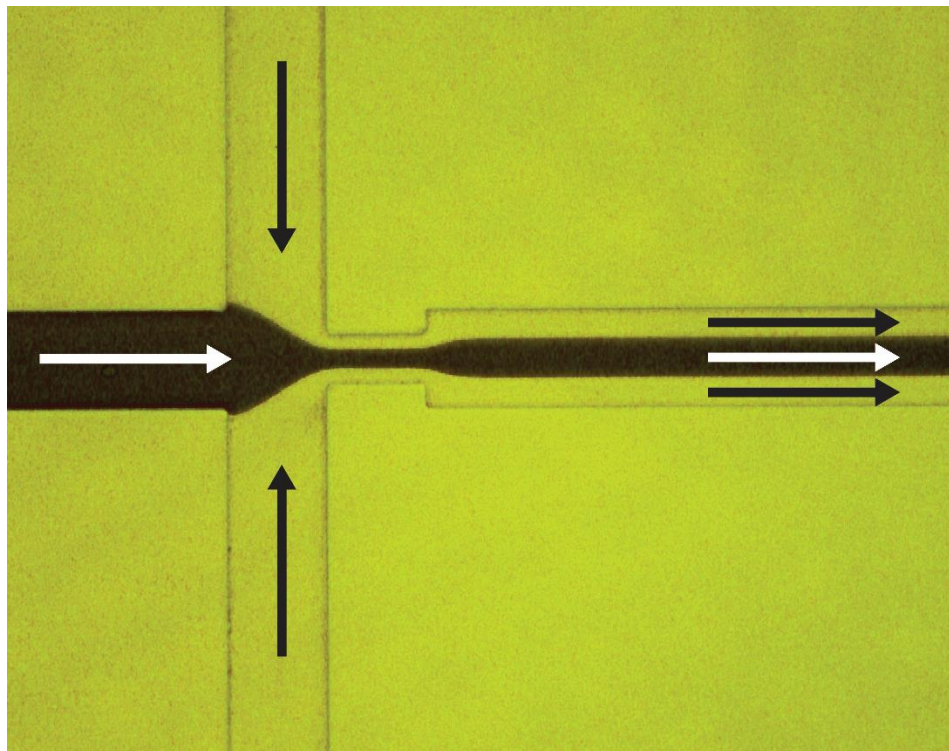
Figure 1-12. Coaxial flow of two solutions from three incoming channels achieved via hydrodynamic flow focusing. Laminar flow allows the solutions to flow side by side despite both being aqueous while material can diffuse from one stream to the other. Arrows indicate the direction of flow.

1.6.2.3 Droplet formation

Droplet forming microfluidics refers to the formation of discrete volumes of sample in the continuous flow of micro-sized channels via various techniques and channel designs. Common microfluidic configurations to form droplets can be observed where the stream of the discontinuous phase is sheared off by the stream of the continuous phase. A stabilising component may be required to maintain the droplets in a stable stream. The processes can generate monodisperse droplets and allow minute volumes of the internal phase to be monitored discretely which is made possible due to laminar flow and the absence of turbulence. Additionally, droplet size can be modulated with flow rates and the viscosity of the fluids.[136]

Channel designs that feature T-junctions, Y-junctions or a 4-channel intersection can enable droplet formation. The T-junction (**Figure 1-13A**) generally contains the dispersed phase in a channel that is the perpendicular to the flow of the continuous phase. It is the continuous flow in the main channel

that shears off the discrete volumes of the incoming perpendicular flow that generates the drop-
lets.[101,137] Additionally, the T-junction can also facilitate for the breaking up of the already formed
droplets into smaller ones.[105] Similarly, a Y-junction can function in the same shearing motion to
generate droplets (**Figure 1-13B**). Hydrodynamic flow focusing is observed in a 4-channel intersec-
tion of which the centre channel is the incoming and outgoing flow, and the side channels are
incoming flow of the continuous phase (one example is shown in **Figure 1-13C**).[104,106,107,114] The in-
coming flow from the side channels focuses and thins the centre flow—much like the co-axial flow
behaviour. As the stream of the dispersed phase flows further from the intersection, there is more
instability, resulting in sections of the stream breaking off to form the droplets. This has been sug-
gested to be the consequence of the imbalance of the shear stress from the external flow and the
interfacial tension.[138]
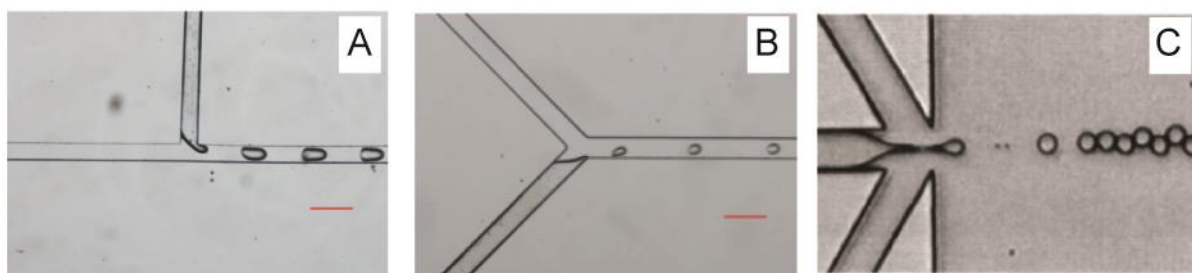
Figure 1-13. Channel designs for chip-based microfluidics. A) n-hexadecane with polyglycerol polyricinoleate
droplets forming in water in a T-junction configuration.[139] B) The droplets formed from same system described
in A via a Y-junction channel design. Images from A) and B) were obtained with permission from Ushikubo *et
al.*[139] C) Hydrodynamic flow focusing in microfluidics which yielded monodisperse droplets from a soybean oil
in an sodium dodecyl sulfate solution.[107]

Capillary-based microfluidics concerns the arrangement of microcapillaries which can also be con-
figured to form droplets as shown in **Figure 1-14**. The internal capillary contains the dispersed phase
which is suspended in a larger capillary containing the continuous phase. As the dispersed phase is
ejected into the continuous phase, similar to the mechanism of hydrodynamic flow focusing, the
fluid buds off into droplets.[103,140]
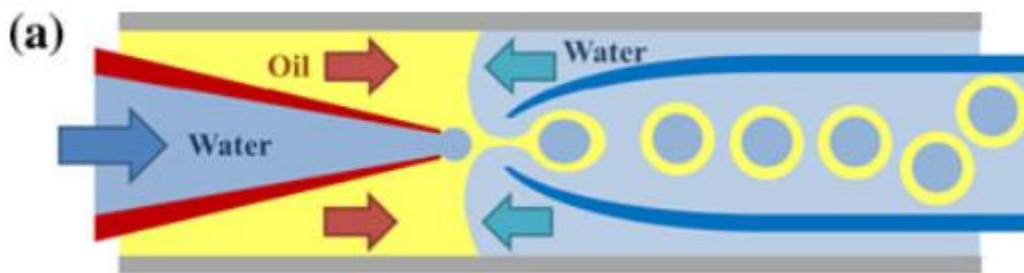
Figure 1-14. Capillary-based microfluidics developed by the Weitz research group which demonstrates the formation of a water-in-oil-in-water emulsion.[140]

1.7 Potential for microfluidics integrated analysis of liquid crystal nanoparticles

To date, microfluidics has been mostly employed for biological applications,[94] and to a lesser extent, it has been translated to other soft matter such as liquid crystals. Liposomes[102,110,111,141–144] and thermotropic liquid crystals[106,114] have also been produced using microfluidics. However, studies with regard to cubosomes and hexosomes are limited.[119,145] In particular, the ability to inspect these structures on a micro-scale highlights a different perspective of understanding not available with bulk scale processes.

In one method to generate liposomes in microfluidics, researchers would combine a stream of lipid dissolved in ethanol with an aqueous stream in a commercial available device (NanoAssemblr by Precision Nanosystems, Inc.).[110,111] As the solutions mix along the herringbone structures, a co-solvent system is formed where the solubility of the lipid in this co-solvent system is less than if it were in the lone solvent. The decrease in solubility prompts the "precipitation" of the lipid molecule and its self-assembly to form the liquid crystal nanostructures. This resembles the emulsion dilution method described by Spicer *et al.* for the production of cubosomes.[22] They had noted there was a greater particle size distribution with this bulk mixing method, but microfluidic translation appears to afford more control for more uniform self-assembly at least in the case of liposome production.[111] It should be noted that structural data for the liposome dispersions was acquired subsequent to mixing in the chip upon collection using microscopy-based techniques.

Recently and during the conduct of this thesis, there has been growing interest in the manipulation of non-lamellar based LCNPs analysed with microfluidics. Researchers have attempted to form cubic and hexagonal phases *in situ* in these microchannels and integrate them with SAXS to interrogate the mesophases. This can be performed dynamically or at equilibrium whilst still *in situ*.

Khvostichenko *et al.* aimed to develop a method to determine the phase behaviour of a lipid, water and surfactant system in the form of a microfluidic device.[115] The device was comprised of PDMS and COC layers and exhibited various interconnected chambers, isolated by pressure valves. Each chamber contained a raw component (monoolein, water and β-octylglucoside) which was released by the valves allowing contact between all three. The components were combined via the action of the pneumatic valves and further assisted using a freeze-thaw method that facilitated the mixing of the more viscous cubic phase. Additionally, these bulk samples were frozen after mixing for up to 3 days and then equilibrated to 25° C prior to SAXS measurements. The experiment presented a promising preliminary device to probe the transformations of the mesophase using 300-fold less material. However, it required lengthy equilibration times and could only analyse a fixed number of samples in any one device, necessitating more devices if experiments needed to be completed in the limited access to the SAXS equipment.

Other non-lipid-based systems have been analysed using microfluidics to observe the phase behaviour such as for ionic surfactants. Leng *et al.* employed a PDMS-based microfluidic device to facilitate the evaporation of a binary system (docusate sodium salt and water).[146] The porosity of the PDMS facilitated the escape of the vapours. They monitored the phase structure and growth kinetics using high-magnification optical microscopy with cross-polarisers and stereomicroscope, respectively. Simple vesicular systems of a cetyl trimethylammonium bromide, dodecyl benzene sulfonic acid and water ternary system have been observed alternatively via fluorescence in a glass-based microfluidic device by Lee *et al.*[147]

There have been other microfluidics-based experimental designs that have been utilised to analyse other nanoparticles aside from the lipid-based LCNPs. The structure of smectic liquid crystals comprising of n-octyl-4-cyanobiphenyl (8CB) were analysed in microfluidic devices using SAXS.[106,114] Both designs by Dootz *et al.*[114] and Otten *et al.*[106] featured two intersecting microchannels employed for hydrodynamic flow focusing, however only the latter study used it for the formation of droplets. Additionally, Otten *et al.* used this design to also encapsulate DNA into the bilayers of multilamellar vesicles. They monitored the changes in interlamellar spacing and DNA interaxial distance along the length of the microchannels to denote the successful encapsulation (**Figure 1-15**). In continuously forming the droplets, Otten *et al.* were able to resolve the kinetic interactions of the individual droplets as they traversed the length of the channel.
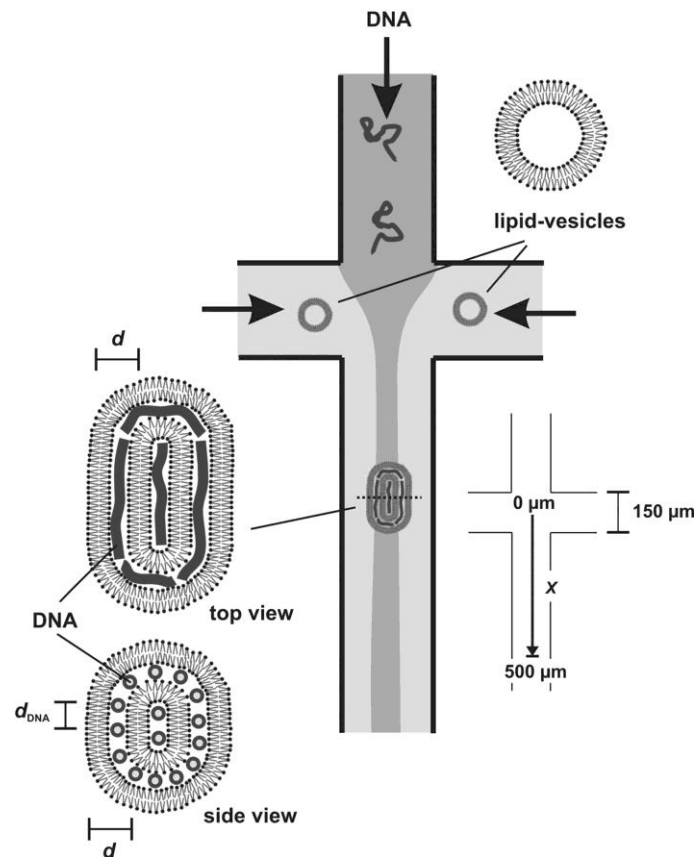
Figure 1-15. A microfluidic design which features a hydrodynamic flow focusing design to encapsulate DNA molecules into the lipid vesicle. Figure adapted from Otten *et al.* [106]

Perhaps the most relevant application of microfluidics with the kinetics of liquid crystalline systems has been demonstrated by Ghazal *et al.* as seen in **Figure 1-16Figure 1-15**.[119] Their custom designed thiol-ene chip integrated with SAXS, displayed a channel design much like that described by Otten *et al.* in **Figure 1-15**, and the structural kinetics were monitored along the straight channel after the intersection. Their initial lipid formulation consisted of a combination of phytantriol and dioleoyl-phosphatidylglycerol which formed cubosomes of the *Im3m* geometry in excess water. When under flow in the microfluidic device and sheathed by the Ca^{2+} ion solution, they were able to observe the emergence of a coexisting *Pn3m* phase with the *Im3m* phase within 0.27 secs of reaction time. The thiol-ene chip was able to exhibit X-ray transparency whilst allowing the structural kinetics to be tracked.
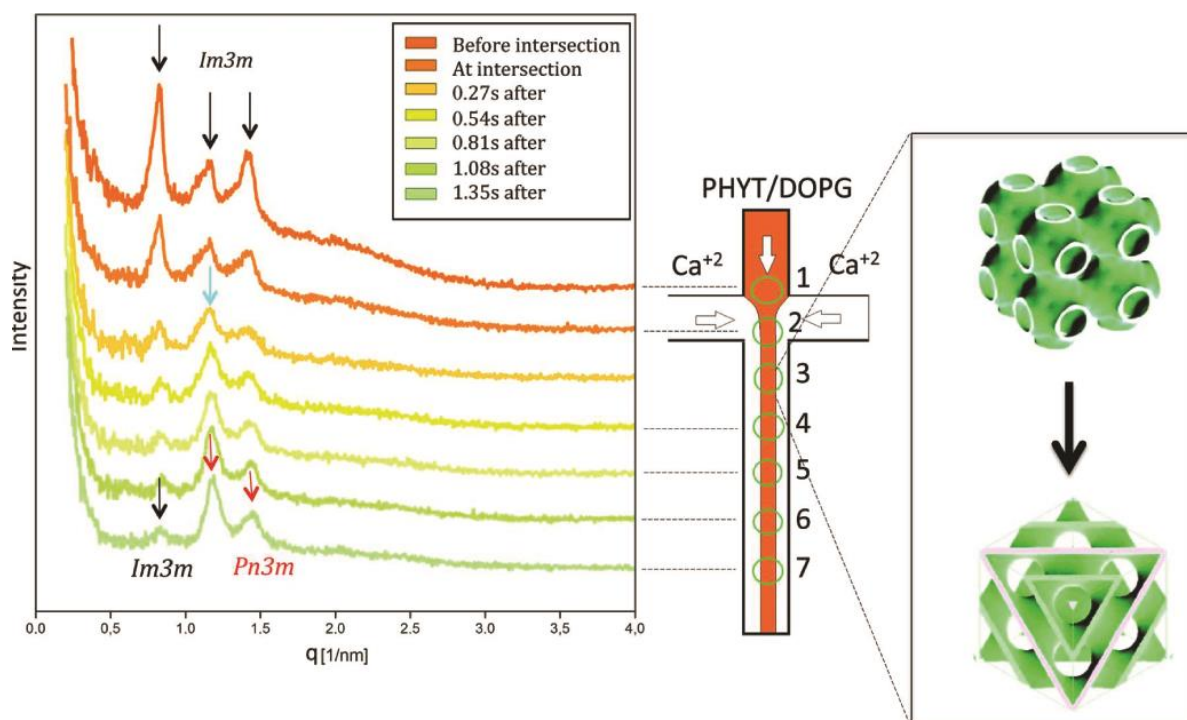
Figure 1-16. Time-resolved monitoring of the incorporation of calcium ions into a phytantriol and di-oleoylphosphatidylglycerol dispersion using a microfluidics-SAXS configuration. Two channels containing a solution of calcium ions and one channel containing the dispersion converged into a co-axial flow by the hydrodynamic flow focusing design. The system was observed to transition from the cubic Im3m phase to a mixed phase of both *Im3m* and *Pn3m* phase. Image adapted from Ghazal *et al.*[119]

The limitation with this device as with most other microfluidic devices for this type of analysis however, is that despite manipulating the flow rates, there is an extent to how much of the kinetics can be observed. The length of the microchannel, which is determined during the device fabrication, fixes the maximum reaction time for a given experiment at any one flow rate. In other words, a restricted time limit for the phase transition. Hence, systems where the kinetics may be significantly slower, the device will not have sufficient length to resolve this, unless the syringe driver used is capable of low enough flow rates. On the contrary, with systems where intermediate structures may form rapidly, there may be insufficient time for the Ca^{2+} ions to fully diffuse into the centre of the channel to yield a homogeneous system within the given length before the non-equilibrium data can be acquired. Another limitation of this device is that it requires a thiol-ene coating to prevent the adhesion of materials to the wall. The coating may not be compatible with all materials and adds another layer of complexity to the microfluidic device.

1.8 Summary

This introduction has outlined the issues surrounding the current techniques to characterise the phase transitions of stimuli-responsive LCNPs along with the expansive possibilities that microfluidics

can offer to overcome them. There is a wealth of knowledge in microfluidics yet to be explored and applied to LCNPs therefore this thesis will endeavour to answer the overarching research question: what can microfluidics reveal about stimuli-responsive LCNPs?

1.9   Project hypotheses

Limitations with the current approaches to analysing phase transitions of LCNPs impede on the generation of reliable and consistent data, and consequently the optimisation and understanding of these systems. The proposal of using microfluidics to address these issues will be covered in the following chapters by these general hypotheses:

1. That controlling the mixing behaviour of the starting materials by diffusion via a fixed interface can regulate the kinetics of the transformation of LCNPs *in situ*.

2. That mixing of homogeneous ratios of starting materials will allow more consistent phase transitions for characterisation.

3. That integrating both the mixing and analysis vessels into one experimental configuration will enable any kinetic structures earlier in the transformation to be defined.

4. That microfluidics is more suited than the traditional pH-stat method (or equivalent) for synchrotron-SAXS experiments as the kinetic analysis is not limited to the acquisition time of data collection, allowing kinetics of rapidly transforming systems to be resolved.

5. That microfluidics can allow a uniform dose of stimulus to be applied to all droplets/particles in the system such that all transformations that take place are homogeneous.

6. That mixed phases will be observed within individual droplets via a gradient before equilibrium is achieved during transformations.

1.10 Project aims

To achieve the aforementioned hypotheses, the aims were defined as the following:

1. To develop a microfluidic device that can control the delivery and mixing of lipid-based formulation with solution containing stimuli material, and that is compatible with advanced analytical techniques such as SAXS.

2. To calculate and characterise the mixing behaviour in the microfluidic device.

3. To characterise the phase transitions of stimuli-responsive LCNPs in microfluidic devices including digestion-, pH-, and ionic strength-sensitive systems.

      a. To identify any intermediate liquid crystalline structures present immediately after complete mixing.

      b. To compare the ability to track the phase transitions of LCNPs with the equivalent experiments in traditional approaches.

      c. To understand the mechanism of phase transitions of stimuli-responsive LCNPs.

4. To manipulate the flow rates and concentrations of the starting materials, and examine their effects on the kinetics of transformation of LCNPs.

5. To observe the change in optical behaviour with CPLM within a droplet of the lipid-based formulation using droplet-based microfluidics.

1.11 References

(1) Singh, R.; Lillard, J. W. Nanoparticle-Based Targeted Drug Delivery. *Exp. Mol. Pathol.* **2009**, *86*, 215–223.

(2) Bhatia, S. Nanoparticles Types, Classification, Characterization, Fabrication Methods and Drug Delivery Applications. In *Natural Polymer Drug Delivery Systems*; Springer, Cham, 2016; pp. 33–93.

(3) Fong, W. K.; Hanley, T.; Boyd, B. J. Stimuli Responsive Liquid Crystals Provide "On-Demand" Drug Delivery In Vitro and In Vivo. *J. Control. Release* **2009**, *135*, 218–226.

(4) Phan, S.; Fong, W. K.; Kirby, N.; Hanley, T.; Boyd, B. J. Evaluating the Link Between Self-Assembled Mesophase Structure and Drug Release. *Int. J. Pharm.* **2011**, *421*, 176–182.

(5) Bisset, N. B.; Boyd, B. J.; Dong, Y. D. Tailoring Liquid Crystalline Lipid Nanomaterials for Controlled Release of Macromolecules. *Int. J. Pharm.* **2015**, *495*, 241–248.

(6) Du, J. D.; Liu, Q.; Salentinig, S.; Nguyen, T. H.; Boyd, B. J. A Novel Approach to Enhance the Mucoadhesion of Lipid Drug Nanocarriers for Improved Drug Delivery to the Buccal Mucosa. *Int. J. Pharm.* **2014**, *471*, 358–365.

(7) Negrini, R.; Fong, W.-K.; Boyd, B. J.; Mezzenga, R. pH-Responsive Lyotropic Liquid Crystals and Their Potential Therapeutic Role in Cancer Treatment. *Chem. Commun.* **2015**, *51*, 6671–6674.

(8) Misiunas, A.; Talaikyte, Z.; Niaura, G.; Razumas, V.; Nylander, T. Thermomyces Lanuginosus Lipase in the Liquid-Crystalline Phases of Aqueous Phytantriol: X-Ray Diffraction and Vibrational Spectroscopic Studies. *Biophys. Chem.* **2008**, *134*, 144–156.

(9) Hong, L.; Salentinig, S.; Hawley, A.; Boyd, B. J. Understanding the Mechanism of Enzyme-Induced Formation of Lyotropic Liquid Crystalline Nanoparticles. *Langmuir* **2015**, *31*, 6933–6941.

(10) Lyon, P. C.; Griffiths, L. F.; Lee, J.; Chung, D.; Carlisle, R.; Wu, F.; Middleton, M. R.; Gleeson, F. V; Coussios, C. C. Clinical Trial Protocol for TARDOX: A Phase I Study to Investigate the Feasibility of Targeted Release of Lyso-Thermosensitive Liposomal Doxorubicin (ThermoDox ®) Using Focused Ultrasound in Patients with Liver Tumours. *J. Ther. Ultrasound* **2017**, *5*, 1–8.

(11)   Fong, W. K.; Malic, N.; Evans, R. A.; Hawley, A.; Boyd, B. J.; Hanley, T. L. Alkylation of Spiropyran Moiety Provides Reversible Photo-Control over Nanostructured Soft Materials. *Biointerphases* **2012**, *7*, 3–7.

(12)   Quinn, M. D. J.; Du, J.; Boyd, B. J.; Hawley, A.; Notley, S. M. Lipid Liquid-Crystal Phase Change Induced through near-Infrared Irradiation of Entrained Graphene Particles. *Langmuir* **2015**, *31*, 6605–6609.

(13)   Fong, W. K.; Negrini, R.; Vallooran, J. J.; Mezzenga, R.; Boyd, B. J. Responsive Self-Assembled Nanostructured Lipid Systems for Drug Delivery and Diagnostics. *J. Colloid Interface Sci.* **2016**, *484*, 320–339.

(14)   Hyde, S. T. Identification of Lyotropic Liquid Crystalline Mesophases. In *Handbook of Applied Surface and Colloid Chemistry*; Holmberg, K., Ed.; John Wiley & Sons, Ltd, 2001; pp. 299–332.

(15)   Dong, Y.-D.; Tilley, A. J.; Larson, I.; Lawrence, M. J.; Amenitsch, H.; Rappolt, M.; Hanley, T.; Boyd, B. J. Nonequilibrium Effects in Self-Assembled Mesophase Materials: Unexpected Supercooling Effects for Cubosomes and Hexosomes. *Langmuir* **2010**, *26*, 9000–9010.

(16)   Hope, M. J.; Bally, M. B.; Mayer, L. D.; Janoff, A. S.; Cullis, P. R. Generation of Multilamellar and Unilamellar Phospholipid Vesicles. *Chem. Phys. Lipids* **1986**, *40*, 89–107.

(17)   Israelachvili, J. N.; Mitchell, D. J.; Ninham, B. W. Theory of Self-Assembly of Hydrocarbon Amphiphiles into Micelles and Bilayers. *J. Chem. Soc. Faraday Trans. 2 Mol. Chem. Phys.* **1976**, *72*, 1525–1568.

(18)   Sagalowicz, L.; Leser, M. E.; Watzke, H. J.; Michel, M. Monoglyceride Self-Assembly Structures as Delivery Vehicles. *Trends Food Sci. Technol.* **2006**, *17*, 204–214.

(19)   Israelachvili, J. The Science and Applications of Emulsions - an Overview. *Colloids Surfaces A Physicochem. Eng. Asp.* **1994**, *91*, 1–8.

(20)   Czeslik, C.; Winter, R.; Rapp, G.; Bartels, K. Temperature- and Pressure-Dependent Phase Behavior of Monoacylglycerides Monoolein and Monoelaidin. *Biophys. J.* **1995**, *68*, 1423–1429.

(21)   Ljusberg-Wahern, H.; Nyberg, L.; Larsson, K. Dispersion of the Cubic Liquid Crystalline Phase – Structure, Preparation, and Functionality Aspects. *Chim. Oggi* **1996**, *14*, 40–43.

(22)   Spicer, P. T.; Hayden, K. L.; Chester, W.; Lynch, M. L.; Ofori-boateng, A.; Burns, J. L. Novel Process for Producing Cubic Liquid Crystalline Nanoparticles (Cubosomes). *Langmuir* **2001**, *17*, 5748–5756.

(23)   Martiel, I.; Sagalowicz, L.; Handschin, S.; Mezzenga, R. Facile Dispersion and Control of Internal Structure in Lyotropic Liquid Crystalline Particles by Auxiliary Solvent Evaporation. *Langmuir* **2014**, *30*, 14452–14459.

(24)   Small, D. M. A Classification of Biologic Lipids Based upon Their Interaction in Aqueous Systems. *J. Am. Oil Chem. Soc.* **1968**, *45*, 108–119.

(25)   Ribier, A.; Biatry, B. Cosmetic and Dermatologic Composition Comprising a Stable Aqueous Dispersion of Phytantriol-Based Gel Particles Containing a Long-Chain Surfactant as Dispersant and Stabilizer, 1995.

(26)   McLain, V. C. Final Report on the Safety Assessment of Phytantriol. *Int. J. Toxicol.* **2007**, *26*, 107–114.

(27)   Astolfi, P.; Giorgini, E.; Gambini, V.; Rossi, B.; Vaccari, L.; Vita, F.; Francescangeli, O.; Marchini,

C.; Pisani, M. Lyotropic Liquid-Crystalline Nanosystems as Drug Delivery Agents for 5-Fluorouracil: Structure and Cytotoxicity. *Langmuir* **2017**, *33*, 12369–12378.

(28)   Nguyen, T.-H.; Hanley, T.; Porter, C. J. H.; Larson, I.; Boyd, B. J. Phytantriol and Glyceryl Monooleate Cubic Liquid Crystalline Phases as Sustained-Release Oral Drug Delivery Systems for Poorly Water-Soluble Drugs II. In-Vivo Evaluation. *J. Pharm. Pharmacol.* **2010**, *62*, 856–865.

(29)   Pham, A. C.; Hong, L.; Montagnat, O.; Nowell, C. J.; Nguyen, T. H.; Boyd, B. J. In Vivo Formation of Cubic Phase in Situ after Oral Administration of Cubic Phase Precursor Formulation Provides Long Duration Gastric Retention and Absorption for Poorly Water-Soluble Drugs. *Mol. Pharm.* **2016**, *13*, 280–286.

(30)   Zhai, J.; Hinton, T. M.; Waddington, L. J.; Fong, C.; Tran, N.; Mulet, X.; Drummond, C. J.; Muir, B. W. Lipid-PEG Conjugates Sterically Stabilize and Reduce the Toxicity of Phytantriol-Based Lyotropic Liquid Crystalline Nanoparticles. *Langmuir* **2015**, *31*, 10871–10880.

(31)   Barauskas, J.; Landh, T. Phase Behavior of the Phytantriol/water System. *Langmuir* **2003**, *19*, 9562–9565.

(32)   Dong, Y. D.; Dong, A. W.; Larson, I.; Rappolt, M.; Amenitsch, H.; Hanley, T.; Boyd, B. J. Impurities in Commercial Phytantriol Significantly Alter Its Lyotropic Liquid-Crystalline Phase Behavior. *Langmuir* **2008**, *24*, 6998–7003.

(33)   Qiu, H.; Caffrey, M. The Phase Diagram of the Monoolein/water System: Metastability and Equilibrium Aspects. *Biomaterials* **2000**, *21*, 223–234.

(34)   Warren, D. B.; Anby, M. U.; Hawley, A.; Boyd, B. J. Real Time Evolution of Liquid Crystalline Nanostructure During the Digestion of Formulation Lipids Using Synchrotron Small-Angle X-Ray Scattering. *Langmuir* **2011**, *27*, 9528–9534.

(35)   Barauskas, J.; Svedaite, I.; Butkus, E.; Razumas, V.; Larsson, K.; Tiberg, F. Synthesis and Aqueous Phase Behavior of 1-Glyceryl Monooleyl Ether. *Colloids Surfaces. B Biointerfaces* **2005**, *41*, 49–53.

(36)   Eriksson, P.-O.; Lindblom, G. Lipid and Water Diffusion in Bicontinuous Cubic Measured by NMR. *Biophys. J.* **1993**, *64*, 129–136.

(37)   Tan, G.; Xu, P.; John, V. T. Cryo-Field Emission Scanning Electron Microscopy Imaging of a Rigid Surfactant Mesophase. *Langmuir* **2008**, *24*, 10621–10624.

(38)   Sagalowicz, L.; Michel, M.; Adrian, M.; Frossard, P.; Rouvet, M.; Watzke, H. J.; Yaghmur, A.; De Campo, L.; Glatter, O.; Leser, M. E. Crystallography of Dispersed Liquid Crystalline Phases Studied by Cryo-Transmission Electron Microscopy. *J. Microsc.* **2006**, *221*, 110–121.

(39)   Muir, B. W.; Zhen, G.; Gunatillake, P.; Hartley, P. G. Salt Induced Lamellar to Bicontinuous Cubic Phase Transitions in Cationic Nanoparticles. *J. Phys. Chem. B* **2012**, *116*, 3551–3556.

(40)   Almgren, M.; Edwards, K.; Karlsson, G. Cryo Transmission Electron Microscopy of Liposomes and Related Structures. *Colloids Surfaces A Physicochem. Eng. Asp.* **2000**, *174*, 3–21.

(41)   Meli, V.; Caltagirone, C.; Falchi, A. M.; Hyde, S. T.; Lippolis, V.; Monduzzi, M.; Obiols-Rabasa, M.; Rosa, A.; Schmidt, J.; Talmon, Y.; Murgia, S. Docetaxel-Loaded Fluorescent Liquid-Crystalline Nanoparticles for Cancer Theranostics. *Langmuir* **2015**, *31*, 9566–9575.

(42)   Rosevear, F. B. Liquid Crystals : The Mesomorphic Phases of Surfactant Compositions. *J. Soc. Cosmet. Chem.* **1968**, *594*, 581–594.

(43)   Massoumian, F.; Juskaitis, R.; Neil, M. A. A.; Wilson, T. Quantitative Polarized Light Microscopy. *J. Microsc.* **2003**, *209*, 13–22.

(44)   Boyd, B. J.; Dong, Y.-D.; Rades, T. Nonlamellar Liquid Crystalline Nanostructured Particles: Advances in Materials and Structure Determination. *J. Liposome Res.* **2009**, *19*, 12–28.

(45)   Paar, A. (GmbH). *The SAXS Guide*; Schnablegger, H.; Singh, Y., Eds.; 2nd ed.; Anton Paar: Austria, 2011.

(46)   Rappolt, M. The Biologically Relevant Lipid Mesophases as "Seen" by X-Rays. In *Advances in Planar Lipid Bilayers and Liposomes*; 2006; Vol. 5, pp. 253–283.

(47)   Fraser, S. J.; Mulet, X.; Hawley, A.; Separovic, F.; Polyzos, A. Controlling Nanostructure and Lattice Parameter of the Inverse Bicontinuous Cubic Phases in Functionalised Phytantriol Dispersions. *J. Colloid Interface Sci.* **2013**, *408*, 117–124.

(48)   Mezzenga, R.; Meyer, C.; Servais, C.; Romoscanu, A. I.; Sagalowicz, L.; Hayward, R. C. Shear Rheology of Lyotropic Liquid Crystals: A Case Study. *Langmuir* **2005**, *21*, 3322–3333.

(49)   Cullity, B. D. *Elements of X-Ray Diffraction*; Addison-Wesley Publishing Company, Inc.: Reading, Massachusetts, 1956.

(50)   Sivia, D. S. The Basics of X-Ray and Neutron Scattering. In *Elementary Scattering Theory for X-ray and Neutron Users*; Oxford Scholarship Online, 2011; pp. 20–95.

(51)   Di Cola, E.; Grillo, I.; Ristori, S. Small Angle X-Ray and Neutron Scattering: Powerful Tools for Studying the Structure of Drug-Loaded Liposomes. *Pharmaceutics* **2016**, *8*, 1–16.

(52)   Muller, F.; Salonen, A.; Glatter, O. Phase Behavior of Phytantriol/water Bicontinuous Cubic Pn3m Cubosomes Stabilized by Laponite Disc-like Particles. *J. Colloid Interface Sci.* **2010**, *342*, 392–398.

(53)   Salentinig, S.; Sagalowicz, L.; Glatter, O. Self-Assembled Structures and pKa Value of Oleic Acid in Systems of Biological Relevance. *Langmuir* **2010**, *26*, 11670–11679.

(54)   Yaghmur, A.; Laggner, P.; Sartori, B.; Rappolt, M. Calcium Triggered Lα-H2 Phase Transition Monitored by Combined Rapid Mixing and Time-Resolved Synchrotron SAXS. *PLoS One* **2008**, *3*, 1–11.

(55)   Tang, X. C.; Pikal, M. J.; Taylor, L. S. The Effect of Temperature on Hydrogen Bonding in Crystalline and Amorphous Phases in Dihydropyrine Calcium Channel Blockers. **2002**, *19*, 484–490.

(56)   Liu, Q.; Dong, Y. D; Hanley, T. L.; Boyd, B. J. Sensitivity of Nanostructure in Charged Cubosomes to Phase Changes Triggered by Ionic Species in Solution. *Langmuir* **2013**, *29*, 14265–14273.

(57)   Salentinig, S.; Tangso, K. J.; Hawley, A.; Boyd, B. J. pH-Driven Colloidal Transformations Based on the Vasoactive Drug Nicergoline. *Langmuir* **2014**, *30*, 14776–14781.

(58)   Yaghmur, A.; Laggner, P.; Almgren, M.; Rappolt, M. Self-Assembly in Monoelaidin Aqueous Dispersions: Direct Vesicles to Cubosomes Transition. *PLoS One* **2008**, *3*, 42–46.

(59)   Rappolt, M.; Hickel, A.; Bringezu, F.; Lohner, K. Mechanism of the Lamellar/Inverse Hexagonal Phase Transition Examined by High Resolution X-Ray Diffraction. *Biophys. J.* **2003**, *84*, 3111–3122.

(60)   Mendozza, M.; Montis, C.; Caselli, L.; Wolf, M.; Baglioni, P.; Berti, D. On the Thermotropic and

Magnetotropic Phase Behavior of Lipid Liquid Crystals Containing Magnetic Nanoparticles. *Nanoscale* **2018**, *10*, 3480–3488.

(61)   Fong, W.; Hanley, T. L.; Thierry, B.; Kirby, N.; Waddington, L. J.; Boyd, B. J. Controlling the Nanostructure of Gold Nanorod–Lyotropic Liquid- Crystalline Hybrid Materials Using Near-Infrared Laser Irradiation. *Langmuir* **2012**, *28*, 14450–14460.

(62)   Lajunen, T.; Viitala, L.; Kontturi, L. S.; Laaksonen, T.; Liang, H.; Vuorimaa-Laukkanen, E.; Viitala, T.; Le Guével, X.; Yliperttula, M.; Murtomäki, L.; Urtti, A. Light Induced Cytosolic Drug Delivery from Liposomes with Gold Nanoparticles. *J. Control. Release* **2015**, *203*, 85–98.

(63)   Kulkarni, C. V; Yaghmur, A.; Steinhart, M.; Kriechbaum, M.; Rappolt, M. Effects of High Pressure on Internally Self-Assembled Lipid Nanoparticles: A Synchrotron Small-Angle X-Ray Scattering (SAXS) Study. *Langmuir* **2016**, *32*, 11907–11917.

(64)   Borne, J.; Nylander, T.; Khan, A. Effect of Lipase on Different Lipid Liquid Crystalline Phases Formed by Oleic Acid Based Acylglycerols. *Langmuir* **2002**, *18*, 8972–8981.

(65)   Fong, W. K.; Salentinig, S.; Prestidge, C.; Mezzenga, R.; Hawley, A.; Boyd, B. J. Generation of Geometrically Ordered Lipid-Based Liquid-Crystalline Nanoparticles Using Biologically Relevant Enzymatic Processing. *Langmuir* **2014**, *30*, 5373–5377.

(66)   Wadsater, M.; Barauskas, J.; Nylander, T.; Tiberg, F. Formation of Highly Structured Cubic Micellar Lipid Nanoparticles of Soy Phosphatidylcholine and Glycerol Dioleate and Their Degradation by Triacylglycerol Lipase. *Appl. Mater. Interfaces* **2014**, *6*, 7063–7069.

(67)   Poletto, F. S.; Lima, F. S.; Lundberg, D.; Nylander, T.; Loh, W. Tailoring the Internal Structure of Liquid Crystalline Nanoparticles Responsive to Fungal Lipases: A Potential Platform for Sustained Drug Release. *Colloids Surfaces B Biointerfaces* **2016**, *147*, 210–216.

(68)   Jia, S.; Du, J. D.; Hawley, A.; Fong, W.; Graham, B.; Boyd, B. J. Investigation of Donor – Acceptor Stenhouse Adducts as New Visible Wavelength-Responsive Switching Elements for Lipid-Based Liquid Crystalline Systems. *Langmuir* **2017**, *33*, 2215–2221.

(69)   Tangso, K. J.; Fong, W.; Darwish, T.; Kirby, N.; Boyd, B. J.; Hanley, T. L. Novel Spiropyran Amphiphiles and Their Application as Light-Responsive Liquid Crystalline Components. *J. Phys. Chem. B* **2013**, *117*, 10203–10210.

(70)   Du, J. D.; Hong, L.; Tan, A.; Boyd, B. J. Naphthalocyanine as a New Photothermal Actuator for Lipid-Based Drug Delivery Systems. *J. Phys. Chem. B* **2018**, *122*, 1766–1770.

(71)   Peng, S.; Guo, Q.; Hughes, T. C.; Hartley, P. G. Reversible Photorheological Lyotropic Liquid Crystals. *Langmuir* **2014**, *30*, 866–872.

(72)   Negrini, R.; Mezzenga, R. pH-Responsive Lyotropic Liquid Crystals for Controlled Drug Delivery. *Langmuir* **2011**, *27*, 5296–5303.

(73)   Boyd, B. J. Characterisation of Drug Release From Cubosomes Using the Pressure Ultrafiltration Method. *Int. J. Pharm.* **2003**, *260*, 239–247.

(74)   Yaghmur, A.; Rappolt, M. Structural Characterization of Lipidic Systems under Nonequilibrium Conditions. *Eur. Biophys. J.* **2012**, *41*, 831–840.

(75)   Du, J. D.; Fong, W.-K.; Salentinig, S.; Caliph, S. M.; Hawley, A.; Boyd, B. J. Phospholipid-Based Self-Assembled Mesophase Systems for Light-Activated Drug Delivery. *Phys. Chem. Chem. Phys.* **2015**, *17*, 14021–14027.

(76)   Conn, C. E.; Ces, O.; Mulet, X.; Finet, S.; Winter, R.; Seddon, J. M.; Templer, R. H. Dynamics of Structural Transformations between Lamellar and Inverse Bicontinuous Cubic Lyotropic Phases Dynamics of Structural Transformations between Lamellar and Inverse Bicontinuous Cubic Lyotropic Phases. **2006**.

(77)   Prassl, R.; Pregetter, M.; Amenitsch, H.; Kriechbaum, M.; Schwarzenbacher, R.; Chapman, J. M.; Laggner, P. Low Density Lipoproteins as Circulating Fast Temperature Sensors. *PLoS One* **2008**, *3*, 1–6.

(78)   Fatouros, D. G.; Deen, G. R.; Arleth, L.; Bergenstahl, B.; Nielsen, F. S.; Pedersen, J. S.; Mullertz, A. Structural Development of Self Nano Emulsifying Drug Delivery Systems (SNEDDS) during in Vitro Lipid Digestion Monitored by Small-Angle X-Ray Scattering. *Pharm. Res.* **2007**, *24*, 1844–1853.

(79)   Bisset, N. B.; Webster, G. R.; Dong, Y. D.; Boyd, B. J. Understanding the Kinetic Mixing between Liquid Crystalline Nanoparticles and Agrochemical Actives. *Colloids Surfaces B Biointerfaces* **2019**, *175*, 324–332.

(80)   Banchelli, M.; Nappini, S.; Montis, C.; Bonini, M.; Canton, P.; Berti, D.; Baglioni, P. Magnetic Nanoparticle Clusters as Actuators of ssDNA Release. *Phys. Chem. Chem. Phys.* **2014**, *16*, 10023–10031.

(81)   Baskaran, R.; Madheswaran, T.; Sundaramoorthy, P.; Kim, H. M.; Yoo, B. K. Entrapment of Curcumin into Monoolein-Based Liquid Crystalline Nanoparticle Dispersion for Enhancement of Stability and Anticancer Activity. *Int. J. Nanomedicine* **2014**, *9*, 3119–3130.

(82)   Cervin, C.; Vandoolaeghe, P.; Nistor, C.; Tiberg, F.; Johnsson, M. A Combined in Vitro and in Vivo Study on the Interactions between Somatostatin and Lipid-Based Liquid Crystalline Drug Carriers and Bilayers. *Eur. J. Pharm. Sci.* **2009**, *36*, 377–385.

(83)   Gan, L.; Han, S.; Shen, J.; Zhu, J.; Zhu, C.; Zhang, X.; Gan, Y. Self-Assembled Liquid Crystalline Nanoparticles as a Novel Ophthalmic Delivery System for Dexamethasone: Improving Preocular Retention and Ocular Bioavailability. *Int. J. Pharm.* **2010**, *396*, 179–187.

(84)   Chen, L.-J.; Ling-Li Gong, A.; Lin, Y.-L.; Jin, X.-Y.; Han-Ying Li, B.; Sen-Sen Li, B.; Che, K.-J.; Cai, Z.-P.; James Yang, C. Lab on a Chip Microfluidic Fabrication of Cholesteric Liquid Crystal Core–shell Structures toward Magnetically Transportable Microlasers. *Lab Chip* **2014**, *16*, 1206–1213.

(85)   Li, J.; Wu, L.; Wu, W.; Wang, B.; Wang, Z.; Xin, H.; Xu, Q. A Potential Carrier Based on Liquid Crystal Nanoparticles for Ophthalmic Delivery of Pilocarpine Nitrate. *Int. J. Pharm.* **2013**, *455*, 75–84.

(86)   Lee, D. R.; Park, J. S.; Bae, I. H.; Lee, Y.; Kim, B. M. Liquid Crystal Nanoparticle Formulation as an Oral Drug Delivery System for Liver-Specific Distribution. *Int. J. Nanomedicine* **2016**, *11*, 853–871.

(87)   Gabizon, A.; Catane, R.; Uziely, B.; Kaufman, B.; Safra, T.; Cohen, R.; Martin, F.; Huang, A.; Barenholz, Y. Prolonged Circulation Time and Enhanced Accumulation in Malignant Exudates of Doxorubicin Encapsulated in Polyethylene-Glycol Coated Liposomes. *Cancer Res.* **1994**, *54*, 987–992.

(88)   Surdam, J. W.; Licini, D. J.; Baynes, N. T.; Arce, B. R. The Use of Exparel (liposomal Bupivacaine) to Manage Postoperative Pain in Unilateral Total Knee Arthroplasty Patients. *J. Arthroplasty* **2015**, *30*, 325–329.

(89) Leesajakul, W.; Nakano, M.; Taniguchi, A.; Handa, T. Interaction of Cubosomes with Plasma Components Resulting in the Destabilization of Cubosomes in Plasma. *Colloids Surfaces B Biointerfaces* **2004**, *34*, 253–258.

(90) Lopes, L. B.; Ferreira, D. A.; De Paula, D.; Garcia, M. T. J.; Thomazini, J. a.; Fantini, M. C. a; Bentley, M. V. L. B. Reverse Hexagonal Phase Nanodispersion of Monoolein and Oleic Acid for Topical Delivery of Peptides: In Vitro and in Vivo Skin Penetration of Cyclosporin A. *Pharm. Res.* **2006**, *23*, 1332–1342.

(91) Lai, J.; Chen, J.; Lu, Y.; Sun, J.; Hu, F.; Yin, Z.; Wu, W. Glyceryl Monooleate/Poloxamer 407 Cubic Nanoparticles as Oral Drug Delivery Systems: I. In Vitro Evaluation and Enhanced Oral Bioavailability of the Poorly Water-Soluble Drug Simvastatin. *AAPS PharmSciTech* **2009**, *10*, 960–966.

(92) Rizwan, S. B.; Assmus, D.; Boehnke, A.; Hanley, T.; Boyd, B. J.; Rades, T.; Hook, S. Preparation of Phytantriol Cubosomes by Solvent Precursor Dilution for the Delivery of Protein Vaccines. *Eur. J. Pharm. Biopharm.* **2011**, *79*, 15–22.

(93) Gordon, S.; Young, K.; Wilson, R.; Rizwan, S.; Kemp, R.; Rades, T.; Hook, S. Chitosan Hydrogels Containing Liposomes and Cubosomes as Particulate Sustained Release Vaccine Delivery Systems. *J. Liposome Res.* **2012**, *22*, 193–204.

(94) Francesko, A.; Cardoso, V. F.; Lanceros-Méndez, S. Lab-on-a-Chip Technology and Microfluidics. In *Microfluidics for Pharmaceutical Applications: From Nano/Micro Systems Fabrication to Controlled Drug Delivery*; Santo, H. A.; Liu, D.; Zhang, H., Eds.; William Andrew, 2018; pp. 4–36.

(95) Khan, I. U.; Serra, C. A.; Anton, N. Production of Nanoparticle Drug Delivery Systems with Microfluidics Tools. *Expert Opin. Drug Deliv.* **2015**, *12*, 547–562.

(96) Song, H.; Tice, J. D.; Ismagilov, R. F. A Microfluidic System for Controlling Reaction Networks in Time. *Angew. Chemie - Int. Ed.* **2003**, *42*, 768–772.

(97) Wang, G. R.; Yang, F.; Zhao, W. There Can Be Turbulence in Microfluidics at Low Reynolds Number. *Lab Chip* **2014**, *14*, 1452–1458.

(98) Stroock, A. D.; Dertinger, S. K. W.; Ajdari, A.; Mezic, I.; Stone, H. A; Whitesides, G. M. Chaotic Mixer for Microchannels. *Science* **2002**, *295*, 647–651.

(99) Schmid, L.; Weitz, D. A.; Franke, T. Sorting Drops and Cells with Acoustics: Acoustic Microfluidic Fluorescence-Activated Cell Sorter. *Lab Chip* **2014**, *14*, 3710–3718.

(100) Devendran, C.; Gralinski, I.; Neild, A. Separation of Particles Using Acoustic Streaming and Radiation Forces in an Open Microfluidic Channel. *Microfluid. Nanofluidics* **2014**, *17*, 879–890.

(101) Sesen, M.; Alan, T.; Neild, A. Microfluidic On-Demand Droplet Merging Using Surface Acoustic Waves. *Lab Chip* **2014**, *14*, 3325–3333.

(102) Mizuno, M.; Toyota, T.; Konishi, M.; Kageyama, Y.; Yamada, M.; Seki, M. Formation of Monodisperse Hierarchical Lipid Particles Utilizing Microfluidic Droplets in a Non-Equilibrium State. *Langmuir* **2015**, *31*, 2334–2341.

(103) Stehle, R.; Goerigk, G.; Wallacher, D.; Ballauff, M.; Seiffert, S. Small-Angle X-Ray Scattering in Droplet-Based Microfluidics. *Lab Chip* **2013**, *13*, 1529–1537.

(104) Anna, S. L.; Bontoux, N.; Stone, H. A. Formation of Dispersions Using "Flow Focusing" in Microchannels. *Appl. Phys. Lett.* **2003**, *82*, 364–366.

(105) Link, D. R.; Anna, S. L.; Weitz, D. A.; Stone, H. A. Geometrically Mediated Breakup of Drops in Microfluidic Devices. *Phys. Rev. Lett.* **2004**, *92*, 0545031–0545034.

(106) Otten, A.; Köster, S.; Struth, B.; Snigirev, A.; Pfohl, T. Microfluidics of Soft Matter Investigated by Small-Angle X-Ray Scattering. *J. Synchrotron Radiat.* **2005**, *12*, 745–750.

(107) Xu, Q.; Nakajima, M. The Generation of Highly Monodisperse Droplets through the Breakup of Hydrodynamically Focused Microthread in a Microfluidic Device. *Appl. Phys. Lett.* **2004**, *85*, 3726–3728.

(108) Volpatti, L. R.; Yetisen, A. K. Commercialization of Microfluidic Devices. *Trends Biotechnol.* **2014**, *32*, 347–350.

(109) Khor, S. Y.; Vu, M. N.; Pilkington, E. H.; Johnston, A. P. R.; Whittaker, M. R.; Quinn, J. F.; Truong, N. P.; Davis, T. P. Elucidating the Influences of Size, Surface Chemistry, and Dynamic Flow on Cellular Association of Nanoparticles Made by Polymerization-Induced Self-Assembly. *Small* **2018**, *14*, 1–13.

(110) Kastner, E.; Kaur, R.; Lowry, D.; Moghaddam, B.; Wilkinson, A.; Perrie, Y. High-Throughput Manufacturing of Size-Tuned Liposomes by a New Microfluidics Method Using Enhanced Statistical Tools for Characterization. *Int. J. Pharm.* **2014**, *477*, 361–368.

(111) Kastner, E.; Verma, V.; Lowry, D.; Perrie, Y. Microfluidic-Controlled Manufacture of Liposomes for the Solubilisation of a Poorly Water Soluble Drug. *Int. J. Pharm.* **2015**, *485*, 122–130.

(112) Micronit. Micromixers https://store.micronit.com/microfluidic-chips/micromixers (accessed Jan 23, 2019).

(113) Micronit. Microfluidic starter kit https://www.micronit.com/products/microfluidic-starter-kit.html (accessed Jan 23, 2019).

(114) Dootz, R.; Evans, H.; Köster, S.; Pfohl, T. Rapid Prototyping of X-Ray Microdiffraction Compatible Continuous Microflow Foils. *Small* **2007**, *3*, 96–100.

(115) Khvostichenko, D. S.; Kondrashkina, E.; Perry, S. L.; Pawate, A. S.; Brister, K.; Kenis, P. J. A. An X-Ray Transparent Microfluidic Platform for Screening of the Phase Behavior of Lipidic Mesophases. *Analyst* **2013**, *1338*, 5384–5395.

(116) Schwemmer, F.; Blanchet, C. E.; Spilotros, A.; Kosse, D.; Zehnle, S.; Mertens, H. D. T.; Graewert, M. A.; Rössle, M.; Paust, N.; Svergun, D. I.; von Stetten, F.; Zengerle, R.; Mark, D. LabDisk for SAXS: A Centrifugal Microfluidic Sample Preparation Platform for Small-Angle X-Ray Scattering. *Lab Chip* **2016**, *16*, 1161–1170.

(117) Ghazal, A.; Gontsarik, M.; Kutter, J. P.; Lafleur, J. P.; Ahmadvand, D.; Labrador, A.; Salentinig, S.; Yaghmur, A. Microfluidic Platform for the Continuous Production and Characterization of Multilamellar Vesicles: A Synchrotron Small-Angle X-Ray Scattering (SAXS) Study. *J. Phys. Chem. Lett.* **2016**, *8*, 73–79.

(118) Khaliqi, K.; Ghazal, A.; Azmi, I. D. M.; Amenitsch, H.; Mortensen, K.; Salentinig, S.; Yaghmur, A. Direct Monitoring of Lipid Transfer on Exposure of Citrem Nanoparticles to an Ethanol Solution Containing Soybean Phospholipid by Combining Synchrotron SAXS with Microfluidics. *Analyst* **2017**, *142*, 3118–3126.

(119) Ghazal, A.; Gontsarik, M.; Kutter, J. P.; Lafleur, J. P.; Labrador, A.; Mortensen, K.; Yaghmur, A. Direct Monitoring of Calcium-Triggered Phase Transitions in Cubosomes Using Small-Angle X-Ray Scattering Combined with Microfluidics. *J. Appl. Crystallogr.* **2016**, *49*, 1–10.

(120)   Lee, J.; Jha, A. K.; Bose, A.; Tripathi, A. Supplementary Material Imaging New Transient Nanostructures Using a Microfluidic Chip Integrated with a Controlled Environment Vitrification System for Cryo-TEM. *Langmuir* **2008**, *104*, 1–2.

(121)   Swyer, I.; Soong, R.; Dryden, M. D. M.; Fey, M.; Maas, W. E.; Simpson, A.; Wheeler, A. R. Interfacing Digital Microfluidics with High-Field Nuclear Magnetic Resonance Spectroscopy. *Lab Chip* **2016**, *16*, 4424–4435.

(122)   Liszka, B. M.; Rho, H. S.; Yang, Y.; Lenferink, A. T. M.; Terstappen, L. W. M. M.; Otto, C. A Microfluidic Chip for High Resolution Raman Imaging of Biological Cells. *RSC Adv.* **2015**, *5*, 49350–49355.

(123)   Cristobal, G.; Arbouet, L.; Sarrazin, F.; Talaga, D.; Bruneel, J.-L.; Joanicot, M.; Servant, L. On-Line Laser Raman Spectroscopic Probing of Droplets Engineered in Microfluidic Devices. *Lab Chip* **2006**, *6*, 1140–1146.

(124)   Lee, J. N.; Park, C.; Whitesides, G. M. Solvent Compatibility of Poly(dimethylsiloxane)-Based Microfluidic Devices. *Anal. Chem.* **2003**, *75*, 6544–6554.

(125)   Ren, K.; Zhou, J.; Wu, H. Materials for Microfluidic Chip Fabrication. *Acc. Chem. Res.* **2013**, *46*, 2396–2406.

(126)   Zilio, C.; Sola, L.; Damin, F.; Faggioni, L.; Chiari, M. Universal Hydrophilic Coating of Thermoplastic Polymers Currently Used in Microfluidics. *Biomed. Microdevices* **2014**, *16*, 107–114.

(127)   Jena, R. K.; Yue, C. Y. Cyclic Olefin Copolymer Based Microfluidic Devices for Biochip Applications: Ultraviolet Surface Grafting Using 2-Methacryloyloxyethyl Phosphorylcholine. *Biomicrofluidics* **2012**, *6*, 1–12.

(128)   Tan, S. H.; Nguyen, N. T.; Chua, Y. C.; Kang, T. G. Oxygen Plasma Treatment for Reducing Hydrophobicity of a Sealed Polydimethylsiloxane Microchannel. *Biomicrofluidics* **2010**, *4*, 1–12.

(129)   Abate, A. R.; Krummel, A. T.; Lee, D.; Marquez, M.; Holtze, C.; Weitz, D. A. Photoreactive Coating for High-Contrast Spatial Patterning of Microfluidic Device Wettability. *Lab Chip* **2008**, *8*, 2157–2160.

(130)   Yu, H.; Chong, Z. Z.; Tor, S. B.; Liu, E.; Loh, N. H. Low Temperature and Deformation-Free Bonding of PMMA Microfluidic Devices with Stable Hydrophilicity via Oxygen Plasma Treatment and PVA Coating. *RSC Adv.* **2015**, *5*, 8377–8388.

(131)   Reynolds, O. An Experimental Investigation of the Circumstances Which Determine Whether the Motion of Water Shall Be Direct or Sinuous, and of the Law of Resistance in Parallel Channels. *Philos. Trans. R. Soc. London* **1883**, *174*, 935–982.

(132)   Rott, N. Note on the History of the Reynold's Number. *Annu. Rev. Fluid Mech.* **1990**, *22*, 1–11.

(133)   Lee, C. Y.; Chang, C. L.; Wang, Y. N.; Fu, L. M. Microfluidic Mixing: A Review. *Int. J. Mol. Sci.* **2011**, *12*, 3263–3287.

(134)   Nguyen, N.-T.; Wu, Z. Micromixers—a Review. *J. Micromechanics Microengineering* **2005**, *15*, R1–R16.

(135)   With, S.; Trebbin, M.; Bartz, C. B. A.; Neuber, C.; Dulle, M.; Yu, S.; Roth, S. V; Schmidt, H.; Fo, S.; Forster, S. Fast Diffusion-Limited Lyotropic Phase Transitions Studied in Situ Using Continuous Flow Microfluidics/Microfocus-SAXS. *Langmuir* **2014**, *30*, 12494–12503.

(136)   Tice, J. D.; Lyon, A. D.; Ismagilov, R. F. Effects of Viscosity on Droplet Formation and Mixing in Microfluidic Channels. *Anal. Chim. Acta* **2004**, *507*, 73–77.

(137)   Thorsen, T.; Roberts, R. W.; Arnold, F. H.; Quake, S. R. Dynamic Pattern Formation in a Vesicle-Generating Microfluidic Device. *Phys. Rev. Lett.* **2001**, *86*, 4163–4166.

(138)   Baroud, C. N.; Gallaire, F.; Dangla, R. Dynamics of Microfluidic Droplets. *Lab Chip* **2010**, *10*, 2032–2045.

(139)   Ushikubo, F. Y.; Birribilli, F. S.; Oliveira, D. R. B.; Cunha, R. L. Y- and T-Junction Microfluidic Devices: Effect of Fluids and Interface Properties and Operating Conditions. *Microfluid. Nanofluidics* **2014**, *17*, 711–720.

(140)   Kim, S. H.; Kim, J. W.; Kim, D. H.; Han, S. H.; Weitz, D. A. Enhanced-Throughput Production of Polymersomes Using a Parallelized Capillary Microfluidic Device. *Microfluid. Nanofluidics* **2013**, *14*, 509–514.

(141)   Mijajlovic, M.; Wright, D.; Zivkovic, V.; Bi, J. X.; Biggs, M. J. Microfluidic Hydrodynamic Focusing Based Synthesis of POPC Liposomes for Model Biological Systems. *Colloids Surfaces B Biointerfaces* **2013**, *104*, 276–281.

(142)   Michelon, M.; Oliveira, D. R. B.; de Figueiredo Furtado, G.; Gaziola de la Torre, L.; Cunha, R. L. High-Throughput Continuous Production of Liposomes Using Hydrodynamic Flow-Focusing Microfluidic Devices. *Colloids Surfaces B Biointerfaces* **2017**, *156*, 349–357.

(143)   Balbino, T. A.; Serafin, J. M.; Radaic, A.; de Jesus, M. B.; de la Torre, L. G. Integrated Microfluidic Devices for the Synthesis of Nanoscale Liposomes and Lipoplexes. *Colloids Surfaces B Biointerfaces* **2017**, *152*, 406–413.

(144)   Balbino, T. A.; Aoki, N. T.; Gasperini, A. A. M.; Oliveira, C. L. P.; Azzoni, A. R.; Cavalcanti, L. P.; de la Torre, L. G. Continuous Flow Production of Cationic Liposomes at High Lipid Concentration in Microfluidic Devices for Gene Delivery Applications. *Chem. Eng. J.* **2013**, *226*, 423–433.

(145)   Kim, H.; Sung, J.; Chang, Y.; Alfeche, A.; Leal, C. Microfluidics Synthesis of Gene Silencing Cubosomes. *ACS Nano* **2018**, *12*, 9196–9205.

(146)   Leng, J.; Joanicot, M.; Ajdari, A. Microfluidic Exploration of the Phase Diagram of a Surfactant/Water Binary System. *Langmuir* **2007**, *23*, 2315–2317.

(147)   Lee, J.; Bose, A.; Tripathi, A. Rapid Exploration of Phase Behavior in Surfactant Systems Using Flow in Microchannels. *Langmuir* **2006**, *22*, 11412–11419.

Chapter 2: Evaluation of commercial microfluidic devices for *in situ* scattering measurements of transitions in lyotropic liquid crystalline systems

2.1 Introduction

Liquid crystalline nanoparticles (LCNPs) are a drug delivery system that can be rendered responsive to certain stimuli to enable switching between nanoparticles of different internal structures. These stimuli include pH,[1,2] dilution,[3] enzyme[4,5] and temperature,[6] which when applied to the lipid system containing the corresponding additive can alter the internal structure. The effect can transition a slow-releasing structure such as inverse hexagonal (H_2) phase to one that has a greater rate of release such as cubic (V_2) phase.[7] These liquid crystalline mesophases have been previously described in section **1.2 Lipid-based liquid crystal nanoparticles (LCNPs)**. Thus, the ability to control this with the application and removal of the stimulus can be capitalised for controlled and 'on-demand' drug delivery, where drug can be administered at the required location, when required and for as long as required.

To date, medicines containing stimuli-responsive and lipid-based LCNPs have not reached the market. Camurus® have been at the forefront of advancing lipid-based liquid crystalline systems to the market, of which their systems containing nanoparticles are still undergoing development.[8,9] A temperature-sensitive liposomal system developed by Celsion Corporation is currently the only stimuli-responsive formulation in clinical trials.[10,11] The lack of stimuli-responsive LCNPs on the market and their slow progression into clinical trials may suggest that there are challenges in their optimisation and how they are assessed.

Current experimental configurations to characterise the dynamic phase behaviour of these stimuli-responsive systems are not truly *in situ* as the analysis occurs at a different location from the main reaction. One example of such an experimental configuration is the pH-stat method integrated with small angle X-ray scattering (SAXS) used to measure changes in structure during lipid digestion. The sample (lipid emulsions eg. milk) and solution of stimulus (lipase) are mixed in a bulk digestion vessel before being transferred via a peristaltic pump to a quartz capillary for analysis and then back into the vessel.[4,5,12] The separation of the mixing and analytical vessel is necessary due to a lack of X-ray transparency of the mixing vessel. Additionally, the configuration also requires a pH electrode, burette, magnetic stirring and pumping appendages in the mixing vessel, meaning there is a minimum operating volume of around 10 to 20 mL of sample. Although the experimental configuration may appear to yield sufficient kinetic data, the delay in transport from the mixing vessel to analytical vessel can overlook earlier kinetics and is impractical for components with limited availability. The

mixing of the stimulus with the emulsion is also not instantaneous so compounded with the continuous nature of the pump, mixing ratios and completeness can be inconsistent between replicates which can result in heterogeneous transformations.

Other experimental configurations for the characterisation of kinetics also demonstrate a delay from where the sample is mixed to where analysis occurs. Yaghmur *et al.* had combined a liposomal formulation containing an anionic lipid with calcium ions in a stopped-flow apparatus in-line with SAXS.[13] Mixing was accomplished within 10 msecs before injection into a capillary where the structural data was acquired. A rapid phase transition from lamellar (L_α) phase into the expected H_2 phase was noted within the first second leaving little time for observation of an intermediate phase.[13]

An improved experimental configuration is therefore required to reveal the entire transformation of the system and allow more control over the kinetics. Removal of the delay in transport between different processes could enable elucidation of earlier kinetics. A finer control over the mixing behaviour could also observe more consistent phase transitions. Both aspects are hypothesised to be able to be achieved with the use of microfluidics.

Microfluidics has been applied to mainly biological processes and more recently, has been used for the analysis of LCNPs. Khvostichenko *et al.* used microfluidics to more efficiently generate ternary phase diagrams of lipid, surfactant and water.[14] Their microfluidic design could generate the liquid crystalline structures *in situ*, however the mixing capabilities of the device were unsuitable for real-time kinetic studies.

Microfluidics downscales the manipulation of material into micron-scale channels in a device that has been coined "lab-on-a-chip".[15] A device featuring channels that converge into one outlet flow can combine solutions together so that they mix, facilitating controlled reactions.[16–19] The kinetics of a reaction initiated in the channels can also be monitored along the length where positions can correlate to a specific time point in the reaction equilibrium.[17] Thus, this feature can potentially be useful to track the kinetics of phase transitions for stimuli-responsive LCNPs.

Despite the apparently simple concept of microfluidics, it is a complex device in terms of its fabrication and flow characteristics. The devices themselves can be relatively inexpensive however the facilities and equipment to manufacture them may not be readily accessible nor affordable for the average research lab. While microfluidic devices can be made incredibly complex, simpler off-the-

shelf microfluidic (OTS-MF) devices have been used to achieve similar manipulations of liquid crystalline systems.

More recently, a commercially available microfluidic device was used for the generation of lamellar-based liquid crystalline systems. Using the antisolvent principle the Perrie research group formed liposomes using the microfluidic device from Precision Nanosystems, Inc.[20,21] A precursor solution containing the liposomal lipid in ethanol, and an aqueous buffer solution were fed into the device at varying flow rate ratios. The two streams converged at a Y-junction before flowing through staggered herringbone structures that enhanced the mixing (**Figure 2-1B**). The staggered herringbone mixer passively combined the fluids as they collided into the elevated walls of the herringbone structure. This also resulted in laminar mixing (**Figure 2-1C**) where the layers of fluid fold over one another, increasing the surface area of contact to increase the overall diffusion between components until homogeneous.[22]
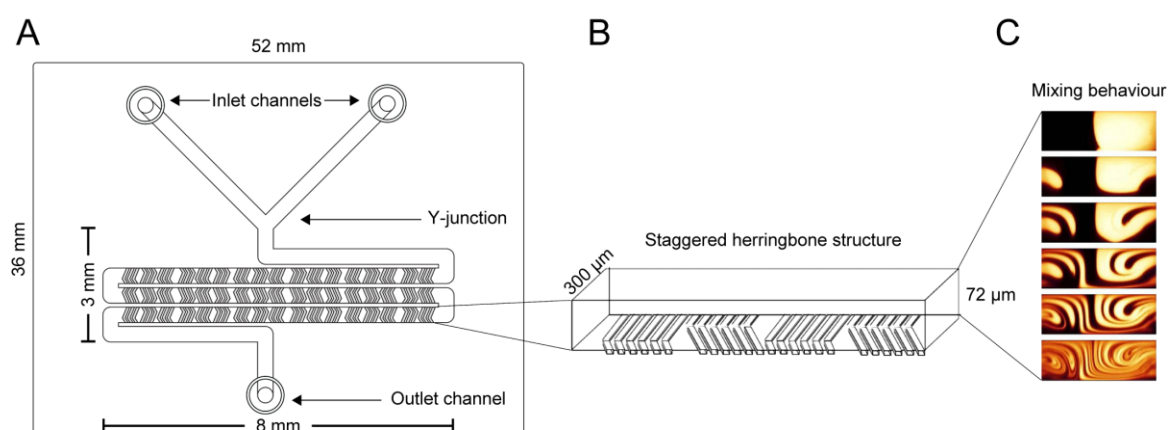
Figure 2-1. A) A not-to-scale schematic of a commercial chip available from Precisions Nanosystems Inc. It features two inlet channels which converge at a Y-junction, staggered herringbone mixers and one outlet channel. B) The close-up of the staggered herringbone structure observed in the microfluidic chip, which is a form of a passive mixer that enables laminar mixing. Figure adapted from Kastner *et al.*[20] C) Flow behaviour of fluorescent solutions along a length of microchannels which contain the staggered herringbone structures. Figure adapted with permission from Stroock *et al.*[22]

Another microfluidic device was also proposed by Bottaro *et al.* to facilitate the formation and loading of liposomes.[23] Unlike the commercially available device described previously, this device was composed of tubing and fittings typically used for high performance liquid chromatography. The device was assembled as shown in **Figure 2-4** where the inlet channels were delivered from the top and side inlets into the T-junction, after which the mixture would flow into the attached capillary.[24] Flow of the two incoming solutions would fill the two semi-circle halves of the capillary, sharing an

interface where material would diffuse from one stream to the other. The researchers noted that despite the T-junction device producing larger particle sizing than the conventional approach, the polydispersity was consistently lower. When loading the liposomes, the difference in particle size turned out to be insignificant between methods.

Although both simple microfluidic devices enabled the formation of LCNPs, it posed the question: could the formation of LCNPs be tracked *in situ*? To test this, the commercial and capillary-based microfluidic devices were integrated with the SAXS apparatus to monitor the phase transitions of known LCNP transformations of systems previously studied using bulk approaches including that of the dilution of a phytantriol-ethanol system[25] and enzyme-sensitive lipid-based formulations.[4,5]

2.2   Hypotheses & aims

It was hypothesised:

- That simple microfluidic devices coupled with SAXS can allow tracking of the structural evolution of stimuli-responsive LCNPs along the microchannels.

The aims were as follows:

- To reconfigure simple microfluidic devices for their integration with SAXS
- To elucidate the mixing within the microfluidic channels using fluorescence
- To monitor the structural evolution of the systems *in situ* in both microfluidic devices

2.2.1   Rationale for selected study formulations

A phase diagram for the phytantriol-ethanol-water system was developed by Han *et al.* as illustrated in **Figure 2-2**.[25] The phase diagram was constructed from phytantriol and ethanol mixtures that were diluted and equilibrated for a week. Phase diagrams are useful for determining the appropriate dilution trajectories to explore in dynamic mixing studies, based on the final equilibrium composition and phase behaviour. The rate of mass transfer of the constituents in the structure and re-structuring of the lipids may also influence the trajectory of the dynamic phase transition.[26,27] A system of 25% w/w phytantriol, 25% w/w ethanol and 50% w/w water (25P25E50W) was selected for testing in the microfluidic device. Selection of this formulation and dilution along the trajectory represented by the red circle and arrow in **Figure 2-2**, was analogous to the dilution occurring with the preparation of liposomes by the Perrie group, except that dilution with an equal volume of water was expected

to transition the system from a milky phase to V_2 phase instead of from an isotropic solution to liposomes. The equilibrium phase diagram was also reconstructed given that different sources of phytantriol could yield different phase behaviours.[6]
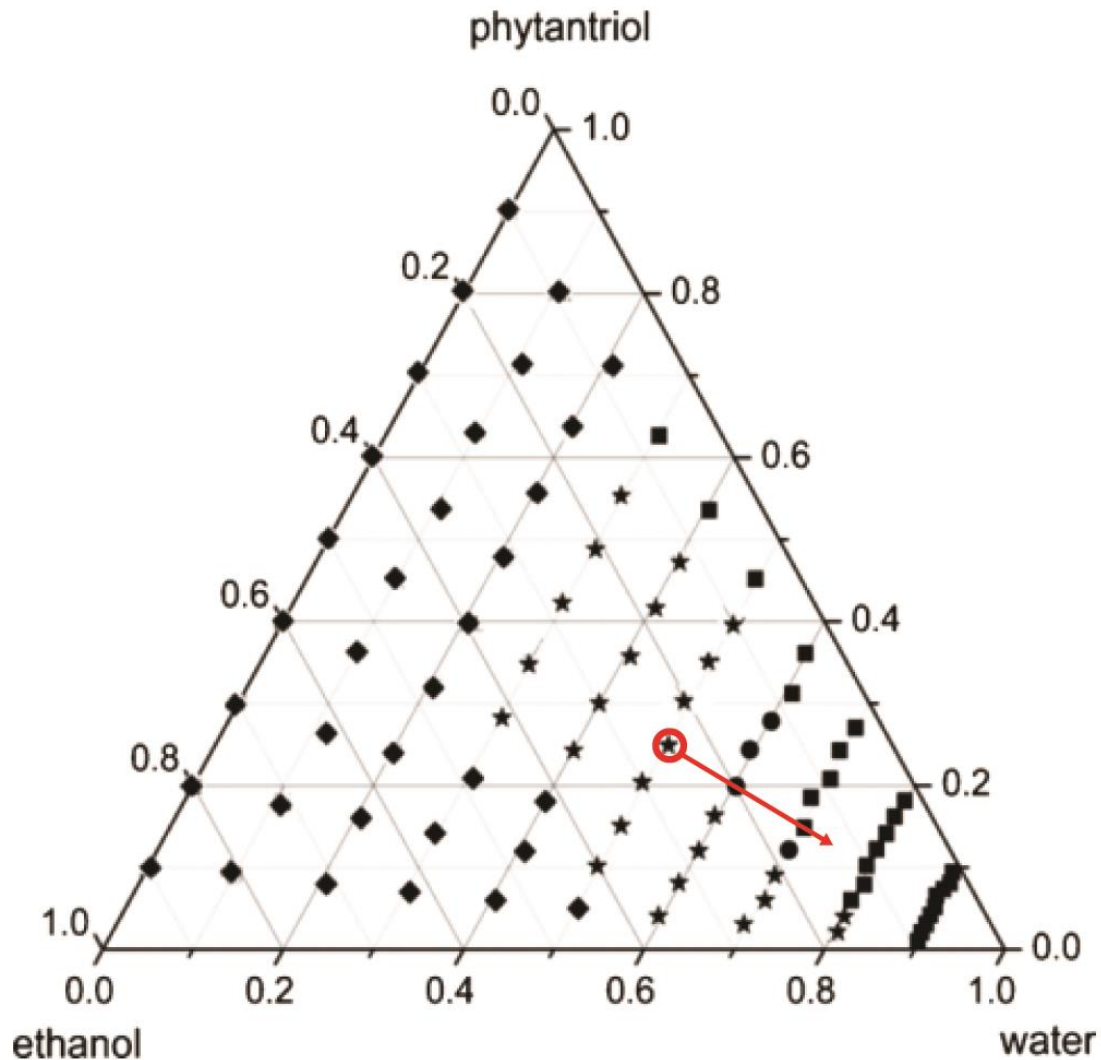
Figure 2-2. Ternary phase diagram of a phytantriol-ethanol-water system (diamond: isotropic solution phase; square: cubic phase; star: milky phase (L_2); circle: lamellar phase). The phase diagram was constructed from samples equilibrated for a week at 25°C. Image adapted with permission from Han *et al.*[25] The red circle denotes the formulation to be tested and the arrow illustrates the expected trajectory of the transformation for a 1:1 dilution starting with the milky phase, transitioning into the lamellar phase, then finishing as the cubic phase.

Monitoring the structural evolution during the digestion of enzyme-sensitive systems was conducted previously using the pH-stat approach with a flow through capillary placed in the X-ray beam. In the experiments conducted by Fong *et al.* and Hong *et al.*, the digestion-sensitive formulations consist of a lyotropic lipid and a triglyceride (eg. tributyrin and tricaprylin) which are dispersed as an emulsion.[4,5] Digestion of the system converted the triglyceride into smaller digestion products

which allowed the lipid molecules to rearrange into the liquid crystal phases such as cubosomes and hexosomes. Two formulations were selected for the current study including an emulsion containing phytantriol with 20% w/w tributyrin (PHYT20TB) and another containing selachyl alcohol with 25% w/w tributyrin (SA25TB) in the microfluidic devices to compare the phase transitions. The PHYT20TB emulsion was anticipated to transition from the inverse micellar (L_2) phase into the cubic *Pn3m* phase, while SA25TB was expected to transition from L_2 phase to the H_2 phase in accordance with the digestion performed previously in the pH-stat approach illustrated in **Figure 2-3**. An emulsion containing phytantriol with 7.5% w/w tributyrin (PHYT7.5TB) was also digested in the microfluidic device, expecting to transform from the inverse hexagonal phase to the cubic *Pn3m* phase. As microfluidics can facilitate a greater control over the kinetics of the transformation, it may be possible to elucidate any transient intermediate structures not observed in the traditional approach.
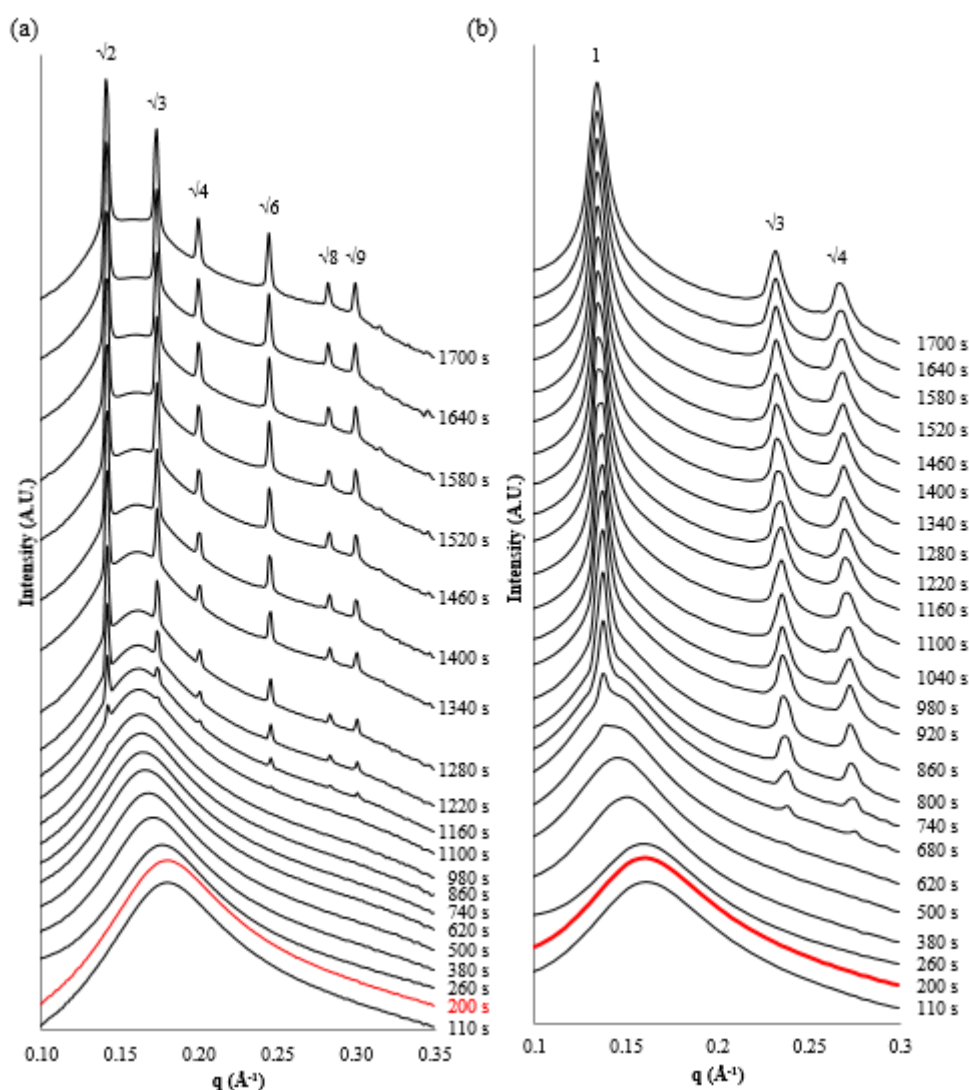
Figure 2-3. Small angle X-ray scattering profiles from emulsions comprising a 'core lipid' and tributyrin during digestion using the pH-stat/flow through capillary method. A) digestion of an emulsion containing phytantriol with 20% w/w tributyrin (PHYT20TB), observing a transition from L_2 phase (as represented by the broad hump) to cubic *Pn3m* phase (as represented by the specific spacing ratios of the peaks: $\sqrt{2}$, $\sqrt{3}$, $\sqrt{4}$, $\sqrt{6}$, $\sqrt{8}$ and $\sqrt{9}$). B) Digestion of an emulsion containing selachyl alcohol with 25% w/w tributyrin (SA25TB), observing a transition from L_2 phase (as represented by the broad hump) to H_2 phase (as represented by the specific spacing ratios of the peaks: 1, $\sqrt{3}$ and $\sqrt{4}$). The red profile at 200 secs indicates the addition of enzyme. Image reproduced with permission from Hong *et al.*[4]

2.3 Methods

2.3.1 Materials

Phytantriol (3,7,11,15-tetramethylhexadecane-1,2,3-triol, PHYT) was purchased from DSM Nutritional Products Ltd, Singapore. Selachyl alcohol (1-glyceryl monooleyl ether, SA) was obtained from Hai Hang Industries, Shang Hai, China. Tributyrin (TB) was obtained from TCI Chemicals, Tokyo Japan.

Pancreatin was purchased from Southern Biological, Nunawading, Australia. Fluorescein sodium salt was purchased from Sigma Aldrich, St Louis, U.S.A.

Sodium chloride was purchased from Chem-Supply, SA, Australia. Trizma maleate was purchased from Sigma-Aldrich, St. Louis, U.S.A. Calcium chloride dihydrate and sodium hydroxide pellets were obtained from Ajax Finechem, NSW, Australia. Sodium azide was obtained from Merck Schuchardt OHG, Darmstadt, Germany. Absolute ethanol was obtained from Merck, Darmstadt, Germany. Milli-Q water was supplied by the Millipore Milli-Q purification system (Billerica, USA) with a 0.22 μm Millipak® filter. Synperonic F108 (Pluronic F108) was purchased from Fluka, France.

2.3.2 Lipid-based formulations

2.3.2.1 Dilution-sensitive systems

Phytantriol was combined in a 20 mL scintillation vial with absolute ethanol and Tris buffer (containing 1% w/w Pluronic F108) in a weight ratio (w/w) of 25:25:50, respectively. Such mixtures were denoted as, in this case, 25P25E50W. The Tris buffer consisted of 150 mM sodium chloride, 50 mM Trizma maleate, 5 mM calcium chloride dihydrate, 6 mM sodium azide, and 37.5 mM sodium hydroxide pellets, all of which were dissolved in Milli-Q water. The ternary mixture was sonicated with a Misonix Ultrasonic liquid processor S-4000 (USA) at 30% amplitude for 2 mins, pulsing on for 4 secs and off for 1 secs. Solutions of sodium hydroxide and hydrochloric acid were used to adjust the pH to 6.5. The aqueous phase that was used to dilute the lipid-based formulation also consisted of Tris buffer with 1% Pluronic F108.

2.3.2.1.1 Equilibrium phase diagram

A ternary phase diagram was also reconstructed with compositions surrounding 25P25E50W to confirm the equilibrium phase behaviour along the dilution trajectory. Phytantriol and ethanol were combined in ratios (w/w) of 4:6, 5:5, 6:4 and 7:3 and diluted with aqueous phase as described by Han *et al.*[25] Samples (200 μL) were loaded in a clear 96-well plate and thermal sealed with an Eppendorf® heat sealer for analysis with SAXS. The plate was mounted upright on a holder and placed in line with the X-ray beam. The experimental stage was programmed to shift in the X- and Y-positions to raster across the plate, taking shot in each well using the same settings for SAXS described below in **2.3.5 Monitoring kinetics of phase transitions**.

2.3.2.2 Enzyme-responsive systems

The lyotropic lipids (PHYT or SA) and TB were weighed in a scintillation vial in the appropriate masses totalling 10% w/w in buffer. The lipids were dispersed into the 50 mM Tris buffer (pH 6.5 and containing 1% Pluronic F108) using the Misonix Ultrasonic liquid processor S-4000 (USA) at 30% amplitude for 2 mins, pulsing on for 4 secs and off for 1 secs. These emulsions then constituted one stream to be mixed with a second stream containing lipase. The lipase suspension was reconstituted from freeze-dried pancreatic lipase at a concentration of 390-400 mg per 1.8 mL of Tris buffer containing 1% w/w Pluronic F108. The freeze-dried lipase was prepared in the method described by Clulow *et al.*[28] The strength of this batch of enzyme was 1000 TBU per mL of digest.

2.3.3 Commercial NanoAssemblr™ microfluidic chip (NA chip)

The polymer-based microfluidic devices were obtained from Precision Nanosystems Inc., Vancouver, Canada. This device, illustrated in **Figure 2-1**, constituted the cartridge in the NanoAssemblr™ that is manufactured with the intention of research scale preparation of particles for applications such as nanomedicine.[20,21] The dimensions of these channels were approximately 300 μm x 79 μm, with the length of the channel stretching approximately 30 mm from the point of convergence (Y-junction) to the outlet. The channel walls featured a series of staggered herringbone structures.

The two independent solutions were delivered to the device via two Harvard Apparatus 11 Plus syringe pumps. The solutions to be mixed were contained within Luer Lock syringes (3 mL) (Livingstone, Korea) which were connected via HPLC fittings and tubing to the NA chip.

2.3.4 Off-the-shelf microfluidic device (OTS-MF device)

The capillary-based microfluidic device was assembled using a T-junction (IDEX P-728 PEEK Tee with a 1.3 mm thru-hole) and a borosilicate glass capillary (1.5 mm OD, 0.84 mm ID, length: 100 mm, World Precision Instruments, U.S.A.) as shown in **Figure 2-4**. The capillary was fitted securely into the T-junction with approximately 7 cm of the length accessible to the X-rays. The solutions to be mixed were filled in separate Luer Lock syringes (3 mL) and delivered to the T-junction via HPLC tubing. Fittings (NanoTight™ PEEK Headless, Short, 10-32 Coned, for 1/16" OD) from IDEX Health and Science (USA) were used to connect the tubing to the T-junction, and the T-junction to the

capillary. The flow rates of both syringes were controlled using two Harvard Apparatus 11 Plus syringe pumps.
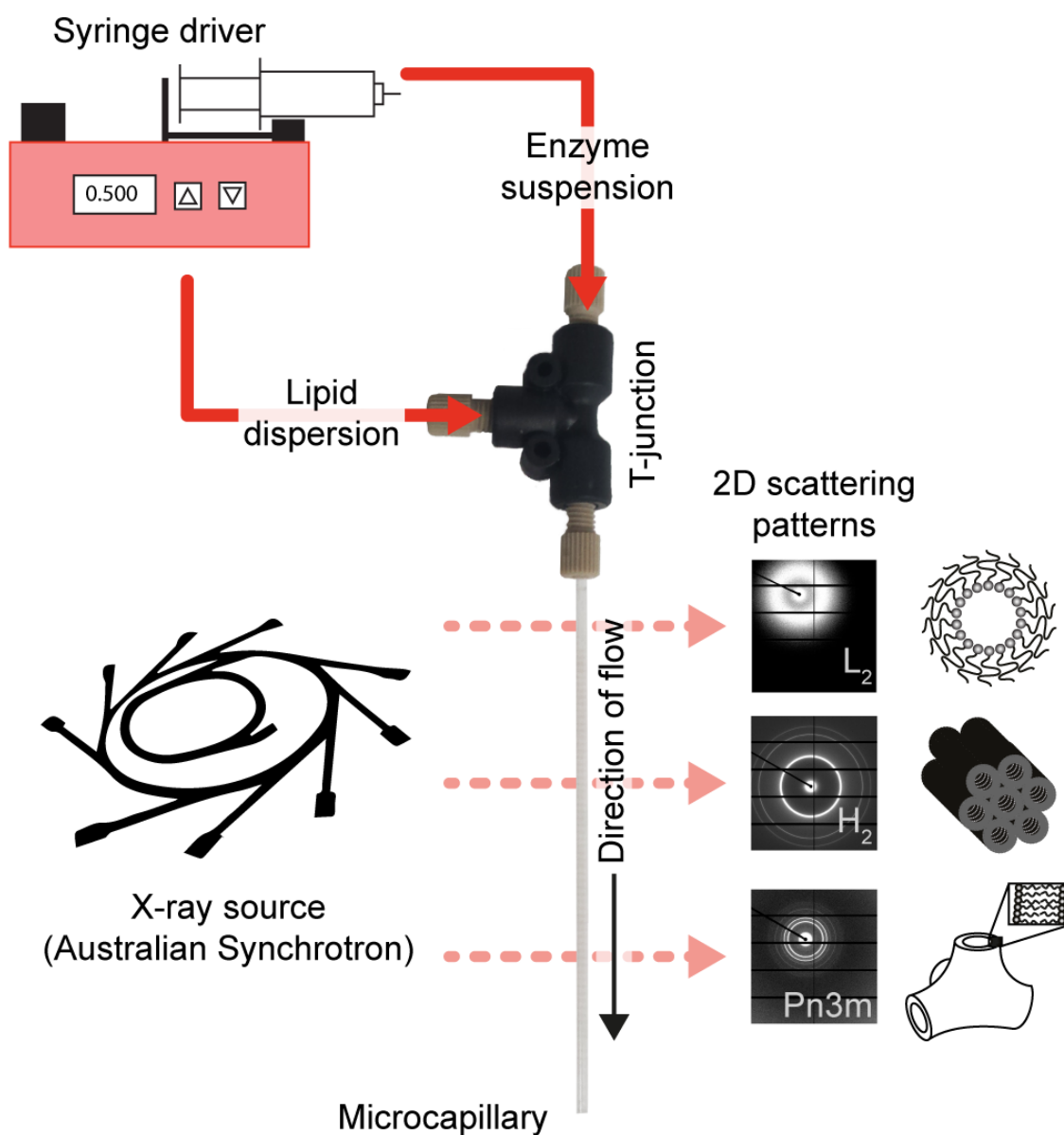
Figure 2-4. Schematic of the OTS-MF device in line with the X-ray beam at the SAXS beamline (Australian Synchrotron). Solutions were delivered to the T-junction via a syringe driver before flowing into the capillary. The X-ray beam scanned the length of the capillary to track the structural kinetics of the digestion.

2.3.5 Monitoring kinetics of phase transitions

Identification of phases was determined using SAXS at the SAXS/WAXS facility at the Australian Synchrotron (Melbourne, Australia). The beamline settings used the 1.13 Å (11 keV) wavelength, with the q range of $0.0169 < q < 0.850$ Å^{-1}. The two-dimensional scattering patterns were acquired over an active area of 169×179 mm^2 with 172 µm pixels, using a Pilatus 1M detector positioned 961 mm

from the sample (determined by calibration against silver behenate). The 2D scattering patterns were then integrated into a one-dimensional scattering function I(q) using the in-house software, Scatterbrain (version 1.15).[29] Identification of the nanostructures from the scattering function was determined by correlating the relative spacing ratios between the positions of the Bragg peaks to literature.[30]

The NA chip was fitted to the aluminium holder provided with the chip (a section of the holder was removed to allow access of the chip to the X-rays). It was then mounted onto a custom designed, 3D printed holder, and positioned in line with the X-ray beam. The OTS-MF device was fixed to a metal support with the capillary placed in-line with the beam. The X- and Y-positions of the experimental stage were adjusted accordingly to track the positions along the length of the channels. The flow rate ratio (FRR) was adjusted to obtain an optimal ratio of both incoming solutions and total flow rate (TFR) was adjusted to resolve the entire phase transitions if the length of the channel was insufficient.

A preliminary test was also conducted using the NA chip which has not been used in SAXS experiments previously, to determine the attenuation of the beam by the polymer, which would limit the ability to detect scattering from the sample. The channels were prefilled with a dispersion of phytantriol-based cubosomes and transmission scattering profiles were obtained to confirm the possibility of observing liquid crystalline structure of the equilibrated cubosome particles inside the microchannel of the device.

2.3.6 Assessment of flow behaviour *in situ*

The division of the two incoming flows at the Y-junction was observed in the NA chip. A video (from the camera directly viewing the sample in line with the X-ray beam) was acquired of the flow at the Y-junction, whilst the X-ray beam was focused at the end of the channel (marked x) to acquire the structure of the equilibrated mixture as illustrated in **Figure 2-5**. This was to confirm the reproducibility of the non-equilibrium structure at the one position depending on the flow behaviour at the Y-junction. Flow rates were selected to ensure an equal division of the two components at the Y-junction, while the magnitude of the flow rates was proposed to yield sufficient retention time for phase transitions to occur *in situ*.
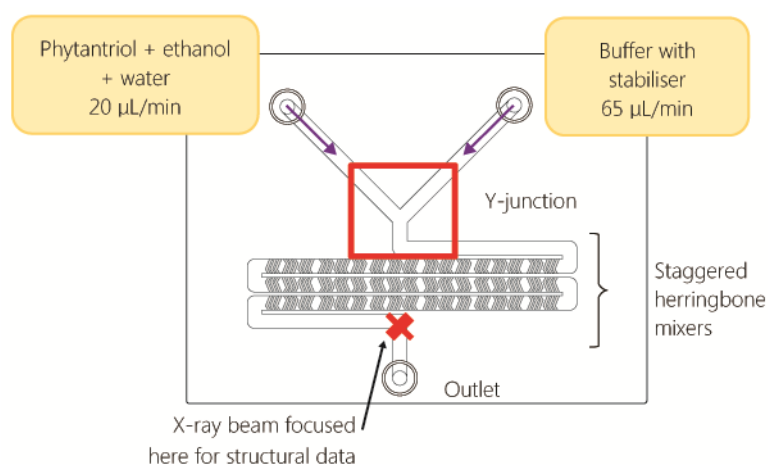
Figure 2-5. Schematic of the NA chip where the lipid formulation was combined with the buffer solution at low flow rates. Video was acquired at the red square encasing the Y-junction whilst the X-ray beam was acquiring the structural data.

The effectiveness of mixing of the two streams on the chip was tested using fluorescence. Sodium fluorescein is known to fluoresce at higher pH, but lose its fluorescence under acidic conditions.[31] Hence by formulating sodium fluorescein at low pH (pH 4) and mixing with the second liquid at pH 10, it was possible to visually interrogate the mixing at different positions along the microchannels. Hence, the dilution-sensitive system was modified to include 50 mg/mL sodium fluorescein in the aqueous phase. The formulation was adjusted to pH 4. The aqueous phase for dilution was adjusted to pH 10. The fluorescence of the mixing was monitored using the Nikon A1R Confocal microscope. Image processing was performed in ImageJ (1.51f).[32]

2.4 Results & discussion

2.4.1 X-ray transparency of the microfluidic devices

The proposed microfluidic devices needed to be compatible with SAXS in order to track structural changes of the lipid-based systems. The capillary in the design of the OTS-MF device is composed of micron-thick borosilicate glass, a commonly used sample holder for SAXS.[33] The NA chip was composed of cyclic olefin copolymer (COC) and had not been used with SAXS prior to these studies, so it was completely unknown whether any scattering would be detected at all from the dispersion loaded into the channels. Using the settings for a typical SAXS experiment in a quartz capillary, four very clear diffraction peaks at q = 0.135, 0.165, 0.190 and 0.233 Å^{-1} which correlate to spacing ratios of √2, √3, √4 and √6 were observed which confirm the detection of the cubic *Pn3m* phase consistent with previous reports (**Figure 2-6**).[6,30] Liposomes have been shown previously to form using this device,[20,21] but not *in situ* meaning this is the first demonstration of the potential to detect the

formation of structured particles in this device *in situ* and that evolution of nanostructured particles from their starting materials could be tracked along the channels in the NA chip.
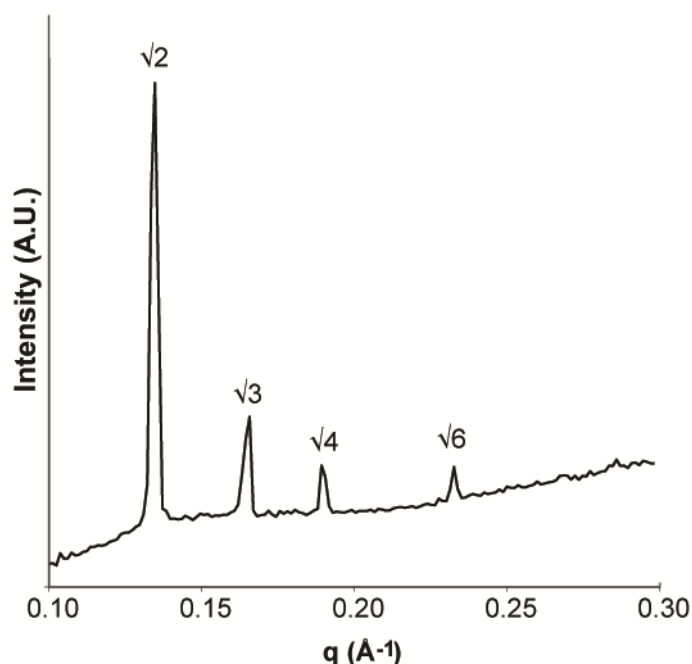
Figure 2-6. SAXS profile of a dispersion of phytantriol-based cubosomes in the COC-based NA chip. The spacing ratios between the peaks indicate the internal structure of the particles was cubic *Pn3m* phase.

2.4.2 Phase characterisation of a dilution-sensitive system

A phase diagram was reconstructed using SAXS for the PHYT, ethanol and water system to allow selection of the most appropriate composition with which to conduct the dilution experiment. The compositions that were re-assessed focused on the trajectories surrounding the sample of interest (25P25E50W) to account for the possibility of subtle changes in the dilution trajectory. The phase structures determined in this study for the phytantriol-ethanol-buffer system are overlaid on the literature phase diagram (**Figure 2-7**) and the phase boundaries were found to be similar. Slight variations could be attributed to the different source of phytantriol and the inclusion of salts in the aqueous phase.[34]
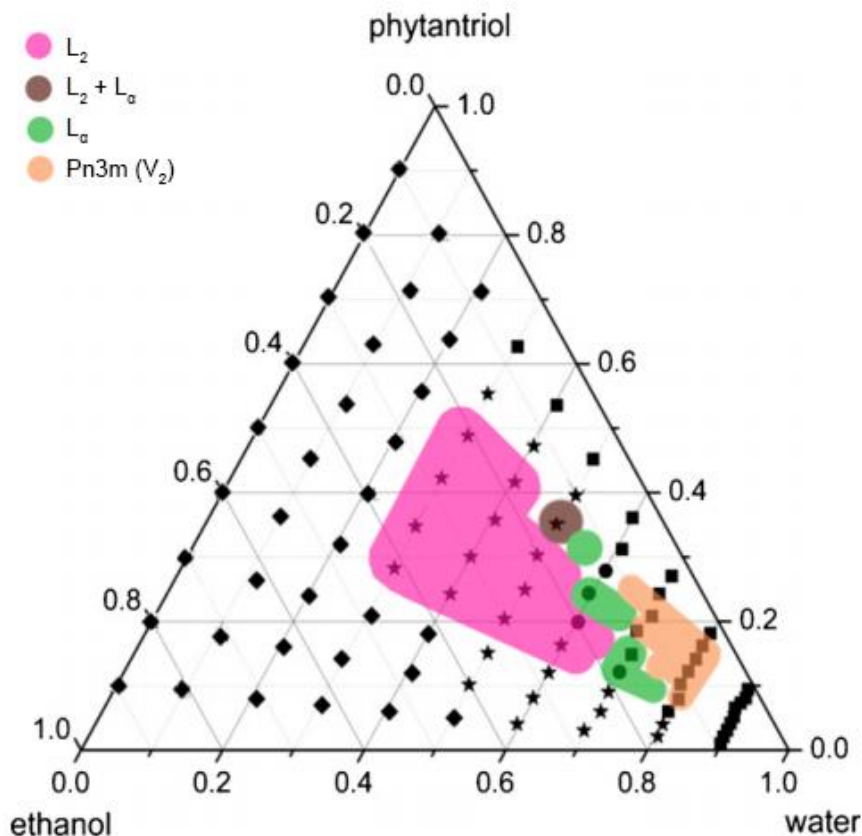
Figure 2-7. Phase diagram of a phytantriol-ethanol-water system reproduced with permission from Han *et al.*[25] with a coloured overlay of the structural data acquired from the phytantriol-ethanol-buffer system. The symbols are from the original source, while the shaded areas are the phase behaviours specific to this experiment. Phase boundaries were found to correspond for the most part. L_2 denotes inverse micellar phase, L_α denotes lamellar phase while *Pn3m* denotes cubic phase.

2.4.3 Monitoring the dynamic phase behaviour of dilution-sensitive LCNP systems in the NA chip

The dilution of the 25P25E50W system was tracked along the microchannels of the NA chip. Flow rates were set to approximately 10-fold slower than that used in a typical NanoAssemblr™ experiment to allow as much retention time *in situ* as practical for the sample to equilibrate. Flow rates for the lipid-based formulation and the aqueous phase were 20 and 65 µL/min, respectively, to achieve an equal division of the two streams as they converged at the Y-junction (attaining equal volumes of the solution along the channel).

It was found that the division of flow at the Y-junction could not be maintained for the duration of the experiment. The proportion of the solutions fluctuated at the Y-junction which resulted in different ratios of the two solutions equilibrating along the length of the channel. It was observed in the one experiment that at times (1.00 to 5.00 sec) there would be approximately equal proportions

of the two flows that would mix along the herringbone structures resulting the cubic *Pn3m* phase

which is represented by the red arrows in the scattering profiles (**Figure 2-8**), in accordance with the

phase diagram (**Figure 2-7**). At other times (0.00 and 6.00 sec), the lipid stream would dominate,

resulting in a less hydrated mixture equilibrating yielding an incomplete transformation. The various

peaks of the accompanying scattering profiles could not be assigned a phase, however it was sus-

pected there were mixed phases present. The inability of this experimental design to reproduce the

same structure at the same position (with the same retention time) could be attributed to the fluc-

tuations of the two streams at the Y-junction.
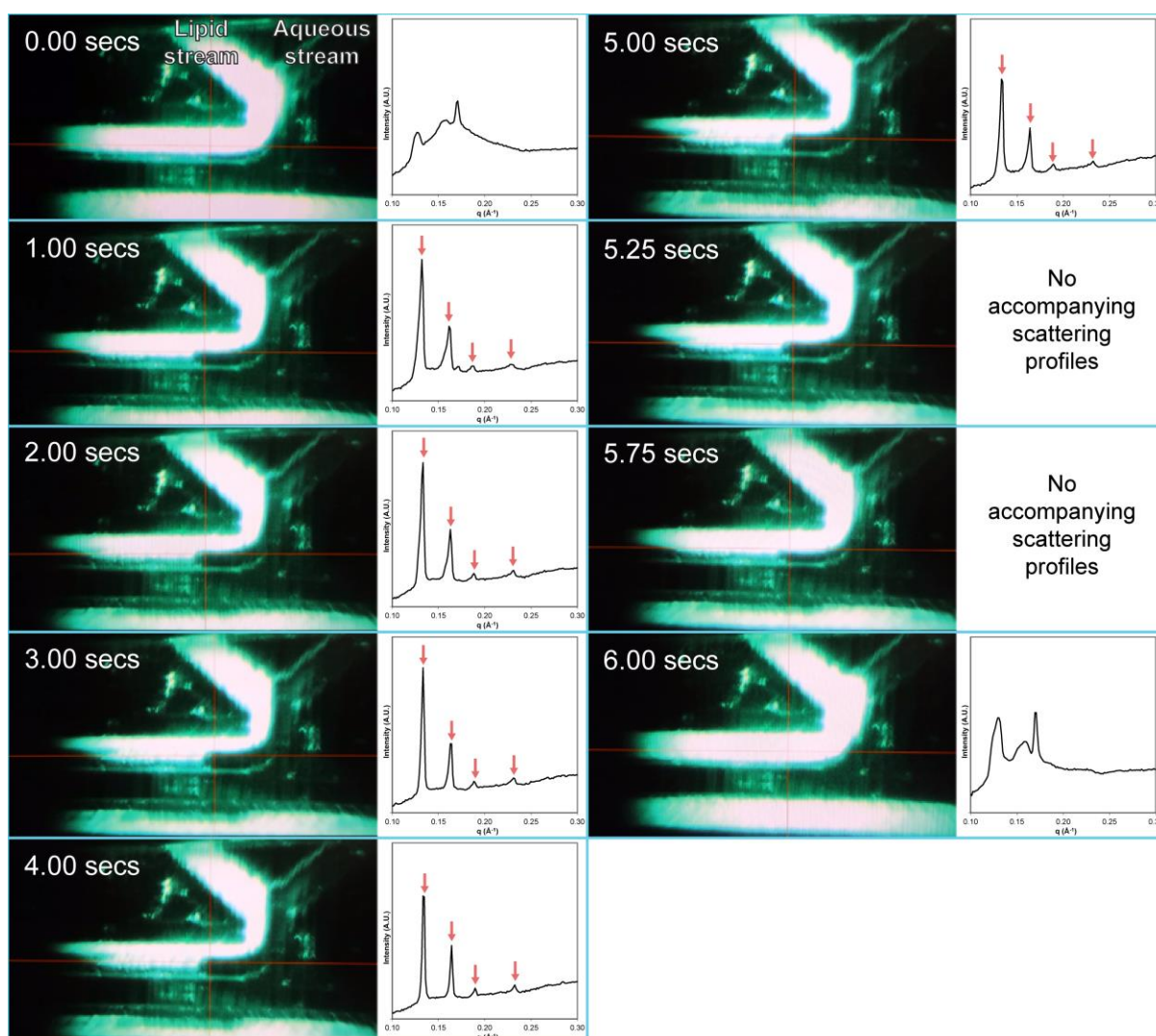
Figure 2-8. Simultaneously tracking the flow behaviour of the phytantriol-ethanol-aqueous phase formulation and aqueous solution at the Y-junction with the structural data (plotted as an intensity vs scattering vector profile) at the same position of the microfluidic channel over time. At flow proportions where there was an approximately equal volume of the lipid and aqueous stream (1.00 to 5.00 secs), cubic *Pn3m* phase resulted as denoted by the red arrows at spacing ratios √2, √3, √4 and √6. When the lipid stream dominated (0.00 and 6.00 secs), peaks were resolved but could not be correlated to any mesophase.

The pulsating behaviour of the two incoming solutions could be attributed to the 10-fold decrease in flow rates compared to typical flow rates used in the NanoAssemblr™. Pendyala *et al*. had noted that where laminar flow is present, the effect of the oscillation becomes more prevalent at lower flow rates in microfluidics.[35] For the configuration of this experiment where the NA chip was repurposed from its original experimental configuration, the oscillations may have also been introduced by the mechanical step nature of the syringe pumps. This can potentially be mitigated by selecting a syringe with an appropriate diameter and volume. More advanced flows can be achieved with pressure pumps which are available from Elve Flow[36] and Dolomite.[37] Pulsing is not observed with this type of pump as the displacement of fluids from the storage vessel does not require contact with mechanical components and is instead via pressure. Nevertheless the experiment was partly successful in generating liquid crystalline structures albeit *in situ* with compromised mixing, and that in this case, differences in mixing at a single spot evident from changes in scattering over time, could be detected spatially to resolve different time points in the reaction.

2.4.4 Monitoring the dynamic phase behaviour of digestion-sensitive LCNP systems in the NA chip

In addition to a dilution-sensitive lipid-based formulation, an enzyme-responsive system was also monitored in the NA chip. An emulsion consisting of phytantriol with 20% w/w tributyrin (PHYT20TB) was digested by lipase after mixing of the emulsion and lipase streams on the chip. After running for 60 mins at a TFR of 4 µL/min and a FRR of 1, no cubic *Pn3m* phase was observed by the end of the channel within the first 2 mins after stabilisation (**Figure 2-9**). The set TFR yielded a retention time of only 11 secs and was likely insufficient time to observe a transformation *in situ*. The syringe drivers in use could not generate a sufficiently slow flow rate to yield a complete transition in the device.

Given that there was no digestion apparent on the chip, the pump was switched off and the scattering acquired over time from the same volume of mixed solutions to confirm whether the short dwell time was responsible. No structure was observed despite the 7 mins of retention time. When the proportion of enzyme in the flow was increased 10-fold relative to the formulation, it became apparent in **Figure 2-9** that V_2 phase could actually be formed and that digestion had occurred *in situ*. Therefore, overall, it appeared that the flow in the NA chip was problematic from a structural determination perspective, so was further investigated using fluorescence microscopy.
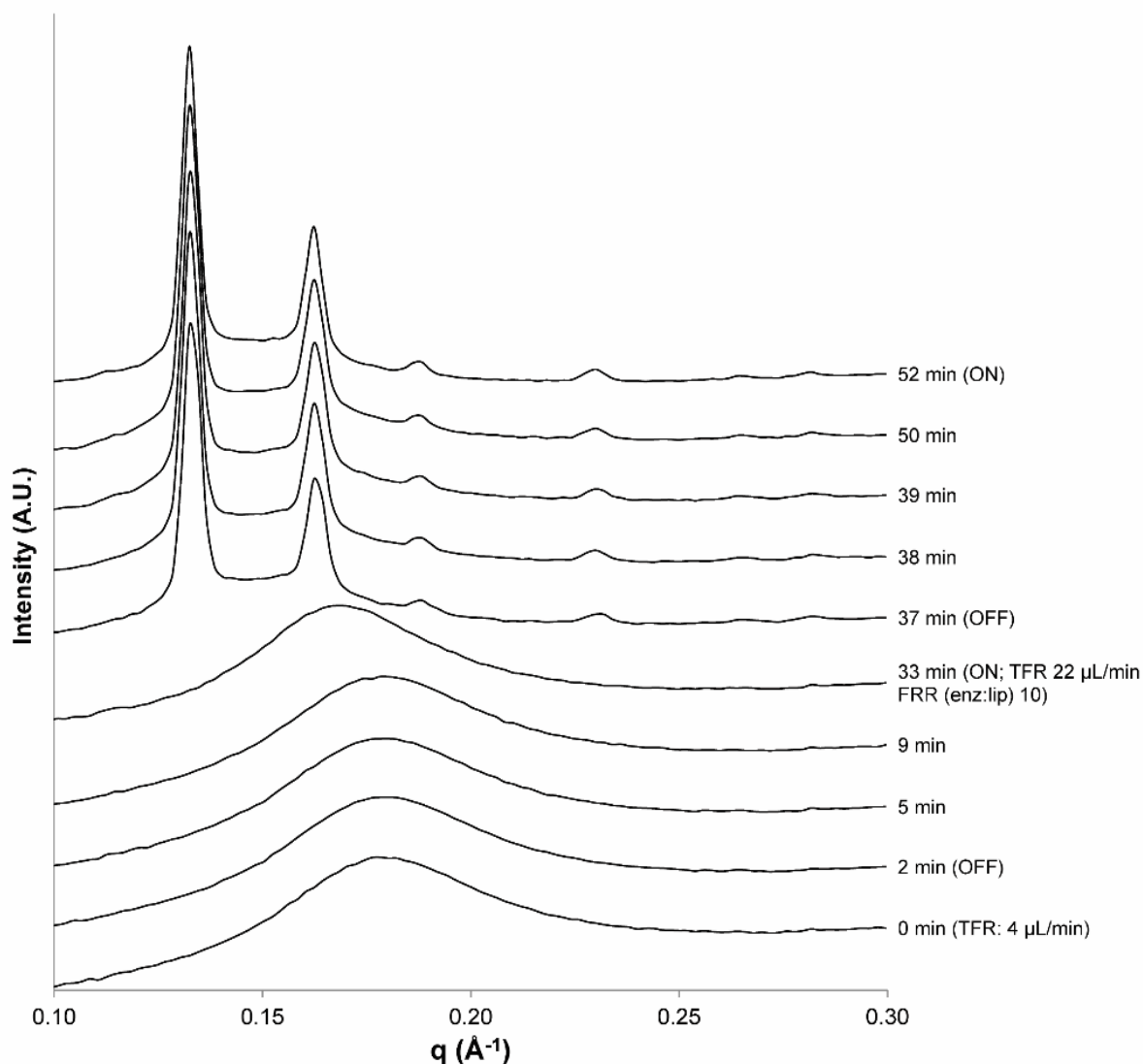
Figure 2-9. Dynamic SAXS profiles monitoring the digestion of the PHYT20TB system in the NA chip at the end point of the microchannel. Initially the system had a TFR of 4 µL/min and a FRR (enzyme:lipid) of 1. The system was allowed to equilibrate for 60 mins before data was acquired. No phase transition was observed so the flow was stopped. After another 30 mins, no transformation was observed. The FRR was then increased to 10 for the next 4 mins before flow was halted, and digestion was apparent *in situ* with the evolution of the six peaks denoting the cubic *Pn3m* phase.

2.4.5 Monitoring flow behaviour in the NA chip

In general, without sufficient mixing and diffusion of the two incoming streams, the kinetics of the reaction may be so slow as to preclude their study *in situ*. Fluctuations in flow at the Y-junction further complicates the behaviour. The presence of staggered herringbone structures introduces chaotic mixing by obstructing the normal flow forcing the two streams to distort,[22] but the effectiveness of this mixing is not clear at least from the structural data obtained thus far.

Consequently, fluorescent dye was used in the channels with a pH shift to interrogate the mixing along the length of the channel using fluorescence microscopy. It was observed that the extent of mixing fluctuated along the channel length (**Figure 2-10**). The fluorescence of the lipid-based formulation mixing with aqueous phase under flow failed to show a consistent gradient from unmixed (blue to green) to fully mixed (red) along the channels. There were sections of the formulation in the channel that would be intensely red, and then later in the channel revert to a less intense red or even green by the end of the channel. Furthermore, the channel filled with premixed sample showed variations in intensity along the length (**Figure 2-10C**). Sections of the channel where the herringbone structures were present showed a relatively more intense fluorescence compared to sections adjacent to the herringbones. The presence of the herringbone structures decreased the local volume which could alter SAXS and fluorescence measurements. Thus, even if the flow behaviour could remain stable for an experiment, the presence of the herringbone structures would alter the local volumes along the channel and the inconsistent mixing behaviour would yield inconsistent transformations.
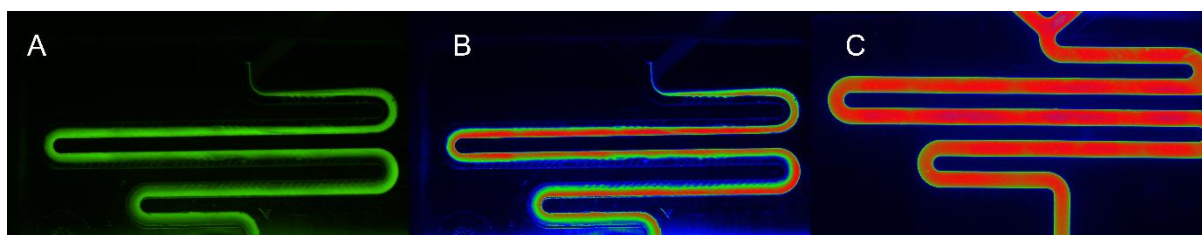
Figure 2-10. A) Micrograph showing the flow behaviour of the fluorescently-dyed dilution-sensitive system (20 µL/min) with the aqueous phase (65 µL/min). B) The same micrograph as A but colours adjusted to Rainbow RGB function for clarity, and C) micrograph of the expected fluorescence should a 50:50 ratio of the two solutions be completely mixed.

Overall, it appeared unlikely that the NA chip could be used to track the transition of stimuli-responsive formulations. Though it may be convenient to repurpose commercially available devices such as the NA chip for such investigations, as revealed in these studies, they must first be heavily scrutinised in terms of mixing behaviour and channel length. Therefore, the NA chip was deemed inappropriate for kinetic studies and another microfluidic device was tested.

2.4.6 Monitoring structural kinetics of digestion-sensitive LCNPs in an "off-the-shelf" microfluidic device

As a very different alternative to the polymer NA chip, a T-mixing device fitted with a microcapillary (OTS-MF device) was studied as another format for *in situ* structural determination. The PHYT20TB

emulsion was digested with lipase in the OTS-MF device (**Figure 2-4**) and the transitions were monitored along the length of capillary using SAXS (**Figure 2-11**). A transition from L_2 phase (broad hump in scattering profile) to cubosomes was observed when scattering was acquired at different positions along the length of capillary. There was an obvious loss of the L_2 phase at 48.2 secs, as shown by the sudden linearity of the baseline**Error! Reference source not found.**. When the TFR was set to 40 μL/min, the mixture was retained in the capillary for up to 82.3 secs, observing the kinetics of the digestion move towards completion with the emergence of V_2 phase (*Pn3m* phase). Vice versa, increasing the flow rate to 100 μL/min shifted the equilibrium towards structures earlier in the digestion, with a prominence in the L_2 phase. The profile at the earliest time of 19.6 secs displayed a minor peak at $q = 0.138$ Å^{-1}, which was associated with the first peak of the cubic *Pn3m* phase, along with the characteristic bump indicative of L_2 phase. Between 47.3 and 49.1 secs there was a sudden loss of the L_2 phase as the baseline flattened out, leaving only the V_2 phase to persist. Structures present earlier in the transformation may have been observed if the TFR had been increased further.
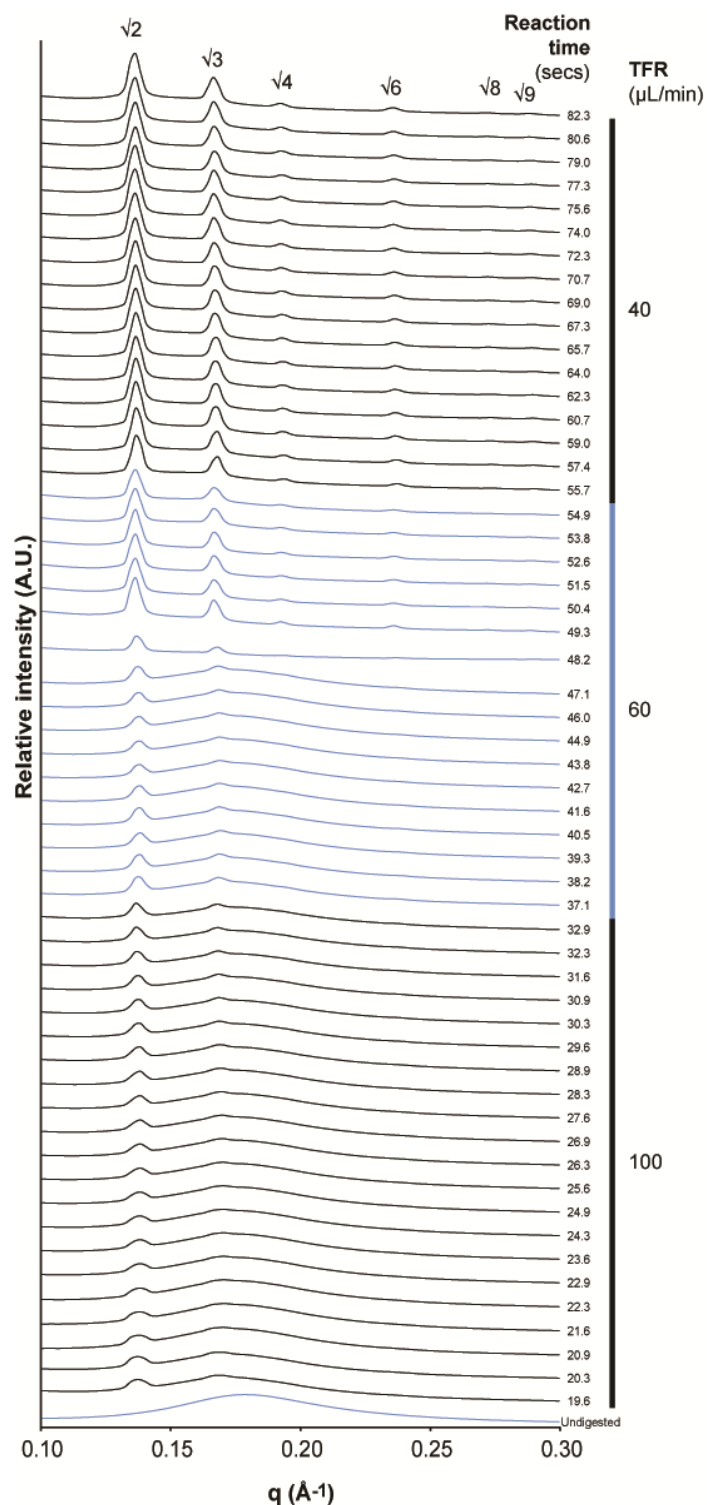
Figure 2-11. Digestion of PHYT20TB in the OTS-MF device as tracked by SAXS along the length of the channel with modification of the TFR. The emulsion displayed a transition from the L_2 phase (characterised by the broad peak) to *Pn3m* phase cubosomes, denoted by the spacing ratio: $\sqrt{2}$, $\sqrt{3}$, $\sqrt{4}$ and $\sqrt{6}$. The corresponding TFR are indicated to the right of the graph. The FRR was fixed at 1 for formulation and enzyme solution. Time points indicate the residence time of the sample in the channels, calculated with the flow rates.

The OTS-MF device was also used to digest a different lipid formulation consisting of another lyotrope, selachyl alcohol. It was expected that the digestion of the selachyl alcohol-based emulsion containing 25% w/w tributyrin (SA25TB) would transition the nanostructure from the L_2 to the H_2 phase in the microfluidic device. The results reflected the expected phase behaviour (**Figure 2-12**). No obvious intermediate phases were identified in the kinetic scattering profiles of this digestion. There was a smaller peak around q = 0.138 $Å^{-1}$ within the TFR of 160 μL/min, and even though this was not the same q value as the eventual first peak of the final H_2 phase (q = 0.130 $Å^{-1}$, lattice parameter = 56.0 Å), both peaks co-existed when the flow rate was set to 80 and 140 μL/min. The peak at q = 0.138 $Å^{-1}$ did not have any additional peaks in the profiles aside from the micellar bump, so no known mesophase could be assigned for this peak. However, it was speculated that this may be another H_2 phase with a smaller lattice parameter (52.4 Å).
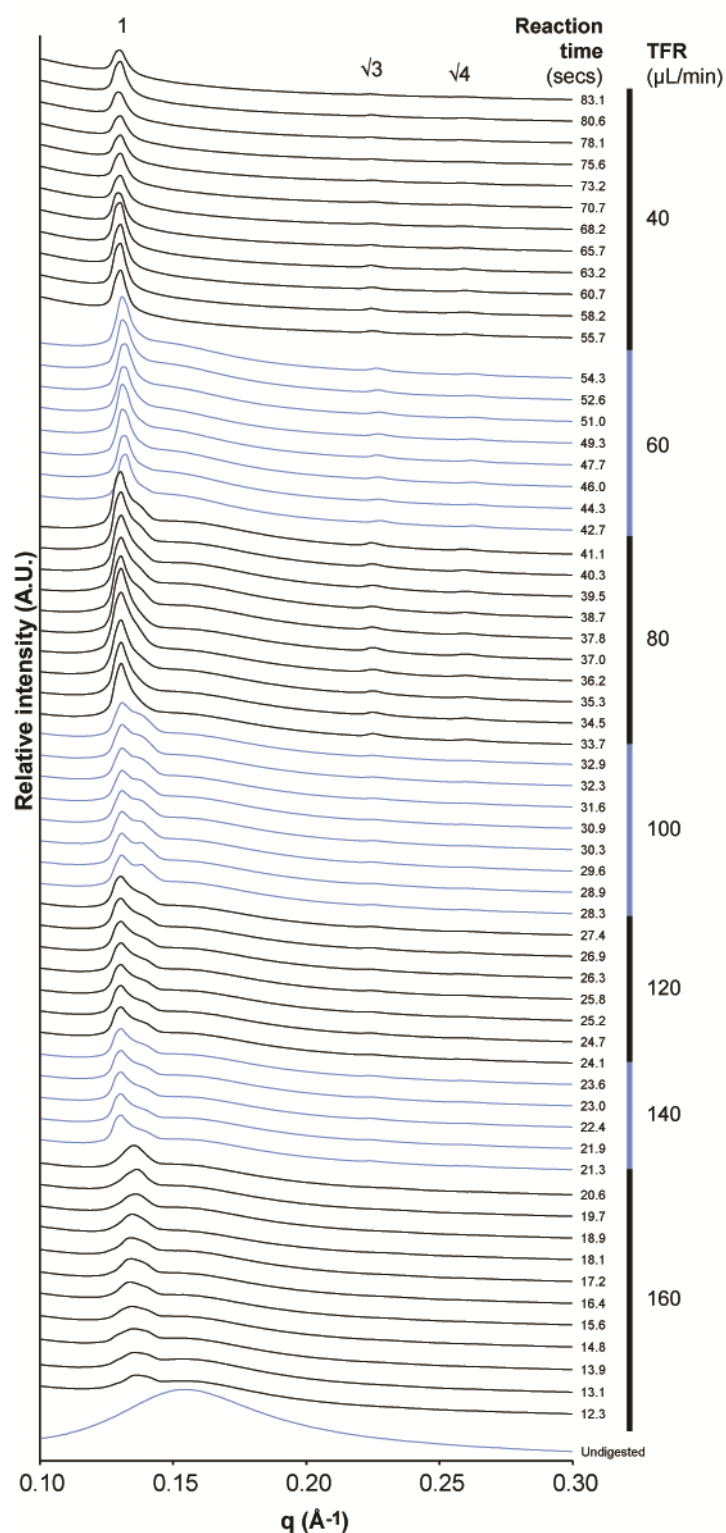
Figure 2-12. Effect of total flow rate on phase structure present at different reaction times in the OTS-MF device of the digestion of SA25TB plotted as an intensity vs scattering vector, q, scattering profile plotted against time. A phase transition from L_2 phase to H_2 phase (denoted by the peaks labelled 1, $\sqrt{3}$ and $\sqrt{4}$) was evident by manipulation of the TFR. The FRR was maintained at 1 for the formulation and enzyme. The corresponding TFR are indicated to the right of the graph. Time points indicate the residence time of the sample in the channels, calculated with the flow rates.

Aside from observing transitions from a disordered L_2 emulsion to liquid crystal dispersion, transformations between liquid crystalline structures were also demonstrated in this microfluidic device. At a lower level of tributyrin (7.5% w/w), the phytantriol emulsion (PHYT7.5TB) can also exist as the H_2 phase.[4] The transition from H_2 to V_2 phase is of particular interest for drug delivery because can demonstrate the transition from slow releasing to fast releasing structure.[7,38] Slow releasing structures would impede the release of drug, enabling drug to be retained for when and where it is needed whilst avoiding unnecessary side effects. Controlling the phase transition to the fast-releasing structure would then enable drug release when required to achieve a greater therapeutic dose where required.[38] In the OTS-MF device, the digestion of the PHYT7.5TB system displayed the anticipated transition from hexagonal to cubic *Pn3m* phase (**Figure 2-13**). More specifically, the decrease in intensity of the H_2 phase peaks and the rise in intensity of the cubic *Pn3m* peaks was observed as the TFR was decreased. The intermediary flow rates showed the emergence of coexisting *Pn3m* phases with different lattice parameters (64.9 and 62.9 Å). There was also a broadening of the peak of the H_2 phase at the 60, 80 and 100 µL/min TFRs likely resulting from particles with more than one set of lattice parameters as with the V_2 phase. It should be noted that even in this more controlled configuration than the pH-stat approach, it is not possible to determine whether there are actually truly mixed phase individual particles or whether there is two discrete populations of particles possessing H_2 phase and V_2 phase. This point is address later in **Chapter 3:Investigating phase transitions of enzyme-responsive lipid-based formulations in chip-based microfluidics**.
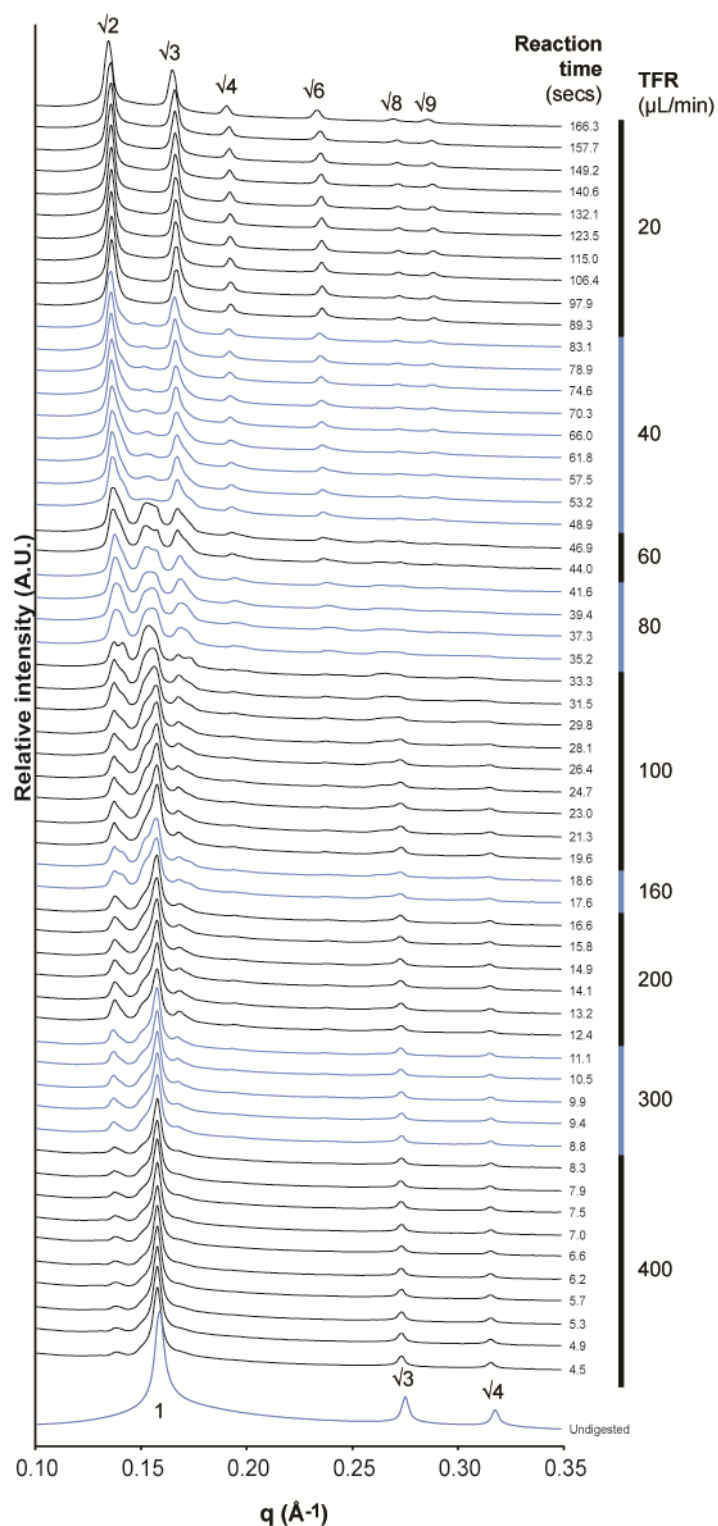
Figure 2-13. The structural evolution of H_2 phase (denoted at the spacing ratio 1, √3 and √4) to V_2 phase of the *Pn3m* geometry (√2, √3, √4, √6, √8, and √9) was exhibited by digestion of PHYT7.5TB in the OTS-MF device. The FRR was fixed at 1 while the TFR was modified to show different stages in the kinetics of the digestion. The corresponding TFR are indicated to the right of the graph. Time points indicate the residence time of the sample in the channels, calculated with the flow rates.

The onset of a phase transition was significantly faster in the OTS-MF device than observed in the pH-stat approach. Formulations in the OTS-MF device showed the emergence of the V_2 phase within 20 secs, whereas up to 1000 secs of reaction time was required before the V_2 phase developed in the pH-stat approach for the digestion of PHYT20TB. One possible explanation for this difference is that the smaller volumes of sample used in the OTS-MF device allowed more access of enzyme to the formulation than seen in the pH-stat approach. It was possible that the relatively greater local concentration of enzyme exposed to the formulation in the format of the OTS-MF device enabled a greater amount of digestion. Hence, phase transitions occurred earlier.

A major flaw noted in this experimental configuration was that there was a noticeable difference between the scattering profiles of adjacent time points from two different TFRs. The sets of kinetic data from different flow rates displayed slightly shifted intensities and positions of the peaks and consequently the lattice parameters despite all results being obtained from the same formulation. The different flow rates used could have results in differing shear stresses that influence the packing behaviour of the lipids during transformation. Microfluidic flows of other liquid crystal systems have previously shown the potential to induce a change in structure[39] or orientation,[40] particularly after disturbances from a linear flow such as the T-junction configuration.

The configuration of the OTS-MF device also did not enable the earliest time points in the digestion to be observed, where the undigested formulation was yet to transition in structure. The earliest time points detected across the digestions was at least 4.5 secs after the fluids meet in the device, by which time digestion was already occurring. This was due to the first 30 mm of capillary being hidden within the T-junction and not accessible to the X-rays. It may be possible to speed up the flow rates to force the structures into the accessible region of the capillary, but the enhanced flow rates may put excess shear stress on the particles, influencing the self-assembly in the phase behaviour and increasing the deviation from the expected non-equilibrium structure.

In spite of its limitations, this OTS-MF device featuring a T-junction was at least able to minimize the consumption of material and simplify the digestion process while still yielding comparable information to the pH-stat approach. Factors such as temperature and pH which were previously controlled in the pH-stat method but absent in this design, did not appear to impose a significant

influence on digestion kinetics, a factor also noted by Phan *et al.* when investigating the experimental parameters in the pH-stat method.[41] The diffusion aspect of this microfluidic design, as well as previous literature designs, appeared sufficient to facilitate the transformation.

2.5   Conclusion

The two microfluidic designs were readily incorporated into the synchrotron SAXS/WAXS beamline to allow high-end analytical structural interrogation by X-ray diffraction. The NA chip could generate LCNPs under specific conditions *in situ*. However, it could not reliably facilitate the tracking of the stimuli-responsive transformations *in situ* due to irreproducibility and inconsistency of the mixing. In contrast, the OTS-MF device allowed monitoring of the phase transitions *in situ*, however the TFR required adjustment to map out an entire phase transformation. These simple devices demonstrated that microfluidics could be used to track changes in phase behaviour, and with more refinement it may be possible to yield more reproducible results.

2.6   References

(1)   Du, J. D.; Liu, Q.; Salentinig, S.; Nguyen, T. H.; Boyd, B. J. A Novel Approach to Enhance the Mucoadhesion of Lipid Drug Nanocarriers for Improved Drug Delivery to the Buccal Mucosa. *Int. J. Pharm.* **2014**, *471*, 358–365.

(2)   Salentinig, S.; Sagalowicz, L.; Glatter, O. Self-Assembled Structures and PKa Value of Oleic Acid in Systems of Biological Relevance. *Langmuir* **2010**, *26*, 11670–11679.

(3)   Spicer, P. T.; Hayden, K. L.; Chester, W.; Lynch, M. L.; Ofori-boateng, A.; Burns, J. L. Novel Process for Producing Cubic Liquid Crystalline Nanoparticles (Cubosomes). *Langmuir* **2001**, *17*, 5748–5756.

(4)   Hong, L.; Salentinig, S.; Hawley, A.; Boyd, B. J. Understanding the Mechanism of Enzyme-Induced Formation of Lyotropic Liquid Crystalline Nanoparticles. *Langmuir* **2015**, *31*, 6933–6941.

(5)   Fong, W. K.; Salentinig, S.; Prestidge, C.; Mezzenga, R.; Hawley, A.; Boyd, B. J. Generation of Geometrically Ordered Lipid-Based Liquid-Crystalline Nanoparticles Using Biologically Relevant Enzymatic Processing. *Langmuir* **2014**, *30*, 5373–5377.

(6)   Dong, Y.-D.; Tilley, A. J.; Larson, I.; Lawrence, M. J.; Amenitsch, H.; Rappolt, M.; Hanley, T.; Boyd, B. J. Nonequilibrium Effects in Self-Assembled Mesophase Materials: Unexpected Supercooling Effects for Cubosomes and Hexosomes. *Langmuir* **2010**, *26*, 9000–9010.

(7)   Phan, S.; Fong, W. K.; Kirby, N.; Hanley, T.; Boyd, B. J. Evaluating the Link Between Self-Assembled Mesophase Structure and Drug Release. *Int. J. Pharm.* **2011**, *421*, 176–182.

(8)   Fong, W.; Negrini, R.; Vallooran, J. J.; Mezzenga, R.; Boyd, B. J. Responsive Self-Assembled Nanostructured Lipid Systems for Drug Delivery and Diagnostics. *J. Colloid Interface Sci.* **2016**, *484*, 320–339.

(9)   Camurus. Development Pipeline https://www.camurus.com/products-grund/ (accessed Dec

22, 2018).

(10) Celsion. Thermodox https://celsion.com/thermodox/ (accessed Dec 25, 2018).

(11) Lyon, P. C.; Griffiths, L. F.; Lee, J.; Chung, D.; Carlisle, R.; Wu, F.; Middleton, M. R.; Gleeson, F. V; Coussios, C. C. Clinical Trial Protocol for TARDOX: A Phase I Study to Investigate the Feasibility of Targeted Release of Lyso-Thermosensitive Liposomal Doxorubicin (ThermoDox ®) Using Focused Ultrasound in Patients with Liver Tumours. *J. Ther. Ultrasound* **2017**, *5*, 1–8.

(12) Warren, D. B.; Anby, M. U.; Hawley, A.; Boyd, B. J. Real Time Evolution of Liquid Crystalline Nanostructure During the Digestion of Formulation Lipids Using Synchrotron Small-Angle X-Ray Scattering. *Langmuir* **2011**, *27*, 9528–9534.

(13) Yaghmur, A.; Laggner, P.; Sartori, B.; Rappolt, M. Calcium Triggered Lα-H2 Phase Transition Monitored by Combined Rapid Mixing and Time-Resolved Synchrotron SAXS. *PLoS One* **2008**, *3*, 1–11.

(14) Khvostichenko, D. S.; Kondrashkina, E.; Perry, S. L.; Pawate, A. S.; Brister, K.; Kenis, P. J. a. An X-Ray Transparent Microfluidic Platform for Screening of the Phase Behavior of Lipidic Mesophases. *Analyst* **2013**, *138*, 5384–5395.

(15) Francesko, A.; Cardoso, V. F.; Lanceros-Mendez, S. Lab-on-a-Chip Technology and Microfluidics. In *Microfluidics for Pharmaceutical Applications: From Nano/Micro Systems Fabrication to Controlled Drug Delivery*; Santo, H. A.; Liu, D.; Zhang, H., Eds.; William Andrew, 2018; pp. 4–36.

(16) Graceffa, R.; Nobrega, R. P.; Barrea, R. A.; Kathuria, S. V.; Chakravarthy, S.; Bilsel, O.; Irving, T. C. Sub-Millisecond Time-Resolved SAXS Using a Continuous-Flow Mixer and X-Ray Microbeam. *J. Synchrotron Radiat.* **2013**, *20*, 820–825.

(17) Song, H.; Tice, J. D.; Ismagilov, R. F. A Microfluidic System for Controlling Reaction Networks in Time. *Angew. Chemie - Int. Ed.* **2003**, *42*, 768–772.

(18) With, S.; Trebbin, M.; Bartz, C. B. A.; Neuber, C.; Dulle, M.; Yu, S.; Roth, S. V; Schmidt, H.; Fo, S. Fast Diffusion-Limited Lyotropic Phase Transitions Studied in Situ Using Continuous Flow Microfluidics/Microfocus-SAXS. **2014**.

(19) Fletcher, P. D. I.; Haswell, S. J.; Zhang, X. Monitoring of Chemical Reactions within Microreactors Using an Inverted Raman Microscopic Spectrometer. *Electrophoresis* **2003**, *24*, 3239–3245.

(20) Kastner, E.; Verma, V.; Lowry, D.; Perrie, Y. Microfluidic-Controlled Manufacture of Liposomes for the Solubilisation of a Poorly Water Soluble Drug. *Int. J. Pharm.* **2015**, *485*, 122–130.

(21) Kastner, E.; Kaur, R.; Lowry, D.; Moghaddam, B.; Wilkinson, A.; Perrie, Y. High-Throughput Manufacturing of Size-Tuned Liposomes by a New Microfluidics Method Using Enhanced Statistical Tools for Characterization. *Int. J. Pharm.* **2014**, *477*, 361–368.

(22) Stroock, A. D.; Dertinger, S. K. W.; Ajdari, A.; Mezic, I.; Stone, H. A; Whitesides, G. M. Chaotic Mixer for Microchannels. *Science* **2002**, *295*, 647–651.

(23) Bottaro, E.; Nastruzzi, C. "Off-the-Shelf" Microfluidic Devices for the Production of Liposomes for Drug Delivery. *Mater. Sci. Eng. C* **2016**, *64*, 29–33.

(24) Terray, A.; Hart, S. J. "Off-the-Shelf" 3-D Microfluidic Nozzle. *Lab Chip* **2010**, *10*, 1729.

(25)   Han, K.; Pan, X.; Chen, M.; Wang, R.; Xu, Y.; Feng, M.; Li, G.; Huang, M.; Wu, C. Phytantriol-Based Inverted Type Bicontinuous Cubic Phase for Vascular Embolization and Drug Sustained Release. *Eur. J. Pharm. Sci.* **2010**, *41*, 692–699.

(26)   Moitzi, C.; Guillot, S.; Fritz, G.; Salentinig, S.; Glatter, O. Phase Reorganization in Self-Assembled Systems through Interparticle Material Transfer. *Adv. Mater.* **2007**, *19*, 1352–1358.

(27)   Salonen, A.; Moitzi, C.; Salentinig, S.; Glatter, O. Material Transfer in Cubosome–Emulsion Mixtures: Effect of Alkane Chain Length. *Langmuir* **2010**, *26*, 10670–10676.

(28)   Clulow, A. J.; Salim, M.; Hawley, A.; Boyd, B. J. A Closer Look at the Behaviour of Milk Lipids during Digestion. *Chem. Phys. Lipids* **2017**, *211*, 107–116.

(29)   Mudie, S. T. ScatterBrain http://www.synchrotron.org.au/aussyncbeamlines/saxswaxs/software-saxswaxs.

(30)   Hyde, S. T. Identification of Lyotropic Liquid Crystalline Mesophases. In *Handbook of Applied Surface and Colloid Chemistry*; Holmberg, K., Ed.; John Wiley & Sons, Ltd, 2001; pp. 299–332.

(31)   Doughty, M. J. PH Dependent Spectral Properties of Sodium Fluorescein Ophthalmic Solutions Revisited. *Ophthalmic Physiol. Opt.* **2010**, *30*, 167–174.

(32)   Schneider, C. A; Rasband, W. S.; Eliceiri, K. W. NIH Image to ImageJ: 25 Years of Image Analysis HHS Public Access. *Nat. Methods* **2012**, *9*, 671–675.

(33)   Hilgenberg. Sample tubes and accessories https://www.hilgenberg-gmbh.de/en/products/test-tubes/sample-tubes/ (accessed Jan 29, 2019).

(34)   Dong, Y. D.; Dong, A. W.; Larson, I.; Rappolt, M.; Amenitsch, H.; Hanley, T.; Boyd, B. J. Impurities in Commercial Phytantriol Significantly Alter Its Lyotropic Liquid-Crystalline Phase Behavior. *Langmuir* **2008**, *24*, 6998–7003.

(35)   Pendyala, R.; Jayanti, S.; Balakrishnan, A. R. Flow and Pressure Drop Fluctuations in a Vertical Tube Subject to Low Frequency Oscillations. *Nucl. Eng. Des.* **2008**, *238*, 178–187.

(36)   ElveFlow. Elve Flow https://www.elveflow.com/ (accessed Sep 10, 2018).

(37)   Dolomite. Dolomite Microfluidics https://www.dolomite-microfluidics.com/ (accessed Sep 10, 2018).

(38)   Fong, W. K.; Hanley, T.; Boyd, B. J. Stimuli Responsive Liquid Crystals Provide "On-Demand" Drug Delivery In Vitro and In Vivo. *J. Control. Release* **2009**, *135*, 218–226.

(39)   Safinya, C. R.; Sirota, E. B.; Plano, R. J. Nematic to Smectic-A Phase Transition under Shear Flow: A Nonequilibrium Synchrotron x-Ray Study. *Phys. Rev. Lett.* **1991**, *66*, 1986–1989.

(40)   Silva, B. F. B. SAXS on a Chip: From Dynamics of Phase Transitions to Alignment Phenomena at Interfaces Studied with Microfluidic Devices. *Phys. Chem. Chem. Phys.* **2017**, *19*, 23690–23703.

(41)   Phan, S.; Salentinig, S.; Hawley, A.; Boyd, B. J. Immobilised Lipase for in Vitro Lipolysis Experiments. *J. Pharm. Sci.* **2015**, *104*, 1311–1318.

Chapter 3: Investigating phase transitions of enzyme-responsive lipid-based formulations in chip-based microfluidics

3.1 Introduction

Part A of this chapter is based on a manuscript that has been submitted to 'Lab on a Chip' hence some of the introduction may be repetitive of previous chapters. Part B will delve further into the kinetics of structural changes by looking more closely at individual drops of formulation.

3.1.1 Part A: Evaluation of a custom-designed microfluidic device to study structure in enzyme responsive LCNP systems

Amphiphilic molecules can self-assemble into a variety of different liquid crystalline geometries, such as cubic or hexagonal phases, when hydrated with solvent.[1] Dispersions of lipidic liquid crystalline phases consist of sub-micron particles that possess the internal phase structure comprising ordered internal hydrophilic and hydrophobic channels.[2] When the bicontinuous cubic (V_2) and inverse hexagonal (H_2) phases are dispersed in excess solvent, the particles are known as cubosomes or hexosomes, respectively. Transitions between structures can be triggered by various stimuli such as enzymes,[3–5] changes in pH[6,7] or a change in ionic strength.[8–10] In application in drug delivery, different phases can exhibit different rates of drug release.[11,12] Thus, there is an opportunity to take advantage of these transformations to control the rate and location of drug availability.

There is a growing recognition that lipid self-assembly during digestion may be crucial to determining interactions with drugs,[13] drug absorption and overall effectiveness of lipid-based drug formulations, and that it could be used to deliberately target specific structural transformations in the gut. Fong *et al.* and Hong *et al.* designed enzyme-responsive lipid-based systems to trigger the structural evolution from an enzyme-responsive and slow-releasing micellar phase structure to a fast-releasing cubic structure.[3,4] Synchrotron-based small angle X-ray scattering (SAXS) coupled to an *in vitro* digestion model (**Figure 3-1A**) was employed to monitor the structural transformations in real time.[14] The initially unstructured emulsion (inverse micellar L_2 phase in **Figure 3-1B**) consisted of the lyotropic lipid phytantriol mixed with a bulky triglyceride, such as tributyrin (**Figure 3-1C**). When together, the triglyceride disrupts the natural tendency of the phytantriol to form the bicontinuous cubic phase. For an emulsion consisting of phytantriol and tributyrin, the scattering initially provided only a broad hump which shifted to the left of the profile as the lipids were digested with the addition of enzyme at 200 secs (**Figure 3-1B**). This implies that the lattice parameter, which can infer the internal water channel dimension, had increased. The hump gradually lessened in prominence dur-

ing digestion as peaks with a spacing ratio of √2, √3, √4, √6, √8, √9 emerged. This specific scattering profile is unique to cubic *Pn3m* phase, which is the structure that phytantriol self-assembles into at these conditions.[15] No apparent intermediate phases were observed.[4]
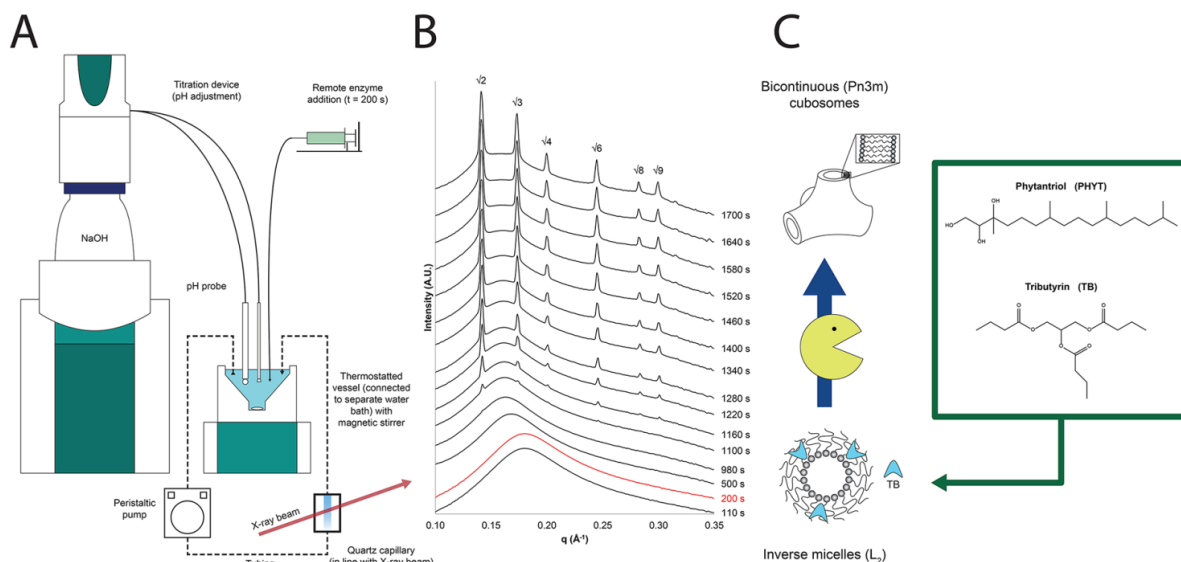
Figure 3-1. A) The experimental configuration for the pH-stat approach integrated with the X-ray beam for SAXS measurements. There are multiple components to the configuration to control parameters such as temperature and pH. B) A set of scattering profiles following the kinetics of the structural evolution during the digestion of a lipid system, showing the transformation from inverse micelles to cubic phase particles after the addition of enzyme at 200 secs. Figure adapted with permission from Hong *et al.*[4] Copyright 2015 American Chemical Society. C) A schematic of the enzyme-induced transformation from the inverse micelle containing phytantriol and tributyrin. The annotation of the peaks with their relative spacing ratios as √2, √3, √4 etc. indicates the presence of the highly ordered cubic phase, forming from the disordered L_2 phase indicated by the broad hump.

Although the pH-stat approach allows tracking of the phase transitions over time, the experimental apparatus required is cumbersome and difficult to incorporate with advanced analytical techniques. The pH-stat equipment, schematically presented in **Figure 3-1**Error! Reference source not found.A, requires at least 20 mL volume to run in flow through mode, which can be prohibitive for investigating special lipid compositions, or where drugs are incorporated into the materials. There is also a delay in formulation transiting from the digestion vessel to the capillary, during which phase transitions are possible. The mixing efficiency inside the vessel is also not well understood. Lastly, the means of remote delivery of the enzyme to the vessel via a syringe driver, means that at early time points there is a non-homogeneous distribution of lipase, presenting uncertainty about non-equilibrium structures and non-uniform compositions. Ideally, the sample should be examined instantaneously once fully mixed.

To reduce the experimental space required by the apparatus, decrease sample consumption, and enable *in situ* analysis of transformations, microfluidics is proposed here as an alternative format.[16] The ability to monitor real-time transformations along the microchannel is a result of the low Reynold's number.[17] This yields laminar flow and diffusion-limited mixing, thus allowing the correlation between the spatial position in the microchannel and the temporal position in the reaction.[18,19]

Microfluidic approaches have been previously applied to assist the analysis of lipid-based systems with conventional techniques.[20] The incorporation of DNA into multilamellar vesicles by Otten *et al.* was determined by a change in the *d*-spacing of the DNA interaxial distance which could be detected with SAXS.[21] The kinetics of this change were monitored along the length of a microfluidic channel where an intersection of three converging channels resulted in the co-axial flow of a DNA solution between two streams containing vesicles. The design of the channels is generalised in **Figure 3-2**. More recently, Ghazal *et al.* monitored a lipidic cubic phase system changing from the *Im3m* phase to the *Pn3m* phase when mixed with calcium ions using a similar channel design.[8] The point of complete diffusion of the ions into the formulation could also be characterised with equations taking into account flow rates and the diffusion coefficient of the substrates among other variables. In both instances, the three co-axial streams allowed diffusion of a stimuli-inducing substance via two interfaces into the stream of the formulation to yield a structural change.
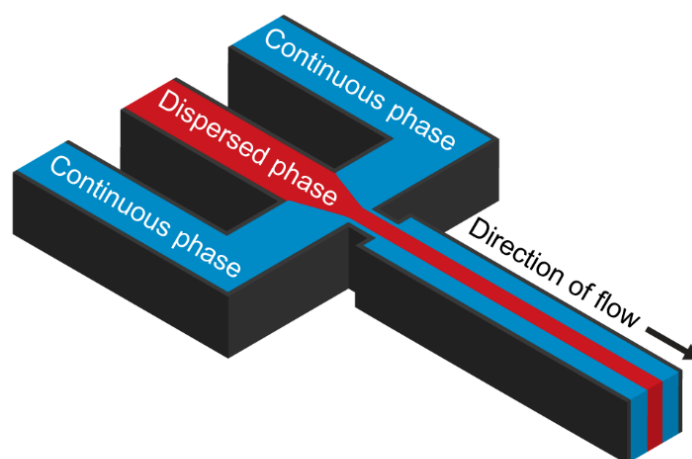

Figure 3-2. Schematic of the channel design used to converge three incoming channels known as hydrodynamic flow focusing. The three flows enter the output channel where the flow of the dispersed phase is sandwiched by the two flows of the continuous phase. There are two interfaces through which substrates can diffuse across for reactions to occur.

A new microfluidic device was conceived to more effectively analyse the phase transitions of stimuli-responsive liquid crystalline nanoparticles (LCNP) taking into consideration channel designs in the aforementioned studies and from devices in the previous chapter. The improved design would feature hydrodynamic flow focusing to exploit the diffusion-controlled mixing of the two solutions. The shortcomings noted in the simpler microfluidic devices in the previous chapters were also taken into account such as the need for a longer length of channel. Therefore, the new device would include hydrodynamic flow focusing channels and an extended length of channel.

Consequently, a custom-fabricated microfluidic chip to study the digestion of lipid-based formulations was assessed for the tracking of structural changes of lipid-based formulations. The performance of the new device was also compared with the standard experimental configuration and the OTS-MF device detailed in an earlier chapter. The suitability of the device would depend on the channel design, flow rate limits, and the compatibility with SAXS.

In contrast to traditional studies where the sample was analysed at a fixed position under a flow-through apparatus, different positions along the channel in the microfluidic devices were able to be aligned with the SAXS beam to allow acquisition of the structural data correlating to different time points in the reaction. The total flow rates (TFR) were manipulated to alter the kinetics of the digestion and enable the observation of the full transition of the stimuli-responsive formulation. Data were then compared to the phase behaviour observed with the pH-stat approach. Two enzyme-sensitive emulsions were examined: phytantriol with 20% w/w tributyrin (PHYT20TB) and phytantriol with 15% w/w tricaprylin (PHYT15TC), selected based on previous studies with these systems.[4] Specifically, the PHYT20TB emulsion was reported previously to transition from the L_2 phase to the cubic *Pn3m* phase with no intermediate phases observed in the pH-stat approach. The PHYT15TC system transitioned from the L_2 phase to the H_2 phase to the cubic *Pn3m* phase. The PHYT20TB system is a well-studied system and a good test case for microfluidics interfacing with SAXS, while the digestion of PHYT15TC is of interest for its transformation across three phases.

3.1.2 Part B: Using droplet-based microfluidics to interrogate the digestion of individual droplets

Characterising the non-equilibrium structures formed during phase transitions of stimuli-responsive lipid-based formulations is important for optimising drug release and formulation design.[22] Non-

equilibrium structures arising during stimuli-initiated phase transitions can influence the intermediate behaviour of drug release which can affect the therapeutic effect as different structures exhibit different rates of release.[11,23] Therefore, by identifying the non-equilibrium (or intermediate) phases, formulators can tailor the formulation to the desired phase transitions.

Kinetic studies of stimuli-responsive systems so far have been conducted on dispersions or bulk phases in configurations where there is inefficient distribution of the stimulus which can lead to heterogeneous transformations, as has been previously explored in **Chapter 1:Introduction**. An uneven application of stimulus can result in particles undergoing phase transformations at different times so the occurrence of multiple phases (or mixed phases) existing at one time point is possible. Monitoring the transformation using SAXS would then sample all the heterogeneously transforming particles and average the data into one scattering profile for that time point. This can be misleading for kinetic studies as the phase transitions were a result of the experimental configuration and not the system itself.

Although mixed phases have been documented to coexist within one particle,[24] to date, it has not been observed as an intermediate structure during dynamic phase transitions. The occurrence of mixed phases is common during phase transitions of milk systems,[25,26] emulsions,[4,8,9] and liquid crystalline dispersions.[27,28] Whether the phases coexist altogether in one particle during the dynamic transformation, forming a gradient of one phase to another, or if each of the phases exist in separate particles has yet to be elucidated. These two concepts have been illustrated in **Figure 3-3**. For example, mixed phases were noted between the transitions of a fast-releasing cubic phase to a slow releasing H_2 phase by Tangso *et al.*[28] The localisation of the phases within the particles would influence the release of drug. In this scenario, if the H_2 phase were to surround the outside of the particles with V_2 phase existing at the centre of the particle, then drug release could be impeded, while if the two phases existed in separate droplets, then the proportion of the two phases would affect the rate. Therefore, determining the mechanism in which each droplet transforms can give a better indication of rate of release.
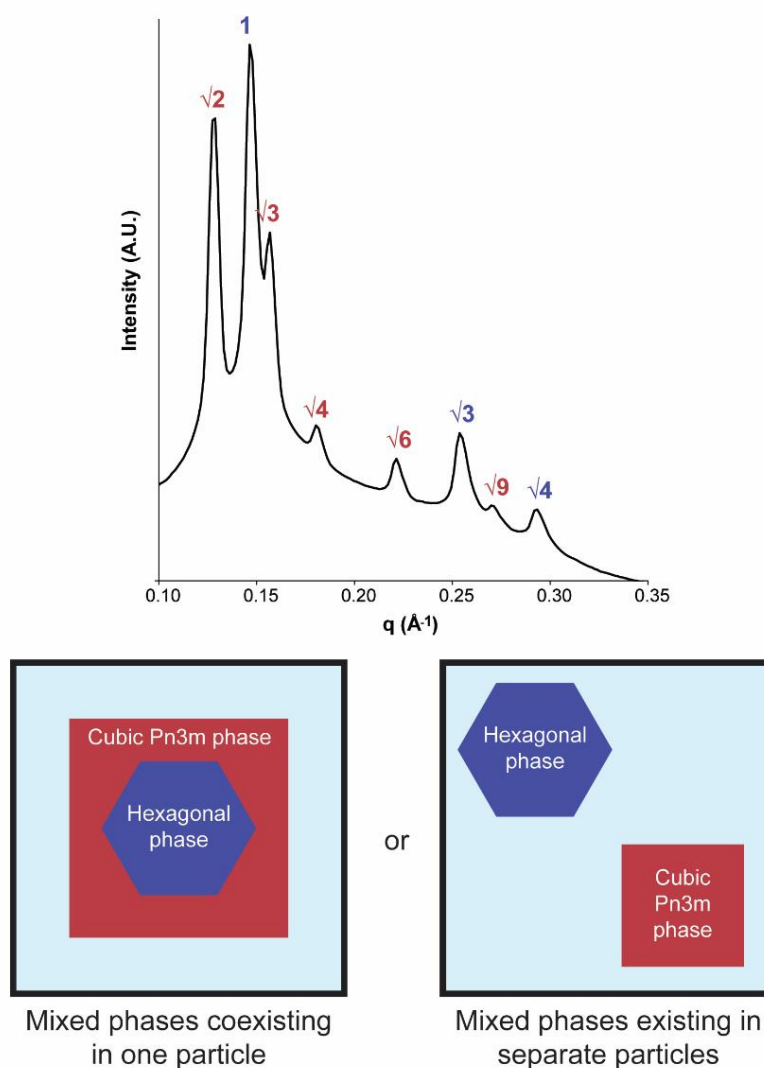
Figure 3-3. The scattering pattern above illustrates the presence of two phases, but because traditional SAXS measurements give an additive picture from all the scattering elements in the beam path, in an LCNP dispersion many particles in all different orientations are giving rise to the overall scattering. Hence it is not possible to differentiate whether the two phases are present in a single particle or are in separate particles of exclusively each phase.

Droplet-based microfluidics can potentially facilitate the monitoring of the individual droplets and particles during phase transitions. The hydrodynamic flow focusing in the previously described S-MF device can facilitate the formation of droplets. Depending on the surface tension and viscosity of the solutions, it is possible to form droplets of the formulation *in situ*.[29,30] Individual droplets or discrete volumes of sample can subsequently be scrutinised using SAXS or microscopy as the analytical technique for example, instead of collecting an average across multiple droplets/particles, offering an alternative perspective to analysing these systems.

The digestion of lipid-based formulations in a droplet format has previously been investigated using microscopy. Droplets were formed using microfluidics with a flow focusing junction and trapped.[31–33] The process was monitored with fluorescence microscopy, where digestion process resulted in a decrease in the diameter of the droplets as the water-soluble digestion products were removed along the flow.

The following work uses crossed polarised light microscopy (CPLM) to capture the phase transitions during the digestion of droplets composed of selachyl alcohol with 25% w/w tributyrin (SA25TB). This particular formulation was chosen as it transitions from a non-birefringent L_2 phase to H_2 phase.[4] The latter phase is anisotropic which exhibits birefringence under polarised light and can be easily detected using CPLM as a bright and textured pattern.[34] The design of the experiments was configured for droplet-based microfluidics in two channel designs: serpentine and droplet trapping.

3.2 Hypotheses and aims

3.2.1 Part A

The contents of this chapter address the same hypotheses as the previous, focusing on an improved microfluidic device, whilst taking into account the lessons learnt from the former devices:

- That a microfluidic device with a sufficiently long length of channel (>30 cm) can access more time points in a reaction to enable complete observation of the phase transformation at one TFR as opposed to off-the-shelf devices.

The following aims were developed to address these hypotheses:

- To fabricate a microfluidic device with a sufficient length of channel and track the full phase transition in a lipase responsive system
- To compare the ability of the improved microfluidic device with former experimental configurations to track phase transitions.

3.2.2 Part B

It was hypothesized:

- That mixed phases exist as a transient gradient within a particle during a transformation of a stimuli-responsive LCNP system.

The following aims addressed these hypotheses:

- To observe the phase transitions during the digestion of discrete volumes of a lipid-based formulation.

3.3 Methods

3.3.1 Materials

Phytantriol (3,7,11,15-tetramethylhexadecane-1,2,3-triol, PHYT) was from DSM Nutritional Products Ltd, Singapore. Selachyl alcohol (SA) was obtained from Hai Hang Industries, China. Tributyrin (TB) and tricaprylin (TC) were obtained from TCI Chemicals, Tokyo, Japan. Sodium chloride was from Chem-Supply, SA, Australia. Trizma maleate, butyric acid (BA), caprylic acid (CA) and 1-mono-capryloyl-rac-glycerol (C8:0, MC) were obtained from Sigma-Aldrich, MO, U.S.A. Calcium chloride dihydrate and glycerol (GLY) were from Ajax Finechem, NSW, Australia. Sodium azide was from Merck Schuchardt OHG, Darmstadt, Germany. Sodium hydroxide pellets were from Ajax Chemicals, NSW, Australia. Water was from a Milli-Q water purification unit (Millipore, Australia). Synperonic F108 (Pluronic F108) was purchased from Fluka, France. Pancreatin was obtained from Southern Biological, VIC, Australia. 4-bromophenylboronic acid (4-BPBA) was acquired from Aldrich, China. Methanol was obtained from Merck KGgA, Darmstadt, Germany. All chemicals were used without further purification.

3.3.2 Sample preparation

3.3.2.1 Digestible lipid formulations

In a scintillation vial (20 mL), phytantriol was weighed out with TB (20% w/w of lipid content) or TC (15% w/w of lipid content). The lipid mixtures were heated until they flowed at 60 °C and vortexed until homogeneous. Lipid (10% w/w) was then dispersed in a Tris buffer solution (containing 1% w/w Pluronic F108), using a Misonix Ultrasonic liquid processor S-4000 (USA) at 30% amplitude for 2.5 min, pulsing on for 4 secs and off for 1 sec. Tris buffer at pH 6.5 was comprised of the following: 150 mM sodium chloride, 50 mM Trizma maleate, 5 mM calcium chloride dihydrate, 6 mM sodium azide, and 50 mM sodium hydroxide.

3.3.2.2 Static simulated 'digested' lipid formulations

Different proportions of the phytantriol, triglyceride and digestion products (fatty acids and mono-glyceride or glycerol) were dispersed in Tris buffer containing 1% Pluronic F108 and processed as

described with the aforementioned formulations. Each formulation contained the same amount of phytantriol with the remainder of the lipid component comprised of required amounts of triglyceride and digestion products. As the amount of triglyceride was decreased in the formulation, the equivalent mass decreased was replaced by the appropriate mol ratios of the fatty acid and monoglyceride or glycerol. To determine the compositions of the simulated 'digested' formulations, it was assumed that TB was digested to yield a 1:3 glycerol:fatty acid mol ratio,[35] while TC digested to a 1:2 monocaprylin:caprylic acid mol ratio.[36] The compositions of each formulation have been described in **Table 3-1** and **Table 3-2** for PHYT20TB and PHYT15TC, respectively.

Table 3-1. Composition of formulations to construct the phase diagram of the 'digested' PHYT20TB emulsion. The formulation code contains the % w/w of TB and the % w/w of the digestion products (DP) in the formulation.

Formulation	Buffer (g)	PHYT (g)	TB (g)	3BA+GLY (g)
20TB-0DP	2.700	0.240	0.012	0.057
18TB-2DG	2.700	0.240	0.011	0.058
16TB-4DP	2.700	0.240	0.010	0.059
14TB-6DP	2.700	0.240	0.008	0.061
12TB-8DP	2.700	0.240	0.007	0.062
10TB-10DP	2.700	0.240	0.006	0.064
0TB-20DP	2.700	0.240	0.000	0.071

Table 3-2. Composition of formulations to construct the phase diagram of the 'digested' PHYT20TB emulsion. The formulation code contains the % w/w of TB and the % w/w of the digestion products (DP) in the formulation.

Formulation	Buffer (g)	PHYT (g)	TC (g)	2CA+MC (g)
15TC-0DP	2.700	0.255	0.045	0.000
12TC-3DP	2.700	0.255	0.036	0.009
9TC-6DP	2.700	0.255	0.027	0.018
6TC-9DP	2.700	0.255	0.018	0.027
3TC-12DP	2.700	0.255	0.009	0.036
0TC-15DP	2.700	0.255	0.000	0.045

3.3.2.3 Lipid-only mixture (LOM)

Selachyl alcohol (at room temperature) and tributyrin (25% w/w) were weighed out in a 20 mL scintillation vial. The mixture was mixed by vortex for 1 min until it was isotropic.

3.3.2.4 Enzyme suspension

A lipase suspension was rehydrated from a freeze-dried preparation of pancreatic lipase with Tris buffer (containing 1% w/w Pluronic F108) prepared according to the method described by Clulow *et al.*[26] Activity was determined to be 500 TBU/mL of digest.

3.3.3 Equilibrium phase behaviour

The static simulated 'digested' lipid formulations were loaded into quartz capillaries for SAXS measurements. The formulations were analysed using an X-ray wavelength λ = 0.954 Å (equivalent to energy = 13 keV) and a sample to detector distance of 1531 mm (determined by calibration with silver behenate) which provided a q range of 0.0111 - 0.659 Å^{-1}, where q is the scattering vector determined by the equation: $q = 4\pi/\lambda \sin(\theta/2)$, where θ is the scattering angle. Acquisition time of the data was set to 5 secs. The two-dimensional scattering patterns were acquired using a Pilatus 1M detector with an active area of 169 × 179 mm^2 with 172 μm pixel size. The scattering patterns were then integrated into a one-dimensional scattering function I(q) using the in-house software, Scatterbrain (version 1.15).[37]

Identification of the nanostructures from the scattering function was determined by correlating the relative spacing ratios between the positions of the Bragg peaks to literature.[38]

3.3.4 Microfluidic devices

3.3.4.1 "Off-the-shelf" microfluidic device (OTS-MF)

Refer to Chapter 2 (**2.3.4 Off-the-shelf microfluidic device (OTS-MF device)**).

3.3.4.2 Serpentine microfluidic device (S-MF)

The custom microfluidic device illustrated in **Figure 3-4** was fabricated at the South Australian node of the Australian National Fabrication Facility. The device featured microchannels dry etched into quartz to a depth of approximately 60 μm. The same device but with a channel height of 30 μm was used for the microscopy studies. The channel design included two inlet channels where one inlet port divided into two channels and converged at the intersection with the other inlet channel. Flow proceeded through a serpentine length of channel of length ~350 mm before exiting from

the outlet port. Two syringes (1 mL, from BD, U.S.A.) driven by a syringe driver as described for OTS-MF delivered the solutions to the device via PTFE tubing (0.012"ID x 0.030"OD, Cole-Parmer, U.S.A.).
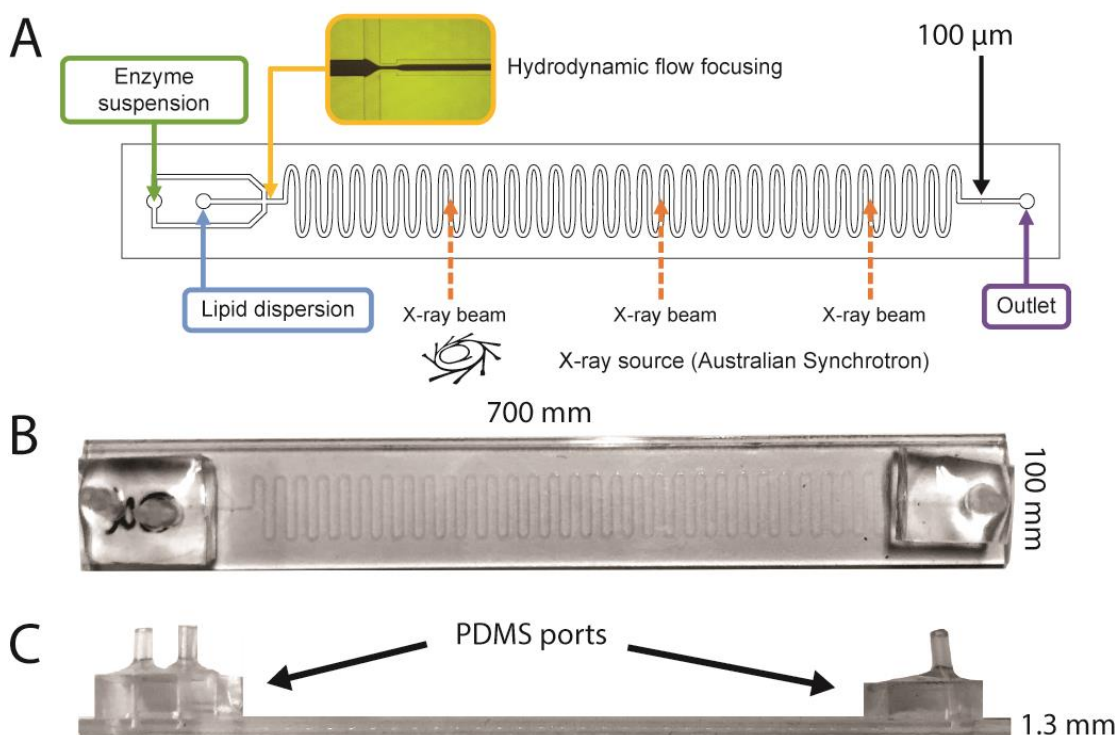
Figure 3-4. A) Diagram of the S-MF device and how it was used in line with SAXS. The enzyme solution and lipid dispersion were delivered to the inlet channels on the left via syringe pump. When the solutions converged at the intersection, the enzyme solution pinched the lipid dispersion to form a co-flow of solutions known as hydrodynamic flow focusing (inset). The X-ray beam was focused at various positions along the microchannel to track the kinetic nanostructures. B) Top view of the device. C) Side view of the device. There were three ports in which the tubing can be inserted to deliver the solutions into the channels (left) or remove waste (right).

3.3.4.3 Droplet-trapping microfluidic device (DT-MF)

The droplet-trapping microfluidic (DT-MF) device was fabricated using the same process as the S-MF device. The first half of this device features hydrodynamic flow focusing exactly like that shown in the S-MF device. The latter half features five sets of droplet-trapping designs (**Figure 3-5**). In these features, the incoming channel splits into three channels (**Figure 3-5B**):

- one channel continues in the same direction but widens into two consecutive round openings where the droplets can be trapped, then narrows
- two other channels flow around the droplet traps forming a circle.

All three channels reconverge before flowing to the next set of trapping features.
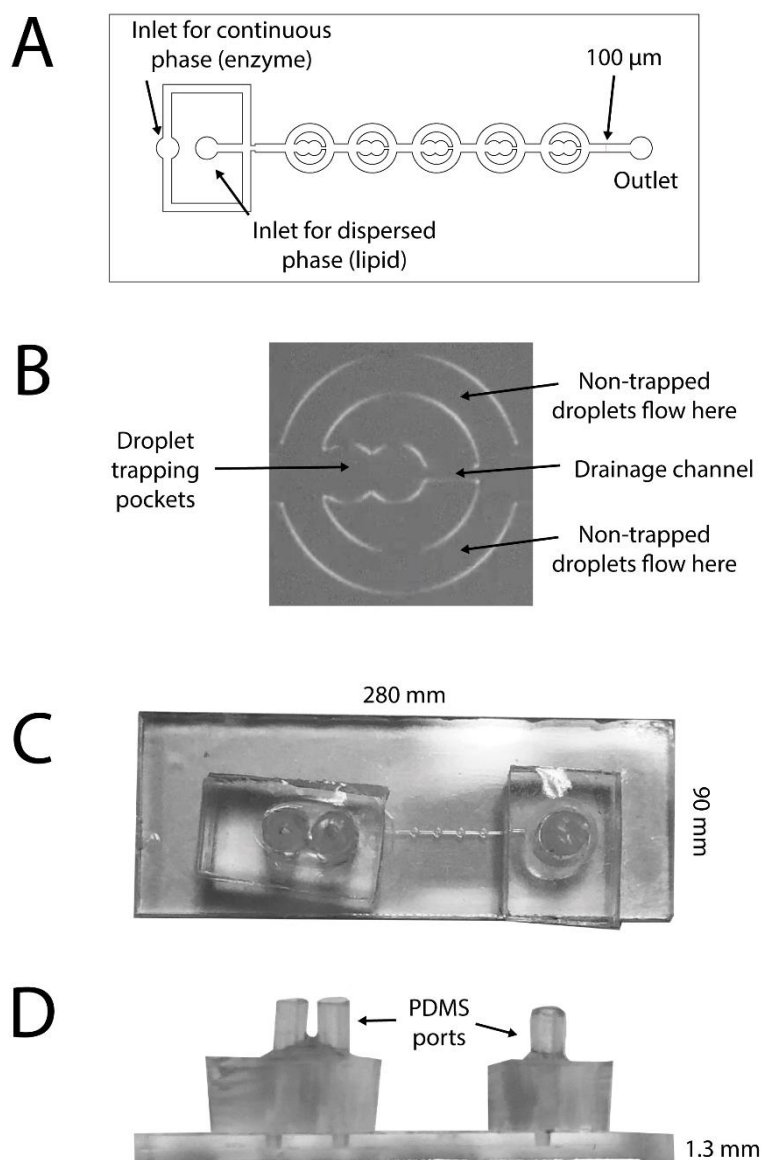
Figure 3-5. A) A not-to-scale schematic of the channels in the DT-MF device. It features two inlet channels which converge at an intersection for hydrodynamic flow focusing. B) Droplets formed within the device can be passively trapped within the doubly circular pockets for an extended amount of time. Excess droplets not trapped in the pockets continue to the flow around the pockets towards the outlet port. The flow of continuous phase can still pass around the trapped droplets and drain back into the main flow via the drainage channel. C) Top view of the device. D) Side view of the device. There were three ports in which the tubing can be inserted to deliver the solutions into the channels or remove the waste.

3.3.4.3.1   Formation of droplets

The LOM and enzyme suspension were drawn up into separate Luer-Lok syringes (1 mL, from BD, U.S.A) with a 30G needle (BD, U.S.A.). After filling the syringes, the 30G needle was replaced with a 27G syringe tip (Nordson Corporation, U.S.A.) attached to PTFE tubing (0.012"ID x 0.030"OD, Cole-Parmer, U.S.A.). The tubing was connected to the corresponding inlets of the microfluidic device.

Formation of droplets was achieved with the LOM flowing at 2 μL/hr with the New Era 4000 syringe pump (U.S.A.) and the enzyme suspension flowing at 50 μL/hr with the Harvard Apparatus 11 plus syringe pump. Formation of droplets required up to 1 hr to stabilise. Experiments were run at ambient temperatures.

3.3.5 Monitoring the real-time evolution of structure during digestion

3.3.5.1 In microfluidic devices

Structural kinetic studies were performed on the SAXS/WAXS beamline at the Australian Synchrotron, VIC, Australia.[39] The microfluidic devices were fixed to a metal support, with the microchannels positioned in-line with the X-ray beam. The enzyme and lipid formulation were flowed to the devices via the syringe driver at a flow rate ratio of 1 and variable TFR. The system was stabilized for an appropriate amount of time before structural data were acquired. Data were acquired at consistent increments along the length of the microchannels, noting the exact locations to determine the corresponding reaction time points. Specifically, for the S-MF device, a table is provided in **Supplementary table 3-1** at a TFR of 10 μL/hr indicating where along the channel the X-ray beam was focused and the correlated time point (or retention time). Experiments were run at hutch temperature (~27 °C).

The scattering experiments conducted with the OTS-MF device with the setting described in **3.3.3 Equilibrium phase behaviour**. The S-MF device in other experiments required a wavelength of 0.620 Å (20 keV) with sample to detector distance of 1561 mm which provided a q range of 0.0193 - 0.611 Å^{-1}. Acquisition time of the data was set to 30 secs.

3.3.5.2 In the pH-stat apparatus

To compare with microfluidic experiments, equivalent experiments were run with the pH-stat apparatus. The pH-stat apparatus was set up to digest 1 mL of formulation with 1 mL of enzyme, and the mixture diluted to 17 mL with Tris buffer to facilitate a flow-through digestion as described by Warren *et al.*[14] The settings for SAXS were the same as for the OTS-MF device. Digestions were run at 37 °C, while the pH was maintained at 6.5 with automated titration (0.2 M NaOH). Once digested to completion at 380 secs, 1 mL of the digested solution was added to 10 μL of 5 mg/mL 4-BPBA in methanol for particle size testing.

3.3.6   Determination of the completion of diffusive mixing

The digestion of the lipid in the microfluidic devices was limited by the diffusion of the enzyme at the lipid-enzyme solution interface to the far edge or centre of the lipid stream for the OTS-MF and S-MF devices, as represented by x_2 and x_3 respectively in **Figure 3-6**. To determine the position of complete diffusion along the microchannel, the time of complete mixing, t, was first calculated using **Equation 3-1**:

Equation 3-1. Equation to determine the time of complete mixing across a distance, x, and taking into account the diffusion coefficient, D.

$$t = {x^2}/{2D}$$

This equation takes into account the lateral distance the solute, x, in this case is lipase, must travel across (which has been illustrated in **Figure 3-6**), and its diffusion coefficient, D.[8,40] For the OTS-MF device, the distance that the enzyme needed to diffuse across was 100 µm which is half the width of the X-ray beam and the only relevant region for calculating the diffusion. The diffusion coefficient of the pancreatic lipase was obtained from literature[41] and adjusted for Taylor-Aris dispersion using **Equation 3-2**.[42]

Equation 3-2. Equation used to adjust the diffusion coefficient of molecules, taking into account the Taylor-Aris dispersion.

$$\frac{K}{D} = 1 + \frac{1}{210}\left(\frac{Ud}{D}\right)^2$$

The complete mixing time was then converted to a distance along the length of the microchannel using **Equation 3-3**.

Equation 3-3. Equation to determine the distance of complete mixing along a microchannel.

$$Distance = Linear\ velocity \times t$$

The linear velocity was determined from the flow rates and the volume of the channels. An example of these equations used for the total flow rate of 1200 µL/hr can be found in

Supplementary table 3-2. The distances of complete diffusion with adjusted diffusion coefficients for the pancreatic lipase are shown in **Supplementary table 3-3** and **Supplementary table 3-4** for the OTS-MF and S-MF device, respectively.
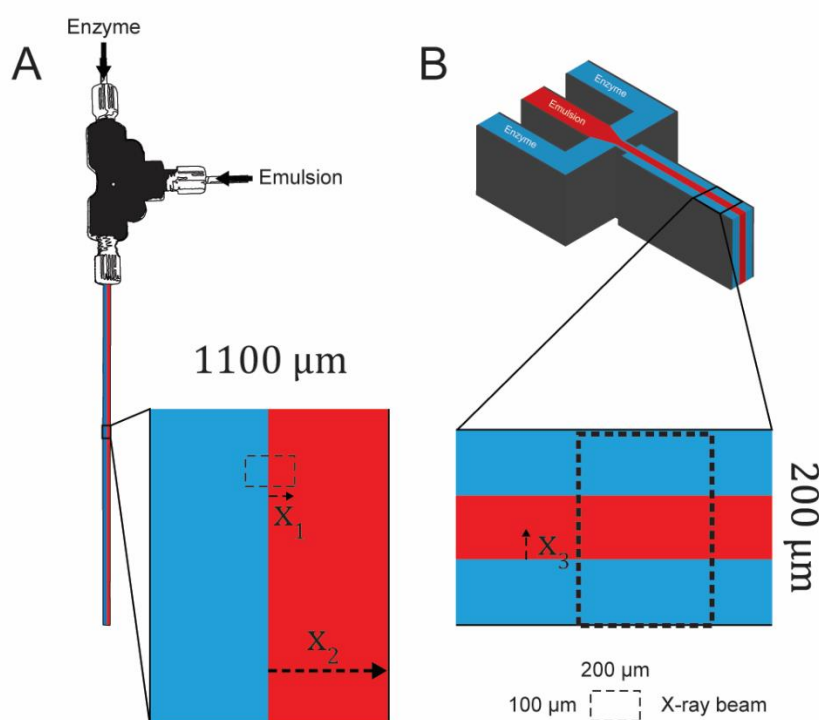
Figure 3-6. Schematic depicting the distance, x, the enzyme in the blue stream needs to traverse across the flow of the emulsion (red) to be considered fully mixed in the two microfluidic devices. A) The enzyme needed to travel 420 μm, which was half the width of the capillary of the OTS-MF device (x_2) to access all droplets in the emulsion. However, given the X-ray beam was only 200 μm in width and focused at the centre of the channel, calculations only needed to take into account half this dimension (x_1). B) As there were two streams of enzyme on either side of the stream of emulsion, enzyme only needed to travel to the centre of the enzyme flow (x_3) to be considered fully diffused.

3.3.7 Comparing particle size between the pH stat and microfluidics techniques

Dynamic light scattering (Zetasizer Nano ZS, Malvern Instruments, UK) was performed on samples obtained from the end point of digestion of PHYT20TB in the microfluidic devices at different TFR. The digested sample was collected (2 μL), diluted in 995 μL of Milli-Q-grade water and run immediately without inhibitor. Experiments were run in triplicate. Inhibited samples collected from the pH-stat digestions were also assessed with the same protocol.

3.3.8 Microfluidic devices in line with CPLM

Both of the following microfluidic devices were secured to a glass microscope slide and placed on an upright microscope fitted with crossed polarizing filters (Nikon ECLIPSE Ni−U). A digital camera

(DS-U3) from Nikon, Tokyo, Japan (4x and 10x objectives) was used to acquire the images with a frame rate of 4.45 frames per second in conjunction with the software NIS-Elements (version f 4.0). The arrangement is shown in **Figure 3-7**. The freeware, ActivePresenter (version 7.3.3), was used to acquire screen video of the microchannels.
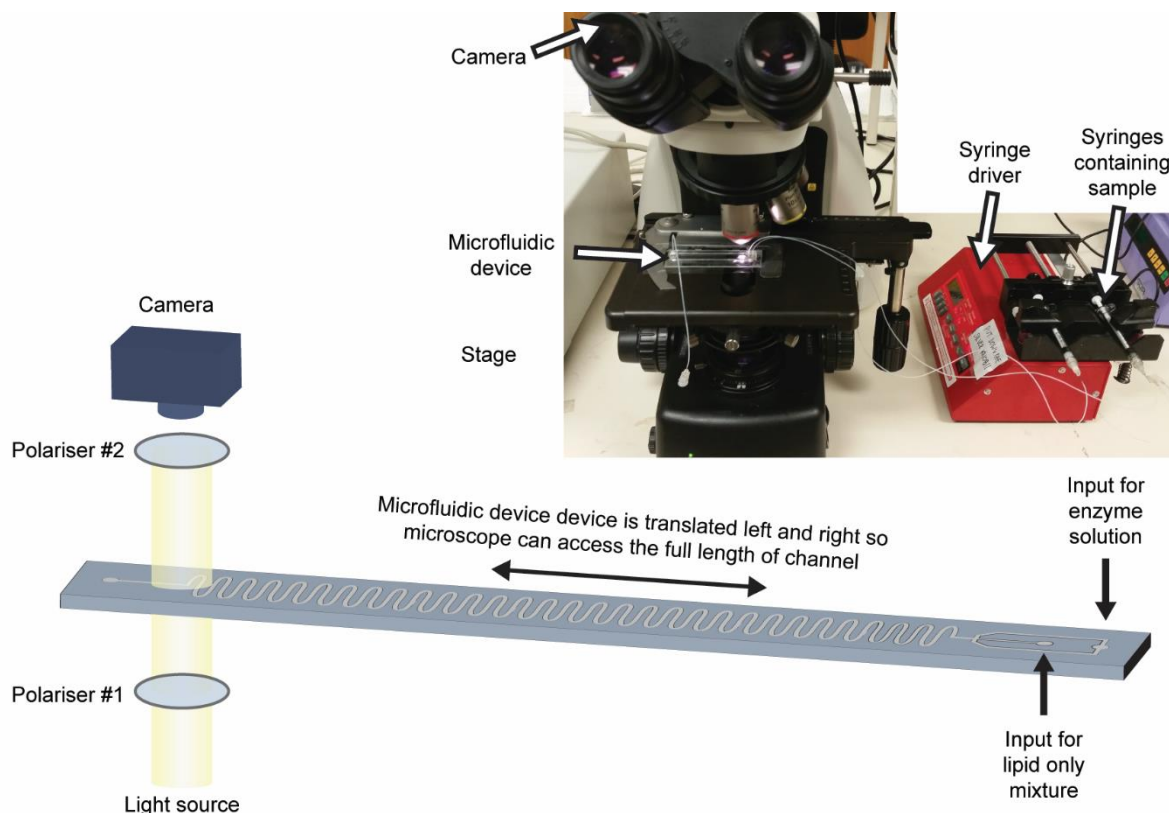
Figure 3-7. Schematic and photo (top right) of the microfluidic device (applicable for both the S-MF and the DT-MF device) in line with CPLM. The device is fixed to the glass slide which is also fixed to the holder on the stage, allowing it to be moved around to access all lengths of the microchannel. The schematic shows a simplified configuration of the microfluidic device in between the two polarisers of the microscope. This configuration where the camera was focused at the end position of the S-MF device was used to acquire the results in **Figure 3-15**.

3.4   Part A: Results and discussion

The use of microfluidics in conjunction with traditional analytical techniques to investigate the transformations of enzyme-responsive liquid crystalline systems can enable greater control over experiments. Microfluidics can also be customized to achieve any experimental manipulations through alterations in channel designs, material or the device, or additional electronic components. The custom designed and manufactured microfluidic device was assessed for factors including mixing

efficiency, resolution of the device in relation to SAXS and particle sizing. Results were also compared with equivalent digestion performed in the pH-stat approach and the previously reported OTS-MF device.

3.4.1 Influence of microchannel design on mixing

Channel design determines the flow of solutions and mixing efficiency in microfluidic devices. The OTS-MF device featured a T-junction allowing the convergence of the lipid formulation and enzyme suspension. The two solutions flowed as two streams along the length of the capillary, sharing one interface between them as can be seen in **Figure 3-8**. As such, enzyme could only diffuse through one interface of the lipid stream to induce digestion. The S-MF device featured three converging channels that resulted in hydrodynamic flow focusing and the co-axial flow of three streams (lipid emulsion sheathed by two enzyme streams).[8,18] This provided relatively more interfacial area through which the enzyme can diffuse.
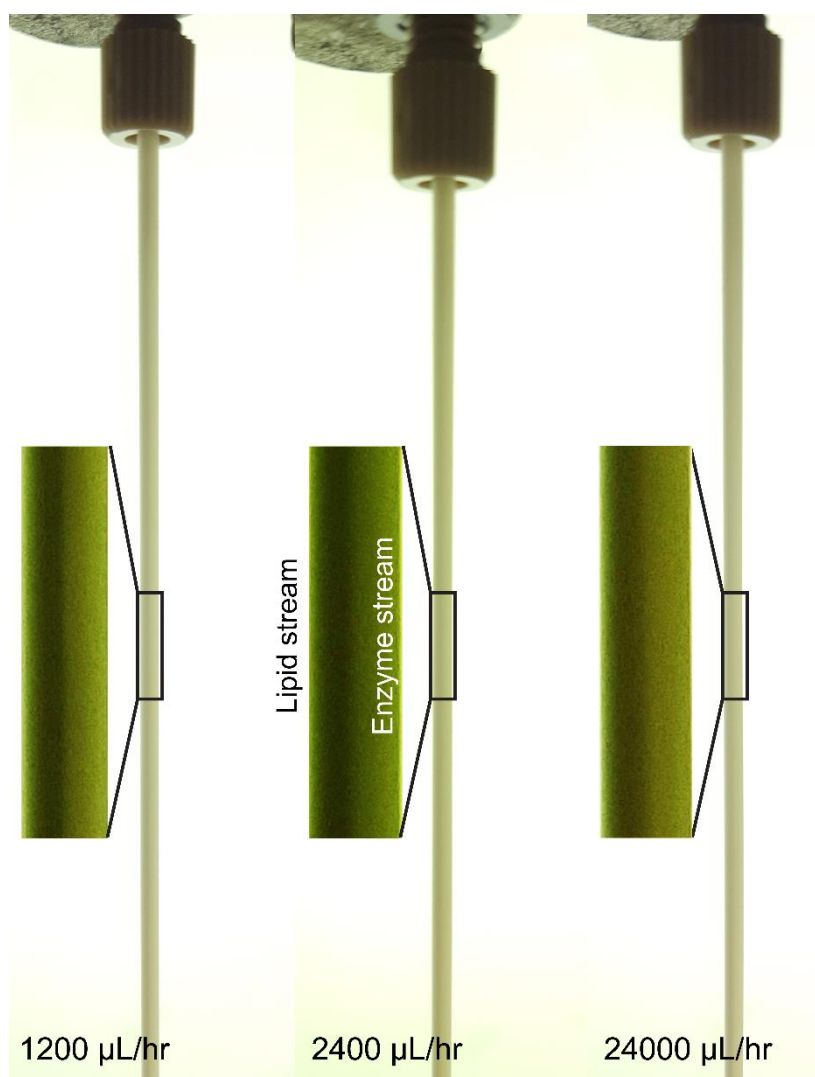
Figure 3-8. Image of the digestion of PHYT20TB in the OTS-MF device at various flow rates (FRR was 1:1). The inset figures have the contrast increased to highlight the division of the two streams. The darker section is the lipid stream which is opaque, while the enzyme stream is semi-transparent.

The position of complete mixing relative to the full length of the respective microchannels was calculated to occur earlier along the channel for experiments in the S-MF device than in the OTS-MF device, and slower TFR were calculated to delay the diffusion process. At the slowest TFR (10 μL/hr) used in the S-MF device, complete diffusion was calculated to occur by 8% of the entire length of the channel (28 mm from the point of initial contact) while complete mixing was anticipated to occur by 2% of the channel length at 40 μL/hr (7 mm from the point of initial contact). A similar trend was calculated for the OTS-MF device where shorter distances of complete diffusion were calculated for faster TFR (0.14% of the channel when set to 12000 μL/hr), and vice versa longer distances were calculated for slower TFR (14.4% of the channel when set to 120 μL/hr). The greater flow rates enhanced the Taylor-Aris dispersion effect and consequently the diffusion coefficient of the lipase. As such, the position of complete diffusion into the lipid stream was calculated to occur earlier along the channel. Although the distance to complete mixing in the OTS-MF device was at most 14.4 mm from the point of convergence, this distance was within the section of capillary hidden in the T-junction and inaccessible to X-rays (or any other analytical technique), therefore data obtained at all positions along the remaining length of the capillary reflected completely mixed systems, and any non-equilibrium structures would not be due to incomplete mixing. As for the S-MF device, the position of complete mixing occurred within the first 8% of the channel, leaving more than 32 cm of the channel available for tracking phase transitions.

3.4.2 Phase diagram of samples representing equilibrium compositions expected during 'digestions'

The structure of samples at specific compositions representing different stages of digestion were measured using SAXS to compare to the structures formed during the dynamic digestion experiments (**Figure 3-9**). The relative spacing between the peaks was used to determine the different phases and the lattice parameters of the different structures were also calculated over time.

Each formulation comprised of the same amount of structure forming lipid, PHYT, and varying amounts of triglyceride and/or the digestion products (DP). The DP were comprised of the fatty acids and monoglycerides or glycerol in their appropriate mol ratios. The ratio of triglyceride to DP was varied to represent different extents of digestion and was described in **Table 3-1** and **Table 3-2**.

Without any digestion products being present, i.e. the starting formulation at time = 0, the PHYT20TB emulsion was in the L_2 phase as demonstrated by the broad hump (20TB-0DP) in **Figure 3-9A**. In the case of the PHYT20TB system, the DP consisted of 3 mol of butyric acid and 1 mol glycerol. At 18% w/w TB and 2% w/w DP (18TB-2DP), peaks with a spacing ratio of √2, √3, √4, √6, √8, √9 in coexistence with the emulsion were apparent, signifying the presence of the ordered cubic *Pn3m* phase. As the proportion of triglyceride was replaced by fatty acids and glycerol/monoglyr-cerides (**Table 3-1**), the characteristic hump became more level with the background scattering while the peaks for cubic phase became more pronounced, signifying a clear range of concentrations over which the system transitioned from L_2 phase to the bicontinuous cubic phase structure.

As was the case for PHYT20TB, without addition of digestion products the PHYT15TC was an emul-sion (L_2 phase) as denoted by the hump as shown in **Figure 3-9B**. The H_2 phase, indicated by the peaks with a spacing ratio of 1, √3 and √4, formed at 9% w/w TC and 6% w/w DP (where in this case DP was 2 mol caprylic acid and 1 mol of monocaprylin) (9TC-6DP). At 3% w/w TC and 12% w/w DP (3TC-12DP), the H_2 phase persisted and the L_2 phase was no longer evident; instead, peaks with relatively low intensity were apparent that indicated the presence of cubic *Pn3m* phase, demon-strated by the minor peaks labelled √2 and √3. Only the cubic *Pn3m* phase remained when all of the TC was replaced with digestion products in the formulation (0TC-15DP). With increasing amount of DP in these static systems, the peak positions were shifting towards lower q which correlated with the increase in lattice parameter illustrated in **Figure 3-9D** as the nanoparticles swelled with aqueous phase.
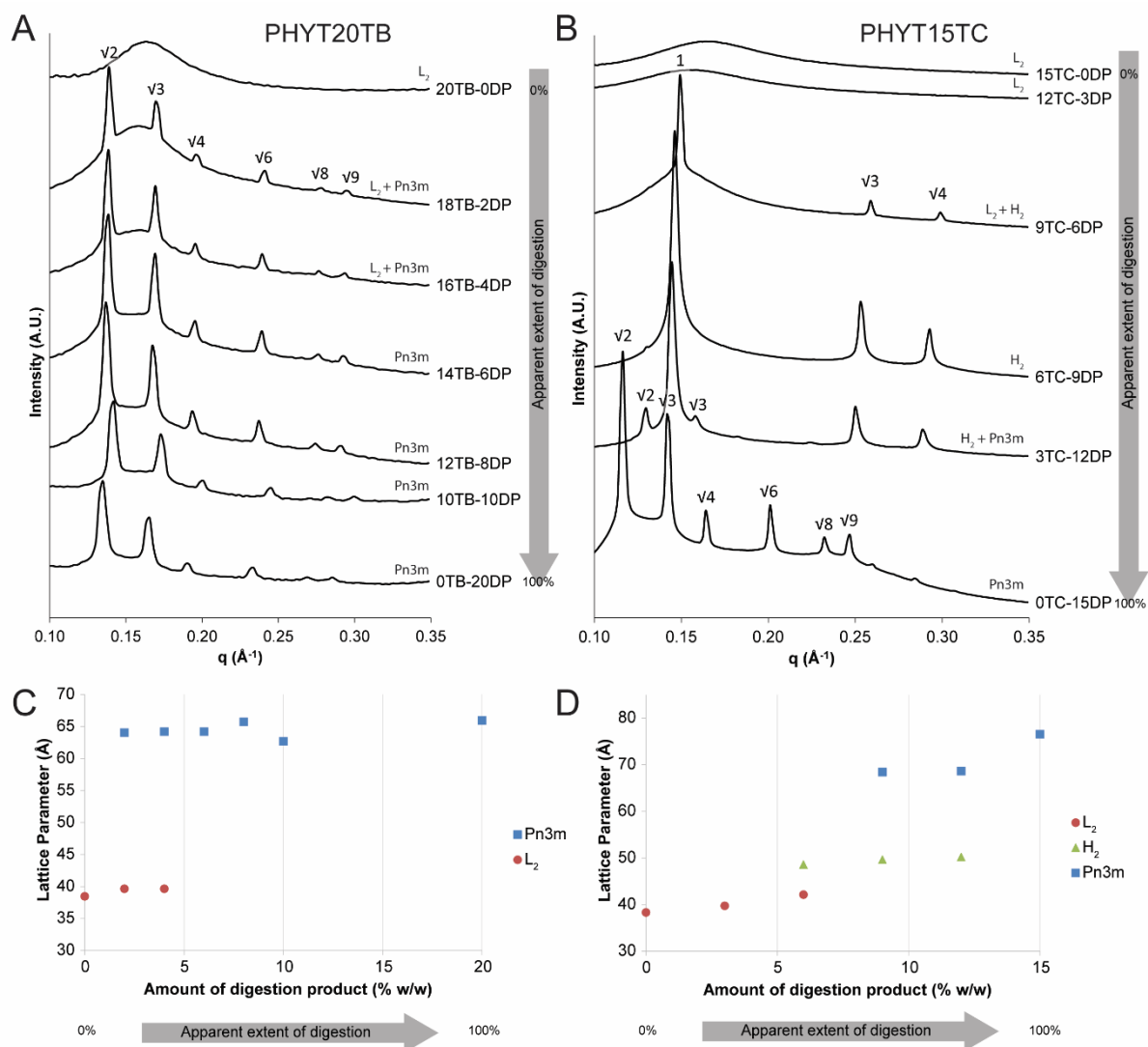
Figure 3-9. Phase diagrams of different compositions of the formulations with % w/w triglyceride (tributyrin: TB; tricaprylin: TC) and % w/w digestion product (DP). Each formulation simulated the composition of the digested formulation at various stages of hydrolysis of the triglyceride showing the apparent extent of digestion of the enzyme-sensitive emulsions. A) PHYT20TB transitioned from L_2 phase to cubic *Pn3m* phase at 18% w/w TB (18TB-2DP), and B) PHYT15TC transitioned from L_2 phase to H_2 phase and finally cubic *Pn3m* phase upon complete replacement of TC with digestion products of the triglyceride (0TC-15DP). The data is also plotted as a lattice parameter vs. the amount of digestion product in the system in C) for the TB system and in D) for the TC system.

3.4.3 Device sensitivity

To track the structural changes during the digestion of lipid-based formulations, the devices needed to be compatible with SAXS. Ideally, a device composed of X-ray transparent material with thin walls or windows would permit optimal detection, and a larger transmission distance/pathlength through the sample would enable greater signal as the X-rays see more scattering material from the sample (but not so thick that multiple scattering effects occur). To determine the relative sensitivity across

the three experimental configurations, the intensity of the peaks for the cubic *Pn3m* phase was compared between devices in **Figure 3-10**.
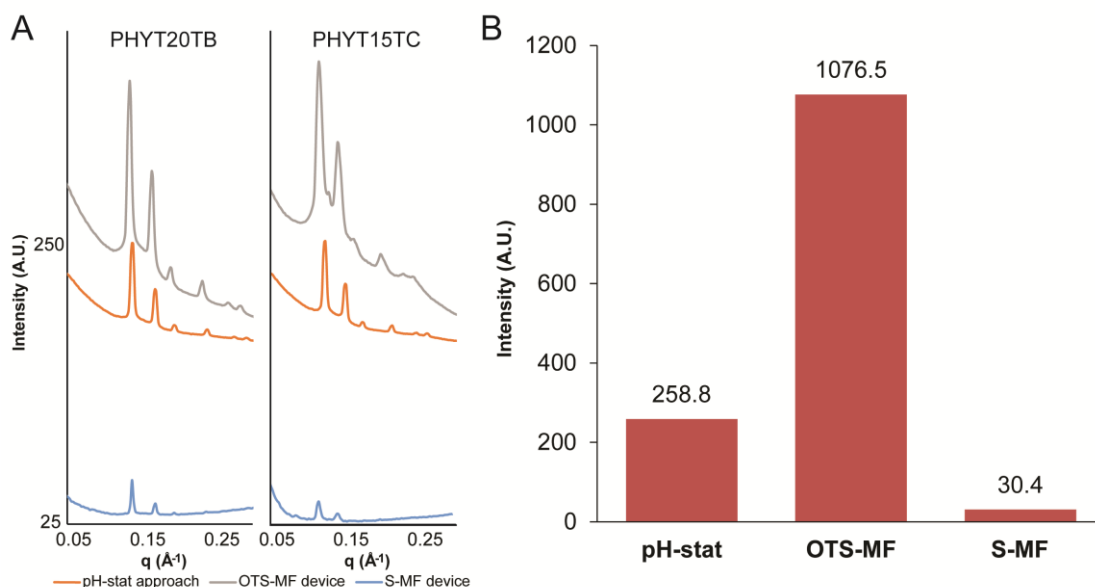
Figure 3-10. Comparison of the sensitivity for detection of diffraction peaks of the different devices. A) Scattering profiles of the cubic *Pn3m* phases generated after the digestion of PHYT20TB and PHYT15TC samples within the pH-stat approach, OTS-MF device and S-MF devices (extracted from **Figure 3-11**). B) An average of intensities of the first cubic phase peak from the digestions.

The OTS-MF device exhibited high sensitivity for the liquid crystal structures. An X-ray energy setting of 13 keV was sufficient to yield signals from sample within the borosilicate glass capillary. This was expected as the device was constructed from a capillary similar in material and diameter to the capillaries typically used in experiments for static samples. In fact, it appeared that the OTS-MF capillary yielded at least a threefold greater signal than the capillary used in the pH-stat apparatus (**Figure 3-10**) which could be a result of the microcapillary having a larger capillary diameter and so a greater sample distance.

Comparatively, the S-MF device exhibited a lower sensitivity with SAXS. This was due to the ratio of path length through the sample compared to that through the quartz (or thickness of the sample holder), which was much lower than that observed in the OTS-MF device. This required the energy of the X-ray beam to be increased to 20 keV and an additional increase from the usual acquisition time of 5 secs to 30 secs to counteract the loss of signal. Even after this optimisation, the resultant signal was observed to be about 10 times lower than the standard capillary signals at 13 keV. However, the background signal was also lower, meaning that the diffraction peaks from the sample could still be readily identified.

3.4.4 Kinetic structural evolution during digestion

Kinetics of the phase transitions of PHYT20TB and PHYT15TC were monitored in all three experimental configurations integrated with synchrotron-based SAXS. **Figure 3-11** displays the scattering profiles obtained from the systems during digestion in the pH-stat approach, OTS-MF device, and S-MF device, while **Figure 3-12** presents changes in the lattice parameters of the mesophases in the nanoparticles during digestion.

PHYT20TB is a well-studied system that transitions from L_2 phase to the parent cubic *Pn3m* phase during digestion in the pH-stat approach.[3,4] At the start of digestion in the pH-stat approach (**Figure 3-11A**), the q-position of the broad hump (indicative of L_2 phase) shifted to the left which suggested the lipid droplets were swelling with water.[43] The shift to lower q was also noted between 20TB-0DP and 18TB-2DP for the L_2 phase in **Figure 3-9A**. At approximately 20 secs, two peaks with a spacing ratio of √2 and √3 became visible, sufficient to be identified as cubic *Pn3m* phase.[38] There was a minor amount of cubic phase forming at this stage hence a low intensity signal that was insufficient for the latter peaks (√4, √6, √8, √9 etc.) to be noticeable. Thereafter, the scattering for the cubic *Pn3m* phase remained constant in terms of q-position, number of peaks and intensity for the remainder of the digestion where the lattice parameter of the cubosomes in the dynamic digestion was 64.4 Å (**Figure 3-12A**) which was similar to that of 14TB-6DP in **Figure 3-9A** (64.4 Å) indicating that the formulation contained at least 6% w/w digestion products (consisting of glycerol and butyric acid) at that point (which was the equivalent of at least 40% digestion). In addition to the cubic phase in the scattering profile at 20 secs, there was an additional peak between the peaks at √2 and √3 at q = 0.155 Å^{-1}. This peak would suggest the coexistence of another structure. No phases aside from L_2 and cubic phases existed in the static samples that represented the various stages of digestion (**Figure 3-9A**). So, it is possible that the peak could be a second *Pn3m* phase with a smaller lattice parameter or an H_2 phase. The exact structure, however, cannot be confirmed given the presence of only one peak. The presence of the unidentified phase in the pH-stat method may suggest that there was an uneven distribution of the enzyme solution during mixing and the initial transport. A greater proportion of enzyme may have impacted on the packing of the lipids to induce the formation of the intermediate phase. This difference in phase behaviour, although subtle, was also not evident in the data from the literature pH-stat experiment,[4] serving to highlight the possible inconsistencies in mixing or lack of resolution associated with studying such transitions when using the pH-stat method.

Digestion in the OTS-MF device, shown in **Figure 3-11C**, exhibited a relatively smooth transition within each set of TFR (as denoted by the separate colours) however, the sets of kinetic data between the different TFR were noticeably different. The expected phase transition was observed from L_2 to cubic *Pn3m* phase with increasing intensities. However, scattering profiles of adjacent time points from the different sets of TFR were vastly different in regards to the peak heights and peak positions. Between the yellow (6000 µL/hr, or 100 µL/min) and green (2400 µL/hr, or 40 µL/min) sets of data, the first peak for the *Pn3m* phase abruptly increased almost 50% in intensity and the second peak suddenly became prominent also. Compared to the same digestion in **Chapter 2:Figure 2-11**, the jump in intensity between adjacent time points of different TFR was significantly more pronounced, and it could be due to the larger difference in TFR used to compile the kinetic data. The greater difference in TFR would have applied a greater shear stress of the self-assembly of the molecules[44] that appeared to push more structures towards the equilibrium phase earlier in time (or earlier positions in the channel). In **Figure 3-12C**, the digestion yielded cubosomes with a lattice parameter measuring 66.9 Å, which did not correlate with the lattice parameters of the cubic phases in **Figure 3-9C** where the maximum lattice parameter measured was 65.9 Å, which would suggest that the particles formed in this microfluidic device were hydrated to a greater extent as a result of the configuration. The lipase, which was absent in the equilibrium formulations, could have influenced a greater hydration of the particles.

A smoother transition was observed from L_2 to cubic phase when digested in the S-MF device (**Figure 3-11E**), showing no intermediate phases. The gradual transition as opposed to an almost instantaneous change observed in the pH-stat approach could suggest that the transformation was more controlled with the configuration of the S-MF device. Similar to the pH-stat approach, the lattice parameter of the cubosomes at the last time point reached only 64.6 Å, implying that digestion was at least 40% complete.
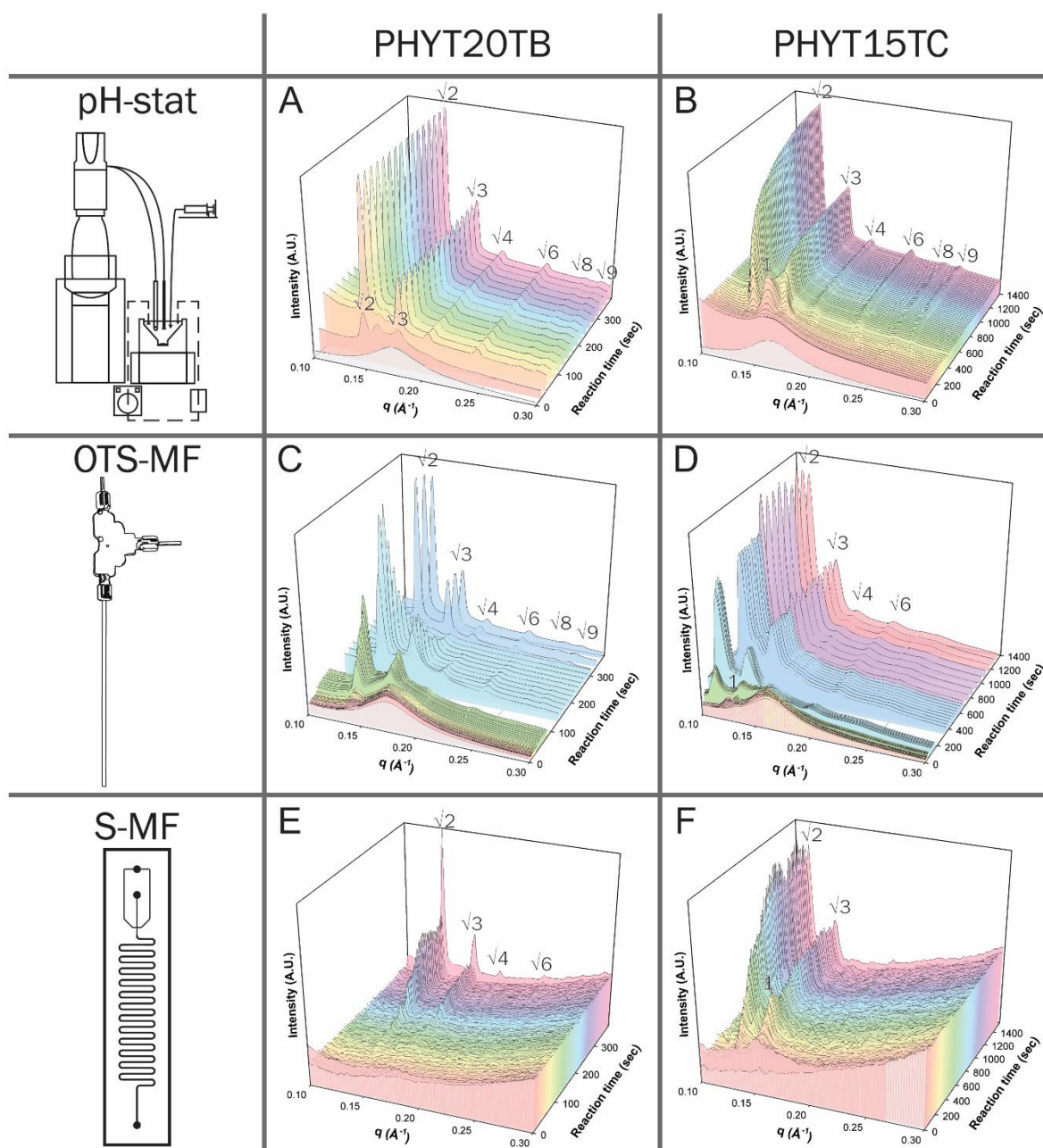
Figure 3-11. Tracking the phase transitions with SAXS during the digestion of PHYT20TB (A, C, E) and PHYT15TC (B, D, F) in the pH-stat apparatus, OTS-MF and S-MF devices, respectively, illustrated as intensity vs. scattering vector, q, plot against time. All six digestions showed a broad hump at time 0, indicative of the unstructured emulsion for PHYT20TB and PHYT15TC. As the formulation underwent digestion, the hump flattened out while other peaks emerged, suggesting a restructuring of the lipid molecules into ordered phases. At the conclusion of all the digestions, at least two peaks were visible in the spacing ratio √2, √3, √4, √6, √8, √9 which is representative of the cubic *Pn3m* phase. For the digestions performed in the OTS-MF device (C, D), experiments performed at the same TFR are grouped with the same colour to differentiate from those done at different TFR.

Between the digestions of PHYT20TB in the three experimental configurations, the onset of the cubic *Pn3m* phase in the pH-stat method was the fastest, followed by the OTS-MF device, then the

S-MF device. The cubic phase, which is the equilibrium phase after the complete digestion of PHYT20TB, was apparent in the first 20 secs of digestion in the pH-stat method, and within 12 secs for the OTS-MF device. The lattice parameter for the cubic phase formed in the pH-stat experiment (**Figure 3-12A**) remained stable for the remainder of digestion after 40 secs despite at least 40% digestion of the tributyrin which may imply that digestion was complete. The lattice parameter for the cubic phase gradually increased over time during digestion in the OTS-MF device. Interestingly, despite the cubic phase forming quite rapidly in the OTS-MF device, the initial L_2 phase persisted for another 200 secs thereafter. Additionally, the characteristic distance was also trending towards higher values (**Figure 3-12C**) which could suggest that the undigested micelles outside of the sampling range of the X-ray beam may have diffused into this space. The increase in characteristic distance appears logical given that there was a lower concentration of micelles in the sampling range owing to their conversion into cubosomes. This was contrary to the kinetics observed in the S-MF device required only one TFR for the data set where the cubic phase appeared after 120 secs and the lattice parameter of the cubic phases fluctuated slightly (**Figure 3-12E**).
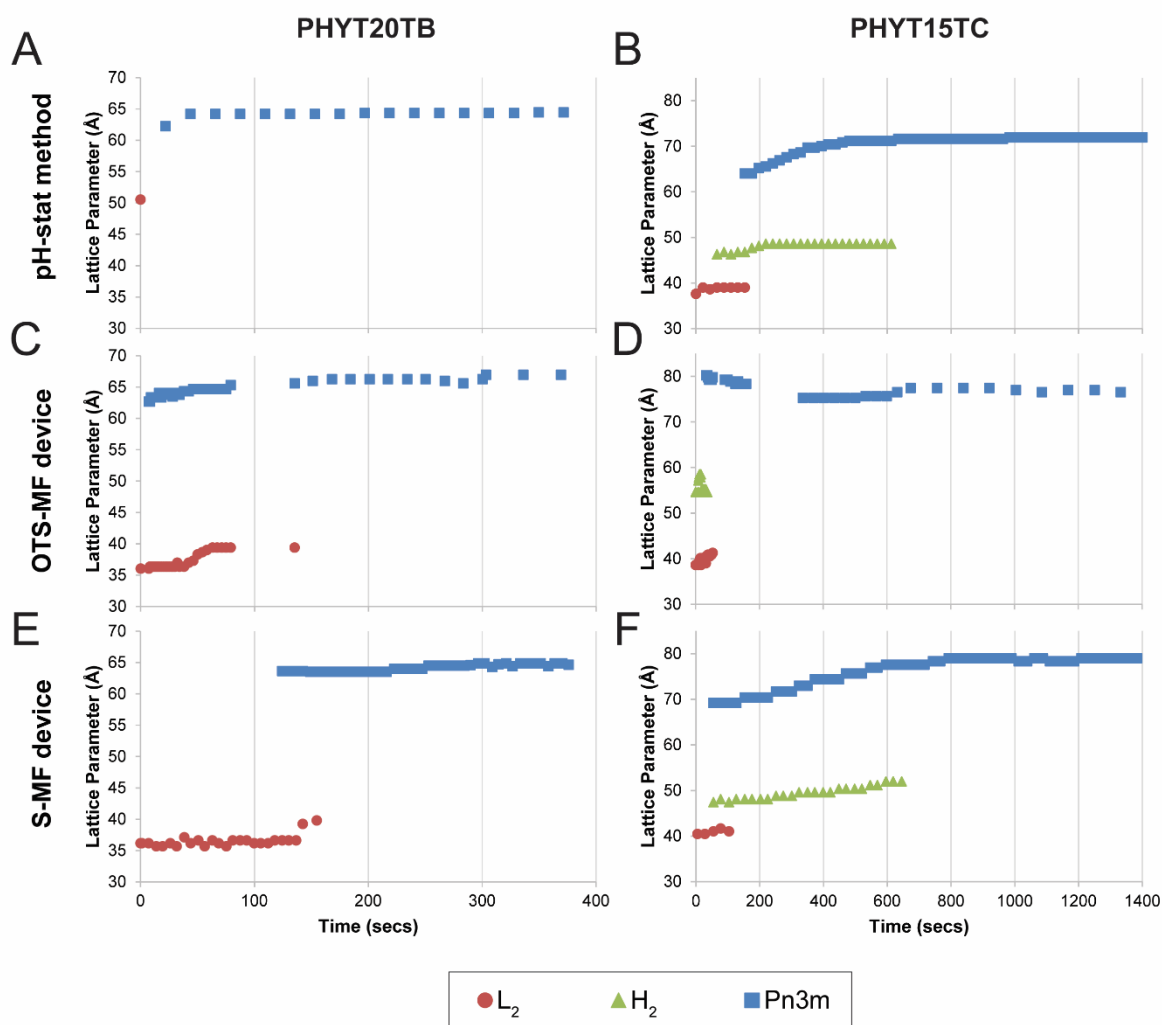
Figure 3-12. Tracking the change in lattice parameter (or characteristic distance for the L_2 phase) of the mesophases formed during the digestion of PHYT20TB in the pH-stat method (A), OTS-MF device (C) and S-MF device (E), and PHYT15TC in the pH-stat method (B), OTS-MF device (D) and S-MF device (F). Lattice parameters were calculated from the peak maxima, and peak broadening was not accounted for.

It was previously shown that the PHYT15TC system undergoes a change from L_2 phase to the coexistence of *Pn3m* phase with H_2 phase before completely transforming into the equilibrium *Pn3m* phase of the hydrated lyotropic lipid mixture.[4] When the PHYT15TC emulsion was digested in the pH-stat apparatus (**Figure 3-11B**), a transition from the starting L_2 phase to a broad peak (marked '1') likely to be the first peak indicating the H_2 phase occurred. The broad peak then decayed concurrent with appearance of peaks at q = 0.137 and 0.168 Å^{-1} (which index at √2 and √3) indicating the formation of cubic *Pn3m* phase particles. The scattering profiles for the cubic phase shifted to lower q indicating the system was taking up water until the first peak for the cubic phase stabilised at q = 0.124 Å^{-1}. The attribution of the peak marked '1' to the first H_2 phase peak was inferred from the static samples where the first peak of the H_2 phase was in the same q range (**Figure 3-9B**) and

yielding comparable lattice parameters (**Figure 3-9B** and **Figure 3-12B**). The broadening of the peak was likely due to heterogeneous transformations, resulting in the formation of H_2 phase with a range of lattice parameters. This would suggest that the configuration of the pH-stat prevented uniform mixing of the enzyme which yielded heterogeneous nanostructures as a consequence. Should an intermediate phase persist for a longer duration as a result of the configurations and not the inherent transformation itself, it would then delay the onset of the subsequent structures also. This would impact on the ability to correlate structures with release behaviour when assessing these systems as potential drug delivery systems. Complete digestion of the tributyrin molecules was also not confirmed *in situ* as the lattice parameter of the cubosomes at the final time point (72.0 Å) did not reach that of the equilibrium systems in **Figure 3-9D** (76.6 Å).

Digestions performed in the OTS-MF device did not exhibit reliable transformations as shown in **Figure 3-11D.** Within the first set of kinetic profiles for a TFR of 200 μL/hr (orange), a peak at $q = 0.125$ Å^{-1} emerged and grew. Although lower than the q range expected for the first H_2 phase peak, it was still suspected that it was H_2 phase but with a larger lattice parameter. In the subsequent TFR (yellow), there was a noticeable decrease in intensity and shift in the q-position of the H_2 phase peak, followed by a sharp transition into cubic *Pn3m* phase in the next TFR (green). The shift in q was evident by the corresponding decrease in lattice parameter of the H_2 phase (**Figure 3-12D**). These unusual variations in peak intensities and lattice parameters between each TFR made it difficult to characterise the kinetics of this system using the OTS-MF device. As with PHYT20TB in the OTS-MF device, this could be attributed to variations in shear stress with different TFR that alter the structural behaviour. Furthermore, the kinetics of this system appeared to exhibit a nonsense order of phase transformations where the H_2 phase disappeared before the disappearance of the L_2 phase, inconsistent with the digestion in literature[4] which could also be attributed to diffusion of the L_2 phase from the bulk flow of the formulation into the collection volume of the X-ray beam.

In contrast to use of the OTS-MF device, the equivalent digestion in the S-MF device exhibited a clear transition from L_2 phase to H_2 phase to cubic phase (**Figure 3-11F**). The improvement in resolution may imply the diffusion-limited digestion of the coaxial flow facilitated a uniform application of the enzyme for more consistent transformations across all particles and droplets in the system, supported by the gradual increase in lattice parameters of the different mesophases present during digestion (**Figure 3-12F**). As particles were able to transform homogeneously, the lattice parameters

of the resulting particles were similar which yielded more pronounced Braggs peaks as opposed to broader peaks. This may indicate that the kinetics observed in the pH-stat approach are in part dictated by the apparatus which is more susceptible to variation in the uniformity of the application of lipase, and therefore, not representative of the system. Digestion of PHYT15TC in the S-MF device produced cubosomes with a lattice parameter (79.0 Å, **Figure 3-12F**) which was approximately 3% greater than the expected dimension from the equilibrium formulations, showing that all TC had digested. However, the mismatch of these corresponding dynamic and equilibrium structure may highlight that comparing lattice parameters is not a reliable indicator of extent of digestion.

As the design of the S-MF device facilitated the uniform application of enzyme to the formulation, the activity of the lipase was increased to confirm that enhanced activity would lead to faster rate of reaction on the chip, and therefore faster structural transitions (**Figure 3-13**). When the activity of the lipase was doubled to 1000 TBU/mL of digest, digestion of the PHYT20TB occurred more rapidly. The onset of the peaks indicative of the *Pn3m* phase appeared at approximately the same position on the chip, indicating the same time (~90 secs) as that observed at half the enzyme strength (**Figure 3-11E**). However, the intensity of the peaks stabilised by 150 secs compared to 300 secs for the half-strength digestion. By controlling and limiting the access of lipase to the formulation the kinetics of digestion can be modulated.
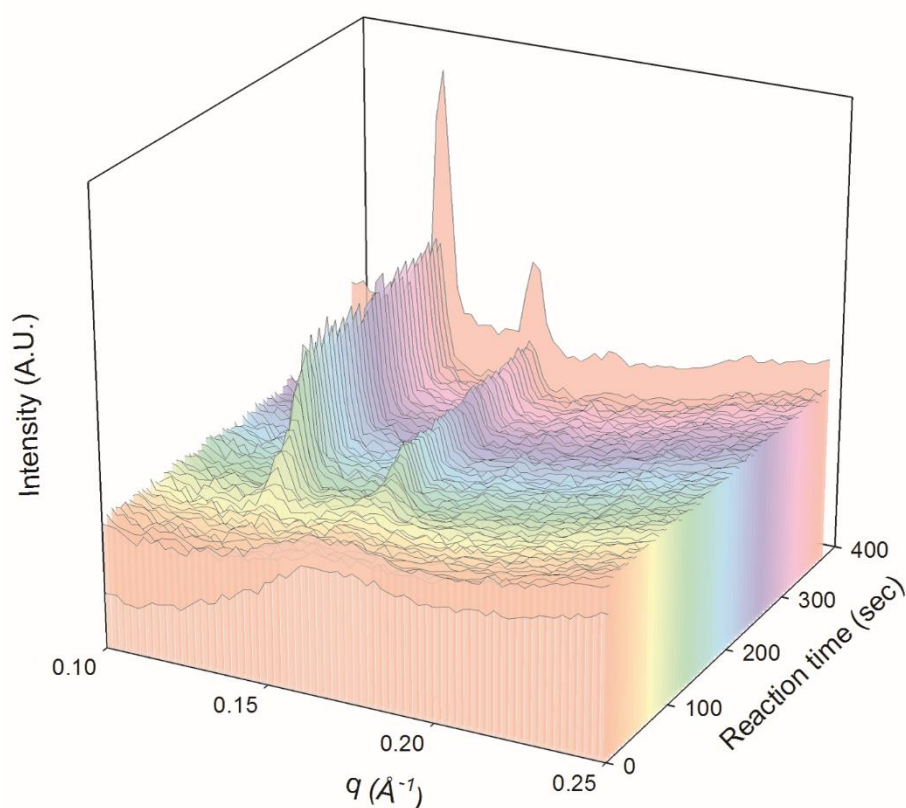
Figure 3-13. Digestion of PHYT20TB in the S-MF device with twice the strength of enzyme than the experiment in **Figure 3-11E**. The emergence of the peaks indicative of the cubic *Pn3m* phase occurred at approximately 90 secs. The intensity of the peaks stabilised at a relatively constant height by 150 secs.

3.4.5 Particle size uniformity

When comparing the resulting particle size of the digested liquid crystal nanostructures between the two MF devices, there was no significant difference in the particle size distributions compared to the emulsion prior to digestion (**Figure 3-14**). There was also no difference when compared to the mean particle size of the nanoparticles formed in the equivalent experiments performed in the pH-stat approach, implying that the particles with internal structures produced after digestion in any of these devices were the same but the transformation pathway to get there may be different. There was a noticeable increase in variability with results for the pH-stat approach, which could be attributed to some background light scattering by the lipase. In addition for the microfluidic systems, the entire system is closed and completely free of opportunity for contamination by dust, while the pH-stat system is open, and opportunistic dust can give rise to larger polydispersity index in dynamic light scattering measurements.
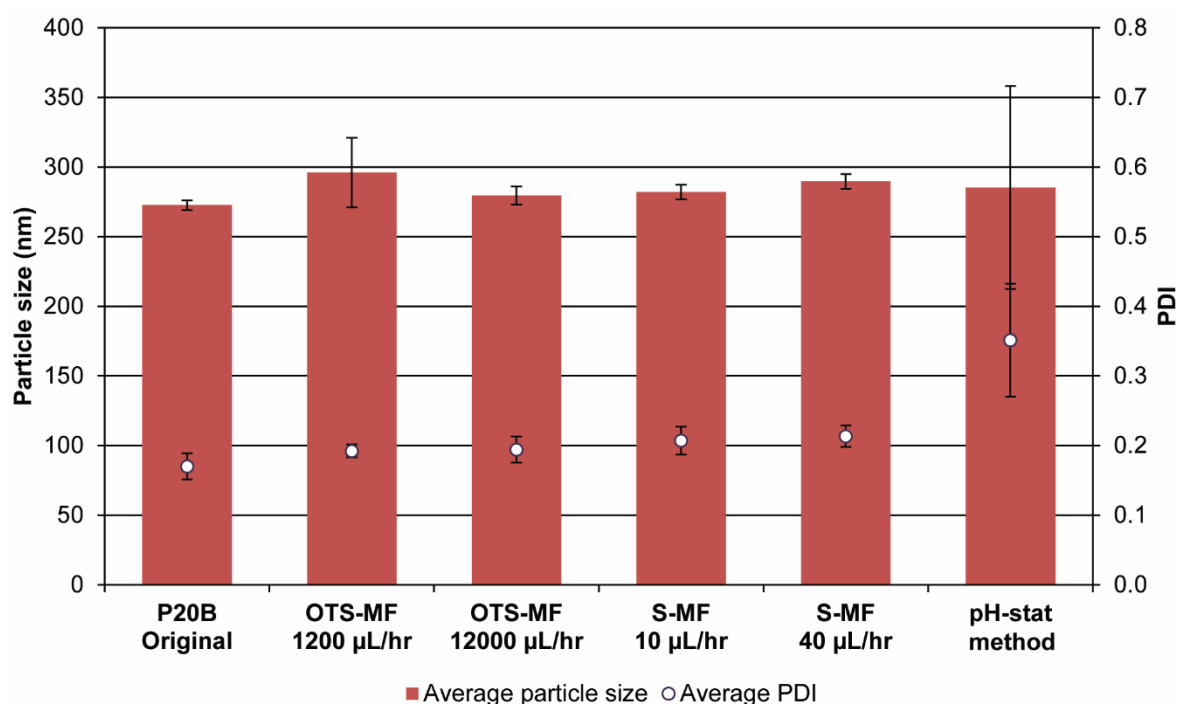
Figure 3-14. Particle size distribution of the undigested PHYT20TB emulsion compared to the cubic phase nanoparticles produced during the digestion of PHYT20TB in the S-MF and OTS-MF devices at the specified flow rates, and the pH-stat approach. The TFR of the experiments are listed below.

3.4.6 Overall comparison

Microfluidics showed clear improvements to studying structural transformations in digestion studies when compared to the pH-stat approach. Integration of the mixing and analysis components over-came problems associated with the separation and transit of materials. In both microfluidic devices, the point of complete mixing occurred sufficiently early in the channels that it did not impede phase transitions which was not the case in the commercial NA chip described in Chapter 2:**2.4.4 Monitoring the dynamic phase behaviour of digestion-sensitive LCNP systems in the NA chip**. Additionally, factors such as temperature and pH, which were previously controlled in the pH-stat method and absent in either microfluidic devices, were found not to exert a significant influence on digestion kinetics which was also a factor concluded by Phan *et al.*[45]

The OTS-MF device could identify phase transitions, however there were inconsistencies in the transition behaviour that were not apparent in the previous chapter. The transitions were not consistent when changing the flow rate to account for the limited capillary length. This could be due to the different shear stresses applied to the transformation with increasing flow rates as Ghazal *et al.* noted more anisotropy in their liposomes formed above flow rates of 15 μL/min in the microchannels.[46] Sections of the capillary were also hidden due to the configuration of the T-junction, therefore

a faster flow rate would be required to observe these earlier time points but at the expense of greater sample consumption. The advantage of the device was its simplicity, cost, and its high sensitivity to qualitatively discern the structures. It may also be possible to use a longer length of capillary so that more time points could be collected for any one TFR, however this is dependent on the space limitations with the experimental stage at the synchrotron and availability of commercial capillaries that are sufficiently long and uniform in diameter.

Although the S-MF device exhibited low sensitivity due to greater absorption of the beam by the quartz housing, it enabled the monitoring of an entire digestion experiment at a fixed flow rate. Up to four peaks could be identified for the cubic *Pn3m* phase as opposed to only two observable for the device used in the work by Ghazal *et al.*[8] Additionally, for the S-MF device the >300 mm of channel length allowed the full transformation (of up to 25 mins) to be mapped from the instant the lipase made contact with the formulation through to the endpoint, including the point of complete mixing. Phase transitions in the S-MF device were also slower compared to the digestions performed in the pH-stat approach. The kinetics may be attributed to the lipid stream-enzyme stream interface restricting digestion to a fixed volume of enzyme per volume of lipid. This was not the case with the pH-stat approach where the excess enzyme had access to all the lipid all at once in the mixing vessel so that the mixing efficiency would be unpredictable as solution was continually being drawn up by the peristaltic pump. Mixing was diffusion-limited in the S-MF device and thus more controlled.

3.5 Part A: Conclusion

The S-MF device produced controlled and gradual phase transitions with sharper peaks than traditional approaches and the kinetics could be modulated with changes in concentration of the stimuli. The full phase transition could be observed using one TFR, whereas the OTS-MF device necessitated manipulations of the TFR to achieve transformations between phases. Thus, the S-MF device can be used instead of current experimental configurations to monitor the structural evolution of stimuli-responsive lipid-based formulations, requiring less consumption of material and less additional instrumentation.

3.6 Part B: Results and discussion

3.6.1 Examining the digestion of individual droplets of lipid-based formulations in the S-MF device

Microscopy was used to visualise the digestion of a lipid-based formulation in the S-MF device. Digestion of the SA25TB droplets was expected to transition from L_2 phase to H_2 phase.[4] The presence of H_2 phase can be implied by a bright texture, known as birefringence under polarised light in microscopy.[34] Using the experimental configuration illustrated in **Figure 3-7**, the birefringence of digesting droplets was determined at fixed time points in the reaction. At the end of the serpentine channel during the digestion of the SA25TB droplets illustrated in **Figure 3-15**, frame A, C and D had a mixture of birefringent and non-birefringent droplets (filled and open white arrows, respectively), while frame B had mostly birefringent droplets. The presence of both the birefringent and non-birefringent lipid droplets in frames A, C and D could imply the digestion may not have reached completion. Therefore, at the end of the microchannel the reaction may not have been complete, and the system was digested to an intermediate time point with the coexistence of L_2 phase (insufficiently digested droplets) with the H_2 phase (birefringent droplets). The presence of each phase existing in separate particles at this intermediate time point would suggest that while the droplets digested, the tributyrin was still diffusing throughout the droplet and maintaining an overall concentration within the droplet above the phase transition concentration. Only when a critical point of digestion or lower threshold concentration of tributyrin was reached could the droplet transition entirely. However, the proportion of the digested and insufficiently digested droplets was inconsistent at the same position along the channel at different time points. As such, the reliability of this design was questionable for this purpose. In theory, each position would have sample that has traversed the same distance of microchannel and so should have the same reaction time.[19] Thus, it was expected that droplets at each position should exhibit the same behaviour structurally. Alternatively, the polydisperse droplets may have different onsets of digestion but this could not be confirmed as the diameter of the droplets could not be discerned from the recording.
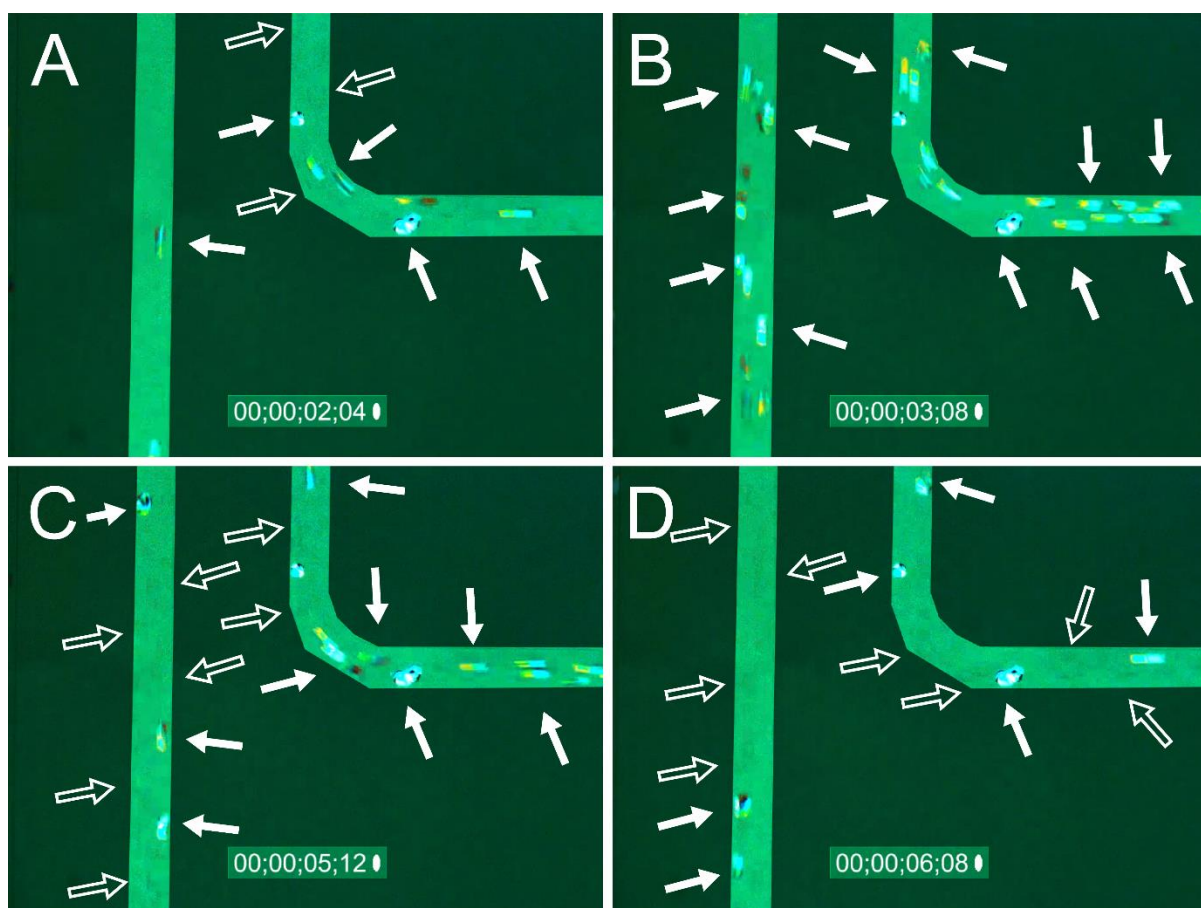
Figure 3-15. Micrographs of the same end position of the microchannel monitoring the digestion of lipid-only droplets containing SA25TB in the S-MF device. Droplets were travelling with a linear velocity of approximately 2.4 mm/sec (flow rate 52 µL/hr). All four frames showed inconsistent droplet behaviours despite all droplets at this point sharing the same reaction time *in situ*. Birefringent particles (bright regions) indicate the presence of H_2 phase and thus digestion. Insufficiently digested droplets are not clear given the quality of the recording but are highlighted by the open white arrows; H_2 phase droplets are denoted by the filled white arrows. The associated time code is interpreted as [hours]:[minutes]:[seconds]:[frame number (out of 30)]. A video of this digestion can be viewed on Youtube: https://youtu.be/TCzu-lxHl_o

3.6.2 Digestion of droplets of lipid-based formulations in the DT-MF device

As the continuous flow of the droplets made it difficult to get quality images of the digesting lipid droplets in the S-MF device, the possibility of device that would enable stationary droplets with a solution of enzyme still flowing around them was also explored. Droplets were trapped indefinitely in the DT-MF device (illustrated in **Figure 3-5**) allowing a clearer recording and analysis. **Figure 3-16** displays the micrographs of three trapped SA25TB droplets in the pockets of the DT-MF device. From left to right, the diameters of the droplets (C), (B), and (A) were approximated to 62, 48 and 84 µm, respectively. Digestion was apparent when isotropic droplets transition into birefringent droplets which would indicate the transition to H_2 phase. The medium-sized droplet closest to the incoming stream of enzyme (C) was first to develop a birefringent appearance about 5 mins after

its trapping (frame 4), despite being trapped later than droplets (A) and (B). The earlier onset of birefringence would indicate that droplet (C), being closest to the flow of the continuous phase, had a greater access to the enzyme that may have induced an earlier phase transition. A complete phase transition across the droplet was apparent within 2 secs as the birefringence (indicative of H_2 phase) was spread from left to right of the droplet (frames 4-7). However, complete digestion of the droplet may not have occurred as the texture of the birefringence had rotated and changed in the following frames, suggesting that the droplet was still digesting and the lipid molecules were still in the process of self-assembly or the droplet was reorientated possibly due to the flow (frames 7-9).[47] The smallest droplet in the middle (B) was next to exhibit birefringence approximately 7.5 mins after it was trapped (frame 10). The full coverage of the droplet with birefringence was observed within 3.5 secs—taking almost twice as long as the droplet that was 1.3 times greater in diameter (frames 10-12). Finally, droplet (A) required 3.63 mins for the birefringence to spread across the area of the droplet, 12.6 mins after it was isolated (frames 17-20). **Figure 3-17** compares the times required before birefringence was first observed in the droplets, showing no correlation between the sizes of the droplets. However, the time of onset did correlate with the location of the droplet in relation to the incoming flow of enzyme where droplets closer to the flow were observed to transform earlier.
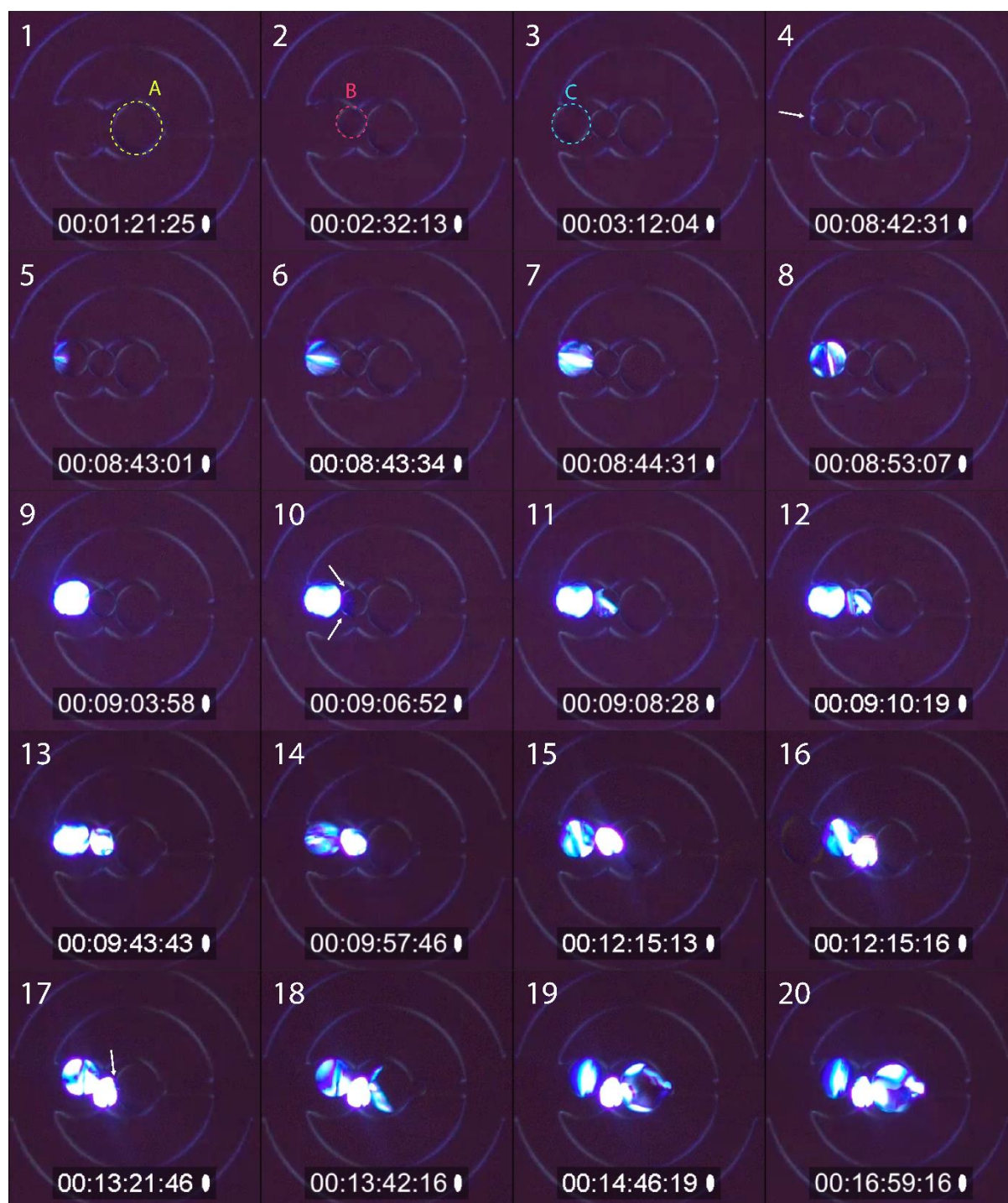
Figure 3-16. A collection of micrographs tracking the digestion of SA25TB droplets trapped in the pockets of a microfluidics device. Frames 1 to 3 show the trapping of three droplets (A), (B), and (C) in the same pocket after already traversing the channels for approximately 0.76 secs. Droplet (C) expressed birefringence first as shown in frames 4-7 with the onset highlighted by the white arrow. Frame 10 to 12 showed the phase transition of droplet (B), and frames 17 to 20 showed the phase transition of droplet (A). Frame 8 to 9, and frames 13 to 16 displayed the alterations of the birefringent pattern in the droplets under flow. The associated time code is interpreted as [hours]:[minutes]:[seconds]:[frame number (out of 60)]. A video of this digestion can be viewed here: https://youtu.be/1jNOYqNtBho
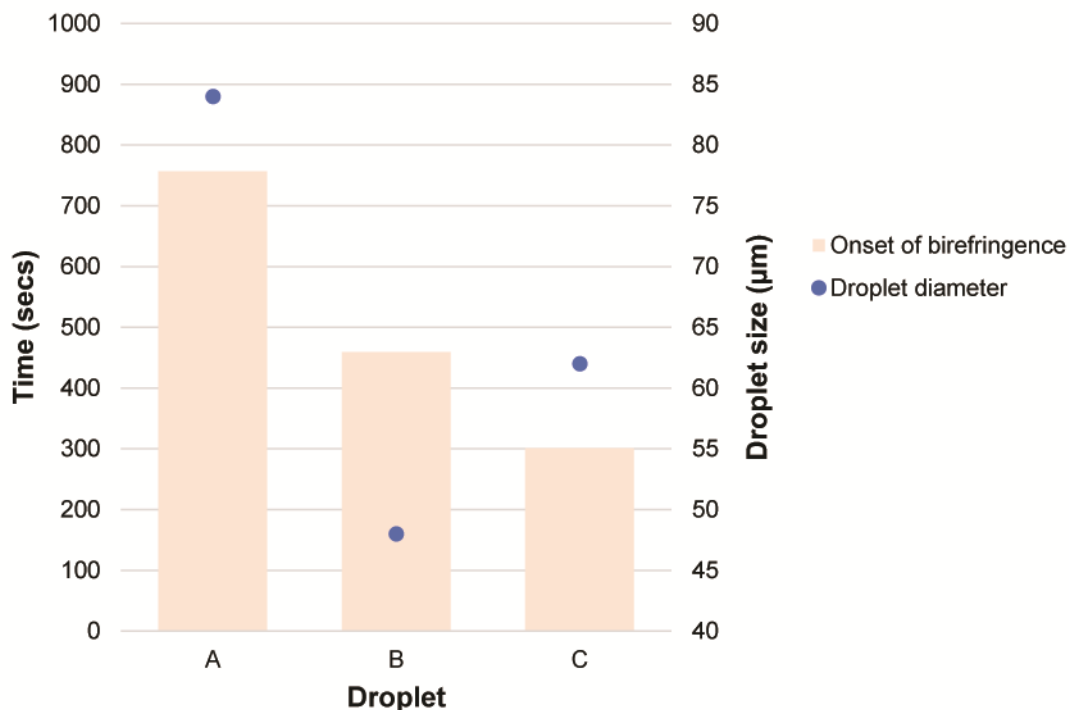
Figure 3-17. Comparison of onset of birefringence between differently sized droplets trapped in the S-MF device. Droplet A was located furthest from the incoming lipase stream, while Droplet C was closest.

The gradient of birefringence that spread across the droplets during digestion would suggest that mixed phases could co-exist within a droplet. Focusing on droplet (C), the phase transition occurred from the left of the droplet (closest to the incoming flow of enzyme) propagating towards the right side, which was also in the direction of flow in the microchannels. This would imply that the aqueous phase was diffusing through the droplet, most likely at an enhanced rate due to the flow rate (52 μL/hr) whilst the tributyrin was digested. The approximate size of the water channel was calculated to be 83.7 Å for a previously digested SA25TB dispersion[4] using **Equation 3-4**.

Equation 3-4. Equation used to approximate the radius of the water channel in a H_2 structure where r is the radius of the water channel, a is the lattice parameter of the H_2 phase and φ is the lipid volume fraction.[48]

$$r = a\sqrt{1-\varphi}\left(\frac{\sqrt{3}}{4\pi}\right)^{1/2}$$

The lipid volume fraction for this system was inferred from the correlation of the lattice parameter of the digestion SA25TB dispersion correlated to water content of the bulk systems in experiments performed by Barauskas *et al.* (**Supplementary figure 3-1**).[49]

This diameter of the water channel was smaller than the unit cell dimensions of a human pancreatic lipase-colipase complex ($a = b = 80$ Å; $c = 251$ Å)[50] which would prevent the diffusion of enzyme

into the lipid droplet. Although the pancreatic lipase used in these experiments was porcine, another study by Hermoso *et al.* had found that the dimensions of the human and porcine lipase complexes were comparable.[51] Therefore, for digestion to occur, it would be more likely that the hydrophobic and small tributyrin molecules diffused through the selachyl alcohol towards the surface of the droplets where enzymatic cleavage could occur. As the local concentration of the tributyrin decreased due to its migration, water was concurrently diffusing inwards to enable the self-assembly of the lyotropic lipid to form the H_2 phase. The formation of the birefringence appeared to originate from only one edge of the droplet, implying that the lipase-colipase complex had only managed to adhere to this end. Being the edge perpendicular to the incoming stream of continuous phase containing the enzyme, the lipase had a high chance of adhesion to this surface of the droplet as opposed to the other regions which were more in parallel with the direction of flow, possibly due to displacement of lipase from the interface due to the flow along the droplet surface. Furthermore, the gradient of birefringence was maintained without reversion to the L_2 phase during the transition despite the proposed migration of tributyrin through the H_2 phase to the droplet surface as its local concentration did not exceed the threshold for the destruction of H_2 phase.

Droplet (A), being the largest out of the three droplets, digested in a radial process towards its centre more so than from one edge of the droplet to another. The droplet was shielded by the other two droplets from the main supply and flow of lipase as it was the deepest in the trapping pocket. It was still exposed to enzyme throughout the experiment, however, the longer onset of the phase transition could be attributed to the lack of force of the incoming flow of continuous phase driving the diffusion of the aqueous phase through the droplet that was noted for the other two droplets. With a relatively more stagnant flow of continuous phase around the droplet, there was more opportunity for the enzyme to adhere to the droplet surface at other regions aside from the first impact of continuous flow. Consequently, the tributyrin could diffuse towards the circumference of droplet from the centre, resulting in the radial growth of the H_2 phase. The diffusion and phase transformation also required more time due to the larger diameter.

The lipid-only droplets were also expected to increase in diameter during digestion due to liquid crystalline phases tending to swell with aqueous phase as observed for the dispersions in **Figure 3-14**. The broad hump of the micellar phase was noted to shift to lower q values in the kinetic profile of the digestion of the equivalent dispersion.[4] This would imply swelling of the lipid droplet due to

an increase in water channels and subsequently, the diameter would be expected to increase. However, there was no observed increase in diameter for these droplets in the micrographs. That is not to say that there was no increase in the height of the droplets though as the experimental configuration did not permit visualisation of the height of the droplets. There was another possibility that the digestion products (including glycerol and butyric acid molecules which are water-soluble) were removed by the continuous flow of the enzyme suspension. This phenomena was noted in the digestion of tricaprylin(C8)-based droplets[31,32] which is a higher molecular weight triglyceride than tributyrin (C4). Tributyrin constituted 25% w/w of the lipid-only droplets so the removal of the digestion products may counteract the increase in size due to the swelling by the aqueous phase. This could then suggest that the aqueous phase constituted up to 25% w/w of the digested droplet, assuming the digestion products were completely removed.

Visualisation of these droplets as they underwent digestion demonstrated that microfluidics could be used in conjunction with CPLM to monitor kinetics. Information regarding when the droplets first digested, and how long they required to digest could be gauged with this technique. Using this as a basis, formulations can be optimised and compared under the same conditions. Likewise, the same formulation could be assessed under different conditions such as at different pH conditions or using fed and fasted state intestinal fluids.

Unfortunately, the polydispersity of the droplets and trapping of multiple droplets appeared to skew the results. It would be expected that complete diffusion of the enzyme would occur earlier for smaller droplets due to the higher surface area to volume ratio as opposed to larger droplets. This was not observed due to the stacking of multiple droplets of differing sizes in the same pockets which may have impeded on the access of enzyme to the droplets further inside the pockets. The monodispersity of the droplets could have been maintained by investing in a higher precision or pressure driven syringe pump.[52]

3.7 Part B: Conclusion

Analysing droplets of lipid-based formulations on the micro-scale showed that phase transitions occurred via a gradient as the enzyme diffused into it. Mixed phases can exist within the same droplet during transformations. The kinetics of the phase transitions from contact with enzyme to its complete transformation were in the order of minutes, however, the apparent full phase transition to H_2 phase across the droplet could occur within seconds. CPLM, along with this style of microfluidic

design, can thus be a powerful screening tool to assess larger scale systems prior to further analysis with accessible techniques such as synchrotron-based SAXS. There may also be opportunities for the droplet-trapping design to be interfaced with SAXS, if the size of the beam spot was sufficiently small to enable spatial resolution within the droplets, which is not the case at the accessible facility at the Australian Synchrotron where the rest of the studies in this thesis were performed.

3.8 References

(1)   Hyde, S.; Ninham, B.; Andersson, S.; Larsson, K.; Landh, T.; Blum, Z.; Lidin, S. Lipid Self-Assembly and Function In Biological Systems. In *The Language of Shape*; Elsevier: New York, 1997; pp. 199–235.

(2)   Gustafsson, J.; Ljusberg-Wahren, H.; Almgren, M.; Larsson, K. Submicron Particles of Reversed Lipid Phases in Water Stabilized by a Nonionic Amphiphilic Polymer. *Langmuir* **1997**, *13*, 6964–6971.

(3)   Fong, W. K.; Salentinig, S.; Prestidge, C.; Mezzenga, R.; Hawley, A.; Boyd, B. J. Generation of Geometrically Ordered Lipid-Based Liquid-Crystalline Nanoparticles Using Biologically Relevant Enzymatic Processing. *Langmuir* **2014**, *30*, 5373–5377.

(4)   Hong, L.; Salentinig, S.; Hawley, A.; Boyd, B. J. Understanding the Mechanism of Enzyme-Induced Formation of Lyotropic Liquid Crystalline Nanoparticles. *Langmuir* **2015**, *31*, 6933–6941.

(5)   Wadsater, M.; Barauskas, J.; Nylander, T.; Tiberg, F. Formation of Highly Structured Cubic Micellar Lipid Nanoparticles of Soy Phosphatidylcholine and Glycerol Dioleate and Their Degradation by Triacylglycerol Lipase. *Appl. Mater. Interfaces* **2014**, *6*, 7063–7069.

(6)   Salentinig, S.; Sagalowicz, L.; Glatter, O. Self-Assembled Structures and PKa Value of Oleic Acid in Systems of Biological Relevance. *Langmuir* **2010**, *26*, 11670–11679.

(7)   Du, J. D.; Liu, Q.; Salentinig, S.; Nguyen, T. H.; Boyd, B. J. A Novel Approach to Enhance the Mucoadhesion of Lipid Drug Nanocarriers for Improved Drug Delivery to the Buccal Mucosa. *Int. J. Pharm.* **2014**, *471*, 358–365.

(8)   Ghazal, A.; Gontsarik, M.; Kutter, J. P.; Lafleur, J. P.; Labrador, A.; Mortensen, K.; Yaghmur, A. Direct Monitoring of Calcium-Triggered Phase Transitions in Cubosomes Using Small-Angle X-Ray Scattering Combined with Microfluidics. *J. Appl. Crystallogr.* **2016**, *49*, 1–10.

(9)   Yaghmur, A.; Laggner, P.; Sartori, B.; Rappolt, M. Calcium Triggered Lα-H2 Phase Transition Monitored by Combined Rapid Mixing and Time-Resolved Synchrotron SAXS. *PLoS One* **2008**, *3*, 1–11.

(10)   Khaliqi, K.; Ghazal, A.; Azmi, I. D. M.; Amenitsch, H.; Mortensen, K.; Salentinig, S.; Yaghmur, A. Direct Monitoring of Lipid Transfer on Exposure of Citrem Nanoparticles to an Ethanol Solution Containing Soybean Phospholipid by Combining Synchrotron SAXS with Microfluidics. *Analyst* **2017**, *142*, 3118–3126.

(11)   Phan, S.; Fong, W. K.; Kirby, N.; Hanley, T.; Boyd, B. J. Evaluating the Link Between Self-Assembled Mesophase Structure and Drug Release. *Int. J. Pharm.* **2011**, *421*, 176–182.

(12)   Negrini, R.; Mezzenga, R. PH-Responsive Lyotropic Liquid Crystals for Controlled Drug

Delivery. *Langmuir* **2011**, *27*, 5296–5303.

(13)   Khan, J.; Rades, T.; Boyd, B.; Boyd, B. The Precipitation Behavior of Poorly Water-Soluble Drugs with an Emphasis on the Digestion of Lipid Based Formulations. **2016**, 548–562.

(14)   Warren, D. B.; Anby, M. U.; Hawley, A.; Boyd, B. J. Real Time Evolution of Liquid Crystalline Nanostructure During the Digestion of Formulation Lipids Using Synchrotron Small-Angle X-Ray Scattering. *Langmuir* **2011**, *27*, 9528–9534.

(15)   Barauskas, J.; Landh, T. Phase Behavior of the Phytantriol/Water System. *Langmuir* **2003**, *19*, 9562–9565.

(16)   Khan, I. U.; Serra, C. A.; Anton, N.; Vandamme, T. Microfluidics: A Focus on Improved Cancer Targeted Drug Delivery Systems. *J. Control. Release* **2013**, *172*, 1065–1074.

(17)   Rott, N. Note on the History of the Reynold's Number. *Annu. Rev. Fluid Mech.* **1990**, *22*, 1–11.

(18)   With, S.; Trebbin, M.; Bartz, C. B. A.; Neuber, C.; Dulle, M.; Yu, S.; Roth, S. V; Schmidt, H.; Fo, S.; Forster, S. Fast Diffusion-Limited Lyotropic Phase Transitions Studied in Situ Using Continuous Flow Microfluidics/Microfocus-SAXS. *Langmuir* **2014**, *30*, 12494–12503.

(19)   Song, H.; Tice, J. D.; Ismagilov, R. F. A Microfluidic System for Controlling Reaction Networks in Time. *Angew. Chemie - Int. Ed.* **2003**, *42*, 768–772.

(20)   Ghazal, A.; Lafleur, J. P.; Mortensen, K.; Kutter, J. P.; Arleth, L.; Jensen, G. V. Recent Advances in X-Ray Compatible Microfluidics for Applications in Soft Materials and Life Sciences. *Lab Chip* **2016**, *16*, 4263–4295.

(21)   Otten, A.; Köster, S.; Struth, B.; Snigirev, A.; Pfohl, T. Microfluidics of Soft Matter Investigated by Small-Angle X-Ray Scattering. *J. Synchrotron Radiat.* **2005**, *12*, 745–750.

(22)   Yaghmur, A.; Rappolt, M. Structural Characterization of Lipidic Systems under Nonequilibrium Conditions. *Eur. Biophys. J.* **2012**, *41*, 831–840.

(23)   Fong, W. K.; Hanley, T.; Boyd, B. J. Stimuli Responsive Liquid Crystals Provide "On-Demand" Drug Delivery In Vitro and In Vivo. *J. Control. Release* **2009**, *135*, 218–226.

(24)   Tran, N.; Hawley, A. M.; Zhai, J.; Muir, B. W.; Fong, C.; Drummond, C. J.; Mulet, X. High-Throughput Screening of Saturated Fatty Acid Influence on Nanostructure of Lyotropic Liquid Crystalline Lipid Nanoparticles. *Langmuir* **2016**, *32*, 4509–4520.

(25)   Salentinig, S.; Phan, S.; Hawley, A.; Boyd, B. J. Self-Assembly Structure Formation during the Digestion of Human Breast Milk. *Angew. Chemie* **2015**, *127*, 1620–1623.

(26)   Clulow, A. J.; Salim, M.; Hawley, A.; Boyd, B. J. A Closer Look at the Behaviour of Milk Lipids during Digestion. *Chem. Phys. Lipids* **2017**, *211*, 107–116.

(27)   Fong, W.; Hanley, T. L.; Thierry, B.; Kirby, N.; Waddington, L. J.; Boyd, B. J. Controlling the Nanostructure of Gold Nanorod–Lyotropic Liquid- Crystalline Hybrid Materials Using Near-Infrared Laser Irradiation. *Langmuir* **2012**, *28*, 14450–14460.

(28)   Tangso, K. J.; Fong, W.; Darwish, T.; Kirby, N.; Boyd, B. J.; Hanley, T. L. Novel Spiropyran Amphiphiles and Their Application as Light-Responsive Liquid Crystalline Components. *J. Phys. Chem. B* **2013**, *117*, 10203–10210.

(29)   Stehle, R.; Goerigk, G.; Wallacher, D.; Ballauff, M.; Seiffert, S. Small-Angle X-Ray Scattering in Droplet-Based Microfluidics. *Lab Chip* **2013**, *13*, 1529–1537.

(30)   Zhu, P.; Wang, L. Passive and Active Droplet Generation with Microfluidics: A Review. *Lab*

Chip **2017**, *17*, 34–75.

(31)   Marze, S.; Algaba, H.; Marquis, M. A Microfluidic Device to Study the Digestion of Trapped Lipid Droplets. *Food Funct.* **2014**, *5*, 1481–1488.

(32)   Nguyen, H. T.; Marquis, M.; Anton, M.; Marze, S. Studying the Real-Time Interplay between Triglyceride Digestion and Lipophilic Micronutrient Bioaccessibility Using Droplet Microfluidics. 1 Lab on a Chip Method. *Food Chem.* **2019**, *275*, 523–529.

(33)   Scheuble, N.; Iles, A.; Wootton, R. C. R.; Windhab, E. J.; Fischer, P.; Elvira, K. S. Microfluidic Technique for the Simultaneous Quantification of Emulsion Instabilities and Lipid Digestion Kinetics. *Anal. Chem.* **2017**, *89*, 9116–9123.

(34)   Rosevear, F. B. Liquid Crystals : The Mesomorphic Phases of Surfactant Compositions. *J. Soc. Cosmet. Chem.* **1968**, *594*, 581–594.

(35)   Wu, H.-S.; Tsai, M.-J. Kinetics of Tributyrin Hydrolysis by Lipase. *Enzyme Microb. Technol.* **2004**, *35*, 488–493.

(36)   Sek, L.; Porter, C. J. H.; Charman, W. N. Characterisation and Quantification of Medium Chain and Long Chain Triglycerides and Their In Vitro Digestion Products, by HPTLC Coupled with In Situ Densitometric Analysis. *J. Pharm. Biomed. Anal.* **2001**, *25*, 651–661.

(37)   Mudie, S. T. ScatterBrain http://www.synchrotron.org.au/aussyncbeamlines/saxswaxs/software-saxswaxs.

(38)   Hyde, S. T. Identification of Lyotropic Liquid Crystalline Mesophases. In *Handbook of Applied Surface and Colloid Chemistry*; Holmberg, K., Ed.; John Wiley & Sons, Ltd, 2001; pp. 299–332.

(39)   Kirby, N. M.; Mudie, S. T.; Hawley, A. M.; Cookson, D. J.; Mertens, H. D. T.; Cowieson, N.; Samardzic-Boban, V. A Low-Background-Intensity Focusing Small-Angle X-Ray Scattering Undulator Beamline. *J. Appl. Crystallogr.* **2013**, *46*, 1670–1680.

(40)   Brody, J. P.; Yager, P.; Goldstein, R. E.; Austin, R. H. Biotechnology at Low Reynolds Numbers. *Biophys J* **1996**, *71*, 3430–3441.

(41)   Donnér, J. Preparation of Porcine Pancreatic Lipase Free of Co-Lipase Activity. *Acta Chem. Scand.* **1976**, *30*, 430–434.

(42)   Dutta, D.; Ramachandran, A.; Leighton, D. T. Effect of Channel Geometry on Solute Dispersion in Pressure-Driven Microfluidic Systems. *Microfluid. Nanofluidics* **2006**, *2*, 275–290.

(43)   Bisset, N. B.; Boyd, B. J.; Dong, Y. Da. Tailoring Liquid Crystalline Lipid Nanomaterials for Controlled Release of Macromolecules. *Int. J. Pharm.* **2015**, *495*, 241–248.

(44)   Safinya, C. R.; Sirota, E. B.; Plano, R. J. Nematic to Smectic-A Phase Transition under Shear Flow: A Nonequilibrium Synchrotron x-Ray Study. *Phys. Rev. Lett.* **1991**, *66*, 1986–1989.

(45)   Phan, S.; Salentinig, S.; Hawley, A.; Boyd, B. J. Immobilised Lipase for in Vitro Lipolysis Experiments. *J. Pharm. Sci.* **2015**, *104*, 1311–1318.

(46)   Ghazal, A.; Gontsarik, M.; Kutter, J. P.; Lafleur, J. P.; Ahmadvand, D.; Labrador, A.; Salentinig, S.; Yaghmur, A. Microfluidic Platform for the Continuous Production and Characterization of Multilamellar Vesicles: A Synchrotron Small-Angle X-Ray Scattering (SAXS) Study. *J. Phys. Chem. Lett.* **2016**, *8*, 73–79.

(47)   Massoumian, F.; Juskaitis, R.; Neil, M. A. A.; Wilson, T. Quantitative Polarized Light Microscopy. *J. Microsc.* **2003**, *209*, 13–22.

(48) Mezzenga, R.; Meyer, C.; Servais, C.; Romoscanu, A. I.; Sagalowicz, L.; Hayward, R. C. Shear Rheology of Lyotropic Liquid Crystals: A Case Study. *Langmuir ACS J. surfaces colloids* **2005**, *21*, 3322–3333.

(49) Barauskas, J.; Svedaite, I.; Butkus, E.; Razumas, V.; Larsson, K.; Tiberg, F. Synthesis and Aqueous Phase Behavior of 1-Glyceryl Monooleyl Ether. *Colloids Surfaces. B Biointerfaces* **2005**, *41*, 49–53.

(50) Tilbeurgh, H. Van; Sardat, L.; Verger, R.; Cambillau, C. Structure of the Pancreatic Lipase-Procolipase Complex. **1992**, *65*, 159–162.

(51) Hermoso, J.; Pignol, D.; Kerfelec, B.; Crenon, I.; Chapus, C.; Fontecilla-camps, J. C. Lipase Activation by Nonionic Detergents. *J. Biol. Chem.* **1996**, *271*, 18007–18016.

(52) Zeng, W.; Jacobi, I.; Li, S.; Stone, H. A. Variation in Polydispersity in Pump- and Pressure-Driven Micro-Droplet Generators. *J. Micromechanics Microengineering* **2015**, *25*, 115015–115018.

3.9 Appendix

Supplementary table 3-1. Positions along the microchannel of the S-MF device where the X-rays are focused on for the SAXS experiments. The distances were converted to reaction time using the linear velocity. The values in this table are for the TFR of 10 µL/hr, with a linear velocity of 0.234 mm/sec.

Shot number	Position along channel relative to flow focusing junction (mm)	Reaction time (secs)	Shot number	Position along channel relative to flow focusing junction (mm)	Reaction time (secs)
1	0.0	0.0	33	179.1	766.0
2	1.1	4.7	34	185.4	792.7
3	6.6	28.1	35	190.6	815.2
4	12.8	54.9	36	196.9	841.9
5	18.1	77.3	37	202.1	864.4
6	24.3	104.0	38	208.4	891.1
7	29.6	126.5	39	213.6	913.6
8	35.8	153.2	40	219.9	940.3
9	41.1	175.7	41	225.1	962.8
10	47.3	202.4	42	231.4	989.5
11	52.6	224.9	43	236.6	1012.0
12	58.8	251.6	44	242.9	1038.7
13	64.1	274.1	45	248.1	1061.2
14	70.3	300.8	46	254.4	1087.9
15	75.6	323.3	47	259.6	1110.3
16	81.8	350.0	48	265.9	1137.1
17	87.1	372.5	49	271.1	1159.5
18	93.3	399.2	50	277.4	1186.3
19	98.6	421.7	51	282.6	1208.7
20	104.8	448.4	52	288.9	1235.5
21	110.1	470.8	53	294.1	1257.9
22	116.3	497.6	54	300.4	1284.7
23	121.6	520.0	55	305.6	1307.1
24	127.8	546.8	56	311.9	1333.8
25	133.1	569.2	57	317.1	1356.3
26	139.3	596.0	58	323.4	1383.0
27	144.6	618.4	59	328.6	1405.5
28	150.9	645.2	60	334.9	1432.2
29	156.1	667.6	61	340.1	1454.7
30	162.4	694.4	62	346.4	1481.4
31	167.6	716.8	63	351.6	1503.9
32	173.9	743.5			

Supplementary table 3-2. The variables used to calculate the position of complete diffusion of lipase from stream of enzyme to the stream of emulsion during a digestion in the OTS-MF device.

Width of channel	0.84	mm
Enhanced diffusion coefficient of pancreatic lipase (for TFR 120 µL/hr)	2.08×10^{-5}	cm^2/sec
Lateral distance to travel in recipient stream, x	0.1	mm
Total flow rate	1200	µL/hr
Cross sectional area	0.554	mm^2
Flow rate (enzyme suspension)	600	µL/hr
Flow rate (emulsion)	600	µL/hr
FRR (enzyme:emulsion)	1	
Time of complete mixing	2.4	sec
Distance of complete mixing	1.44	mm

Supplementary table 3-3. Enhanced diffusion coefficients and the distance of complete mixing for each flow rate ratio for experiments conducted in the OTS-MF device.

TFR (µL/hr)	120	300	600	1200
K	0.3	1.9	7.8	31.1
Enhanced D (cm^2/s)	2.09E-07	1.30E-06	5.21E-06	2.08E-05
Time of complete mixing (sec)	239.8	38.4	9.6	2.4
Distance of complete mixing (mm)	14.4	5.8	2.9	1.4
Distance of complete mixing (% of full channel length)	14.4%	5.8%	2.9%	1.4%
TFR (µL/hr)	2400	3600	6000	12000
K	124.5	280.0	777.8	3111.4
Enhanced D (cm^2/s)	8.34E-05	1.88E-04	5.21E-04	2.08E-03
Time of complete mixing (sec)	0.600	0.267	0.096	0.024
Distance of complete mixing (mm)	0.721	0.481	0.289	0.144
Distance of complete mixing (% of full channel length)	0.72%	0.48%	0.29%	0.14%

Supplementary table 3-4. Enhanced diffusion coefficients and the distance of complete mixing for each flow rate ratio for experiments conducted in the S-MF device.

TFR (µL/hr)	10	40
K	1.55E-01	1.22E+00
Enhanced D (cm^2/s)	1.04E-07	1.67E-06
Time of complete mixing (sec)	119.98	7.50
Distance of complete mixing (mm)	28.05	7.02
Distance of complete mixing (% of channel length)	8.02	2.00
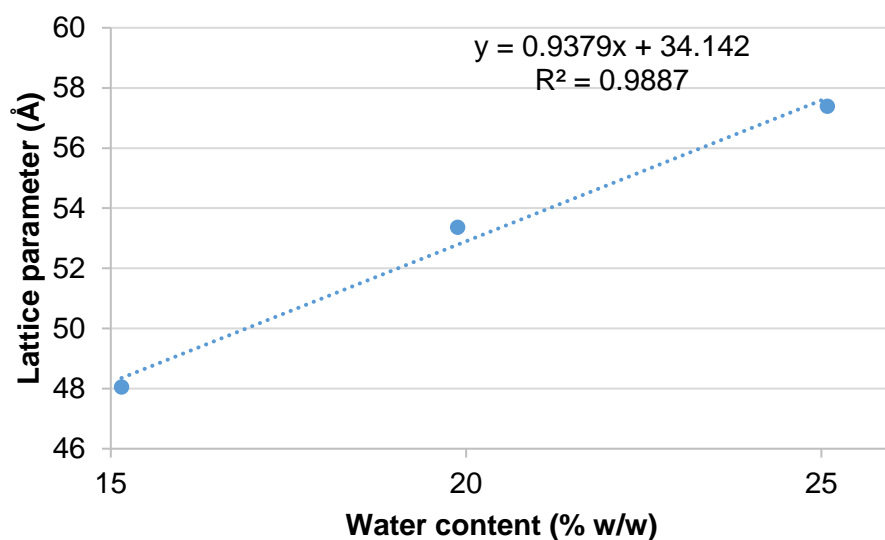
Supplementary figure 3-1. A calibration curve of correlating the water content to the lattice parameter based on data from the work of Barauskas *et al.* for the hydration of selachyl alcohol-based H_2 phase at 25 °C.[49]

Chapter 4: Salt and vinegar on a chip—Microfluidics for inducing transitions in lipid-based systems responsive to changes in pH and ionic strength

4.1 Introduction

While the oral application of liquid crystalline systems is useful for compliance issues, other routes of administration of LCNPS have also been reported including mucosal and intravenous ocular applications[1–3] In the case of intravenous application of LCNPs to treat conditions such as cancer, these carriers can protect the drug particles from metabolism, thereby decreasing frequency of administration.[4,5] In the case of mucosal delivery, the shift in pH has already been shown to induce a change to a mucoadhesive LCNP system which could be retained for longer for sustained release of triamcinolone.[6] The ability to transition from one structure to another (stimuli-responsiveness) presents a useful property for drug delivery. Therefore, in order to probe the behaviour of LCNPS in these environments it is desirable to understand their kinetic transformation behaviour. Bulk mixing systems could achieve this, however the kinetics in the data may be unreliable given the inefficient mixing behaviour.

In principle, a bulk mixing flow-through model such as the pH-stat approach, coupled to small angle X-ray scattering (SAXS), could be used to monitor the kinetics and structural aspects of transformations in stimuli-responsive lipid-based formulations.[7–11] However, in addition to the issues discussed in previous chapters regarding these bulk processes, there are also limitations with the acquisition of data. Each time point in the phase transition is representing SAXS analyses collected over a range of time. It is common to have an exposure time of the X-ray beam set to 5 secs or more, however, the result is the average structure of all particles exposed to the beam in that acquisition.[12] In other words, scattering collected over multiple time points are combined into one scattering profile, meaning that systems that appear as mixed phases could actually have been two different phases existing independently at different time points. This can be particularly problematic for systems which have rapid reaction times. Ultimately, if the phase transitions cannot be accurately or consistently characterised, then the efficiency of formulation development may be impeded.

Combining the mixing and analytical vessel into one apparatus in the form of microfluidics has been demonstrated in the previous chapters to overcome these issues. Microfluidics can continuously facilitate the coaxial flow of the formulation and solution containing the stimulus material via hydrodynamic flow focussing.[13,14] The entire process including the initial convergence of the solutions can be observed through an appropriate X-ray transparent device, such as the S-MF device developed in this thesis. Additionally, the retention time of sample within the device, as signified by the position

along the channel, can be correlated to a time point in the reaction.[15] Thus, acquiring data for a short or long time at a given position theoretically should display the same scattering profile, albeit with varied total intensity. Monitoring the kinetics of reactions is therefore not limited by the instrumental acquisition time as it is in a bulk mixing flow through configuration. With the analysis of the enzyme-triggered lipid-based formulation on the S-MF device that was explored in previous chapters, the lipase must diffuse across the adjacent formulation stream before digestion can proceed. As such, the process is controlled and can be characterised by diffusional equations[13] as opposed to the random mixing observed in the bulk mixing pH-stat approach. The concept can conceptually be translated also to trigger changes using other solution-based systems such as ionic strength and pH changes for appropriately responsive liquid crystalline nanoparticle (LCNP) systems.

Previous chapters have focused on developing and optimising microfluidic devices for the understanding of the kinetics of digestion- and dilution-responsive LCNPs. In this chapter, the microfluidics approach is further extended to probe LCNP systems that are responsive to changes in pH and tonicity, both stimuli that are particularly relevant to *in vivo* conditions.

4.2 Hypotheses and aims

It was hypothesised:

- That phase transition trajectories observed in equilibrium phytantriol-based samples varying in pH and ionic strength can be generated *in situ* using the custom microfluidic device described in **3.3.4.2 Serpentine microfluidic device (S-MF)**.
- That the custom microfluidics device can resolve early kinetic structures of rapidly-transforming pH and ionic strength-sensitive systems without hindrance of acquisition time from the analytical instrument.

To address these hypotheses, the follow aim was achieved:

- To determine structural changes upon mixing of pH- and ionic strength-sensitive systems *in situ* using SAXS

4.2.1 pH-sensitive systems

Lipid systems that form bicontinuous cubic (V_2) and inverse hexagonal (H_2) phases are inevitably uncharged (or at most zwitterionic). For example, phytantriol,[16,17] glyceryl monooleate,[18] and selachyl alcohol[19] are all non-ionic lipid amphiphiles; the chemical structures are shown in **Figure 4-1**. As a consequence, systems prepared from these lipids in water are not sensitive to changes in pH and ionic strength unless there is a component present to induce a change in the packing behaviour, such as oleic acid. Thus, in order to render these systems responsive to pH and ionic strength, an additional component needs to be added that imparts this responsiveness,[20] such as molecules which can impart an ionic charge to the system as those shown in **Figure 4-1**.[6,13,21–25] These components have been termed 'actuators'. The usual approach with such 'actuators' is to determine the influence of the actuator on the phase diagram of the host lipid and water system. Upon identification of the threshold amount of actuator required to induce a change away from the phase formed by the host system without actuator present, then determine the degree of stimulus required to 'neutralise' the effect of the actuator.
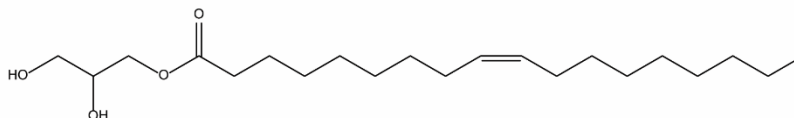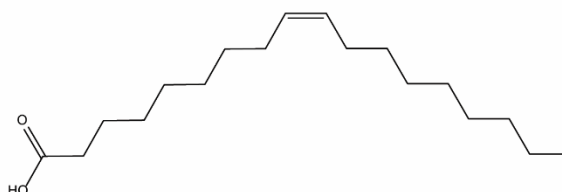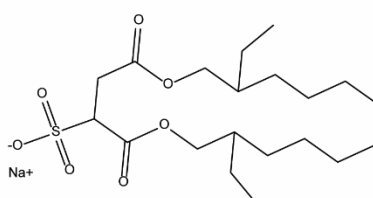
Phytantriol (PHYT)
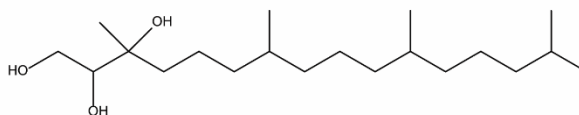
Selachyl alcohol
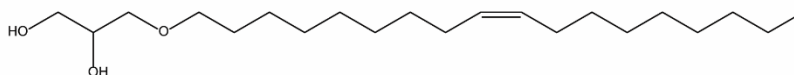
Glyceryl monooleate

Oleic acid (OA)

Sodium dioctyl sulfosuccinate (AOT)
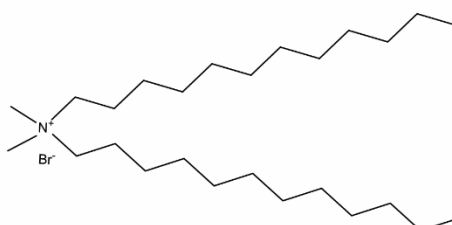
Didodecyldimethylammonium bromide (DDAB)

Figure 4-1. From the top, illustrated are the chemical structures of core lyotropic lipids: phytantriol, selachyl alcohol and glyceryl monooleate, and actuators: oleic acid which contains an ionisable carboxylic acid with a reported pKa value of approximately 9.85;[26] sodium dioctyl sulfosuccinate which is an anionic surfactant; and didodecyldimethylammonium bromide which is a cationic double-chained surfactant.

Lipid-based formulations can be rendered responsive to changes in pH through the addition of an ionisable actuator. These systems are particularly relevant for drug delivery as they can exploit the different regions of the body with different pH.[27] A shift in pH can be used to ionise or protonate the actuator in the system. In the case of a weakly basic system (pH ~7), Negrini and Mezzenga reported a cubic *Im3m* phase composed of monolinolein as the lyotropic lipid and linoleic acid as the actuator. The proposed drug delivery system would transition to the H$_2$ phase at low pH where the linoleic acid remains uncharged, observed within the stomach, which would hinder the untimely

release of drug.[27] The formulation would revert to its original structure in the relatively more basic environment of the intestines and induce drug release.[27] The addition of fatty acid to a core lipid system renders the system pH-sensitive through alteration of the charged state of the acid, which changes the apparent polar head group size.[6,23] Subsequently, the packing behaviour of the lipids was affected, resulting in a phase transition. Salentinig *et al.* studied the addition of oleic acid to the glyceryl monooleate system and found that increasing the pH of the system induced the ionisation of the fatty acid which increased the size of the hydrophilic head group and thus decreased the critical packing parameter. A monoolein dispersion containing 30% w/w oleic acid was found to change from a microemulsion to the *Fd3m* phase to the H_2 phase. The process was reversible upon decreasing the pH to below the pKa, which was also found to deviate from literature values given the change in microenvironment. Du *et al.* followed up the work of Salentinig *et al.* with a subsequent study of the phytantriol and oleic acid system, constructing a phase diagram shown in **Figure 4-2** using the SAXS-flow-through configuration.[6] Kinetic changes in this system were not examined because the mixtures were allowed to equilibrate before data acquisition. As kinetics of acid-base reactions can occur in the order of microseconds and even down to picoseconds,[28] it may not have been possible to probe the kinetics of the ensuing formation of the non-equilibrium structures in the flow through-SAXS apparatus.[7]
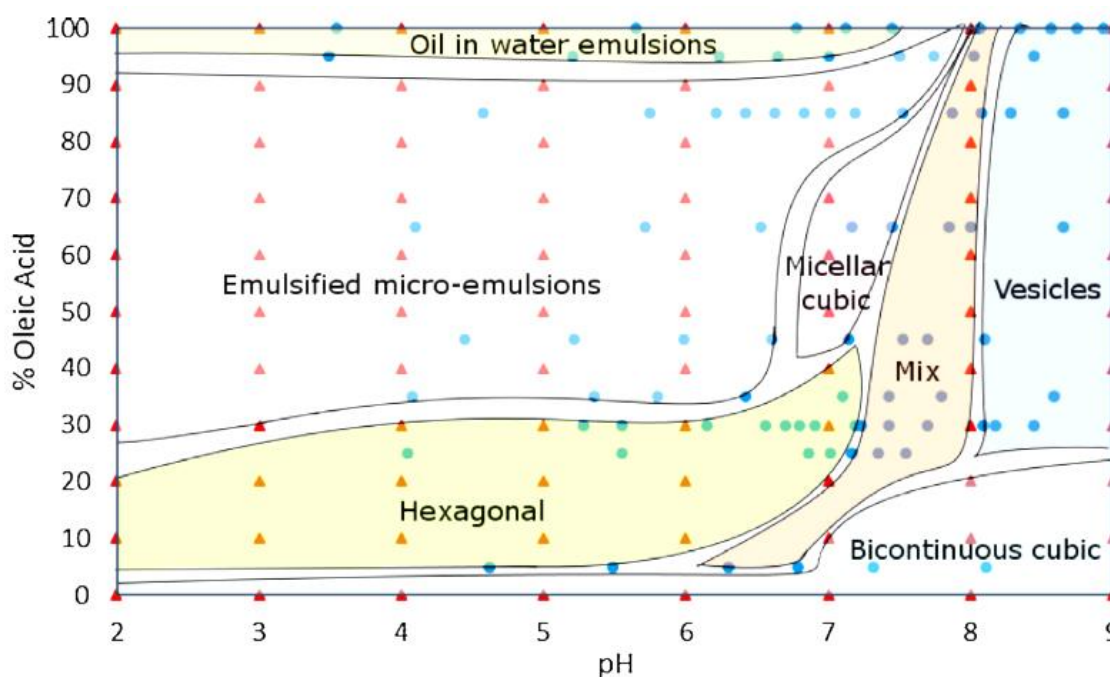

Figure 4-2. Phase diagram of a PHYT dispersion containing increasing amounts of oleic acid, and with increasing pH. Figure adapted from Du *et al.*[6]

4.2.2 Ionic strength-responsive systems

Ionic surfactants can be incorporated as an actuator into LCNP systems, enabling phase transitions to occur in response to changes in tonicity. The neutralisation of the charged head groups of these molecules can be modulated with the concentration of salts in the formulation, which alters the apparent size of the head group and can result in a change to the nanostructure of the self-assembled system. Liu *et al.* had constructed a phase diagram for the phytantriol and water system containing sodium dioctyl sulfosuccinate (AOT) or didodecyldimethylammonium bromide (DDAB) illustrated in **Figure 4-3**.[29] Formulations were equilibrated before SAXS analyses and phase identification so kinetic studies were not performed.
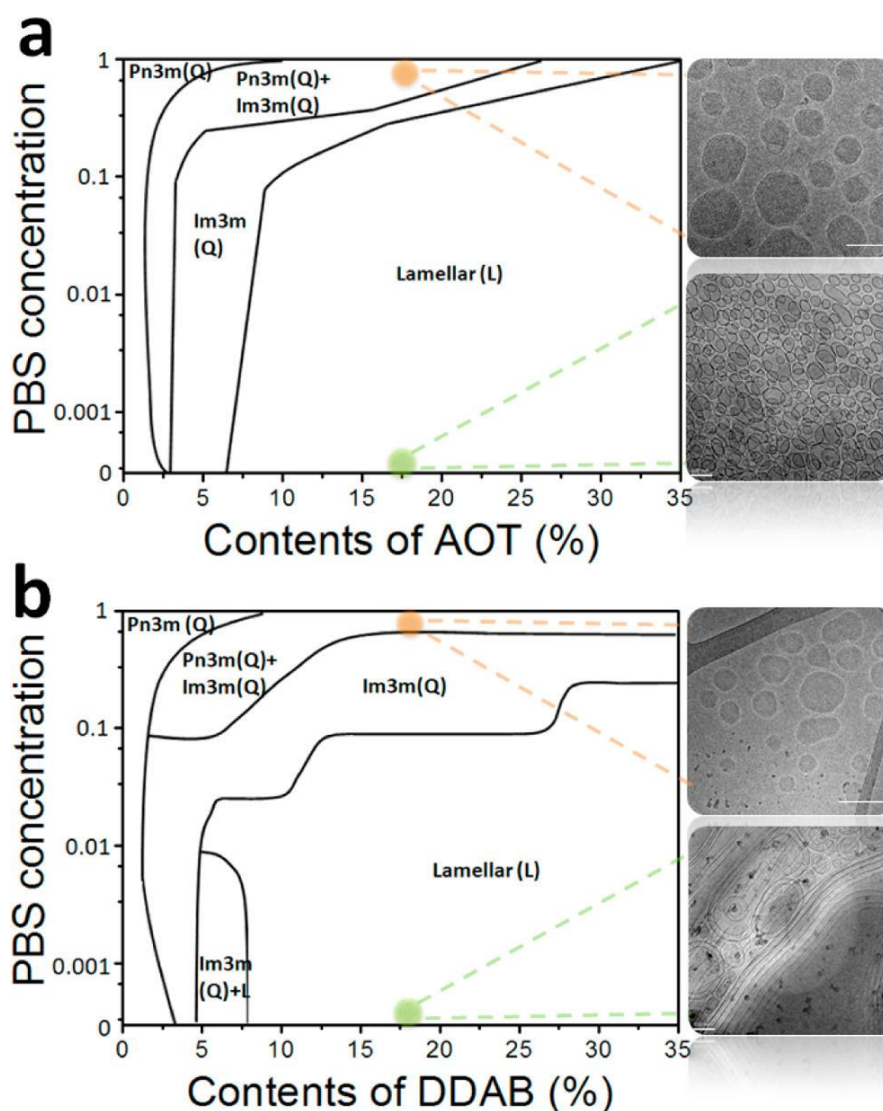

Figure 4-3. Phase diagram of PHYT systems containing increasing amounts of AOT or DDAB with increasing concentrations of phosphate buffered saline. Figure adapted with permission from Liu *et al.*[29]

This chapter will therefore expand on the application of the pre-established custom microfluidics device beyond digestion and explore stimuli-responsive phase transitions induced through changes in solution conditions. Dispersions of phytantriol (PHYT) with oleic acid (OA) and dispersions of PHYT with ionic surfactants (DDAB or AOT) were selected because, as described above, the phase diagrams, and therefore trajectories to expect on introduction of the stimulus were already known.

4.2.3 Projected trajectories for phase transitions

Specifically, for the pH responsive studies, phytantriol with 60% w/w OA (PHYT60OA), with 30% w/w OA (PHYT30OA) and with 10% w/w OA (PHYT10OA) were selected for the pH-responsive systems, and the trajectories are illustrated in **Figure 4-4A**. Each formulation was combined with a HCl solution in the S-MF device. PHYT60OA (**Trajectory I**) was expected to transition from L_α to micellar cubic phase (*Fd3m*) and finally an emulsified microemulsion, assuming a linear and horizontal trajectory. With a similar trajectory, PHYT30OA (**Trajectory II**) was predicted to transition from vesicles to H_2 phase to a microemulsion. PHYT10OA (**Trajectory III**) was anticipated to transition from the V_2 phase to H_2 phase.
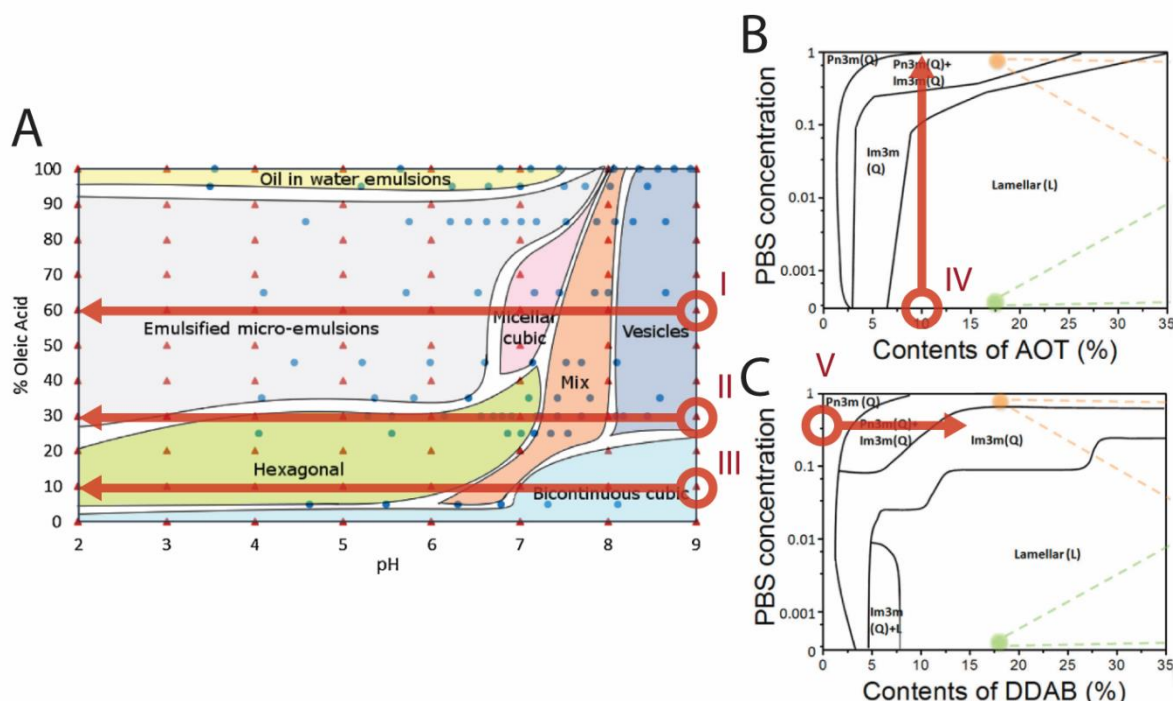

Figure 4-4. Expected trajectories of the phase transitions of phytantriol and OA systems (A) for PHYT60OA in trajectory I, PHYT30OA in trajectory II, PHYT10OA in trajectory III; phytantriol and AOT system (B) in trajectory IV for PHYT10AOT; and a phytantriol with DDAB formulation (C) in trajectory V for 0.3PHYTV$_2$. The trajectories are tabulated in **Table 4-1**.

The ionic-strength responsive systems were studied using two different salt related transitions. Phytantriol with 10% AOT (PHYT10AOT) was combined with a buffered saline solution (to be equilibrated at 1xPBS after dilution) and anticipated to transition from lamellar phase to mixed cubic phases (*Pn3m* and *Im3m*) indicated by **Trajectory IV** in **Figure 4-4B**. For the other trajectory in **Figure 4-4C**, a simple phytantriol-based cubosome dispersion was combined with a solution of DDAB and was expected to transition from the cubic *Pn3m* phase to the *Im3m* phase (**Trajectory V**).

Table 4-1. Summary of the trajectories of phase transitions for pH- and ionic strength-sensitive lipid-based systems.

Trajectory	Formulation	Initial phase	Stimulus	Expected phase after equilibration
I	PHYT60OA (pH 9)	L_α	0.1M HCl	Microemulsion
II	PHYT30OA (pH 9)	L_α	0.1M HCl	Microemulsion
III	PHYT10OA (pH 9)	V_2	0.1M HCl	H_2 phase
IV	PHYT10AOT	L_α	2xPBS solution	*Pn3m* and *Im3m*
V	$0.3PHYTV_2$	*Pn3m*	3% w/w DDAB in 0.3xPBS	*Im3m*

4.3 Methods

4.3.1 Materials

Phytantriol (3,7,11,15-tetramethylhexadecane-1,2,3-triol, PHYT) was purchased from DSM Nutritional Products Ltd, Singapore. Samples for pH systems incorporated oleic acid sourced from Croda International in Yorkshire, UK. Ionic strength studies consisted of didodecyldimethylammonium bromide (DDAB) obtained from Fluka, Analytical in Switzerland (98% purity), and sodium dioctyl sulfosuccinate (AOT) obtained from Cytec Industries, N.J., U.S.A.

Sodium chloride was purchased from Chem-Supply, SA, Australia. Potassium chloride was purchased from Sigma-Aldrich, St. Louis, MO, U.S.A. Di-sodium hydrogen orthophosphate, potassium dihydrogen orthophosphate and sodium hydroxide pellets were obtained from Ajax Finechem, NSW, Australia. Milli-Q water was supplied by the Millipore Milli-Q purification system (Billerica, USA).

Synperonic F108 (Pluronic F108) was purchased from Fluka, France, and Lutrol F127 (Pluronic F127) was purchased from BASF AG, Ludwigshafen, Germany.

4.3.1.1 Sample preparation

4.3.1.1.1 Lipid dispersions

PHYT was heated to 60° C, weighed and combined with the required additive in a scintillation vial (7 mL). Compositions of each formulation are described in **Table 4-2**. The mixture was then briefly vortexed to distribute the additive throughout the lipid. Aqueous phase (containing 1% w/w Pluronic F108) was added so that the lipid content of the formulation was 10% w/w, unless otherwise stated. The dispersions were initially treated with 10 mins of sonication in a water bath (Branson 2210R-MT Ultrasonic Cleaner) until warm before being subjected to ultrasonication (Misonix Ultrasonic liquid processor S-4000, USA) for 2.5 mins at 30% amplitude, pulsing on for 4 secs and off for 1 sec to ensure complete homogenisation.

Table 4-2. Composition of the lipid-based formulations for the study of systems responsive to changes in pH and salt concentration. MQ = Milli-Q grade water; F108 = 1% w/w Pluronic F108; PBS = phosphate buffered saline; F127 = 1% w/w Pluronic F127; PHYT = phytantriol; OA = oleic acid; AOT = sodium dioctyl sulfosuccinate.

Formulation	MQF108 (g)	0.3xPBSF127 (g)	MQF127 (g)	PHYT (g)	OA (g)	AOT (g)
PHYT60OA (Trajectory I)	2.700	-	-	0.120	0.180	-
PHYT30OA (Trajectory II)	2.700	-	-	0.210	0.090	-
PHYT10OA (Trajectory III)	2.700	-	-	0.270	0.030	-
PHYT10AOT (Trajectory IV)	-	-	2.850	0.135	-	0.015
0.3PHYTV$_2$ (Trajectory V)	-	2.700	-	0.300	-	-

As described above the three pH-sensitive phytantriol-based formulations contained 10%, 30% w/w and 60% w/w oleic acid. The resulting dispersions were all adjusted to pH 9.0 to ensure the formation of uni-lamellar vesicles. The dispersions were mixed with hydrochloric acid solution (0.1 M) in the microfluidic devices.

The first trajectory for ionic strength studies used a 5% w/w lipid dispersion (**Trajectory IV**), prepared in the same methods as above, wherein the lipid content consisted of phytantriol with 10% w/w dioctyl sulfosuccinate (PHYT10AOT).[29] This formulation, expected to be liposomes, was combined with a 2x PBS solution (also containing 1% w/w Pluronic F108) in the microfluidic device. The second trajectory (**Trajectory V**) required the mixing of a 10% w/w phytantriol dispersed in 0.3x PBS solution

containing 1% w/w Pluronic F127 (0.3PHYTV$_2$) with a 3% w/w solution of DDAB (also containing 1% w/w Pluronic F127).

PHYT10AOT was mixed with a 2x PBS solution and monitored *in situ* with SAXS and shown in **Figure 4-9**. The formulation initiated as a L$_\alpha$ system at time = 0 secs. If the system was diluted in the microfluidic device with a 2xPBS solution the system would equilibrate to a 1xPBS solution at a flow rate ratio of 1.

4.3.1.1.2 Buffers

Sodium chloride (1.369 mM), potassium chloride (0.268 mM), disodium hydrogen orthophosphate (0.10 mM) and potassium dihydrogen orthophosphate (0.018 mM) were weighed out and made up to volume with Milli-Q grade water to produce a 10x phosphate buffered saline (PBS) solution for studies on ionic strength-sensitive systems. The PBS solution was later diluted down with Milli-Q grade water to the appropriate concentration as needed and combined with Pluronic F127 (1% w/w).

4.3.2 Tracking phase transitions using microfluidics- interfaced with small angle X-ray scattering

The quartz-based serpentine microfluidic (S-MF) device described in 3.3.4.2 Serpentine microfluidic device (S-MF) was fitted to a custom 3D printed holder that was secured in the 96-well plate holder available at the SAXS/WAXS beamline at the Australian Synchrotron. The formulation and solution containing the stimuli were manually drawn into 0.5 mL syringes and the two streams were delivered to the device via a syringe driver (NE-4000 2 channel syringe pump from New Era Pump System Inc., U.S.A.) that controlled the flow rates. Fixing the device to the digitally controlled experimental stage allowed the device to be shifted as needed in the X- and Y- directions.

SAXS experiments were undertaken at the Australian Synchrotron on the SAXS/WAXS beamline.[30] The wavelength of the X-ray was set to 0.620 Å (20 keV). The size of the beam spot was 200 μm in width and 100 μm in height. The sample to detector distance was set to 1538 mm giving a *q* range of 0.0142 Å^{-1} to 0.975 Å^{-1} after calibration with silver behenate. Flux was adjusted to 100% and the acquisition time at each position was 30 secs. A Pilatus 1M detector acquired 2D scattering patterns over an active area of 169 × 179 mm^2, where the dimensions of each pixel was 172 μm.

Data were then converted to a 1D scattering function I(q) using the in-house-developed software package scatterBrain.[31] Phases were identified based on the spacing ratios of the Braggs peaks according to literature.[32]

To measure the end points of mixing for comparison to the dynamic mixing experiments described above, equal volumes of the formulations and the corresponding solution of stimulus were combined in a centrifuge tube and vortexed for 1 min. These premixed systems were filled into glass capillaries and measured with a 5 sec acquisition time using the parameters described above.

4.4 Results and discussion

4.4.1 Analysis of phase transitions induced through changes in solution conditions

4.4.1.1 pH-induced transformations

Acidification of the PHYT60OA system with 0.1M HCl (**Trajectory I**) showed a transition from L_α structure to H_2 phase (**Figure 4-5**). Almost immediately after contact with the acid, the L_α structure was lost. There appeared to be a peak within the q-range 0.117 to 0.151 Å^{-1} that evolved over time while shifting to lower q. By 200 secs, the peak had reached its maximum intensity at q = 0.133 Å^{-1} and began to decrease in intensity while shifting slighting to higher q (corresponding to a smaller lattice parameter). The peak had shifted to q = 0.145 Å^{-1} at 334 secs, and the peak began to increase in intensity again and return to the original q-position. The intensity of this peak also stabilised for the remainder of the transformation. The peak of interest here (0.117 < q < 0.151 Å^{-1}) did not correlate to the scattering for the *Fd3m* phase or microemulsion. Instead, it correlated with the q-position of the first peak for H_2 phase in the premixed solution containing equal volumes of PHYT60OA and 0.1M HCl (**Supplementary figure 4-1**). This suggests that instead of the expected horizontal trajectory from the right to the left of the phase diagram, the transformations may prefer formation of the H_2 phase over the *Fd3m* phase. As a phase diagram is based on equilibrium structures, it is possible that the dynamic structures observed in these studies were not fully equilibrated which could lead to the formation of other structures. This observation was noted as a supercooling effect by Dong *et al.* who remarked the formation of unexpected phases when monitoring phase changes under different 'stimulus' such as heating and cooling.[17]
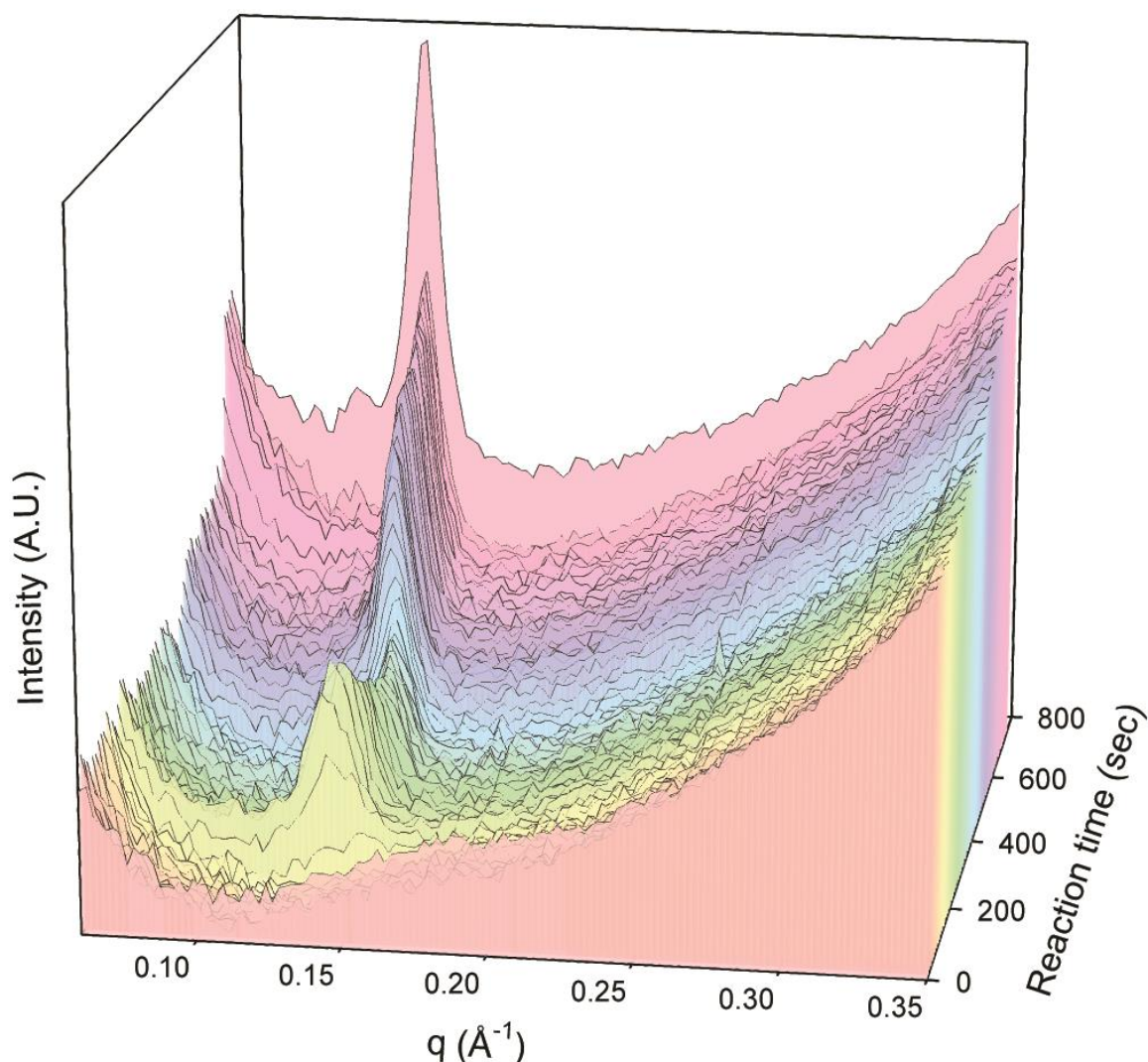
Figure 4-5. Monitoring the structural progression during the dynamic incorporation of a 0.1M solution of HCl with PHYT60OA (pH 9) in the S-MF device. The formulation initiated as vesicles at time 0. Upon contact with the acidic solution, there was an immediate loss of the scattering for L_α phase. A peak at 0.117 Å^{-1} < q < 0.151 Å^{-1} grew in intensity whilst shifting to lower q at a maximum of q = 0.133 Å^{-1} before decreasing in intensity and shifting slightly to higher q and then back again. The peak stabilised at a constant intensity and q-position by 334 secs for the remainder of the transformation. The first profile at 0 secs has been omitted for clarity and the full kinetic profile can be seen in **Supplementary figure 4-2**.

Similar to the previous formulation, the L_α phase of PHYT30OA was completely disrupted upon contact with 0.1M HCl (**Trajectory II**). The formulation was expected to transition from L_α vesicles to H_2 phase and then an emulsified microemulsion. However, a rapid transition of the scattering of the L_α phase to a broad hump, with a sharp apex was observed in the S-MF device (**Figure 4-6**). The two features were most likely indicative of the H_2 phase and microemulsion co-existing, despite not being observed in the literature phase diagram. By 140 secs, there was an evolution of a sharp peak at q = 0.109 Å^{-1}. Identification of the phase from this peak alone cannot be confirmed. While the q-

position of this peak does not match the position of the first H_2 phase peak of the premixed system (**Supplementary figure 4-1**), the peak could still be associated with a H_2 phase with a greater lattice parameter when formed *in situ*. The putative 'H_2 phase' peak decayed within 185 secs and a broad hump persisted for the remainder of the transformation, fluctuating slightly in lattice parameter. The broad peak is attributed to the scattering from the microemulsion which was the expected equilibrium structure at lower pH.
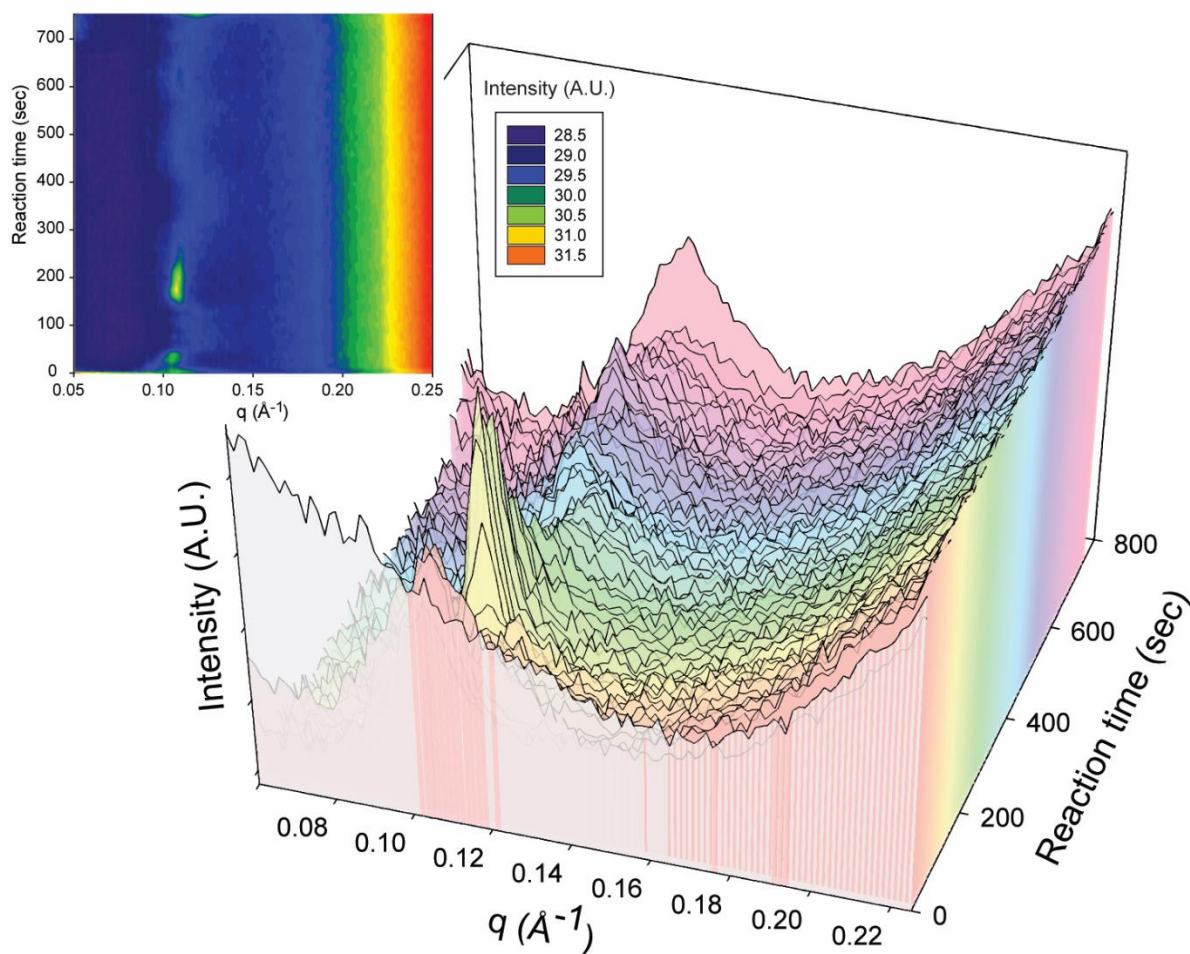

Figure 4-6. Monitoring the structural progression during the dynamic incorporation of a 0.1M solution of hydrochloric acid with PHYT30OA (pH 9) in the S-MF device. The formulation initiated as vesicles as illustrated by the gradual slope at time 0. Upon contact with the hydrochloric acid, there was an almost immediate loss of the L_α scattering profile, replaced with a broader but more distinct hump. The intensity of the hump decreased as a sharp peak at $q = 0.109$ Å^{-1} evolved and decayed within the span of 185 secs. The broad hump persisted for the remaining 500 secs, fluctuating slightly in q, which is evident in the inset containing the contour plot.

Trajectories I and **II** were expected to provide transitions through three different structures on mixing, while PHYT10OA (**Trajectory III**) was only expected to transition through two phases and was observed to do so almost instantaneously in **Figure 4-7**. The initial cubic *Pn3m* phase observed for the

formulation was fully transformed into H_2 phase when combined with the hydrochloric acid solution *in situ* within 0.03 secs. Although this was the projected transformation, the rapid transition was unexpected. The rapid delivery of the protons to the oleic acid molecules could be explained by its fast diffusion coefficient and the proton-hopping mechanism,[33,34] however the restructuring of the phytantriol—a molecule with a molar mass of 330.55 g·mol^{-1}—was equally as fast. The use of microfluidics for this particular system highlights the potential to analyse rapidly transforming systems, especially given that the exposure times for SAXS can exceed 5 secs in the bulk mixing approaches and would therefore not resolve these subsecond transitions.
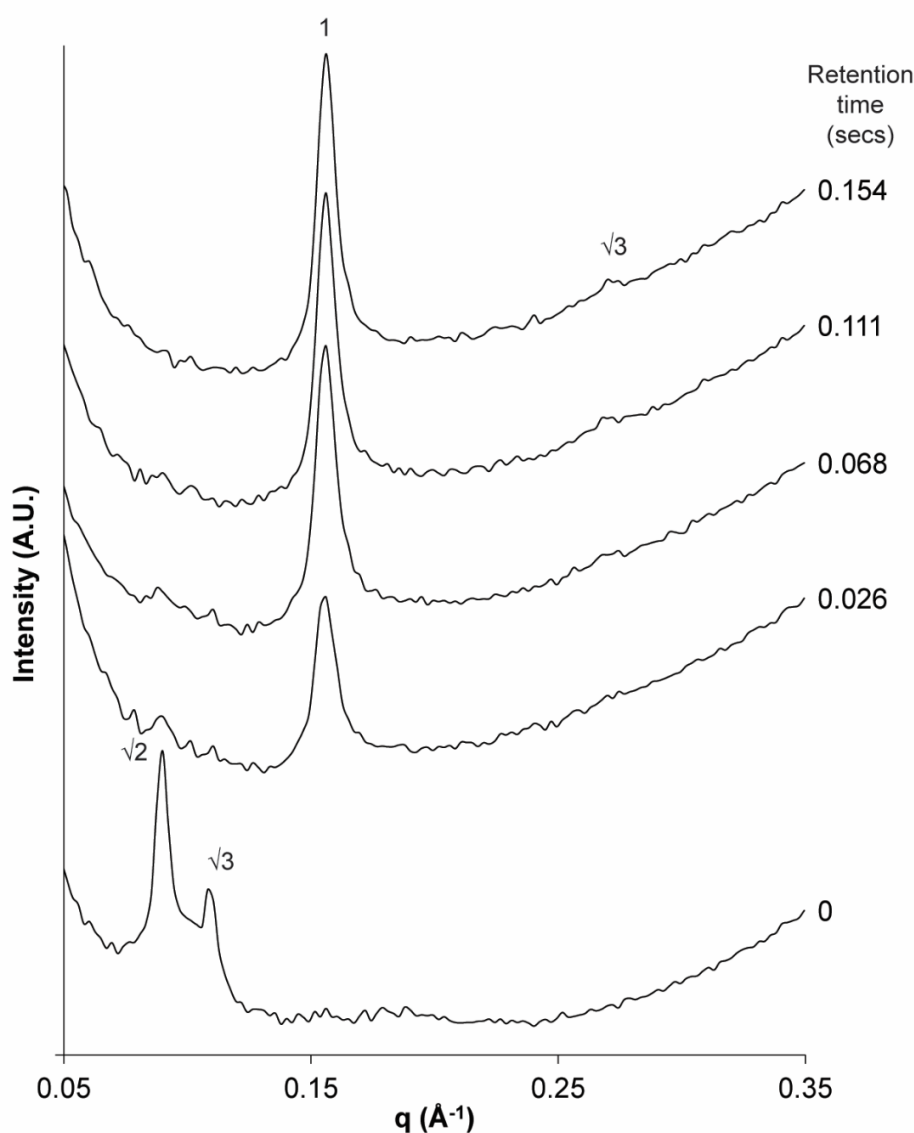

Figure 4-7. Monitoring the structural progression during the dynamic incorporation of a 0.1M solution of hydrochloric acid with PHYT10OA (pH 9) in the quartz microfluidic device. The formulation was initially observed to be a dispersion of cubic *Pn3m* nanoparticles which immediately transformed completely to H_2 phase within 0.02 secs.

4.4.1.2 Ionic-strength-induced transformations

The PHYT10AOT system in combination with an increased salt concentration (2xPBS solution) demonstrated the expected phase transition from L_α phase to a mixed phase of cubic *Pn3m* and *Im3m*, although with low sensitivity. When the two solutions were mixed at a 1:1 volumetric ratio, the system would equilibrate to PHYT10AOT in 1xPBS solution, which according to the phase diagram in **Figure 4-4B** (**Trajectory IV**), two cubic phases (*Im3m* and *Pn3m* geometries) would be present. In monitoring the kinetics of this mixing *in situ* (**Figure 4-8Figure 4-9**), there was a slight change in the scattering profile by 100 secs. The background scattering of this experiment was incredibly noisy compared to other experiments, so identification of peaks was not very confident for the intermediate time points. The decrease in signal could be attributed to the lower concentration of the lipid (5%) as a 10% w/w dispersion was too viscous to flow through the microfluidic channel. However, at the last time point (the last turn of the microchannel), the area of sample to acquire from was relatively larger so a clearer scattering profile was resolved. From this scattering profile, three peaks were observed with a spacing ratio of $\sqrt{2}$, $\sqrt{4}$ and $\sqrt{6}$. Although the profile could be identified as the cubic *Im3m* phase, it did not correspond with the expected trajectory of the literature phase diagram in the region of the two cubic phases. The peak labelled $\sqrt{4}$ was unusually intense for the second peak of the *Im3m* phase. In this respect, it is then possible to index the latter two peaks as $\sqrt{2}$ and $\sqrt{3}$ which would be indicative of the *Pn3m* phase as was observed in the mixed phase system of Ghazal *et al.*[13] It was also noted that the ratio of the lattice parameters of the cubic *Im3m* phase (111.5 Å) and the cubic *Pn3m* phase (79.3 Å) was 1.41. The ratio can be compared to the documented Bonnet transformation where the ratio of the lattice parameters of the two phases in equilibrium together is 1.28.[35] Although there was a 10% positive deviation with the theoretical values, the ratio from this work fell within the range of experimental values from other non-equilibrium studies (1.36 -1.41).[13] The discrepancy in values could be due to the 1.41 value being derived from non-equilibrium studies while the literature values were from equilibrated samples. The coexistence of these two phases would align with the expected trajectory of the phase diagram.
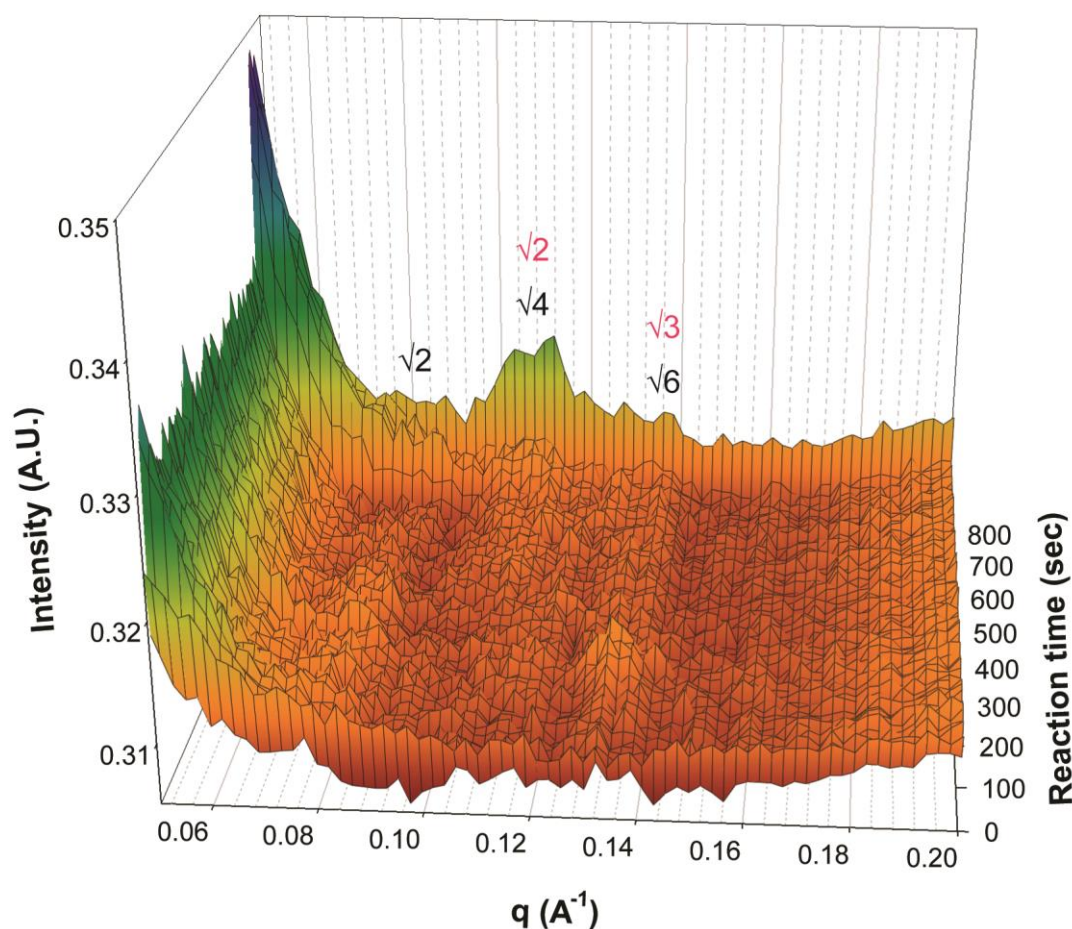
Figure 4-8. Monitoring the structural progression during the dynamic incorporation of a solution of 2xPBS solution to PHYT10AOT system. The style of this figure is different to previous graphs to emphasize the incredible low intensity signals of the system. The initial L_α structure was replaced by an apparent mixed phase of cubic *Im3m* (black data labels) and *Pn3m* (red data labels) phase.

The structural evolution of 0.3PHYTV$_2$ combined with a DDAB solution (**Trajectory V**) in the S-MF device was monitored and the results are presented in **Figure 4-9**. The formulation was initially the cubic *Pn3m* phase. This was denoted by the spacing ratios of the peaks at $\sqrt{2}$, $\sqrt{3}$, $\sqrt{4}$ and $\sqrt{6}$ in the scattering profile at 0 secs. Upon contact with a 3% w/w solution of DDAB, a transition to the *Im3m* structure was expected according to the equilibrated phase diagram in **Figure 4-3** which was also confirmed by **Supplementary figure 4-1**. As DDAB is hydrophobic in nature, it is anticipated that when introduced, it would mostly associate with the lipidic structures so that the local concentration would equilibrate to at least 15% w/w of DDAB. However, the *in situ* combination of both components did not yield *Im3m* phase, instead showing what appeared to be a loss of all nanostructure over 100 secs. Alternatively, the system could also be L_α phase as the scattering profile exhibited a similar pattern to the scattering profiles for PHYT60OA (**Figure 4-5**) and PHYT10AOT (**Figure 4-8**) at

0 secs under flow, both of which were L_α phase. Muir *et al.* had also noted a similar scattering pattern for a 15% w/w solution of DDAB using SAXS and cryoTEM.[36] The formation of L_α phase under flow was possible given that certain compositions of PHYT and DDAB can form L_α phase, especially given the log scale of the PBS concentration in the original phase diagram.[29] Otherwise, DDAB at low concentrations can self-assemble into L_α phase.[37] In this scenario, the formation of L_α phase may have been preferred for the composition of DDAB and the method for processing (diffusion as opposed to vortexing or sonicating). The liposomes could have then solubilised a sufficient amount of PHYT molecules to disrupt the V_2 phase but not enough to induce a phase transition in the L_α phase.
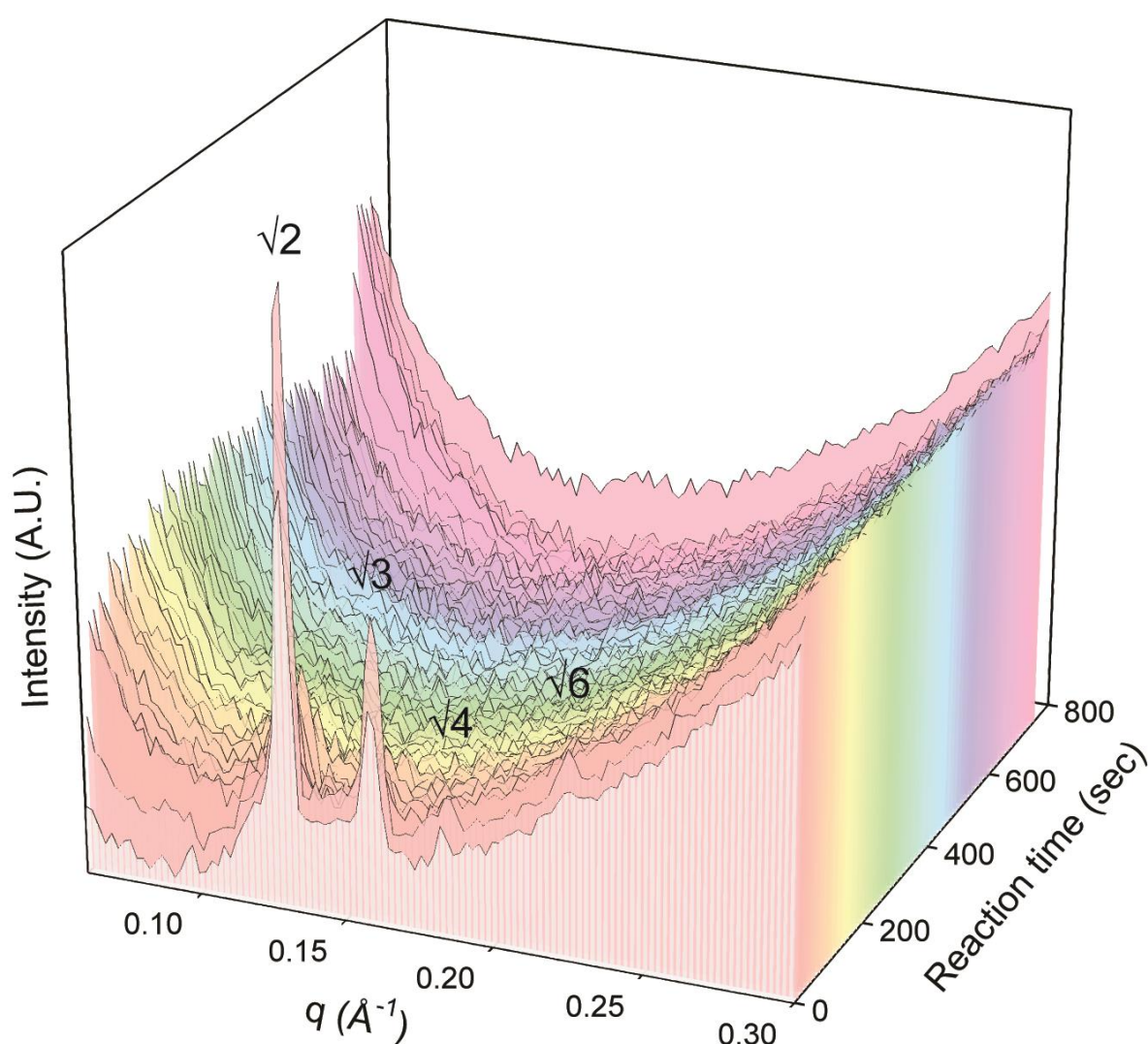

Figure 4-9. Monitoring the structural progression during the dynamic incorporation of a solution of 3% w/w DDAB with 0.3PHYTV$_2$. The initial cubic *Pn3m* structure disappeared gradually within 100 secs but no Bragg peaks evolved for the remaining time.

Overall, the sensitivity of phase transitions of the ionic strength-sensitive systems was poor due to lack of definitive peaks resolved during the phase transition. The device may have been more suited to the pH-responsive systems due to rapid equilibration of the structures that could be resolved within the length of channel. The ionic strength-sensitive systems may require a microfluidic device with longer channel lengths or a rigorous mixing feature which could mimic the energy input of sonication. Thus, the S-MF device may not be useful for every LCNP systems.

4.5 Conclusion

Microfluidics is a highly customisable and versatile tool that can aid in the understanding of stimuli-responsive LCNPs and their transformations. The kinetics of transformation of some pH- or ionic strength-sensitive systems can be almost instantaneous and would be ideal in cases where immediate drug release is required. This information elucidated the non-equilibrium behaviour during the phase transitions that would not have been observed with traditional equilibrium analysis, which may provide greater insight to designing stimuli responsive drug delivery.

4.6 References

(1)   Han, S.; Shen, J.; Gan, Y.; Geng, H.; Zhang, X.; Zhu, C.; Gan, L. Novel Vehicle Based on Cubosomes for Ophthalmic Delivery of Flurbiprofen with Low Irritancy and High Bioavailability. Acta Pharmacol. Sin. 2010, 31, 990–998.

(2)   Carvalho, F. C.; Campos, M. L.; Peccinini, R. G.; Gremião, M. P. D. Nasal Administration of Liquid Crystal Precursor Mucoadhesive Vehicle as an Alternative Antiretroviral Therapy. Eur. J. Pharm. Biopharm. 2013, 84, 219–227.

(3)   Gan, L.; Han, S.; Shen, J.; Zhu, J.; Zhu, C.; Zhang, X.; Gan, Y. Self-Assembled Liquid Crystalline Nanoparticles as a Novel Ophthalmic Delivery System for Dexamethasone: Improving Preocular Retention and Ocular Bioavailability. Int. J. Pharm. 2010, 396, 179–187.

(4)   Astolfi, P.; Giorgini, E.; Gambini, V.; Rossi, B.; Vaccari, L.; Vita, F.; Francescangeli, O.; Marchini, C.; Pisani, M. Lyotropic Liquid-Crystalline Nanosystems as Drug Delivery Agents for 5-Fluorouracil: Structure and Cytotoxicity. Langmuir 2017, 33, 12369–12378.

(5)   Baskaran, R.; Madheswaran, T.; Sundaramoorthy, P.; Kim, H. M.; Yoo, B. K. Entrapment of Curcumin into Monoolein-Based Liquid Crystalline Nanoparticle Dispersion for Enhancement of Stability and Anticancer Activity. Int. J. Nanomedicine 2014, 9, 3119–3130.

(6)   Du, J. D.; Liu, Q.; Salentinig, S.; Nguyen, T. H.; Boyd, B. J. A Novel Approach to Enhance the Mucoadhesion of Lipid Drug Nanocarriers for Improved Drug Delivery to the Buccal Mucosa. Int. J. Pharm. 2014, 471, 358–365.

(7)   Warren, D. B.; Anby, M. U.; Hawley, A.; Boyd, B. J. Real Time Evolution of Liquid Crystalline Nanostructure During the Digestion of Formulation Lipids Using Synchrotron Small-Angle X-Ray Scattering. Langmuir 2011, 27, 9528–9534.

(8)   Hong, L.; Salentinig, S.; Hawley, A.; Boyd, B. J. Understanding the Mechanism of Enzyme-

Induced Formation of Lyotropic Liquid Crystalline Nanoparticles. Langmuir 2015, 31, 6933–6941.

(9)   Fong, W. K.; Salentinig, S.; Prestidge, C.; Mezzenga, R.; Hawley, A.; Boyd, B. J. Generation of Geometrically Ordered Lipid-Based Liquid-Crystalline Nanoparticles Using Biologically Relevant Enzymatic Processing. Langmuir 2014, 30, 5373–5377.

(10) Salentinig, S.; Phan, S.; Khan, J.; Hawley, A.; Boyd, B. J. Formation of Highly Organized Nanostructures during the Digestion of Milk. ACS Nano 2013, 7, 10904–10911.

(11) Yaghmur, A.; Laggner, P.; Sartori, B.; Rappolt, M. Calcium Triggered Lα-H2 Phase Transition Monitored by Combined Rapid Mixing and Time-Resolved Synchrotron SAXS. PLoS One 2008, 3, 1–11.

(12) Paar, A. (GmbH). The SAXS Guide; Schnablegger, H.; Singh, Y., Eds.; 2nd ed.; Anton Paar: Austria, 2011.

(13) Ghazal, A.; Gontsarik, M.; Kutter, J. P.; Lafleur, J. P.; Labrador, A.; Mortensen, K.; Yaghmur, A. Direct Monitoring of Calcium-Triggered Phase Transitions in Cubosomes Using Small-Angle X-Ray Scattering Combined with Microfluidics. J. Appl. Crystallogr. 2016, 49, 1–10.

(14) Khaliqi, K.; Ghazal, A.; Azmi, I. D. M.; Amenitsch, H.; Mortensen, K.; Salentinig, S.; Yaghmur, A. Direct Monitoring of Lipid Transfer on Exposure of Citrem Nanoparticles to an Ethanol Solution Containing Soybean Phospholipid by Combining Synchrotron SAXS with Microfluidics. Analyst 2017, 142, 3118–3126.

(15) Song, H.; Tice, J. D.; Ismagilov, R. F. A Microfluidic System for Controlling Reaction Networks in Time. Angew. Chemie - Int. Ed. 2003, 42, 768–772.

(16) Barauskas, J.; Landh, T. Phase Behavior of the Phytantriol/Water System. Langmuir 2003, 19, 9562–9565.

(17) Dong, Y.-D.; Tilley, A. J.; Larson, I.; Lawrence, M. J.; Amenitsch, H.; Rappolt, M.; Hanley, T.; Boyd, B. J. Nonequilibrium Effects in Self-Assembled Mesophase Materials: Unexpected Supercooling Effects for Cubosomes and Hexosomes. Langmuir 2010, 26, 9000–9010.

(18) Ljusberg-Wahren, H.; Herslof, M.; Larsson, K. A Comparison of the Phase Behaviour of the Monoolein Isomers in Excess Water. Chem. Phys. Lipids 1983, 33, 211–214.

(19) Barauskas, J.; Svedaite, I.; Butkus, E.; Razumas, V.; Larsson, K.; Tiberg, F. Synthesis and Aqueous Phase Behavior of 1-Glyceryl Monooleyl Ether. Colloids Surfaces. B Biointerfaces 2005, 41, 49–53.

(20) Fong, W. K.; Negrini, R.; Vallooran, J. J.; Mezzenga, R.; Boyd, B. J. Responsive Self-Assembled Nanostructured Lipid Systems for Drug Delivery and Diagnostics. J. Colloid Interface Sci. 2016, 484, 320–339.

(21) Oka, T.; Saiki, T.; Alam, J. M.; Yamazaki, M. Activation Energy of the Low-PH-Induced Lamellar to Bicontinuous Cubic Phase Transition in Dioleoylphosphatidylserine/Monoolein. Langmuir 2016, 32, 1327–1337.

(22) Oka, T.; Hasan, M.; Islam, M. Z.; Moniruzzaman, M.; Yamazaki, M. Low-PH-Induced Lamellar to Bicontinuous Primitive Cubic Phase Transition in Dioleoylphosphatidylserine/Monoolein Membranes. Langmuir 2017, 33, 12487–12496.

(23) Salentinig, S.; Sagalowicz, L.; Glatter, O. Self-Assembled Structures and PKa Value of Oleic Acid in Systems of Biological Relevance. Langmuir 2010, 26, 11670–11679.

(24)   Kluzek, M.; Tyler, A. I. I.; Wang, S.; Chen, R.; Marques, C. M.; Thalmann, F.; Seddon, J. M.; Schmutz, M. Influence of a PH-Sensitive Polymer on the Structure of Monoolein Cubosomes. Soft Matter 2017, 13, 7571–7577.

(25)   Muir, B. W.; Zhen, G.; Gunatillake, P.; Hartley, P. G. Salt Induced Lamellar to Bicontinuous Cubic Phase Transitions in Cationic Nanoparticles. J. Phys. Chem. B 2012, 116, 3551–3556.

(26)   Kanicky, J. R.; Shah, D. O. Effect of Degree, Type, and Position of Unsaturation on the PKa of Long-Chain Fatty Acids. J. Colloid Interface Sci. 2002, 256, 201–207.

(27)   Negrini, R.; Mezzenga, R. PH-Responsive Lyotropic Liquid Crystals for Controlled Drug Delivery. Langmuir 2011, 27, 5296–5303.

(28)   Donten, M. L.; VandeVondele, J.; Hamm, P. Speed Limits for Acid–Base Chemistry in Aqueous Solutions. Chim. Int. J. Chem. 2012, 66, 182–186.

(29)   Liu, Q.; Dong, Y. Da; Hanley, T. L.; Boyd, B. J. Sensitivity of Nanostructure in Charged Cubosomes to Phase Changes Triggered by Ionic Species in Solution. Langmuir 2013, 29, 14265–14273.

(30)   Kirby, N. M.; Mudie, S. T.; Hawley, A. M.; Cookson, D. J.; Mertens, H. D. T.; Cowieson, N.; Samardzic-Boban, V. A Low-Background-Intensity Focusing Small-Angle X-Ray Scattering Undulator Beamline. J. Appl. Crystallogr. 2013, 46, 1670–1680.

(31)   Mudie, S. T. ScatterBrain
        http://www.synchrotron.org.au/aussyncbeamlines/saxswaxs/software-saxswaxs.

(32)   Hyde, S. T. Identification of Lyotropic Liquid Crystalline Mesophases. In Handbook of Applied Surface and Colloid Chemistry; Holmberg, K., Ed.; John Wiley & Sons, Ltd, 2001; pp. 299–332.

(33)   Lee, S. H.; Rasaiah, J. C. Proton Transfer and the Mobilities of the H+and OH-Ions from Studies of a Dissociating Model for Water. J. Chem. Phys. 2011, 135, 1–10.

(34)   Agmon, N. The Grotthuss Mechanism. Chem. Phys. Lett. 1995, 50, 456–462.

(35)   Hyde, T. Bicontinuous Structures in Lyotropic Liquid Crystals and Crystalline Hyperbolic Surfaces. Curr. Opin. Solid State Mater. Sci. 1996, 1, 653–662.

(36)   Muir, B. W.; Zhen, G.; Gunatillake, P.; Hartley, P. G. Salt Induced Lamellar to Bicontinuous Cubic Phase Transitions in Cationic Nanoparticles. J. Phys. Chem. B 2012, 116, 3551–3556.

(37)   Regev, O.; Marques, E. F.; Khan, A.; Lindman, B.; da Graça Miguel, M. Vesicle Formation and General Phase Behavior in the Catanionic Mixture SDS–DDAB–Water. The Cationic-Rich Side. J. Phys. Chem. B 2002, 103, 8353–8363.

4.7 Appendix
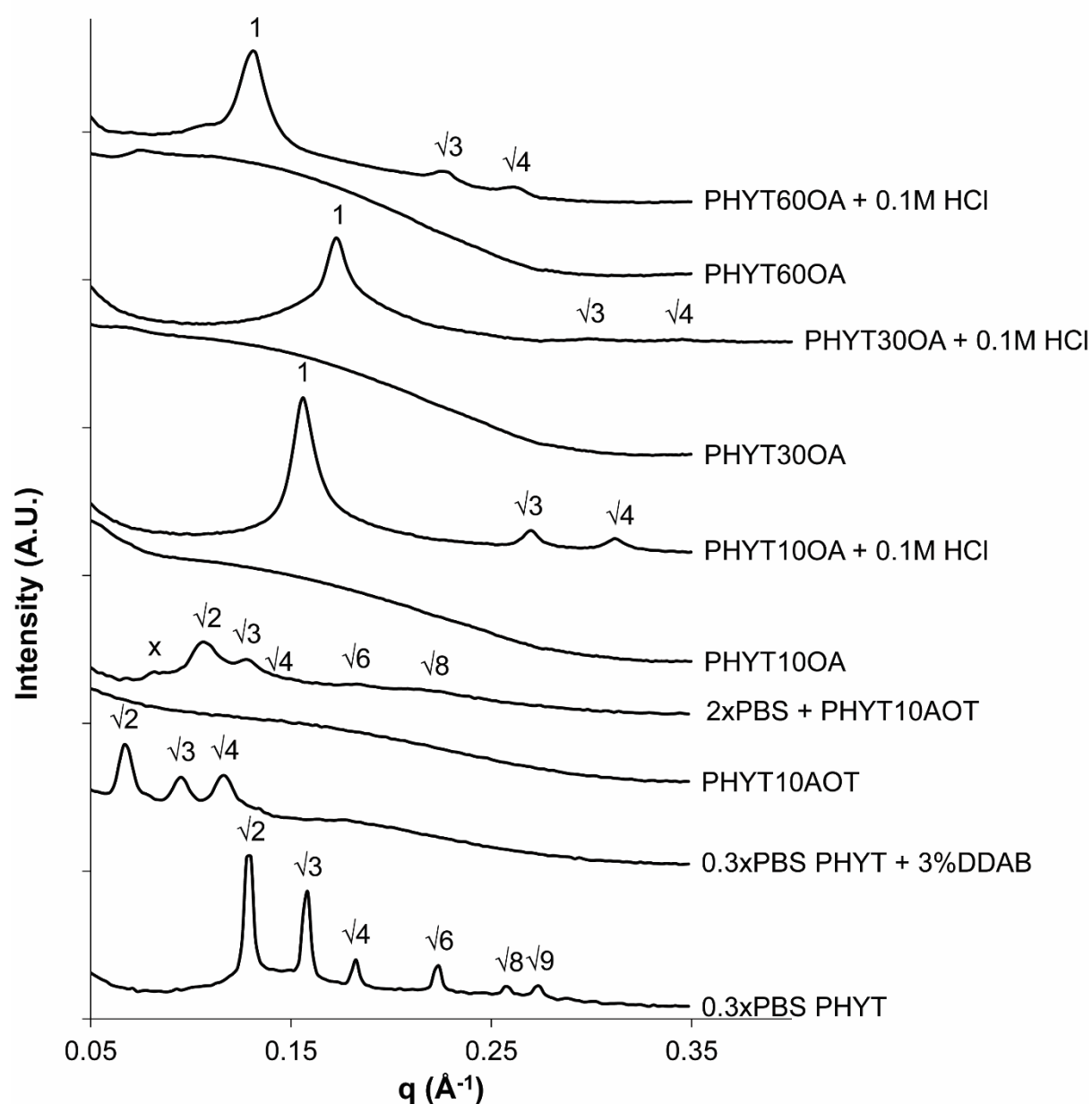
Supplementary figure 4-1. Phases of the different lipid-based systems before and after mixing with equal volumes of the corresponding stimulus. Profiles where the peaks displayed a spacing ratio of 1, √3 and √4 are indicative of the H_2 phase while a spacing ratio of √2, √3, √4 ... indicated the presence of cubic phase (*Pn3m*). The peak labelled x was thought to be the first peak of the Im3m phase.
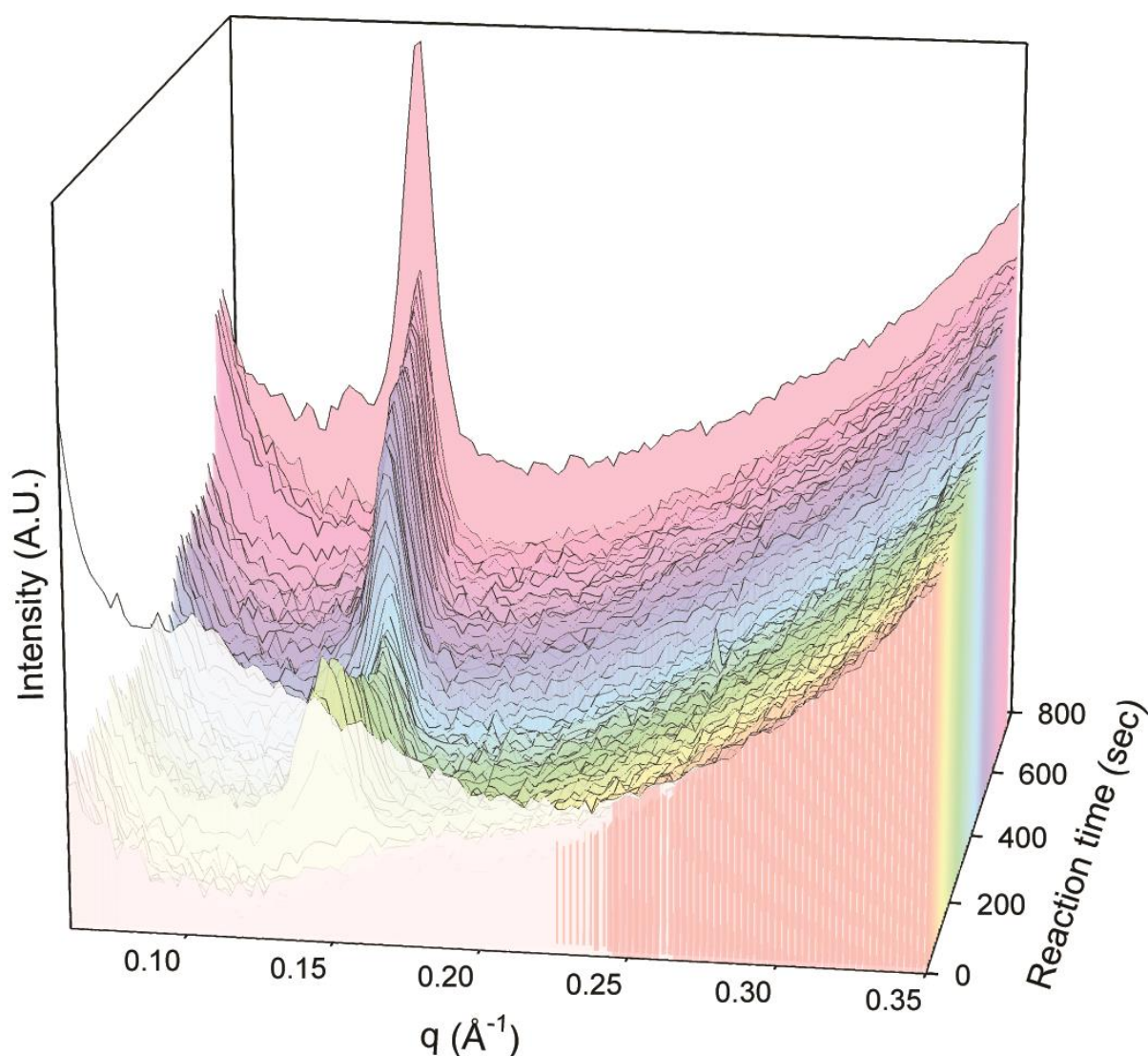
Supplementary figure 4-2. Monitoring the structural progression during the dynamic incorporation of a 0.1M solution of HCl with PHYT60OA (pH 9) in the S-MF device. This profile includes the scattering profile at 0 secs. The formulation initiated as vesicles at time 0. Upon contact with the acidic solution, there was an immediate loss of the scattering for lamellar phase. A peak at 0.117 Å^{-1} < q < 0.151 Å^{-1} grew in intensity whilst shifting to lower q at a maximum of q = 0.133 Å^{-1} before decreasing in intensity and shifting slightly to higher q and then back again. The peak stabilised at a constant intensity and q-position by 334 secs for the remainder of the transformation.

Chapter 5: Conclusion and outlook

5.1 Summary

Stimuli-responsive liquid crystalline systems have potential to improve the delivery and therapeutic outcome of drugs. This property allows the release of content when and where necessary upon exposure to the appropriate stimuli. The ability to control these attributes can potentially reduce side effects and efficiently deliver the dosage of drug without overloading. Thus, these systems are a powerful option for drug delivery. To date though, no stimuli-responsive lipid-based liquid crystalline nanoparticle (LCNP) system exists on the market. Limitations in approaches used to characterise the kinetics of the structural transitions that provide controlled drug release have in part hindered the ability to optimise the formulations. As the rate of drug release is dependent on the nanostructure confining the drug, it is crucial to characterise the phase transitions in order to deliver an accurate dosage.

In vivo studies are often a costly venture on top of all the ethical considerations, so it is important to completely and efficiently assess formulations prior to the necessary *in vivo* validation. Determination of which formulations to test mostly depend on clarity of information from *in vitro* studies. These studies act as preliminary indicators on how the formulation will behave structurally or chemically after administration. Therefore, developing reliable *in vitro* approaches to analysing the performance of formulations will allow researchers to proceed with *in vivo* studies confidently or continue with their optimisation.

The introductory chapter discussed the issues surrounding the traditional experimental configurations used to study the phase transitions of stimuli-responsive LCNP systems. The main issue with the experimental configurations was that the stimulus was not applied uniformly to the formulation, resulting in inconsistent transformations in the bulk mixing process. As a consequence, the associated analytical technique used to determine the structure present at any point in time would potentially sample a portion of the heterogeneous transformation, not necessarily providing an accurate representation of structure. Consequently, the data may be compromised by the experimental configuration rather than being inherent to the formulation itself. Furthermore, the site of interaction of the formulation with the stimulus (such as a mixing vessel) is typically physically separate to the site of analysis (eg. a flow capillary), and so the delay from one location to the other also affects the accuracy of interpretation of the kinetics.

Microfluidics was proposed as the solution to these limitations where the devices incorporated both the site of interaction and analysis into one device in what is commonly referred to as a lab-on-a-chip in the field. And so, the following hypotheses were developed:

1. That controlling the mixing behaviour of the starting materials by diffusion via a fixed interface can regulate the kinetics of the transformation of LCNPs *in situ*.

2. That mixing of homogeneous ratios of starting materials will allow more consistent phase transitions for characterisation.

3. That integrating both the mixing and analysis vessels into one experimental configuration will enable any kinetic structures earlier in the transformation to be defined.

4. That microfluidics is more suited than the traditional pH-stat approach (or equivalent) for synchrotron-SAXS experiments as the kinetic analysis is not limited to the acquisition time of data collection, allowing kinetics of rapidly transforming systems to be resolved.

5. That microfluidics can allow a uniform dose of stimulus to be applied to all droplets/particles in the system such that all transformations that take place are homogeneous.

6. That mixed phases will be observed within individual droplets via a gradient before equilibrium is achieved during transformations.

As custom-built microfluidics can be a costly venture, a simple and inexpensive "off-the-shelf" microfluidic (OTS-MF) device and a commercially available device were initially assessed for the ability to elucidate phase transitions in stimuli-responsive LCNP systems, with the findings detailed in the second chapter. The technology has only recently been introduced to the lipid-based liquid crystal field, having mostly found its application in the production of lipid nanoparticles such as liposomes rather than being used specifically for *in situ* analysis. The OTS-MF device could not enable observation of the full phase transitions along the length of the channel without the need to run at different flow rates to capture different reaction times. For comparison, a commercially available microfluidic chip was also investigated. It was observed that upon mixing of the formulation and the stimulus, even in the presence of the staggered herringbone structures in the channel design, the kinetics could not be tracked *in situ* due to limited length of the fluid path. Insufficient channel length meant that the mixture could not be retained for a sufficient time to observe the full transition kinetics actually on the chip, despite LCNPs being formed in the final collection tube. Additionally,

fluctuations in the proportions of the solutions resulted in different compositions of the system equilibrating along the channel.

As a consequence, in chapter three, a more refined microfluidic device (S-MF) that was custom designed and manufactured to monitor phase transitions was evaluated. The design of the channels took into account the shortcomings of the previously tested devices and featured a longer length of channel (at least 3.5 times longer). Additionally, the configuration of the channels (hydrodynamic flow focusing) allowed a greater interfacial area of contact between the streams and enabling characterisation of the mixing behaviour. Compared to the traditional approach to monitoring the digestion of lipid-based formulations, the S-MF device exhibited more controlled transformations. The Bragg peaks in the scattering profiles arising from the ordered self-assembled structures were sharper and grew more gradually, owing to the diffusion-limited interface of the co-axial flowing streams as opposed to the random mixing of the bulk mixing processes. Depending on the strength of enzyme used, the kinetics of the digestion in the device could also be controlled.

In the aforementioned results chapters, the possibility for microfluidics to control the transformations of stimuli-responsive LCNPs with *in situ* monitoring of the process was demonstrated. The configuration of the OTS-MF and the S-MF devices enabled co-axial flows of the formulation and the stimulus. Consequently, the controlled convergence of the stimulus and formulation saw that each portion of formulation had access to the same amount of stimuli, addressing the first, second and fifth hypotheses. Time points from the moment the formulation came into contact with the stimulus could also be resolved, thereby confirming the third hypothesis. As microfluidics is a spatially-resolved technique, dependent on the retention time at any particular position, the acquisition time for collecting the scattering signal could be increased to 30 secs or more, while continuously collecting the same information without risk of radiation damage or sampling a different time point of the transformation. Therefore, the fourth hypothesis was demonstrated as the flow-through nature of the pH-stat approach is typically limited to 5 secs as it would measuring over a time range of the reaction.

The aforementioned techniques could not resolve the issue of whether multiple phases existed in a single particle or separately when scattering profiles showed an apparent mixed phase composition. Crossed polarised light microscopy (CPLM) was another *in situ* technique used with microfluidics in these studies, allowing visualisation of the morphology of lipid-based formulations during digestion

to interrogate this question. Droplet-based microfluidics was studied with CPLM in two different channel designs. The first was the S-MF design which was not amenable to interrogating this question as the droplets moved too fast to discern the changes in structure within a single individual droplet. The second design consisted of pockets which allowed trapping of specific droplets indefinitely with solution able to flow around those droplets. Phase transitions occurred within the trapped droplets and were observed as a gradient across a droplet showing the co-existence of mixed phases within the one droplet, and thereby aligning with the final hypotheses.

Applications of microfluidics with other stimuli-responsive LCNP systems were explored in the fourth chapter namely systems sensitive to pH or ionic strength. In general, it was found the phytantriol systems with 30 and 60% w/w oleic acid (PHYT30OA and PHYT60OA) observed phase transitions, however the sensitivities of some of the liquid crystal systems was insufficient. Scattering produced one peak which was insufficient for confident phase identification, but was suspected to be the first peak for H_2 phase based on the equilibrated systems. Other systems such as the dispersion with 10% w/w oleic acid (PHYT10OA) observed an almost instantaneous change, suggesting a rapid delivery of stimulus that induced an equally rapid restructuring of the molecules. The change was seen in less than 0.02 secs of reaction time, which would not have been possible to analyse using traditional techniques where the acquisition time is approximately 5 secs, supporting the fourth hypothesis. The PHYT10AOT system that was sensitive to changes in tonicity also underwent the phase changes expected from the premixed equilibrium system, transforming from lamellar phase to the coexistence of cubic *Pn3m* and *Im3m* phase, albeit the sensitivity was low.

Overall, the main aim in this thesis was to use microfluidics as a tool to track the phase transitions of stimuli-responsive LCNP systems. After assessing many different versions of microfluidic devices, the device best suited for this kinetic analysis was found to have a long length of channel and feature a mixing component that could be characterised such as hydrodynamic flow focusing. However, not all lipid-based formulations may be appropriately analysed for any one microfluidic device due to equilibration time constraints and sensitivity. Therefore, it is anticipated that ongoing research will focus on optimising the devices so they may be translated to other lipid-based systems as a high-throughput tool.

5.2 Future directions

Microfluidics is emerging as a rapidly-evolving field that can prepare and analyse samples more efficiently than traditional techniques. Although the contents of this thesis have laid the foundations to better understand the kinetics of stimuli-responsive LCNP systems, microfluidics still has a lot of untapped potential. Aside from optimisation of the device itself, other areas of further studies include the integration of the device with biological components and drug release.

5.2.1 Optimisation of microfluidic devices and X-ray analysis

Sensitivity of the microfluidic device with small angle X-ray scattering (SAXS) was a major issue. In order to compete with the current setups, a sufficient signal was required from the samples *in situ*. However, in some cases, the X-ray beam was attenuated by the material. Consequently, the visibility of peaks in the scattering profiles was hindered such that phases could not be identified. To counteract this deficiency, a few strategies are proposed.

The first improvement could occur during the manufacture of the device with the use of thinner material. A shorter distance of quartz in the custom microfluidic device would see the X-rays travel through less material. Thus, more X-rays would be available to be scattered by the formulation resulting in a greater signal. Under a similar notion, the channel depth could be increased so that the X-rays could be scattered more intensely by more of the sample as it travels through. The width of the channel may also be increased such that the beam spot (although perfectly positioned) does not drift and scatter the walls of the channel which would contribute to the background scattering. Unfortunately, this could not be performed in the duration of the project due to time constraints.

Although the length of channel in the current microfluidic device was sufficient for these systems, it may not be suitable for every stimuli-responsive formulation. In this case, a chip with longer channels may be required but this is not always feasible. Owens *et al.* have generated LEGO-block microfluidic devices which consist of 3D-printed connectable bricks, allowing a combination of variable channel designs.[1] This concept could be used to easily customise channel lengths depending on the equilibrium times of the systems instead of re-manufacturing a new device.

Another option, although costlier and time consuming, would be to access a SAXS beamline at another synchrotron with the required specifications. A facility where the SAXS beamline has a smaller beam spot size would decrease the likelihood of scattering off the walls of the channel. Even though the beam spot size can be decreased at the beamline at the Australian Synchrotron, it would

also decrease the flux of the beam and decrease the signal intensity. A higher energy beam could also counteract the attenuation from the material.

5.2.2 Other stimuli-responsive systems

While digestion-sensitive systems were heavily examined in this thesis along with pH and ionic strength-sensitive systems, other stimuli-responsive systems were also considered but yielded insufficient results and were not included. Light-activated formulations including systems doped with gold nanorods or other photo-actuators such as naphthalocyanine were assessed in the S-MF and OTS-MF devices.[2,3] Light activated systems are of particular interest to potentially improve the treatment of diseases of the back of the eye such as age-related macular degeneration as it is an appropriate stimulus for this application. Briefly, the LCNPs were flowed through the device via one inlet channel (excess inlet channels were blocked) passing a section of the microchannel which was constantly irradiated by an infrared laser (with a wavelength of 808 nm and power set to 400 mW, class IIIB fiber coupled laser system from Changchun New Industries, China). The resulting changes in structures were monitored along the length of the channel as per previous experiments using synchrotron-based SAXS. It was hypothesized that the nanoparticles would undergo a phase transition due to the photothermal heating effect when flowing through the channel exposed to the laser, and then equilibrate back to the original structure as they flow beyond the irradiated region. The gold nanorod formulation did begin to transition as noted by a shift in the position of the q-value of the Braggs peaks (**Figure 5-1**), however no phase transition was evident. Flow rates were slowed to the minimum to increase the exposure time to the laser, however, this was still insufficient. As it would be impractical to procure a larger laser, the laser exposure time of the nanoparticles may be enhanced with nanofluidics which would generate a larger surface area to volume ratio of the sample in the nano-sized channels.
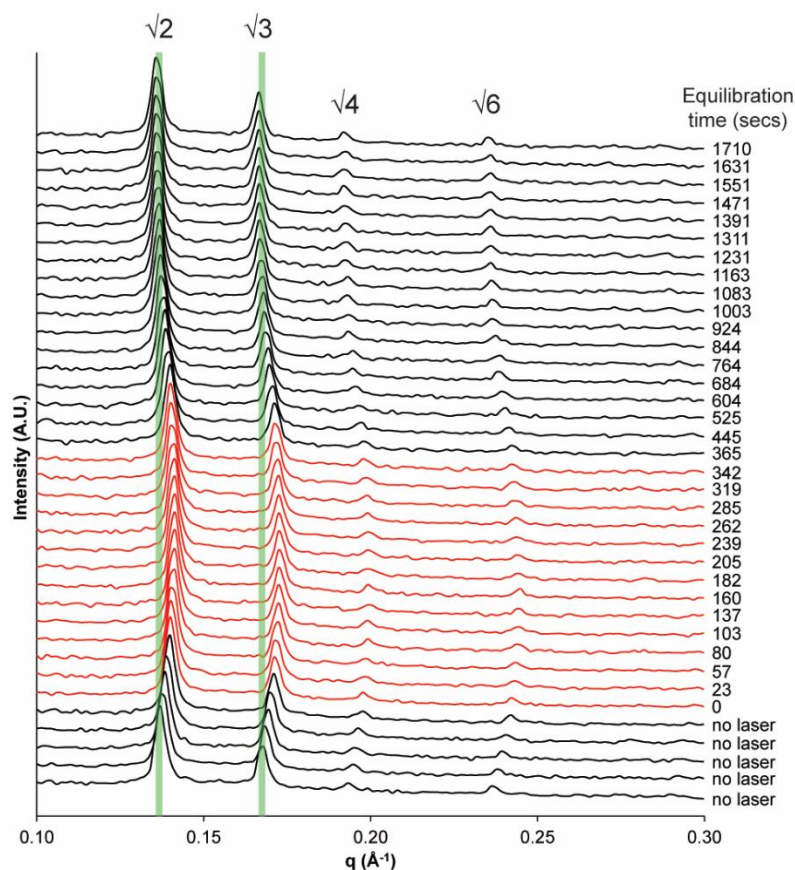
Figure 5-1. Shrinking and swelling of a phytantriol-based cubosomes system doped with gold nanorods in response to infrared irradiation under flow in the OTS-MF device. A transition from the cubic *Pn3m* phase to the L$_\alpha$ phase was expected upon irradiation if the system was heated sufficiently by the photothermal effect of the irradiated nanorods.[2] However, traversing the section of irradiated channel for an exposure time of around 5 mins (profiles highlighted in red), only a shift of the peak positions to higher *q* was observed. As the nanoparticles flowed further from the regions of irradiation, the *q*-position of the peaks shifts back to the original positions, as highlighted by the vertical green lines. The total flow rate was set to 0.5 µL/min and structural data at the top 2 cm of the visible capillary in the OTS-MF configuration were acquired using SAXS.

5.2.3 Alternative uses of microfluidics for the study of stimuli-responsive LCNPs

Microfluidics can be used for many applications depending on its design. Applications can range from the generation of nanoparticles,[4] to observing interactions of formulations with cells,[5] to sorting cells[6] and particles.[7] Studies so far in this thesis have focused on the integration of microfluidics with analytical techniques such as SAXS and CPLM to track the change in nanostructure, however there are other properties of LCNPs that can also be examined. To better characterise the kinetics of these systems, other factors to assess can include release kinetics and interactions with biologically relevant systems.

5.2.3.1 Release studies

The thesis has established microfluidics as a tool to aid in the monitoring of phase transitions, but has yet to correlate the structure with the drug release behaviour which would enable indication of post-administration results. To expand on this, it is possible to also visualise the release of encapsulated drug in response to stimuli from these systems within microfluidics as well. Droplets of the formulation containing a fluorescently labelled substance can be trapped while the intensity of the fluorescence can be used to determine the amount of drug remaining in the droplets.[8,9] Performing the structural analysis alongside the drug release studies can enable direct correlation of the two properties and can thus allow more efficient optimisation of the formulation.

5.2.3.2 Organ-on-a-chip

To advance the stimuli-responsive systems into clinical studies with a greater chance of success, *ex vivo* studies are also required. Literature has shown that LCNPs exhibit interactions with biorelevant systems and vice versa.[10] It has been shown that cubic phases are more damaging to cells than the hexagonal, inverse micellar and sponge phases, for example,[11,12] so the next stage is the assessment of LCNP transformations under flow in these systems to observe the hemolytic and cytotoxic effects. Through modulation of the stimuli-responsive formulation to influence the kinetic changes in structure during a transformation, the occurrence of certain nanostructures may be shortened or removed and the interaction with cells observed. Microfluidic channels can be coated with the relevant cells to mimic the vessels or organs, and their diseased states.[5,13] Additionally, a body on a chip is currently under development which can potentially enable screening of the formulation across an entire human body. With more optimisation and integration with SAXS, there may be opportunity to study the kinetics of structural changes of stimuli-responsive phase transitions along with interactions with the relevant cells.

5.3 Conclusion

In summary, microfluidics has been shown to reliably monitor the structural evolution during the phase transitions of stimuli-responsive lipid-based formulations. A microfluidic device was fabricated specifically to facilitate a controllable and characterisable mixing behaviour to deliver a uniform dose of stimuli to the formulation to yield homogeneous transformations. Not all stimuli-responsive systems were examined in this work so there is, of course, more work to expand on such as stimuli from external sources such as magnets or light-activation which presents more challenges in the configuration of the experiment. Nevertheless, the lessons learnt in this thesis will no doubt impart

a more efficient methodology for researchers looking to fabricate their own devices for kinetic studies which will ultimately accelerate the development and optimisation of these stimuli-responsive drug delivery formulations.

5.4   References

(1)   Owens, C. E.; Hart, A. J. High-Precision Modular Microfluidics by Micromilling of Interlocking Injection-Molded Blocks. *Lab Chip* **2018**, *18*, 890–901.

(2)   Fong, W.; Hanley, T. L.; Thierry, B.; Kirby, N.; Waddington, L. J.; Boyd, B. J. Controlling the Nanostructure of Gold Nanorod–Lyotropic Liquid- Crystalline Hybrid Materials Using Near-Infrared Laser Irradiation. *Langmuir* **2012**, *28*, 14450–14460.

(3)   Du, J. D.; Hong, L.; Tan, A.; Boyd, B. J. Naphthalocyanine as a New Photothermal Actuator for Lipid-Based Drug Delivery Systems. *J. Phys. Chem. B* **2018**, *122*, 1766–1770.

(4)   Khan, I. U.; Serra, C. A.; Anton, N. Production of Nanoparticle Drug Delivery Systems with Microfluidics Tools. *Expert Opin. Drug Deliv.* **2015**, *12*, 547–562.

(5)   Pandya, H. J.; Dhingra, K.; Prabhakar, D.; Chandrasekar, V. Biosensors and Bioelectronics A Micro Fl Uidic Platform for Drug Screening in a 3D Cancer Microenvironment. **2017**, *94*, 632–642.

(6)   Schmid, L.; Weitz, D. A.; Franke, T. Sorting Drops and Cells with Acoustics: Acoustic Microfluidic Fluorescence-Activated Cell Sorter. *Lab Chip* **2014**, *14*, 3710–3718.

(7)   Devendran, C.; Gralinski, I.; Neild, A. Separation of Particles Using Acoustic Streaming and Radiation Forces in an Open Microfluidic Channel. *Microfluid. Nanofluidics* **2014**, *17*, 879–890.

(8)   Nguyen, H. T.; Marquis, M.; Anton, M.; Marze, S. Studying the Real-Time Interplay between Triglyceride Digestion and Lipophilic Micronutrient Bioaccessibility Using Droplet Microfluidics. 2 Application to Various Oils and (pro)Vitamins. *Food Chem.* **2019**, *275*, 661–667.

(9)   Cheng, W. C.; He, Y.; Chang, A. Y.; Que, L. A Microfluidic Chip for Controlled Release of Drugs from Microcapsules. *Biomicrofluidics* **2013**, *7*.

(10)   Tan, A.; Hong, L.; Du, J. D.; Boyd, B. J. Self-Assembled Nanostructured Lipid Systems: Is There a Link between Structure and Cytotoxicity? *Adv. Sci.* **2018**, *6*, 1801223–1801244.

(11)   Tran, N.; Mulet, X.; Hawley, A. M.; Hinton, T. M.; Mudie, S. T.; Muir, B. W.; Giakoumatos, E. C.; Waddington, L. J.; Kirby, M.; Drummond, C. J. Nanostructure and Cytotoxicity of Self-Assembled Monoolein–capric Acid Lyotropic Liquid Crystalline Nanoparticles. *RSC Adv.* **2015**, *5*, 26785–26795.

(12)   Barauskas, J.; Cervin, C.; Jankunec, M.; Spandyreva, M.; Ribokait, K.; Tiberg, F.; Johnsson, M. Interactions of Lipid-Based Liquid Crystalline Nanoparticles with Model and Cell Membranes. *Int. J. Pharm.* **2010**, *391*, 284–291.

(13)   Kimura, H.; Sakai, Y.; Fujii, T. Drug Metabolism and Pharmacokinetics Organ / Body-on-a-Chip Based on Micro Fl Uidic Technology for Drug Discovery. *Drug Metab. Pharmacokinet.* **2018**, *33*, 43–48.

"A stranger to myself and and to the world, armed solely with a thought that negates itself as soon as it asserts, what is this condition in which I can have peace only by refusing to know and to live; in which the appetite for conquest bumps into walls that defy its assaults? To will is to stir up paradoxes."

Albert Camus, The Myth of Sisyphus